

**ANALYSIS OF BIOMARKER IONS AND NUCLEIC ACIDS IN WHOLE  
BACTERIAL CELLS BY MASS SPECTROMETRY**

by

Christy Abbas-Hawks

ProQuest Number: 10796821

All rights reserved

INFORMATION TO ALL USERS

The quality of this reproduction is dependent upon the quality of the copy submitted.

In the unlikely event that the author did not send a complete manuscript and there are missing pages, these will be noted. Also, if material had to be removed, a note will indicate the deletion.



ProQuest 10796821

Published by ProQuest LLC (2019). Copyright of the Dissertation is held by the Author.

All rights reserved.

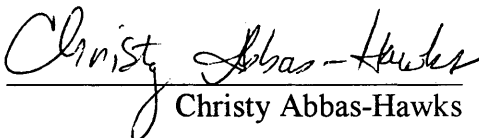
This work is protected against unauthorized copying under Title 17, United States Code  
Microform Edition © ProQuest LLC.

ProQuest LLC.  
789 East Eisenhower Parkway  
P.O. Box 1346  
Ann Arbor, MI 48106 – 1346

A thesis submitted to the Faculty and the Board of Trustees of the Colorado School of Mines in partial fulfillment of the requirements for the degree of Doctor of Philosophy (Applied Chemistry).

Golden, Colorado

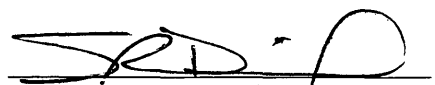
Date July 29, 1999

Signed:   
Christy Abbas-Hawks

Approved:   
Kent J. Voorhees  
Thesis Advisor

Golden, Colorado

Date Aug. 2, 1999

  
Dr. Stephen R. Daniel  
Professor and Department Head  
of Chemistry and Geochemistry

## ABSTRACT

To facilitate the goal of developing bacterial analytical methods and a biomarker database for the chemotaxonomic identification of bacteria, experiments were performed on nucleotides, oligonucleotides, DNA and whole bacterial cells. Two experiments focused on identifying the origins of biomarker ions in whole bacterial cells by pyrolysis tandem mass spectrometry. Twelve statistically/biologically significant ions were analyzed by both low resolution and high resolution pyrolysis tandem mass spectrometry. These ions were found to be fragments of lipids, proteins, carbohydrates and nucleic acids. Fragmentation pathways for the various ions are presented.

The *in situ* methylation products of nitrogen bases were studied by pyrolysis mass spectrometry. The derivatization reagent tetramethylammonium hydroxide was determined to enhance nitrogen base volatility and shift the nitrogen bases to higher masses. These higher mass peaks are used as biomarkers for the nitrogen bases in pure DNA standards and whole bacterial cells.

Another experiment investigated the relationship between the intensities of nitrogen base biomarkers and known percent composition of guanine plus cytosine in nucleotide solutions, pure DNA standards and whole bacterial cells. The intensities of the nitrogen base biomarkers obtained from the Py-mass spectra were used to construct calibration curves. The calibration curves were then used to quantify nitrogen base content in unknowns. The nitrogen base content of four highly pathogenic microorganisms, a pure DNA sample and a free nucleotide solution was calculated with the calibration curves.

## TABLE OF CONTENTS

ABSTRACT.....	iii
LIST OF FIGURES.....	vi
LIST OF TABLES.....	xi
ACKNOWLEDGEMENTS.....	xiii
PREFACE.....	1
Chapter 1: Use of Pyrolysis Tandem Mass Spectrometry to Study Biomarker Pyrolysis Mechanisms in Whole Bacterial Cells.....	5
Abstract.....	5
Introduction.....	5
Experimental.....	7
Results.....	9
Conclusions.....	46
References.....	49
Chapter 2: Identification of Biomarkers in the Desorption Electron Ionization- High Resolution Mass Spectrum of <i>Brucella neotomae</i> .....	50
Abstract.....	50
Introduction.....	50
Experimental.....	55
Results.....	60
Carbohydrate/Nucleic Acid-Based Biomarker Ions.....	73
Protein-Based Biomarker Ions.....	95
Lipid-Based Biomarker Ions.....	105
Biomarker Ions in Gram-positive Bacteria.....	117
Conclusions.....	121
References.....	124
Chapter 3: <i>In Situ</i> Methylation of Nucleic Acids Using Pyrolysis Mass Spectrometry.....	127
Abstract.....	127
Introduction.....	128
Experimental.....	129

Results.....	130
Free nucleotides.....	130
Oligonucleotides.....	137
Calf thymus DNA.....	139
Bacterial Whole Cells.....	139
Conclusions.....	145
References.....	147
Chapter 4: Nitrogen Base Composition Estimation by Mass Spectrometry.....	149
Abstract.....	149
Introduction.....	149
Experimental.....	152
Results.....	160
Nucleotide solutions.....	160
Pure DNA.....	167
Whole Bacterial Cells-Electron Ionization.....	171
Whole Bacterial Cells-Chemical Ionization.....	184
Conclusions.....	191
References.....	193
Appendix.....	194

## LIST OF FIGURES

Figure 1.1.	Instrument diagram of the triple quadrupole mass spectrometer modified for a Curie-point pyrolyzer probe.....	8
Figure 1.2.	Pyrolysis (a) product ion mass spectrum of m/z 67 and (b) precursor ion mass spectrum of m/z 67 from <i>Brucella neotomae</i> .....	12
Figure 1.3.	Proposed structures for biomarker ion 67.....	13
Figure 1.4.	A proposed fragmentation pathway with cytosine origins for biomarker ions 67 and 95.....	14
Figure 1.5.	Pyrolysis (a) product ion mass spectrum of m/z 81 and (b) precursor ion mass spectrum of m/z 81 from <i>Brucella neotomae</i> .....	16
Figure 1.6.	Proposed structures for biomarker ion 81.....	17
Figure 1.7.	A proposed fragmentation pathway with adenine origins for biomarker ion 81.....	18
Figure 1.8.	Pyrolysis (a) product ion mass spectrum of m/z 89 and (b) precursor ion mass spectrum of m/z 89 from <i>Brucella neotomae</i> .....	20
Figure 1.9.	Pyrolysis (a) product ion mass spectrum of m/z 91 and (b) precursor ion mass spectrum of m/z 91 from <i>Brucella neotomae</i> .....	21
Figure 1.10.	A proposed structure for biomarker ion 91.....	22
Figure 1.11.	A proposed fragmentation pathway with phenylalanine origins for biomarker ion 91.....	23
Figure 1.12.	Pyrolysis (a) product ion mass spectrum of m/z 95 and (b) precursor ion mass spectrum of m/z 95 from <i>Brucella neotomae</i> .....	25
Figure 1.13.	Proposed structures for biomarker ion 95.....	26
Figure 1.14.	Pyrolysis (a) product ion mass spectrum of m/z 102 and (b) precursor ion mass spectrum of m/z 102 from <i>Brucella neotomae</i> .....	27
Figure 1.15.	Pyrolysis (a) product ion mass spectrum of m/z 103 and (b) precursor ion mass spectrum of m/z 103 from <i>Brucella neotomae</i> .....	29
Figure 1.16.	A proposed structure for biomarker ion 103.....	30
Figure 1.17.	A proposed fragmentation pathway with phenylalanine and tryptophan origins for biomarker ion 103.....	31
Figure 1.18.	Pyrolysis (a) product ion mass spectrum of m/z 115 and (b) precursor ion mass spectrum of m/z 115 from <i>Brucella neotomae</i> .....	32
Figure 1.19.	A proposed structure for biomarker ion 115.....	33
Figure 1.20.	Pyrolysis (a) product ion mass spectrum of m/z 117 and (b) precursor ion mass spectrum of m/z 117 from <i>Brucella neotomae</i> .....	35
Figure 1.21.	A proposed structure for biomarker ion 117.....	36
Figure 1.22.	A proposed fragmentation pathway with tryptophan origins for biomarker ion 117.....	37

Figure 1.23.	Pyrolysis (a) product ion mass spectrum of m/z 128 and (b) precursor ion mass spectrum of m/z 128 from <i>Brucella neotomae</i> .....	38
Figure 1.24.	A proposed structure for biomarker ion 128.....	39
Figure 1.25.	A proposed fragmentation pathway with alanyl-glycine diketopiperazine origins for biomarker ion 128.....	41
Figure 1.26.	Pyrolysis (a) product ion mass spectrum of m/z 129 and (b) precursor ion mass spectrum of m/z 129 from <i>Brucella neotomae</i> .....	42
Figure 1.27.	A proposed structure for biomarker ion 129.....	43
Figure 1.28.	Pyrolysis (a) product ion mass spectrum of m/z 131 and (b) precursor ion mass spectrum of m/z 131 from <i>Brucella neotomae</i> .....	44
Figure 1.29.	A proposed structure for biomarker ion 131.....	45
Figure 1.30.	A proposed fragmentation pathway with tryptophan origins for biomarker ion 131.....	47
Figure 2.1.	A schematic of an analyzer from the JEOL MStation JMS-700T.....	58
Figure 2.2.	HR-DEI (R=10,000) mass spectrum of m/z 67 from <i>Brucella neotomae</i> .....	61
Figure 2.3.	HR-DEI (R=30,000) mass spectrum of m/z 76 from <i>Brucella neotomae</i> .....	62
Figure 2.4.	HR-DEI (R=10,000) mass spectrum of m/z 79 from <i>Brucella neotomae</i> .....	63
Figure 2.5.	HR-DEI (R=10,000) mass spectrum of m/z 89 from <i>Brucella neotomae</i> .....	64
Figure 2.6.	HR-DEI (R=10,000) mass spectrum of m/z 93 from <i>Brucella neotomae</i> .....	65
Figure 2.7.	HR-DEI (R=10,000) mass spectrum of m/z 95 from <i>Brucella neotomae</i> .....	66
Figure 2.8.	HR-DEI (R=10,000) mass spectrum of m/z 103 from <i>Brucella neotomae</i> .....	67
Figure 2.9.	HR-DEI (R=10,000) mass spectrum of m/z 105 from <i>Brucella neotomae</i> .....	68
Figure 2.10.	HR-DEI (R=30,000) mass spectrum of m/z 115 from <i>Brucella neotomae</i> .....	69
Figure 2.11.	HR-DEI (R=10,000) mass spectrum of m/z 117 from <i>Brucella neotomae</i> .....	70
Figure 2.12.	HR-DEI (R=10,000) mass spectrum of m/z 129 from <i>Brucella neotomae</i> .....	71
Figure 2.13.	HR-DEI (R=30,000) mass spectrum of m/z 131 from <i>Brucella neotomae</i> .....	72
Figure 2.14.	HR-DEI product ion mass spectrum of m/z 67.0547 from <i>Brucella neotomae</i> .....	76

Figure 2.15.	DEI precursor ion mass spectrum of m/z 67 from <i>Brucella neotomae</i> .....	77
Figure 2.16.	Proposed fragmentation pathway of m/z 67.0547 and m/z 95.0861.....	79
Figure 2.17.	HR-DEI (R=10,000) mass spectra of (a) m/z 132, (b) m/z 137 and (c) m/z 149 from muramic acid.....	80
Figure 2.18.	Proposed fragmentation pathway of m/z 67.0421 and m/z 95.0369.....	81
Figure 2.19.	Proposed fragmentation pathway of m/z 67.0296 and m/z 95.0245.....	83
Figure 2.20.	Proposed fragmentation pathway of m/z 67.0184 and m/z 95.0137.....	84
Figure 2.21.	Proposed fragmentation pathway of m/z 76.0150, m/z 103.0411 and m/z 89.0234.....	85
Figure 2.22.	Proposed fragmentation pathway of m/z 79.0296 and m/z 95.0245.....	87
Figure 2.23.	Proposed fragmentation pathway of m/z 79.0178.....	88
Figure 2.24.	Proposed fragmentation pathway of m/z 93.0578.....	90
Figure 2.25.	HR-DEI (R=10,000) mass spectra of (a) m/z 143 and (b) m/z 185 and m/z 186 from N-acetylglucosamine (NAG)....	94
Figure 2.26.	Proposed fragmentation pathway of m/z 76.0313, m/z 79.0417, m/z 89.0392, m/z 103.0543, m/z 115.0533, m/z 117.0567 and m/z 131.0730.....	98
Figure 2.27.	Proposed fragmentation pathway of m/z 79.0545.....	100
Figure 2.28.	Proposed fragmentation pathway of m/z 76.0313 and m/z 103.0543.....	103
Figure 2.29.	Proposed fragmentation pathway of m/z 131.0495.....	106
Figure 2.30.	Proposed fragmentation pathway of m/z 67.0421.....	110
Figure 2.31.	Proposed fragmentation pathway of m/z 79.0545.....	112
Figure 2.32.	Proposed fragmentation pathway of m/z 93.0702.....	113
Figure 2.33.	Proposed fragmentation pathway of m/z 95.0861.....	115
Figure 2.34.	Proposed fragmentation pathway of m/z 105.0704 and m/z 105.0332.....	116
Figure 2.35.	Proposed fragmentation pathway of m/z 129.0913.....	118
Figure 2.36.	Proposed fragmentation pathway of m/z 129.0558.....	119
Figure 2.37.	HR-DEI (R=10,000) mass spectra of m/z 95 from (a) <i>Brucella neotomae</i> and (b) <i>Bacillus anthracis</i> .....	120
Figure 3.1.	Pyrolysis mass spectra of the standards (a) CMP, (b) TMP, (c) AMP and (d) GMP.....	131

Figure 3.2.	Pyrolysis mass spectra showing the <i>in situ</i> methylated standards of (a) CMP + 0.3M TMAH, (b) TMP + 0.03M TMAH, (c) AMP + 0.03M TMAH and (d) GMP + 0.05M TMAH.....	132
Figure 3.3.	DNA bases and their methyl derivatives.....	134
Figure 3.4.	Pyrolysis product-ion spectra of (a) m/z 153 from <i>in situ</i> methylated CMP with 0.01M TMAH, (b) m/z 154 from TMP with 0.01M TMAH, (c) m/z 177 from AMP with 0.01M TMAH and (d) m/z 193 from GMP with 0.01M TMAH.....	136
Figure 3.5.	Pyrolysis mass spectra of the oligonucleotide (a) without and (b) with <i>in situ</i> methylation using 0.03M TMAH.....	138
Figure 3.6.	Pyrolysis mass spectra of calf thymus DNA (a) without and (b) with <i>in situ</i> methylation using 0.03M TMAH.....	140
Figure 3.7.	Pyrolysis product-ion spectra from <i>in situ</i> methylated calf thymus DNA with 0.1M TMAH of (a) m/z 153, (b) m/z 154, (c) m/z 177 and (d) m/z 193.....	141
Figure 3.8.	Pyrolysis mass spectra of <i>B. neotomae</i> whole cells (a) without and (b) with <i>in situ</i> methylation using 0.05M TMAH.....	142
Figure 3.9.	Pyrolysis product-ion spectra from <i>in situ</i> methylated <i>B. neotomae</i> whole cells with 0.05M TMAH of (a) m/z 153 for cytosine, (b) m/z 154 for thymine, (c) m/z 177 for adenine and (d) m/z 193 for guanine.....	144
Figure 3.10.	HR-DEI (R=10,000) mass spectrum of m/z 154 from <i>in situ</i> methylated <i>Brucella neotomae</i> .....	146
Figure 4.1.	Instrument diagram of the field-portable mass spectrometer (CMBS).....	158
Figure 4.2.	Standard plot for quantification of nitrogen bases in free nucleotide solutions.....	162
Figure 4.3.	Standard plot for quantification of nitrogen bases in free nucleotide solutions ( <i>k</i> values included in the % relative intensity calculation).....	165
Figure 4.4.	Py-mass spectrum of a 35% G+C standard solution with <i>in situ</i> methylation using 0.1M TMAH.....	166
Figure 4.5.	Standard plot for quantification of nitrogen bases in pure DNA	170
Figure 4.6.	DEI mass spectrum of salmon sperm DNA with <i>in situ</i> methylation using 0.1M TMAH.....	172
Figure 4.7.	Standard plot for quantification of nitrogen bases in pure DNA ( <i>k</i> values included in the % relative intensity calculation).....	174
Figure 4.8.	Py-mass spectrum of <i>B. licheniformis</i> with <i>in situ</i> methylation using 1.0M TMAH.....	176
Figure 4.9.	Standard plot for quantification of nitrogen bases in whole bacterial cells.....	177

Figure 4.10.	Standard plot for quantification of nitrogen bases in whole bacterial cells ( <i>k</i> values included in the % relative intensity calculation).....	183
Figure 4.11.	HR-DEI ( <i>R</i> =10,000) mass spectra of (a) <i>m/z</i> 154, (b) <i>m/z</i> 165 and (c) <i>m/z</i> 177 from <i>Serratia marcescens</i> .....	186
Figure 4.12.	DCI mass spectrum of <i>S. marcescens</i> with <i>in situ</i> methylation using 0.5M TMAH.....	188
Figure 4.13.	Standard plot for quantification of nitrogen bases in whole bacterial cells (chemical ionization methodology).....	189

## LIST OF TABLES

Table 1.1.	Major product and precursor ions observed in the pyrolysis mass spectra of <i>Brucella neotomae</i> for each of the biomarker ions.....	11
Table 1.2.	Proposed biochemical origins of the selected biomarker ions...	48
Table 2.1.	Standards used to represent the cellular content of proteins.....	53
Table 2.2.	Standards used to represent the cellular content of nucleic acids and carbohydrates.....	74
Table 2.3.	Biomarker ions with proposed carbohydrate and/or nucleic acid origins.....	75
Table 2.4.	Biomarker ions with proposed protein origins.....	96
Table 2.5.	Standards used to represent the cellular content of lipids.....	107
Table 2.6.	Biomarker ions with proposed lipid origins.....	108
Table 2.7.	Proposed biochemical origins of the selected biomarker ions..	122
Table 3.1.	M/z values of the methylated nitrogen base peaks.....	135
Table 3.2.	Nucleic acid biomarker ions for the whole cell, <i>B. neotomae</i> ...	143
Table 4.1.	Free nucleotide solutions used for the construction of a standard curve for calculating % composition of nitrogen bases.....	153
Table 4.2.	Bacterial samples received from the Armed Forces Institute of Pathology.....	155
Table 4.3.	Bacterial samples used for the construction of standard curves for calculating % composition of nitrogen bases in DNA of whole cells.....	156
Table 4.4.	M/z values of the methylated nitrogen bases used as diagnostic peaks for the calculation of percent relative intensity.....	159
Table 4.5.	<i>k</i> values calculated for each of the diagnostic peaks.....	163
Table 4.6.	Comparison of mass spectral quantitation method for mol % G+C in standard solutions with known values.....	168
Table 4.7.	Pure DNA standards used for the construction of a standard curve for calculating % composition of nitrogen bases.....	169
Table 4.8.	Comparison of mass spectral quantitation method for mol % G+C in pure DNA with known values.....	173
Table 4.9.	Comparison of mass spectral quantitation method for mol % G+C in whole cell bacteria with known values.....	178
Table 4.10.	Individual species assessment of mol % G+C determined by mass spectral method.....	180
Table 4.11.	Comparison of mass spectral quantitation method for mol % G+C in whole cell bacteria with known values.....	182

Table 4.12.	Comparison of mass spectral quantitation method (employing <i>k</i> values) for mol % G+C in whole cell bacteria with known values.....	185
Table 4.13.	Comparison of mass spectral quantitation method (chemical ionization) for mol % G+C in whole cell bacteria with known values.....	190

## ACKNOWLEDGEMENTS

Looks like we made it Diddle! I could not have done it without you. Words can not express and thank you seems so small in comparison to what you did for me, but *thank you* for supporting me the entire way. I love you.

I need also to thank my family. You have been my cornerstone; grounding me in what is real. Thanks mom and dad for instructing me in the things that matter.

Thanks to Dr. Voorhees, Franco, Petra, Mike, Alan, Angelo, Curt and Ahmad. You have all made this journey memorable, and my remembrances of you will be fond ones.

## PREFACE

The diverse nature and quantity of research in the bioanalytical field demonstrates the importance associated with this work. New mass spectral ionization techniques, matrix assisted laser desorption ionization (MALDI) and electrospray ionization (ESI), have allowed for the analysis of large biomolecules such as lipids, proteins and nucleic acids. In addition, whole cells have been identified and detected by MALDI and ESI mass spectrometry (1-4). As early as 1975, Anhalt and Fenselau (5) employed pyrolysis-mass spectrometry (Py-MS) for the analysis of bacterial phospholipids and ubiquinones. Pyrolysis allows for the volatilization of high molecular weight and/or polar compounds. Several others have since used Py-MS for the characterization of microorganisms (6-9). Biomarkers (whole bacterial components or fragments characteristic of bacteria) in the mass spectrum are used for the identification of the microorganisms. The ability to rapidly detect and identify microorganisms is accomplished by rapidly identifying and detecting these biomarkers.

As the threat of biological weapons continues to escalate, a real need exists for the rapid detection and identification of these agents. The U.S. Army has selected biomarker detection by pyrolysis mass spectrometry (Py-MS) as the basis of one of their biological detectors. A contract was awarded to Teledyne CME and Bruker Franzen to build an instrument containing a front end consisting of a virtual impactor for size sorting of aerosols and a small tube pyrolyzer (10) connected to an ion trap mass spectrometer. The Bruker Franzen instrument utilizes a silicon membrane in the inlet as an enrichment device. Selectivity is achieved by the differential permeability of the membrane for various compounds. For example, the membrane is permeable to compounds that are soluble in or adsorbed by the membrane. The membrane excludes inorganic materials in the buffer gas (air). As a result, the membrane preferentially allows passage of the organic material into the mass spectrometer with an enrichment factor of approximately 100 (11). Scanning sequences were developed to allow the trap to operate in tandem

mode (MS/MS) (12). A more detailed description of the CBMS instrument will be given in Chapter 4. An aim of the Colorado School of Mines (CSM) research effort has been focused on the development of the membrane-inlet quadrupole ion trap mass spectrometer (termed CBMS for chemical/biological mass spectrometer) with pyrolysis as the bacterial introduction method. This type of instrumentation lends itself to portability, as the instrument samples directly from air, requires low power and can perform analyses in a complex background (12). Along with the development of the instrumentation, much effort has been applied towards the development of bacterial analytical methods and a biomarker database.

The work presented in the following pages represents research into the development of methodology for the analysis of microorganisms by Py-MS, specifically the analysis of nucleic acids. In addition, the work makes a contribution to identifying and classifying biomarker ions in the Py-MS spectra of whole bacterial cells.

Chapter 1 describes a detailed study performed on whole bacterial cells using pyrolysis tandem mass spectrometry to determine possible pyrolysis mechanisms for the formation of biomarker ions. The biochemical origins for most of these ions were determined. Yet, identification of the chemical species that gave rise to each biomarker ion was extremely difficult due to the low resolution nature of the analysis and the large number of common peaks.

Chapter 2 is concerned with the further clarification of the biomarker ions. Since most nominal mass peaks are a consortium of ions, high resolution mass spectrometry (HR-MS) was used to identify these ions. HR-MS provides the capability of identifying the composition of a low resolution mass spectral peak. The knowledge that each nominal mass peak in a whole cell microorganism results from one or more biochemical class was realized by employing HR-MS. Chapter 2 examines this phenomenon.

Chapter 3 is a detailed study performed on free nucleotides, pure DNA and whole bacterial cells using a methylating agent, tetramethylammonium hydroxide (TMAH). This reagent is used for hydrolysis and to increase volatility. Its effect on nitrogen bases

is to enact varying degrees of methylation, when multiple methylation sites are present and increase volatility. Furthermore, the concentration of TMAH was found to have an effect on the methylation process.

Chapter 4 provides an account of the analysis of free nucleotide solutions, pure DNA and whole bacterial cells using Py-MS for the quantification of nitrogen bases. A direct correlation exists between the percent relative intensity of diagnostic peaks in the mass spectrum and the known percent composition of each nitrogen base in the sample. The method of least squares was used to generate calibration curves for each class of samples (nucleotide solutions, pure DNA and whole bacterial cells). Several mass spectrometers were used to verify the legitimacy of this technique.

It is believed that the information contained within these chapters will strengthen the foundation of biomarker classification for rapidly detecting and identifying microorganisms. In addition, the utility of pyrolysis mass spectrometry for the quantitation of nitrogen bases is demonstrated.

**REFERENCES**

- (1) Cain, T.C.; Lubman, D.M.; Weber, W.J. Jr. *Rapid Comm. Mass Spectrom.* **1994**, *8*, 1026.
- (2) Black, G.E.; Fox, A.; Fox, K.; Snyder, A.P.; Smith, P.B.W. *Anal. Chem.* **1994**, *66*, 4171.
- (3) Krishnamurthy, T.; Ross, P.L.; Rajamani, U. *Rapid Comm. Mass Spectrom.* **1996**, *10*, 1992.
- (4) Holland, R.D.; Wilkes, J.G.; Raffi, F.; Sutherland, J.B.; Persons, C.C.; Voorhees, K.J.; Lay, J.O. Jr. *Rapid Comm. Mass Spectrom.* **1996**, *10*, 1227.
- (5) Anhalt, J.P.; Fenselau, C. *Anal. Chem.* **1975**, *47*, 219.
- (6) DeLuca, S.; Sarver, E.W.; Harrington, P.D.B.; Voorhees, K.J. *Anal. Chem.* **1990**, *62*, 1465.
- (7) Voorhees, K.J.; DeLuca, S.; Noguerola, A. *J. Anal. Appl. Pyrolysis* **1992**, *24*, 1.
- (8) Snyder, A.P.; Smith, P.B.W.; Dworzanski, J.P.; Meuzelaar, H.L.C. *Pyrolysis-gas chromatography-mass spectrometry. Detection of biological warfare agents*; American Chemical Society: Washington, 1994.
- (9) Smith, P.B.; Snyder, A.P. *J. Anal. Appl. Pyrolysis* **1993**, *24*, 199.
- (10) DeLuca, S.J.; Voorhees, K.J. *J. Anal. Appl. Pyrolysis* **1993**, *24*, 211.
- (11) Throck Watson, J. *Introduction to Mass Spectrometry*; Lippincott-Raven: Philadelphia, 1997.
- (12) Voorhees, K.J.; Basile, F.; Beverly, M.B.; Abbas-Hawks, C.; Hendricker, A.; Cody, R.B.; Hadfield, T.L. *J. Anal. Appl. Pyrolysis* **1997**, *40,41*, 111.

## Chapter 1

# USE OF PYROLYSIS TANDEM MASS SPECTROMETRY TO STUDY BIOMARKER PYROLYSIS MECHANISMS IN WHOLE BACTERIAL CELLS

### ABSTRACT

A detailed study has been performed on the whole bacterial cells of *Brucella neotomae* using pyrolysis tandem mass spectrometry. The purpose of the study was to determine possible pyrolysis mechanisms for the formation of the observed biomarker ions when pyrolyzing whole cell microorganisms. The results indicate that biomarkers of interest are a collection of fragments from proteins, nucleic acids, carbohydrates and lipids. The pooling of previous analysis on pure cellular components and pure standards with the data collected from the whole bacterial cells facilitates the goal of developing rapid chemotaxonomic assays for microorganism identification. The fragmentation pathways of several important biomarkers are presented.

### INTRODUCTION

As stated in the preface, the U.S. Army has selected biomarker detection by pyrolysis mass spectrometry (Py-MS) as the basis of one of their biological detectors. Upon pyrolysis (*ca* 500<sup>0</sup>C), a biological sample produces an array of pyrolytic and ion chemistry products (biomarkers) resulting in complex mass spectra. The identification of biomarker peaks, therefore, becomes extremely difficult. However, it is of fundamental interest to define the site of origin of pyrolysis products in the macromolecular structure

of a microorganism. The Py-MS spectra of various biological samples (*i.e.* whole cells) were studied to determine specific molecular component peaks termed biomarkers. The biomarkers, at  $m/z$  67, 81, 89, 91, 95, 102, 103, 115, 117, 128, 129 and 131, could be used for the differentiation of microorganisms based upon taxonomic significance. The selection of these ions was based on multivariate statistical analysis (Fisher statistical-weight evaluation) of a large quantity of data with some knowledge of the biomarkers (1, 2). Fisher weights provide a measure of the discriminative ability of a variable in terms of category separation. Fisher weights were calculated to determine which mass spectral features were most (and least) useful for classifying a training set for bacterial separation/identification.

The ability to differentiate between targeted microorganisms and environmental background material is critical to the success of the program. The rationale for the application of a mass spectrometer based biological detector to bacterial identification has been to use a series of product- and precursor-mass spectral scans of the biomarkers. These scans serve to differentiate the various background and biological samples. The need to identify the chemical species and the biochemical precursors for each selected biomarker ion becomes apparent in developing a rapid chemotaxonomic (chemically based) microorganism identification system. That is, the signals for either background or biological sample must be distinguishable. Therefore, a detailed study has been performed on the whole bacterial cells of *Brucella neotomae* using pyrolysis tandem mass spectrometry. The goal of this project was to determine a possible chemical species and biochemical precursor for each of the above-mentioned biomarker ions when pyrolyzing whole cell microorganisms. This type of in-depth investigation using model compounds, product- and precursor-ion scans will provide a database to interpret the information generated in ongoing tests. The proposed structure and fragmentation pathways of these biomarker ions are presented.

## EXPERIMENTAL

### *Bacterial Sample*

Cultures of *Brucella neotomae* (whole cell microorganism), obtained from the Armed Forces Institute of Pathology (Washington, D.C.) were grown at 37<sup>0</sup>C with shaking (225 rpm) in Brucella broth for four days. Cultures were harvested by high-speed centrifugation, washed twice with saline solution and resuspended in distilled water. Cells were gamma killed in a cobalt radiation source. The samples used for this work had an initial cell concentration of 1x10<sup>10</sup> CFU (colony forming units)/ml (in H<sub>2</sub>O).

### *Instrumental*

Pyrolysis mass spectra were obtained using an Extrel Model ELQ-400 triple quadrupole tandem mass spectrometer (MS/MS) fitted with a Fischer Model 0310 (1 kW) rf-generator to supply power to a Curie-point pyrolysis coil (3). Curie-point pyrolysis combined with mass spectrometry (Py-MS) is a powerful technique for producing volatile products from nonvolatile macromolecules. The technique requires the application of sample onto a ferromagnetic wire. As shown in Figure 1.1, the wire is enclosed in a glass reaction tube and then placed in an inductive coil that heats the wire to its Curie-point. At this temperature, the wire no longer absorbs energy and an equilibrium temperature is reached. As the wire is heated and held at its equilibrium temperature, pyrolysis products are formed. The pyrolysis products are then ionized and fragmented by electron ionization, separated by a quadrupole mass filter while the collision cell and third quadrupole are “inactive” (RF only), and detected by an electron multiplier (4). All positive electron ionization (EI+) spectra were obtained at 70 eV ionization energy with Curie-point pyrolysis performed at 510<sup>0</sup>C. The transfer line from the direct probe inlet was maintained at 170<sup>0</sup>C and the ion source temperature at 225<sup>0</sup>C. Full scan spectra were collected with a scan rate of 750 u/s over a range of m/z 60-300, unless otherwise indicated.

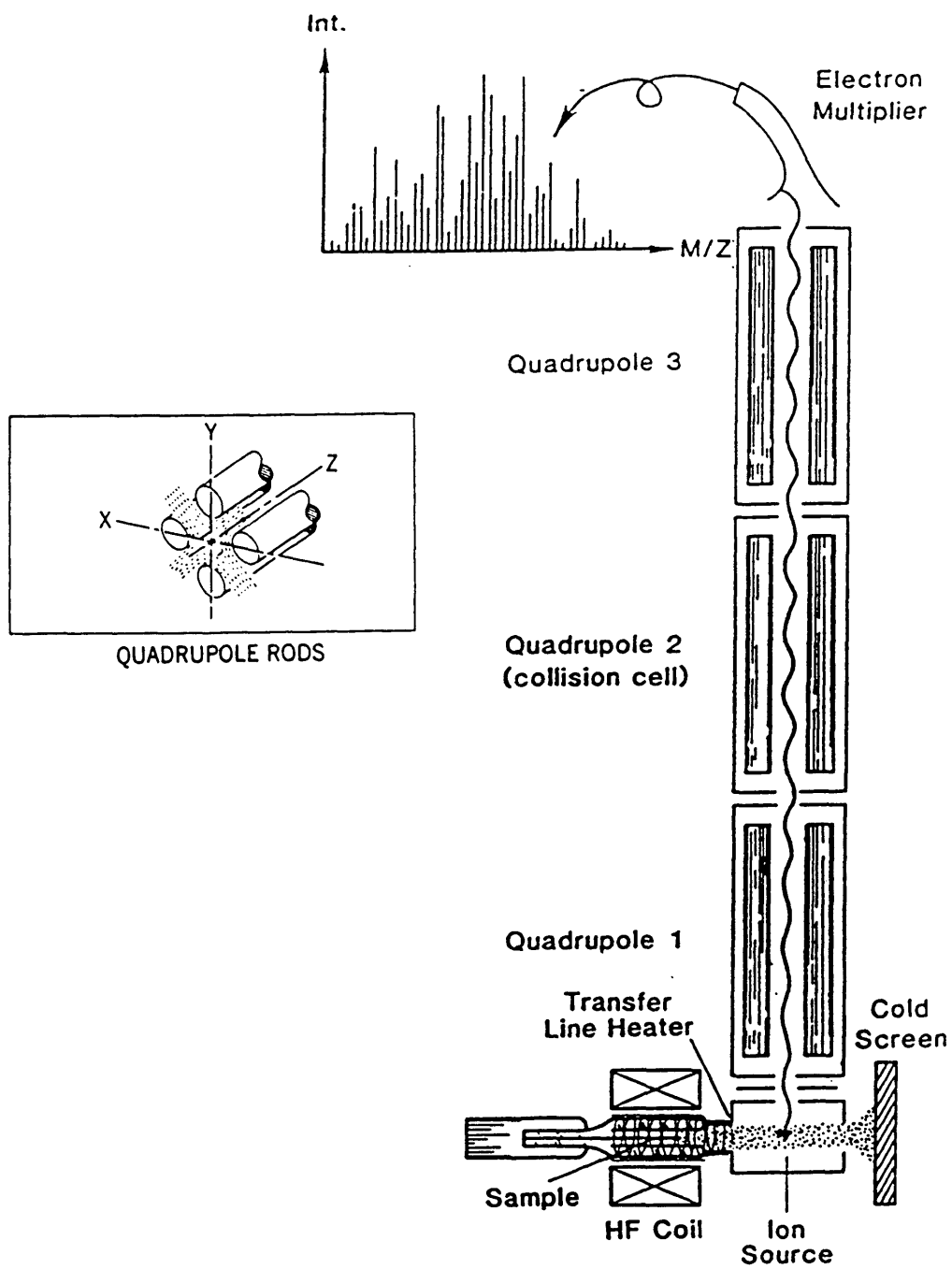


Figure 1.1. Instrument diagram of the triple quadrupole mass spectrometer modified for a Curie-point pyrolyzer probe (4).

Product- and precursor-ion spectra were obtained with argon as the collision gas in quadrupole 2 (Q2) at a pressure of approximately 0.5-1.0 mtorr and a collision energy ( $V_{lab}$ ) of 5.1 eV. Triple quadrupole tandem mass spectrometry (MS/MS) is considerably more powerful as a characterization, identification and structure elucidation tool for biochemical and biological substances than single quadrupole mass spectrometry. Tandem mass spectrometry produces additional information on ionized compounds. Precursor ions are realized by scanning the first mass filter and fixing the third quadrupole (Q3) on the ion mass for which precursors are to be found. Product ions are formed by permitting only ions of a given  $m/z$  to pass through quadrupole one (Q1), fragmenting the ions in the collision cell (Q2) and scanning the resulting fragments in Q3.

#### *Sample preparation*

Cells for Curie-point pyrolysis were prepared by placing 10  $\mu$ L of suspension directly onto a rotating wire (5) followed by solvent evaporation. The rotating wire ensured even coating upon the Curie-point wires. After introduction into the mass spectrometer, the glass sample holder was preheated to 250<sup>0</sup>C before pyrolysis. Pyrolysis was begun five seconds after insertion using the direct probe and was held for 9.9 seconds with a rise time of 100 msec.

## **RESULTS AND DISCUSSION**

The major classes of substances common in living systems are lipids, proteins, nucleic acids and carbohydrates. Assuming this statement to be true, the majority of the biomarker ions, previously listed, will most likely fall into one or more of these classes. By analyzing the selected biomarker ions in the whole cell microorganism by both precursor- and product-ion scan modes, the goal is to propose a possible source and

composition of each selected biomarker ion in addition to presenting a fragmentation pathway. This task is the subject of the present investigation. The results from pyrolysis-low resolution (LR) product- and precursor-ion scans of *B. neotomae* for the biomarker ions are shown in Table 1.1. These ions will be discussed in detail.

### **Biomarker m/z 67**

Fragmentation observed for m/z 67 in the bacterium using a LR-product-ion scan produced product ions at m/z 41 and 39, Figure 1.2a. The origin of the m/z 67 ion of the bacterium was examined using a precursor-ion scan, Figure 1.2b. Major precursor ions included m/z 82, 95 and 109. With the aid of the precursor- and product-ion scans and existing literature, three structures for ion 67 were proposed and are shown in Figure 1.3. Structure A (Figure 1.3) is an amino acid pyrolysis product cited by Merritt and Robertson (6) and Ratcliff *et. al* (7). Although there is no agreed upon list of pyrolysis products of amino acids, the product cited by Merritt, Robertson and Ratcliff is very commonly named. Structure A has been shown to fragment to m/z 41.

The formula given for B (Figure 1.3) was identified as a possible fragment of the nitrogen base cytosine (m/z 111) (8). Cytosine fragments to m/z 95 (loss of NH<sub>2</sub>) followed by the loss of -HCN and -H to produce m/z 67. Ion 95 was observed in the precursor spectrum of m/z 67 in *B. neotomae*. In addition, m/z 95 of the bacterium fragments to m/z 67. A proposed fragmentation pathway based on the precursor- and product-ion scans is given in Figure 1.4. The double-ended arrows confirm the ion in the precursor- and product-ion scans. The single-ended arrows confirm the ion in the precursor- or product-ion scan.

Another source of m/z 67 may be structure C (Figure 1.3). This ion may be a fragment of deprotonated furfural (m/z 95). Furfural is a furan derivative formed by rapid pyrolysis of carbohydrates (9). Furfural readily fragments to m/z 39; an ion observed in the product spectrum of m/z 67 in *B. neotomae*.

Table 1.1. Major product and precursor ions observed in the pyrolysis mass spectra of *Brucella neotomae* for each of the biomarkers.

Biomarker Ion	Product Ions	Precursor Ions
67	41, 39	82, 95, 109
81	67, 53, 41	96, 98, 108, 109, 110, 116, 123, 135, 195, 215, 231
89	63, 39	116, 117
91	65	107, 118, 119, 120, 133, 147
95	81, 68, 67, 55, 41	110, 112, 123, 124, 137, 138, 151, 152, 165, 166
102	77, 76, 31	129, 130
103	77, 76, 51	120, 130
115	97, 87, 70	143, 157, 169, 185, 195, 209, 223, 237
117	99, 90, 62, 37	132, 143, 144, 145, 153, 186, 200
128	113, 101, 85, 84, 77, 72, 57	145, 146, 155, 156
129	102, 87, 84, 73, 57, 55	146, 147, 156, 157, 171, 185, 197, 227, 256
131	117, 104, 103, 91, 86, 77	146, 148, 158, 159, 174, 175, 186, 187, 200, 201, 216, 230, 243

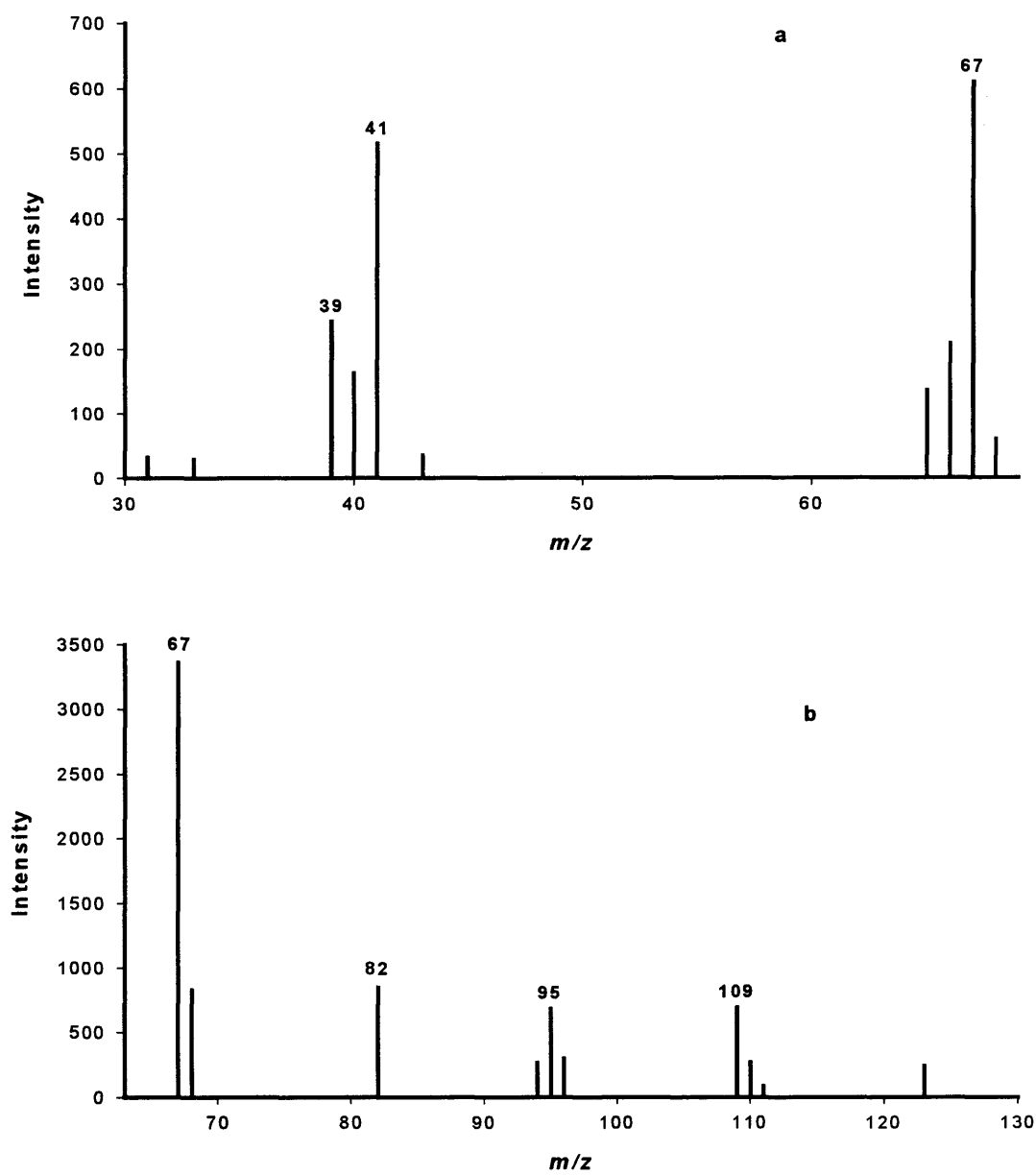


Figure 1.2. Pyrolysis (a) product ion mass spectrum of  $m/z$  67 and (b) precursor ion mass spectrum of  $m/z$  67 from *Brucella neotomae*.

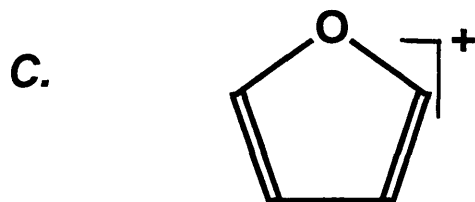
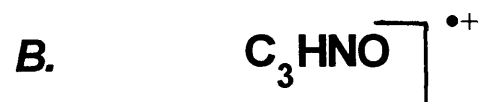


Figure 1.3. Proposed structures and formulas for biomarker ion 67.

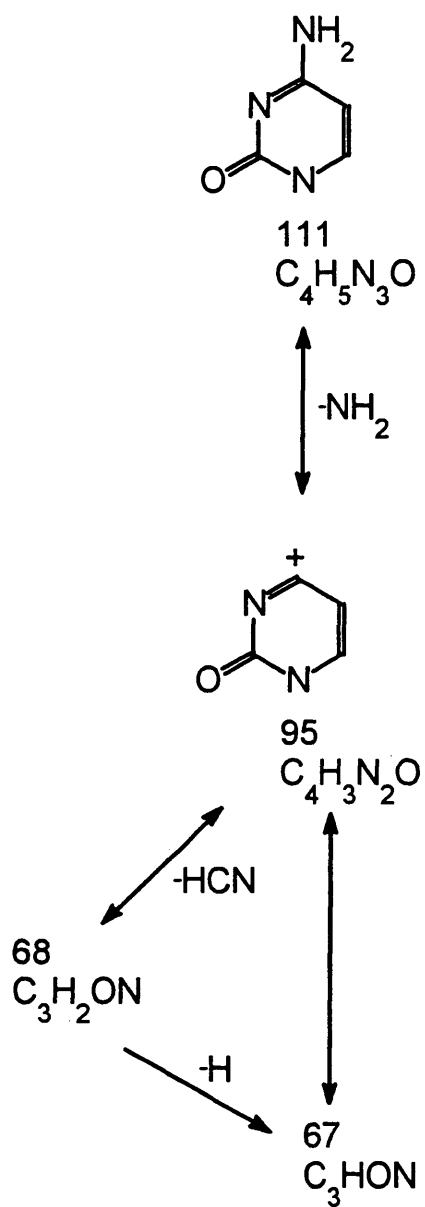


Figure 1.4. A proposed fragmentation pathway with cytosine origins for biomarker ions 67 and 95.

All of the structures/formulas shown in Figure 1.3 are possible sources of biomarker  $m/z$  67. They include a protein, nucleic acid and carbohydrate source. Yet, no exact assignment of origins can be made due to the low resolution character of the analysis and the shared product and precursor ions.

### **Biomarker $m/z$ 81**

The product spectrum (Figure 1.5a) of  $m/z$  81 in the bacterial sample shows fragmentation to  $m/z$  67, 53 and 41 with  $m/z$  53 being the most intense. The precursor ions of  $m/z$  81 in *B. neotomae* were found to be  $m/z$  96, 98, 108, 109, 110, 116, 123, 135, 195, 215 and 231 as shown in Figure 1.5b. Two possible structures/formulas for  $m/z$  81 were proposed, Figure 1.6. The formula given for A (Figure 1.6) is a possible fragment of the nitrogen base adenine ( $m/z$  135) (10). Adenine fragments to  $m/z$  108 (loss of –HCN) which further fragments to  $m/z$  81 and  $m/z$  53 (10). Additionally,  $m/z$  215 has been identified as adenine attached to a sugar moiety (11). Ions 215, 135, 108 and 53 are all associated with adenine and have been observed in the precursor- and product-ion scans of  $m/z$  81 in *B. neotomae*. Furthermore,  $m/z$  135 and 215 in the whole cell microorganism fragment to  $m/z$  108 and 81. Similarly, the product spectrum of  $m/z$  135 for the standard 2'-deoxyadenine indicated product ions at  $m/z$  108 and 81, confirming possible adenine origins to ion 81. A fragmentation pathway for  $m/z$  81 with adenine origins is shown in Figure 1.7.

Structure B (Figure 1.6) represents another possible form of ion 81. This ion may be a fragment of furfural ( $m/z$  96). As discussed previously, furfural is a furan derivative formed by rapid pyrolysis of carbohydrates. Methyl furfural ( $m/z$  110) may also produce structure B. Methyl furfural readily fragments to  $m/z$  81 and 53. In addition, furfuryl alcohol ( $m/z$  98) may also produce structure B. It too fragments readily to  $m/z$  81 and 53. Many of the pyrolysis products identified for sugars are common to all saccharides. In addition, sugars dehydrate and decompose to low mass ions making the assignment of higher mass origins difficult.

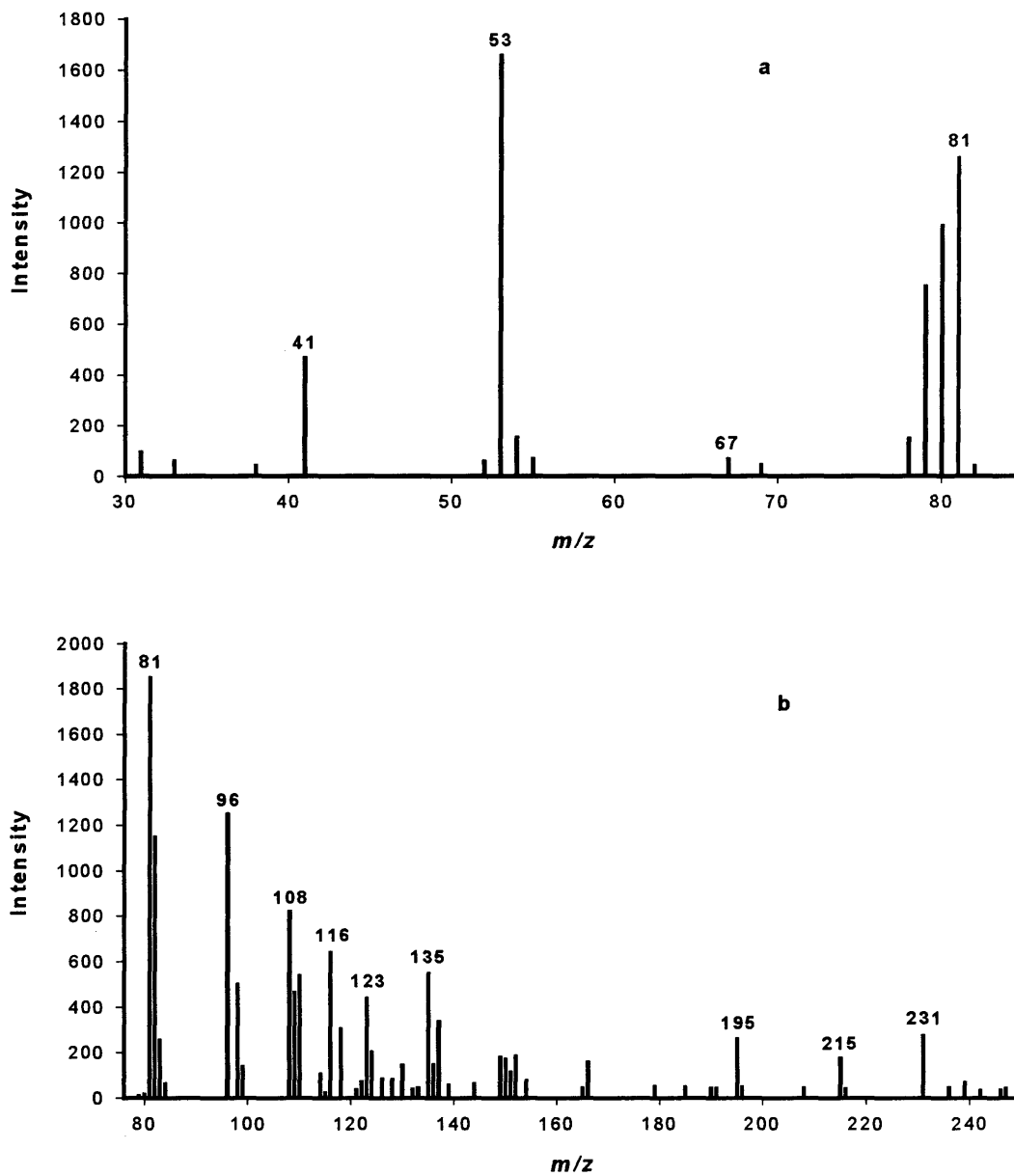


Figure 1.5. Pyrolysis (a) product ion mass spectrum of  $m/z$  81 and (b) precursor ion mass spectrum of  $m/z$  81 from *Brucella neotomae*.

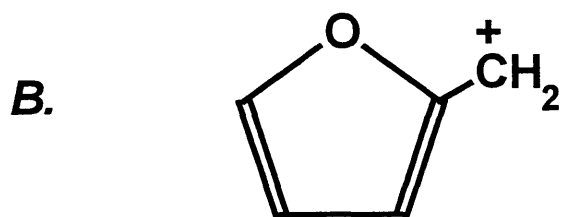
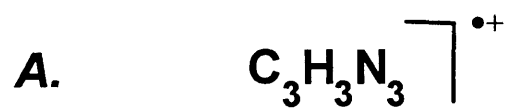


Figure 1.6. Proposed formula and structure for biomarker ion 81.

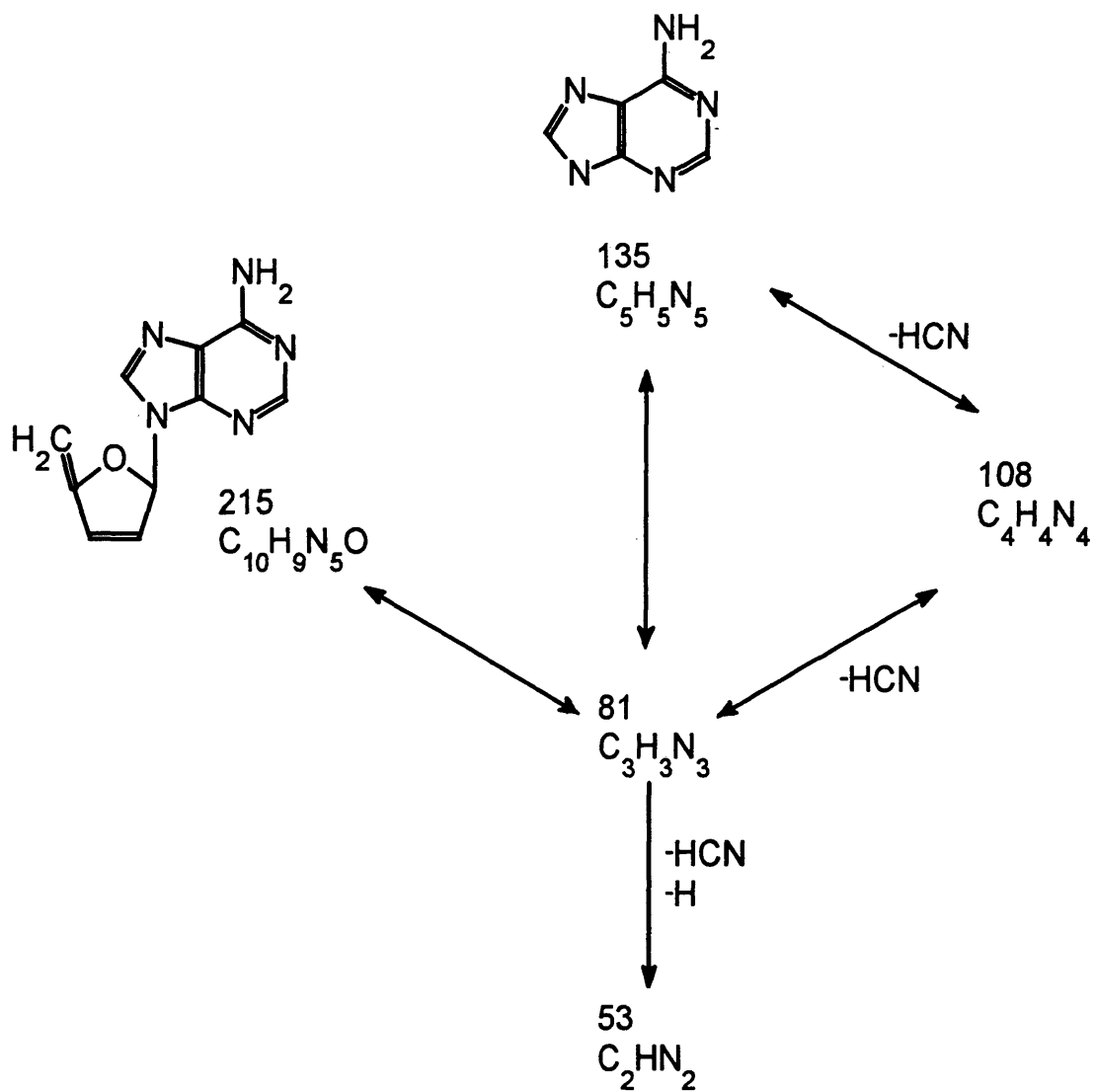


Figure 1.7. A proposed fragmentation pathway with adenine origins for biomarker ion 81.

The species shown in Figure 1.6 are possible sources of biomarker ion 81. It is hypothesized that both nucleic acids and carbohydrates give rise to this ion. However, not exact origin assignment can be made due to the low resolution character of the analysis and shared product and precursor ions.

### **Biomarker m/z 89**

Fragment ions of m/z 89 in the *B. neotomae* include m/z 63 and 39 with m/z 63 being the most intense, Figure 1.8a. Precursor ions include the peaks at m/z 116 and 117 as shown in Figure 1.8b. Ion 89 has been identified as a fragment of the amino acid tryptophan (4). Other fragment ions of tryptophan include m/z 131, 130, 117, 103, 77 and 63. Three of these ions, m/z 131, 117 and 63 are present in the precursor- and product-ion scans of m/z 89 in *B. neotomae*. As m/z 89 has very few precursor ions, the source of this ion is proposed as protein, particularly tryptophan.

### **Biomarker m/z 91**

The product-ion spectrum of m/z 91 in the whole cell microorganism indicates sole fragmentation to m/z 65. Major precursor ions include m/z 107, 118, 119, 120, 133 and 147. These scans are presented in Figure 1.9a and 1.9b. A possible structure for m/z 91 was proposed (Figure 1.10) and is a possible fragment of phenylalanine (m/z 165). Phenylalanine fragments to m/z 147 (dehydration product), 120 (decarboxylation product), 103, 91, 74 and 65 (4, 12). Ions 147, 120 and 65 are associated with phenylalanine, as described above, and have been observed in the precursor- and product-ion scans of m/z 91 in *B. neotomae*. Additionally, m/z 147 and 120 in the bacterium fragments to m/z 91. A fragmentation pathway for m/z 91 with phenylalanine origins is shown in Figure 1.11.

With the aid of the precursor-and product-ion scans and existing literature, it is proposed that proteins, principally phenylalanine, are one source that gives rise to ion 91. However, precursor ions 107, 118, 119 and 133 of m/z 91 have not been identified.

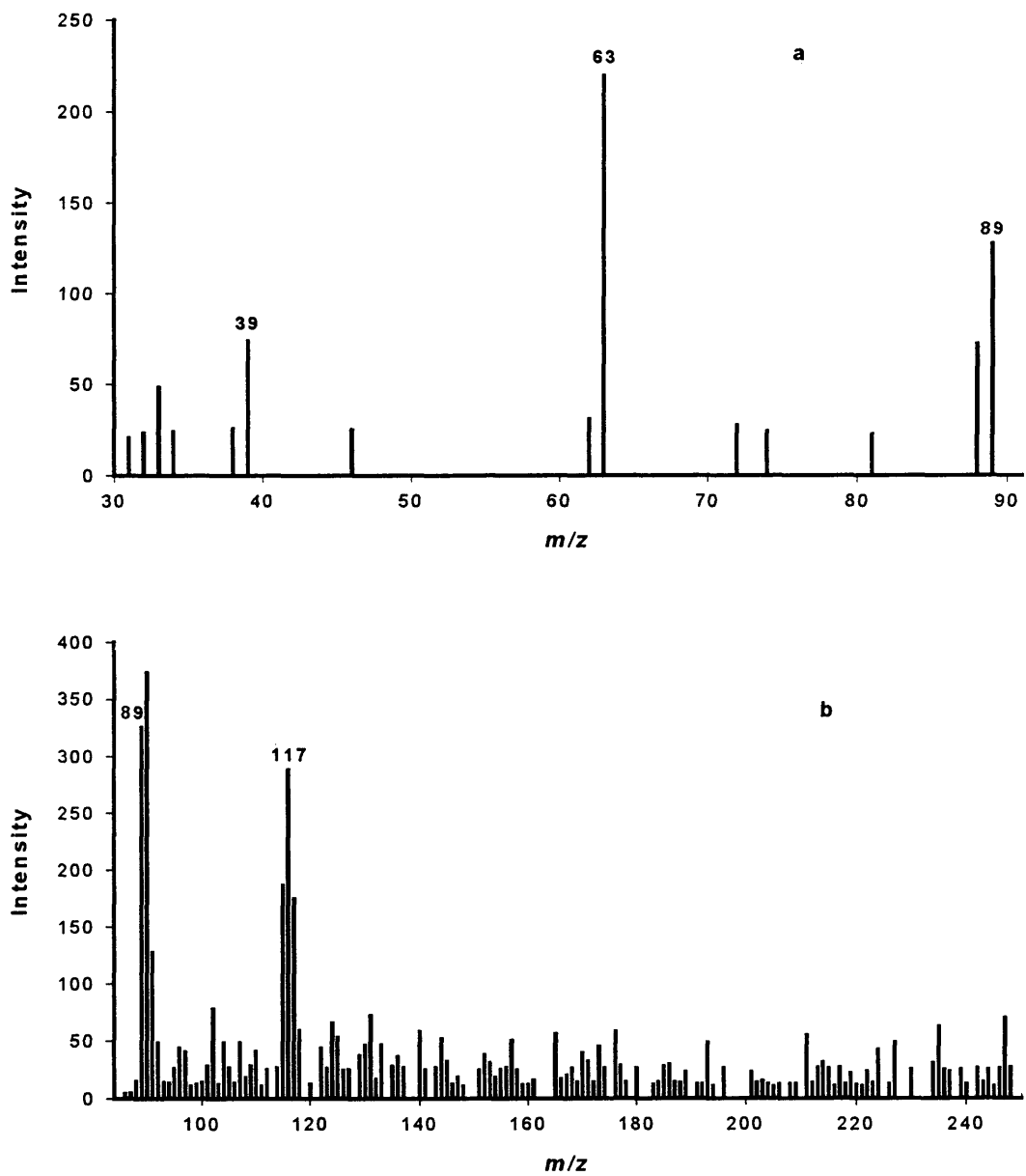


Figure 1.8. Pyrolysis (a) product ion mass spectrum of  $m/z$  89 and (b) precursor ion mass spectrum of  $m/z$  89 from *Brucella neotomae*.

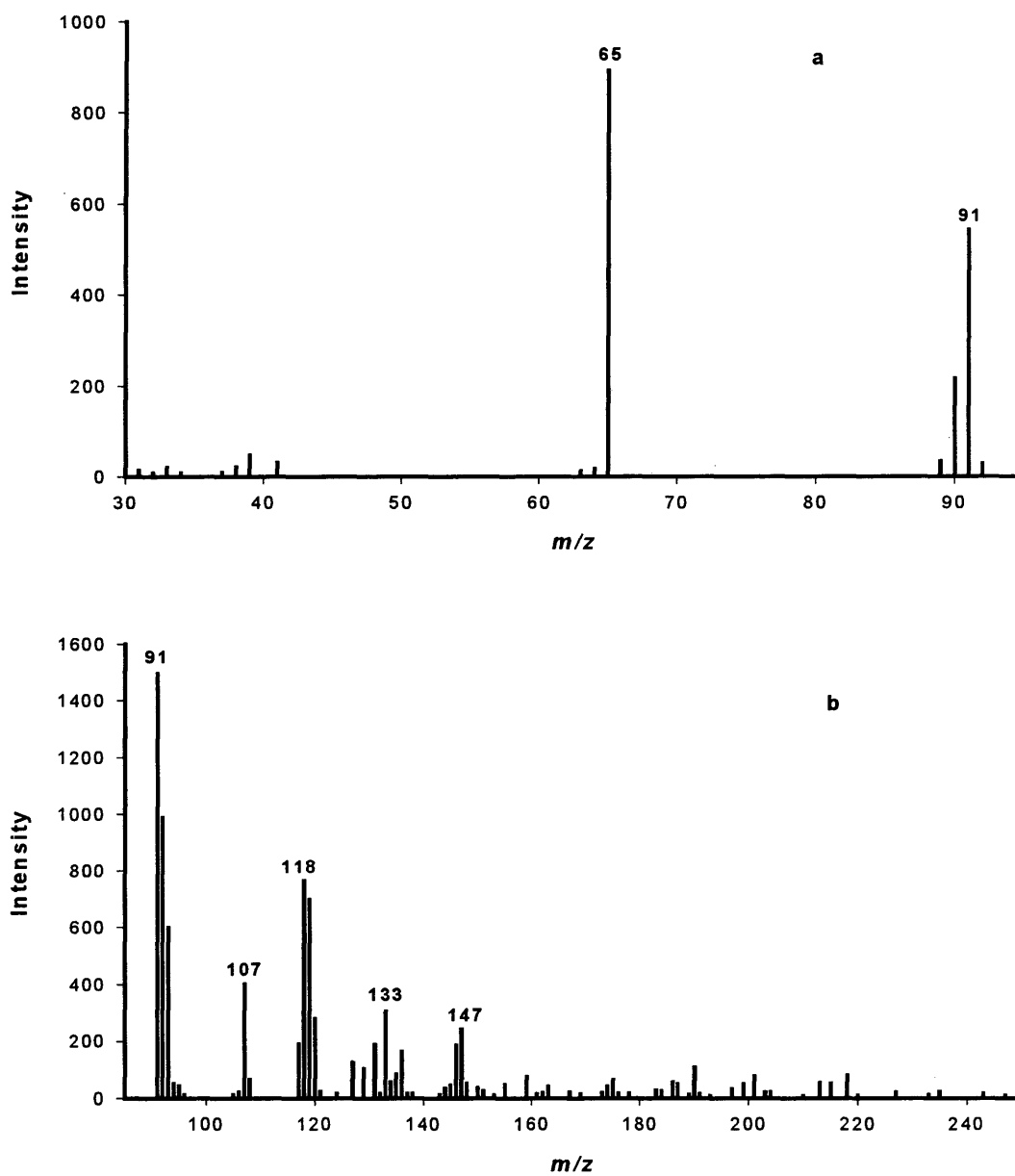


Figure 1.9. Pyrolysis (a) product ion mass spectrum of  $m/z$  91 and (b) precursor ion mass spectrum of  $m/z$  91 from *Brucella neotomae*.

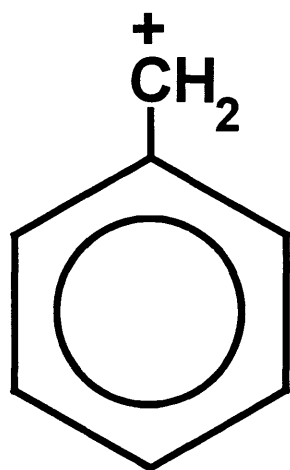


Figure 1.10. A proposed structure for biomarker ion 91.

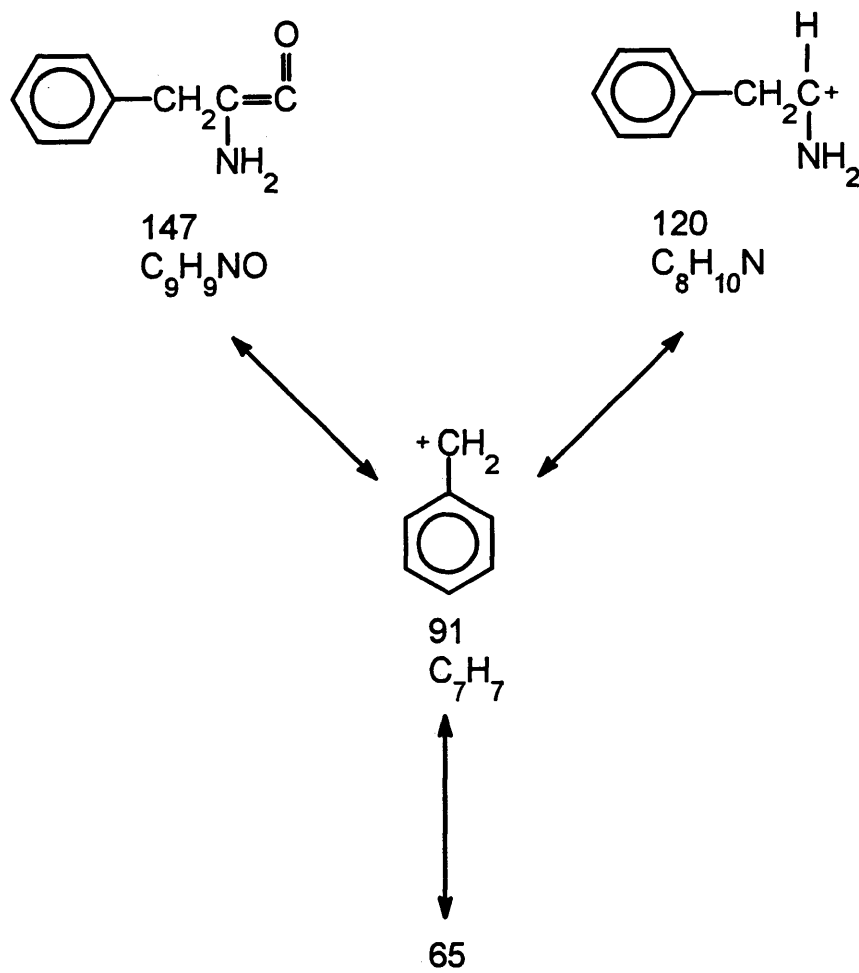


Figure 1.11. A proposed fragmentation pathway with phenylalanine origins for biomarker ion 91.

### **Biomarker m/z 95**

Fragmentation observed for m/z 95 in *B. neotomae* using a LR-product-ion scan produced product ions at m/z 81, 68, 67, 55 and 41, Figure 1.12a. Major precursor ions included m/z 110, 112, 123, 124, 137, 138, 151, 152, 165 and 166 (Figure 1.12b). Employing data obtained from the precursor- and product-ion scans with existing literature, two structures for ion 95 were proposed and are shown in Figure 1.13. Structure A (Figure 1.13) is an EI fragment of cytosine (m/z 111) as postulated by Rice *et. al* (8). Cytosine further fragments to m/z 83, 82, 68 and 67 (4). M/z 111, 68 and 67 are all associated with cytosine and have been observed in the product- and precursor-ion scans of m/z 95 in the whole cell microorganism. A fragmentation pathway for m/z 95 with cytosine origins has been proposed and was shown in Figure 1.4.

Another source of m/z 95 may be structure B, Figure 1.13. This ion may result from furfural minus a hydrogen atom ( $M^+ - H$ ). Methyl furfural (m/z 110), a furanoid product (13), may also produce structure B (Figure 1.13). The intense ion at m/z 110 in the precursor-ion scan of m/z 95 in *B. neotomae* supports this proposal. Moreover, m/z 110 in the whole cell microorganism fragments to m/z 95, 82, 81, 68 and 67 (common sugar peaks).

Both of the structures shown in Figure 1.13 are possible sources of biomarker ion 95. They include a nucleic acid and carbohydrate source. However, no exact assignment of origins can be made due to the low resolution character of the analysis and the shared product and precursor ions. In addition, higher mass precursor ions of m/z 95 have not been identified.

### **Biomarker m/z 102**

The product spectrum of m/z 102 in *B. neotomae* shows fragmentation to m/z 77, 76 and 31, Figure 1.14a. The precursor ions of m/z 102 in the whole cell microorganism were found to be m/z 129 and 130 as shown in Figure 1.14b. The fragmentation observed for m/z 102 is relatively simple. However, ion 102 has not been observed as a

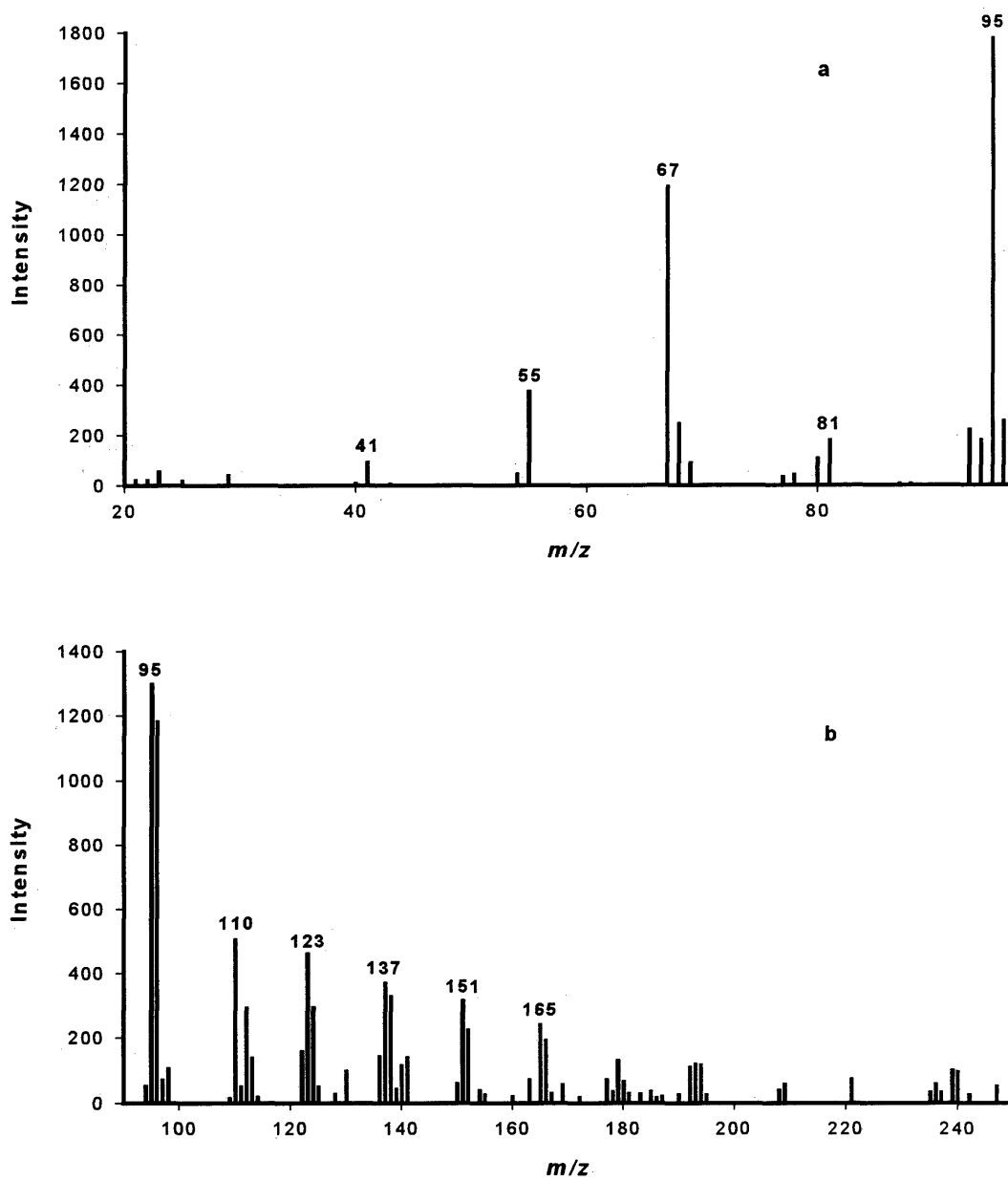


Figure-1.12. Pyrolysis (a) product ion mass spectrum of  $m/z$  95 and (b) precursor ion mass spectrum of  $m/z$  95 from *Brucella neotomae*.

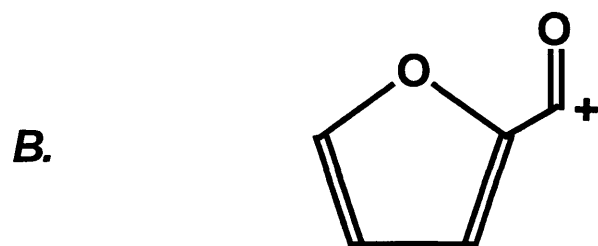
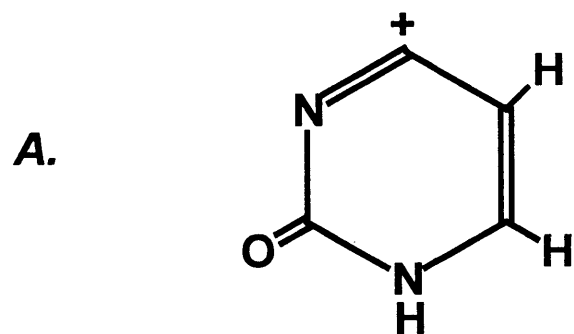


Figure 1.13. Proposed structures for biomarker ion 95.

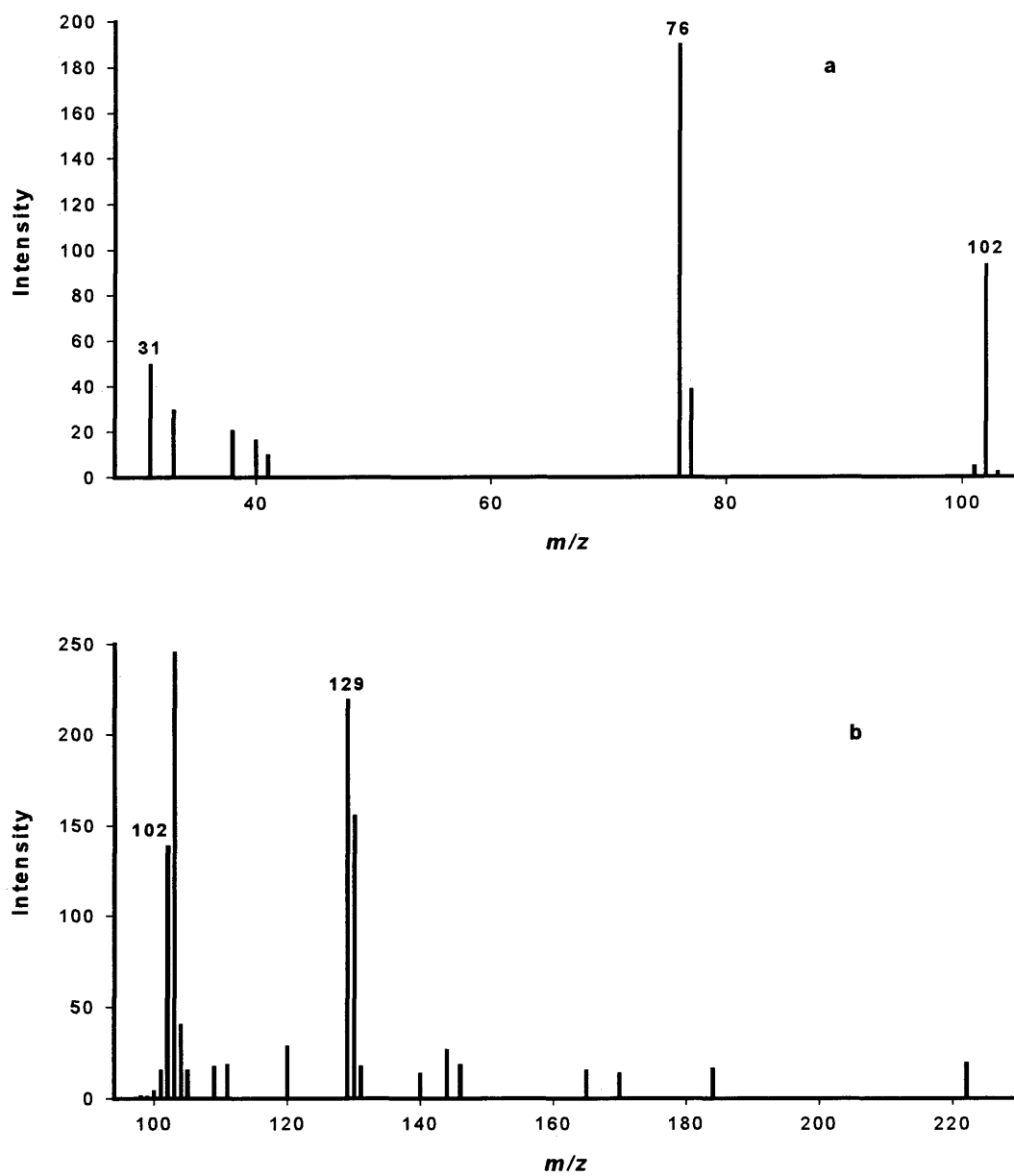


Figure 1.14. Pyrolysis (a) product ion mass spectrum of  $m/z$  102 and (b) precursor ion mass spectrum of  $m/z$  102 from *Brucella neotomae*.

major ion in proteins, nucleic acids, carbohydrates or fatty acids standards. Yet, ion 102 may result from the fragmentation of tryptophan ( $m/z$  204). Tryptophan readily fragments to  $m/z$  130 and 77; ions observed in the precursor- and product-ion scans of  $m/z$  102. To date, no structure for biomarker  $m/z$  102 can be unambiguously assigned.

### **Biomarker $m/z$ 103**

To identify biomarker  $m/z$  103, product- and precursor-ion scans were obtained and are shown in Figures 1.15a and 1.15b. Fragmentation observed for  $m/z$  103 in *B. neotomae* included  $m/z$  77, 76 and 51. Major precursor ions included  $m/z$  120 and 130. A possible structure for  $m/z$  103 is presented in Figure 1.16; a tenable fragment of phenylalanine ( $m/z$  165). Phenylalanine fragments to  $m/z$  120 (decarboxylation product) and  $m/z$  103 (4, 12).  $M/z$  120 in *B. neotomae* also fragments to  $m/z$  103, 91 and 77. Tryptophan ( $m/z$  204) may also produce the structure in Figure 1.16. Tryptophan readily fragments to  $m/z$  130, 103 and 77 (4, 14). In addition,  $m/z$  130 in the whole cell microorganism fragments to  $m/z$  103 and 77. A fragmentation pathway for  $m/z$  103 with phenylalanine and tryptophan origins is shown in Figure 1.17. With the aid of the precursor- and product-ion scans and existing literature, it is surmised that proteins, particularly the amino acids tryptophan and phenylalanine, are the sole source of  $m/z$  103.

### **Biomarker $m/z$ 115**

The fragmentation observed for  $m/z$  115 of *B. neotomae* indicated product ions at  $m/z$  97, 87 and 70. The origin of the  $m/z$  115 ion in the whole cell microorganism was examined using a precursor-ion scan. Major precursor ions included  $m/z$  143, 157, 169, 185, 195, 209, 223 and 237. The product- and precursor-ion scans of  $m/z$  115 are given in Figure 1.18a and 1.18b, respectively. A proposed structure for  $m/z$  115 is shown in Figure 1.19 and is a possible fragment of tryptophan ( $m/z$  204). Tryptophan fragments to  $m/z$  143 (decarboxylation followed by deamination) (14). The presence of  $m/z$  143 in the

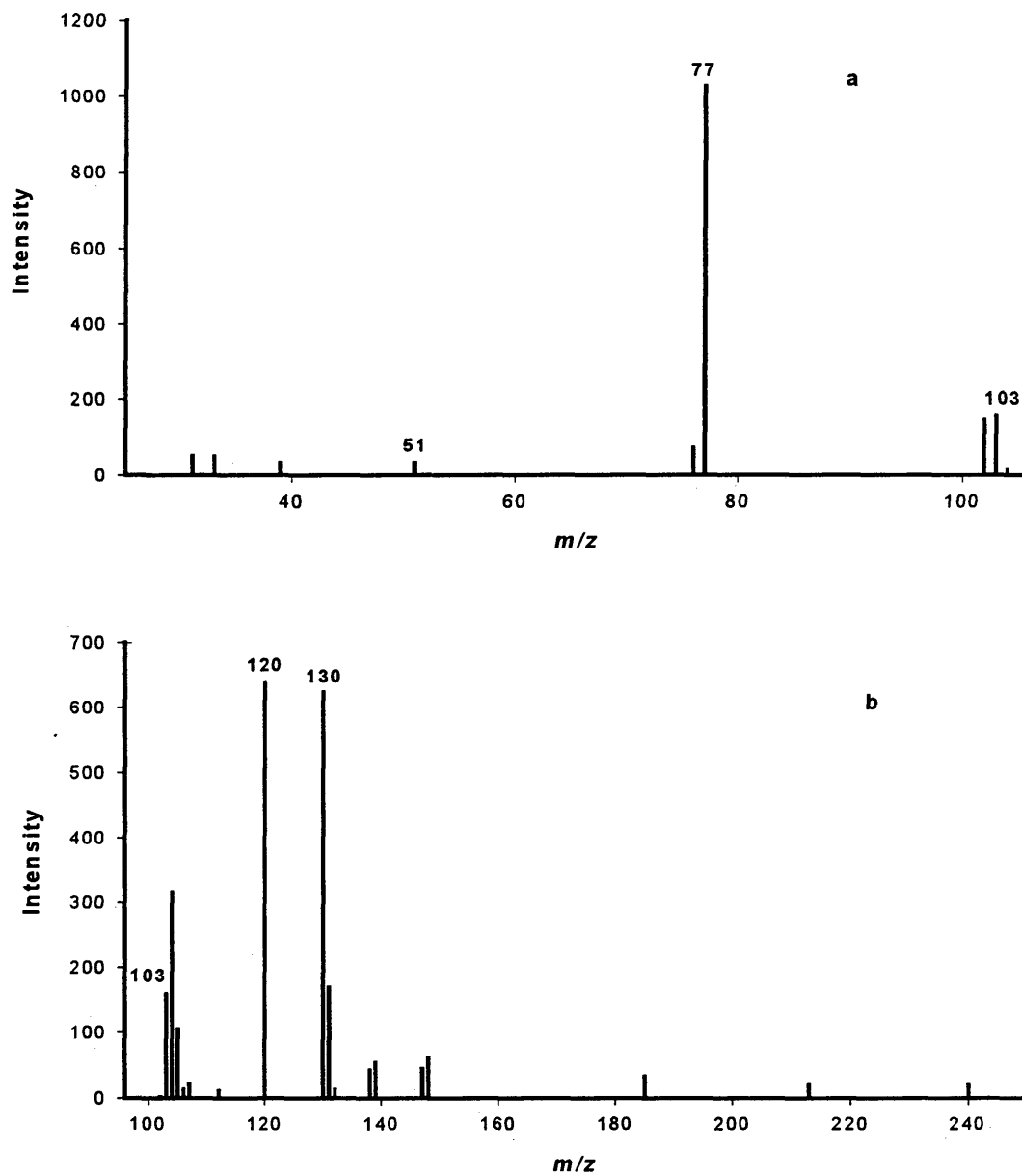


Figure 1.15. Pyrolysis (a) product ion mass spectrum of  $m/z$  103 and (b) precursor ion mass spectrum of  $m/z$  103 from *Brucella neotomae*.

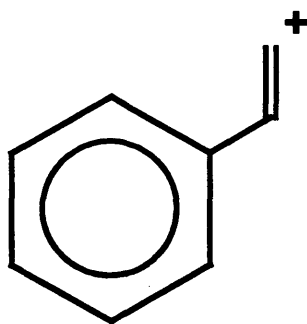


Figure 1.16. A proposed structure for biomarker ion 103.

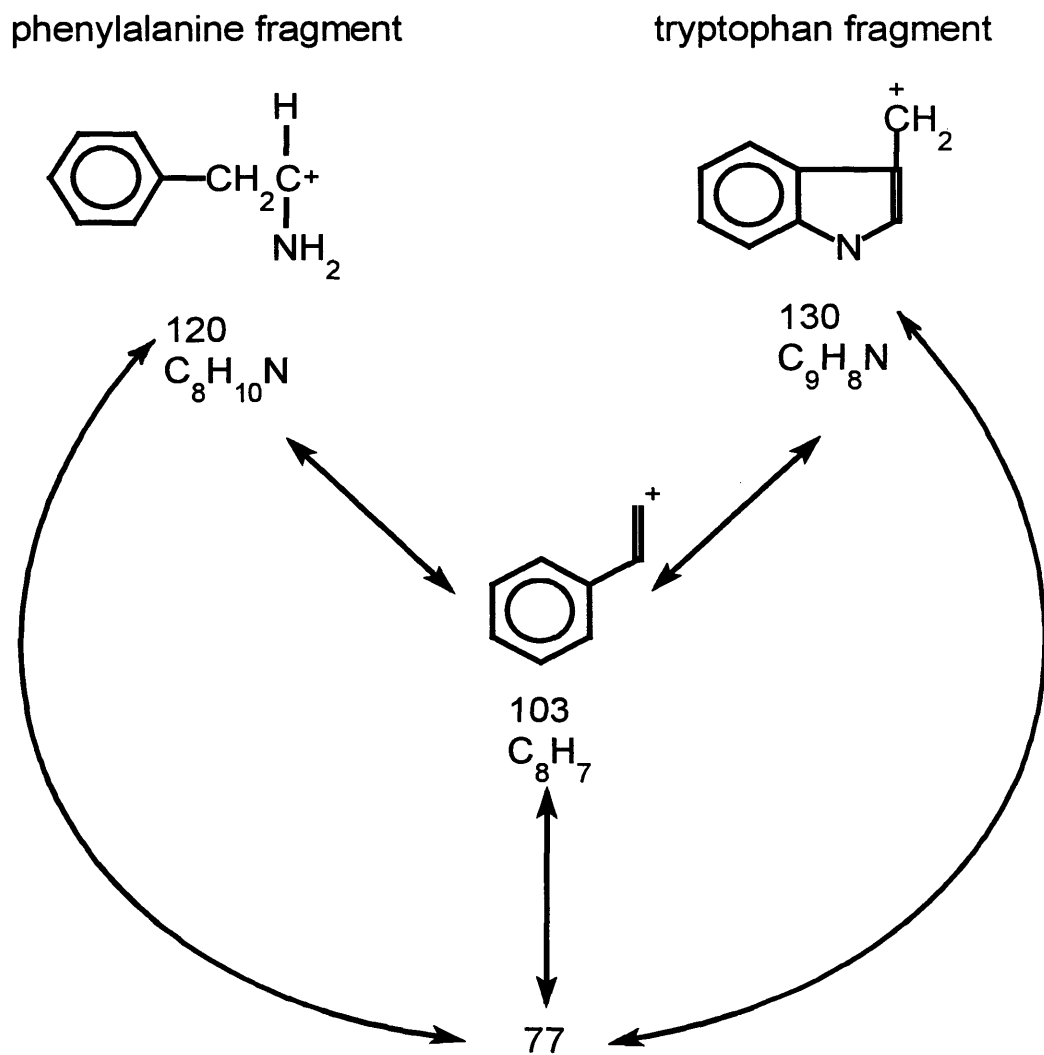


Figure 1.17. A proposed fragmentation pathway with phenylalanine and tryptophan origins for biomarker ion 103.

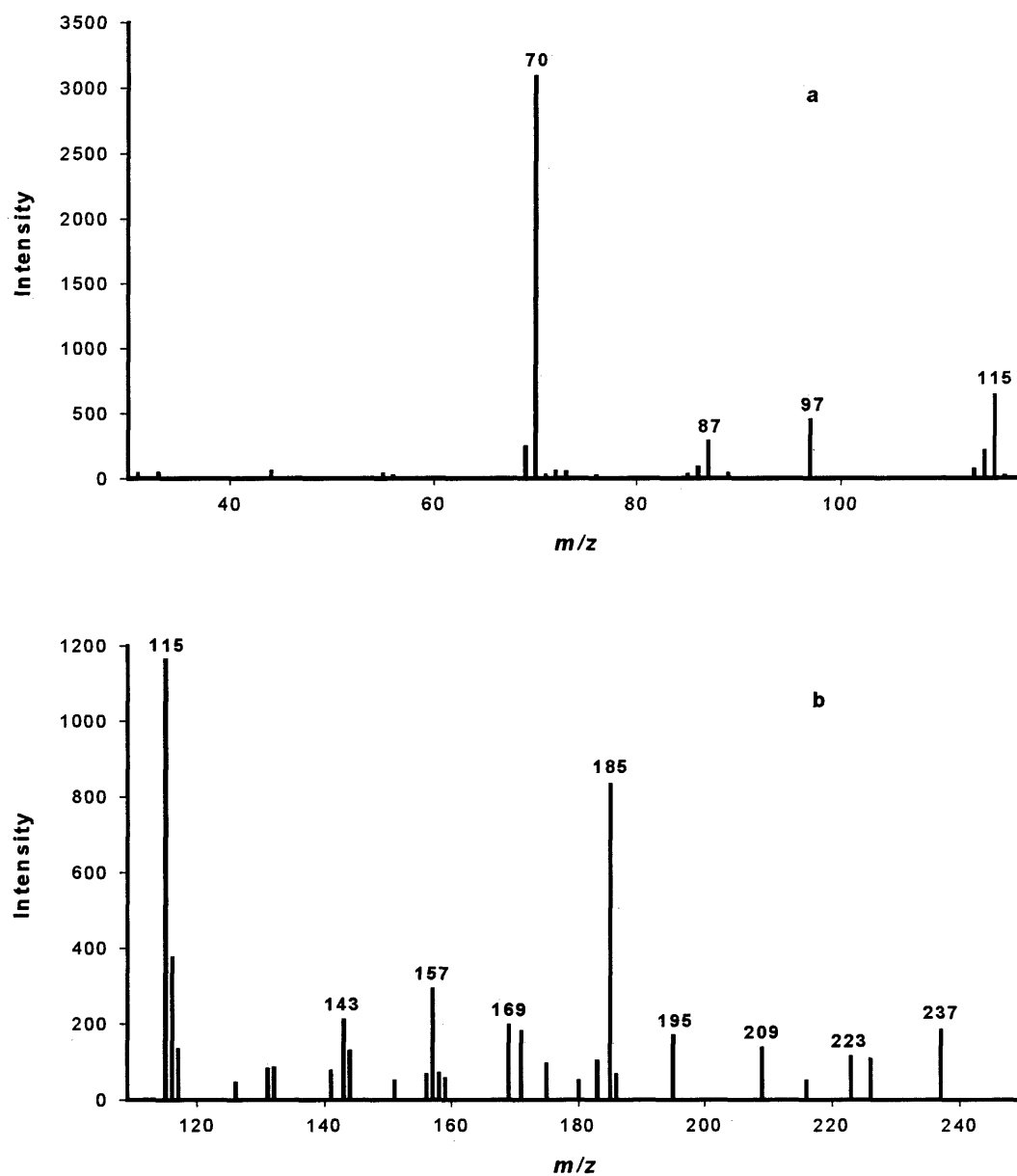


Figure 1.18. Pyrolysis (a) product ion mass spectrum of  $m/z$  115 and (b) precursor ion mass spectrum of  $m/z$  115 from *Brucella neotomae*.

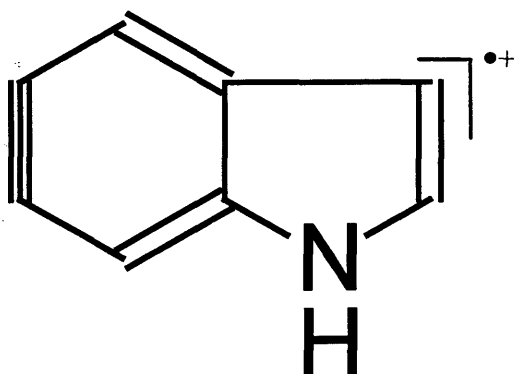


Figure 1.19. A proposed structure for biomarker ion 115.

precursor-ion scan of  $m/z$  115 in *B. neotomae* suggests protein origins for  $m/z$  115. Additionally,  $m/z$  143 in the whole cell microorganism fragmented to  $m/z$  115. Yet, the presence of  $m/z$  87 in the product-ion scan of  $m/z$  115 (loss of  $H_2O$ ) can not be explained by the structure proposed in Figure 1.19. Furthermore, the other precursor ions of  $m/z$  115 have not been identified.

### **Biomarker $m/z$ 117**

The product-ion spectrum (Figure 1.20a) of  $m/z$  117 in *B. neotomae* shows fragmentation to  $m/z$  99, 90, 62 and 37. The precursor ions of  $m/z$  117 in the whole cell microorganism were found to be  $m/z$  132, 143, 144, 145, 153, 186 and 200 as shown in Figure 1.20b. The structure shown in Figure 1.21, indole, is a possible fragment of tryptophan ( $m/z$  204). Tryptophan fragments to  $m/z$  186 (dehydration product), 145, 143 (decarboxylation followed by deamination) and 117 (14).  $M/z$  186 and 143 were observed in the precursor-ion scan of  $m/z$  117 in *B. neotomae*. Moreover,  $m/z$  186 and 145 in the bacterium fragmented to  $m/z$  117. A fragmentation pathway for  $m/z$  117 with tryptophan origins is shown in Figure 1.22.  $M/z$  117 is assumed to originate from the protein-based material of the bacterium, particularly tryptophan.

### **Biomarker $m/z$ 128**

Fragmentation observed for  $m/z$  128 in the whole cell microorganism using a LR-product-ion scan produced product ions at  $m/z$  113, 101, 85, 84, 77, 72 and 57, Figure 1.23a. The origin of the  $m/z$  128 ion of the bacterium was examined using a precursor-ion scan, Figure 1.23b. Major precursor ions included  $m/z$  145, 146, 155 and 156. With the aid of the precursor- and product-ion scans and existing literature, a structure for ion 128 was proposed and is shown in Figure 1.24; a diketopiperazine (DKP) of alanyl and glycine (4). Thermally volatilized dipeptides commonly expel water as the dipeptide cyclizes to form a substituted diketopiperazine (DKP), a cyclo-dipeptide (15). The dipeptide of alanyl-glycine occurs at  $m/z$  146. Fragmentation observed for  $m/z$  128 of

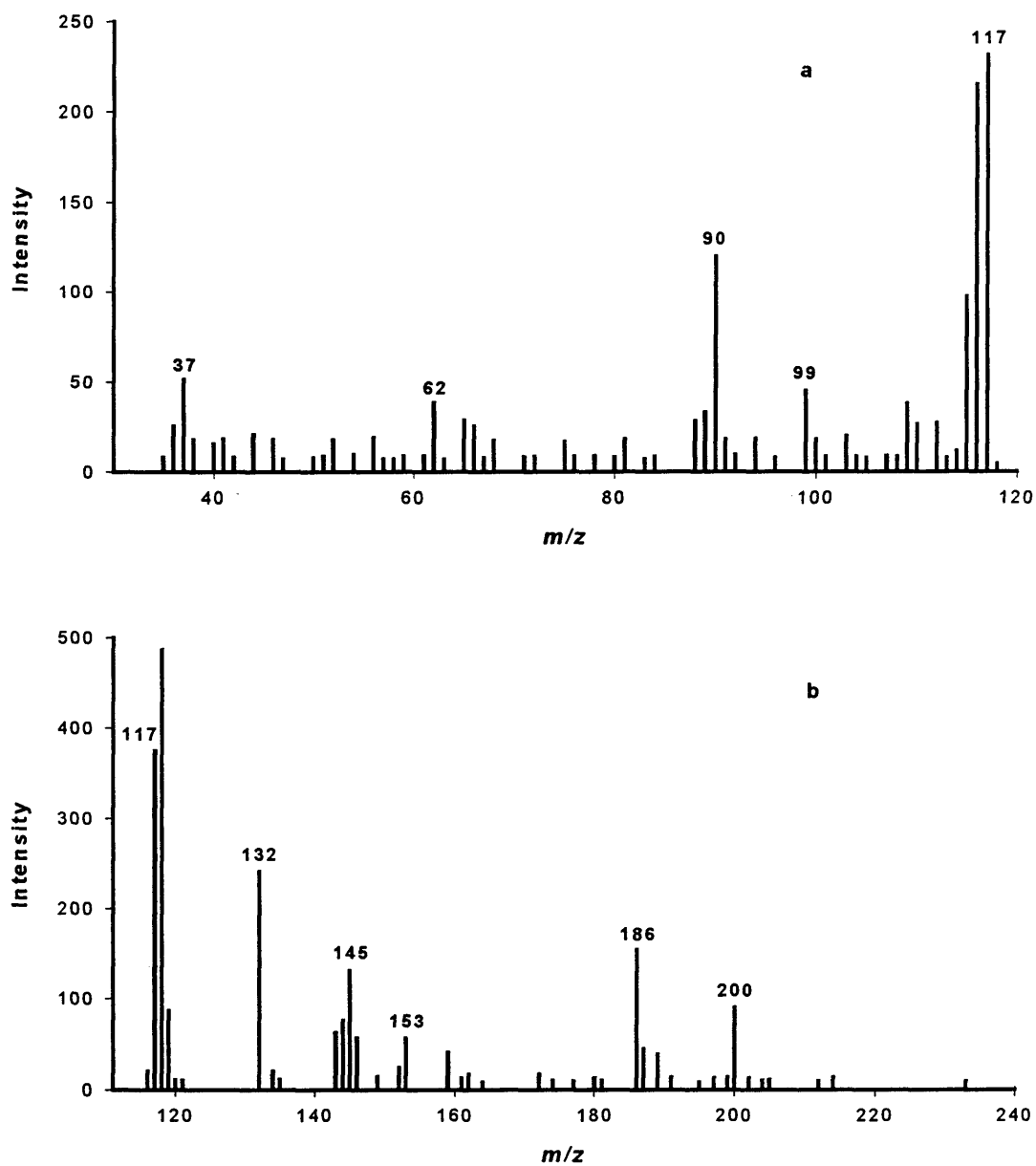


Figure 1.20. Pyrolysis (a) product ion mass spectrum of  $m/z$  117 and (b) precursor ion mass spectrum of  $m/z$  117 from *Brucella neotomae*.

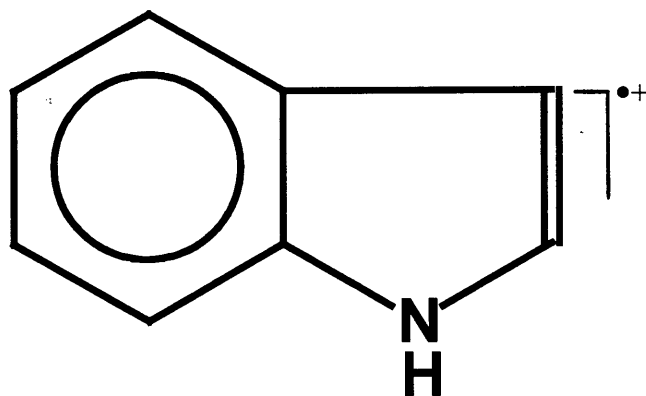


Figure 1.21. A proposed structure for biomarker ion 117.

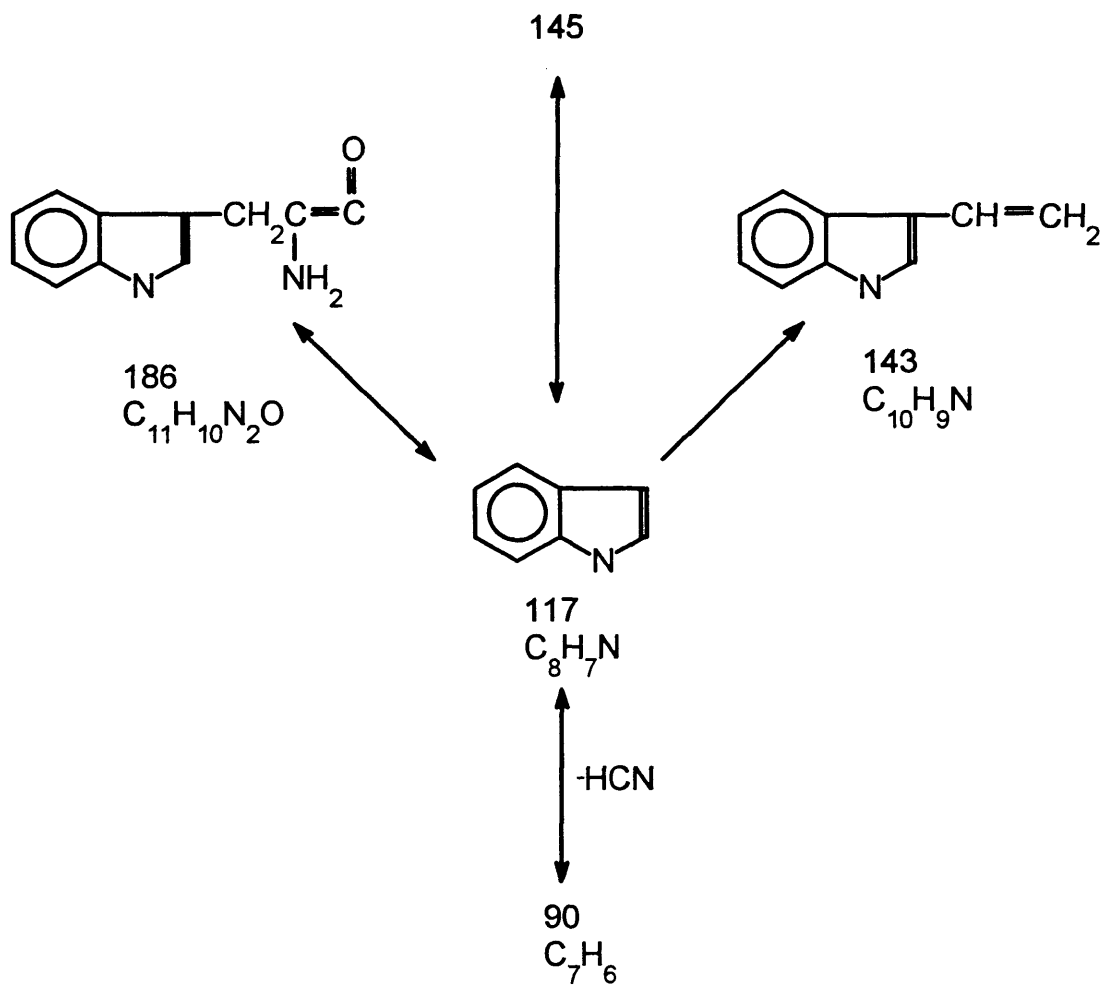


Figure 1.22. A proposed fragmentation pathway with tryptophan origins for biomarker ion 117.

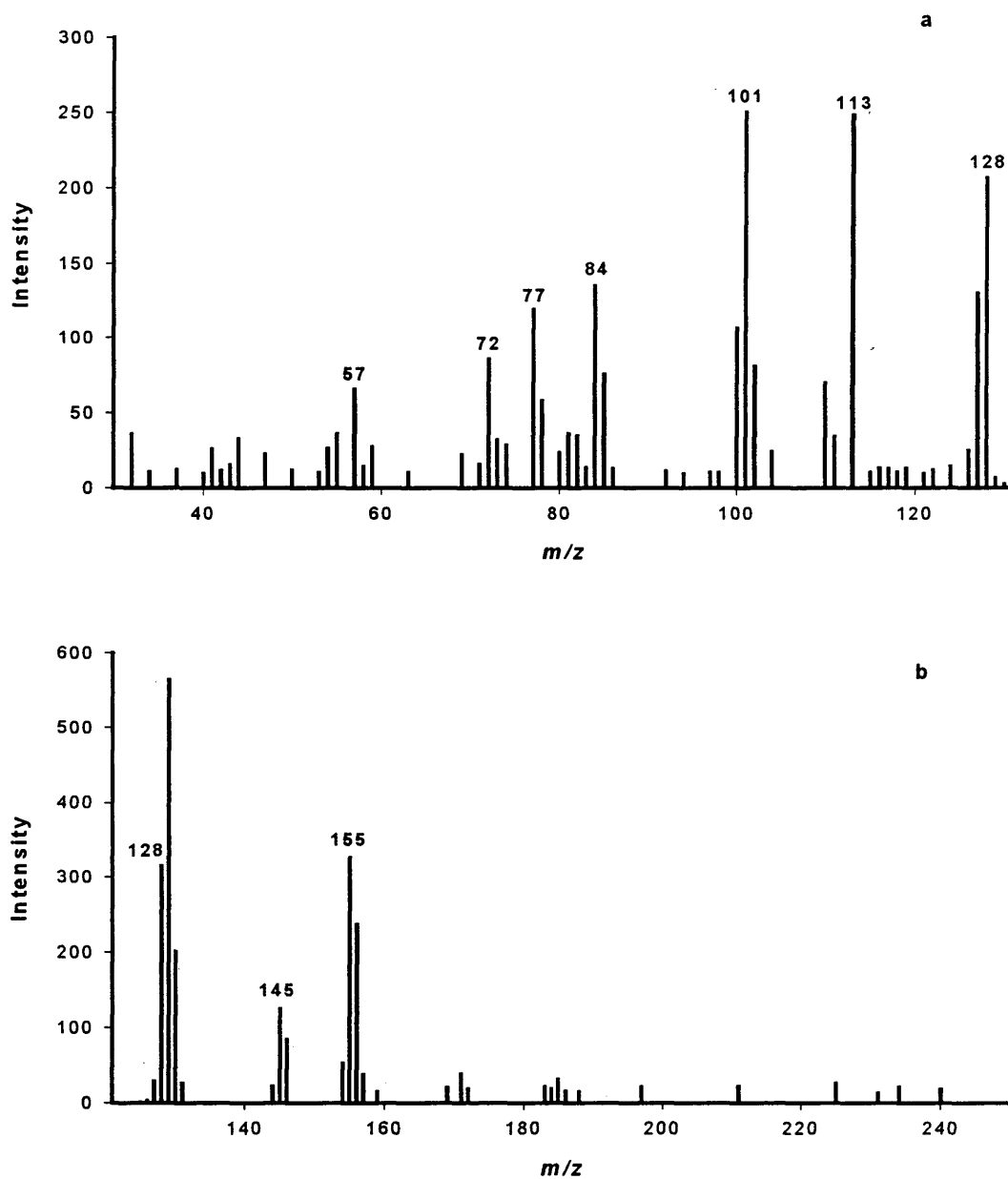


Figure 1.23. Pyrolysis (a) product ion mass spectrum of  $m/z$  128 and (b) precursor ion mass spectrum of  $m/z$  128 from *Brucella neotomae*.

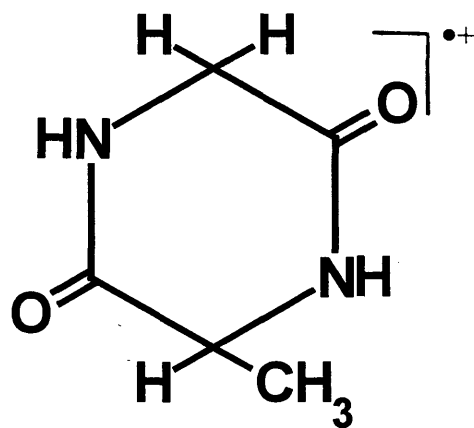


Figure 1.24. A proposed structure for biomarker ion 128.

the alanyl-glycine DKP produced product ions at  $m/z$  85, 72, 58 and 57 (4).  $M/z$  146, 85, 72 and 57 are associated with alanyl-glycine and have been observed in the precursor- and product-ion scans of  $m/z$  128 in the whole cell microorganism. Furthermore,  $m/z$  146 of *B. neotomae* fragmented to  $m/z$  128. A fragmentation pathway for  $m/z$  128 is shown in Figure 1.25. Based on the previously noted data,  $m/z$  128 is considered to originate from proteins.

### **Biomarker $m/z$ 129**

The product-ion spectrum of  $m/z$  129 (Figure 1.26a) in *B. neotomae* shows fragmentation to  $m/z$  102, 87, 84, 73, 57 and 55. The precursor ions of  $m/z$  129 in the whole cell microorganism were found to be  $m/z$  146, 147, 156, 157, 171, 185, 197, 227 and 256 (Figure 1.26b). A structure for  $m/z$  129, identified in Figure 1.27, is a fragment of a fatty acid (16, 17), notably palmitic acid ( $m/z$  256). The mass spectra of free fatty acids are analogous to the spectra of the methyl esters with the exception that the peaks due to the fragments containing the carbomethoxy group are 14 mass units lower. Ions belonging to the carbomethoxy ion series of palmitic acid include, but are not limited to,  $m/z$  185, 171, 157, 129, 87 and 73. The presence of these ions in the precursor- and product-ion scans of  $m/z$  129 in the whole cell microorganism suggests lipid origins for  $m/z$  129.

### **Biomarker $m/z$ 131**

To identify biomarker  $m/z$  131, product- and precursor-ion scans were obtained and are shown in Figures 1.28a and 1.28b. Fragmentation observed for  $m/z$  131 in *B. neotomae* included  $m/z$  117, 104, 103, 91, 86 and 77. Major precursor ions included  $m/z$  146, 148, 158, 159, 174, 175, 186, 187, 200, 201, 216, 230 and 243. One possible structure of  $m/z$  131 is given in Figure 1.29 and is identified as a fragment of the amino acid tryptophan ( $m/z$  204). Tryptophan fragments to  $m/z$  186, 159, 131, 117, 103 and 77 (14). These ions are observed in the precursor- and product-ion scans of  $m/z$  131.

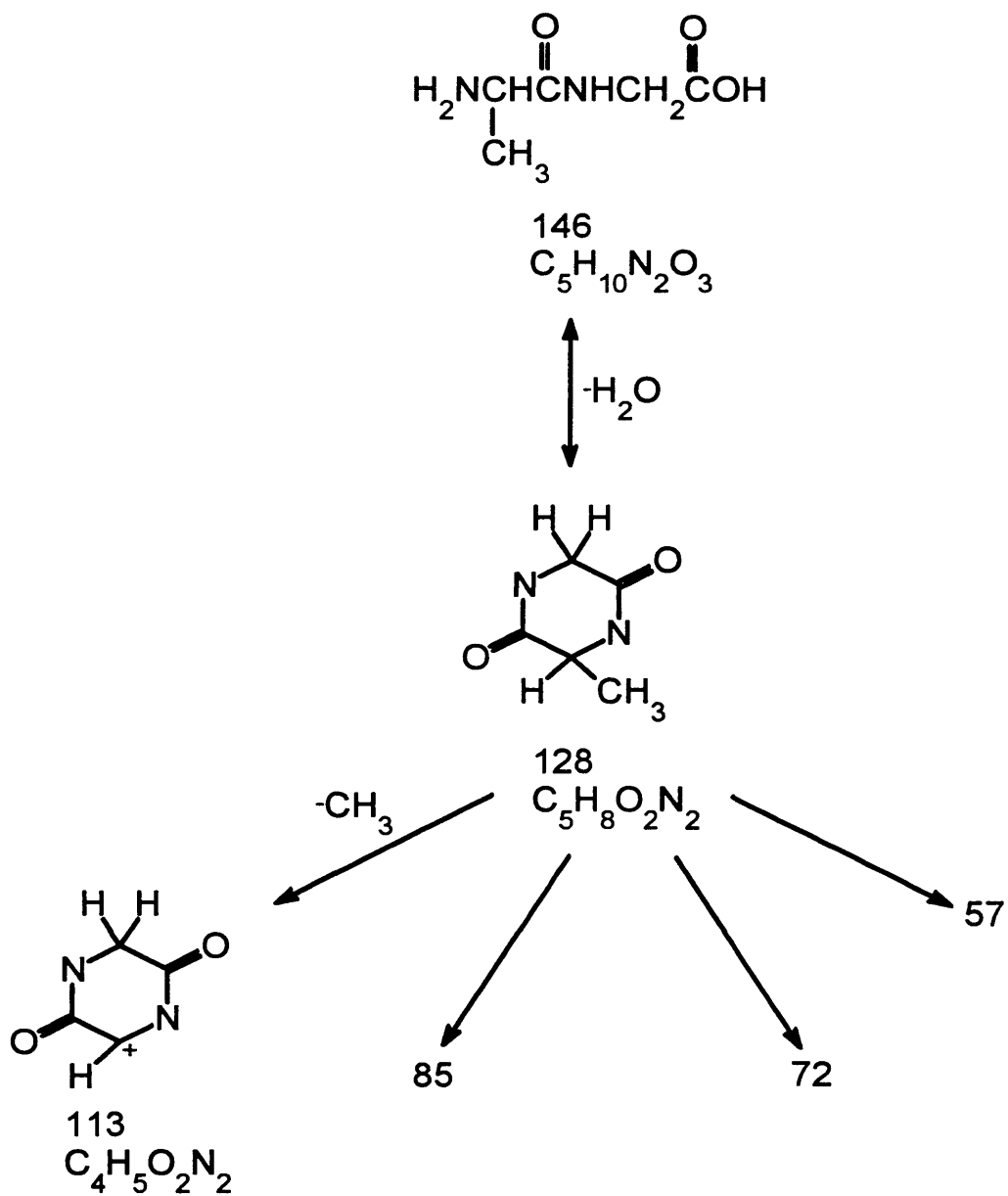


Figure 1.25. A proposed fragmentation pathway with alanyl-glycine diketopiperazine origins for biomarker ion 128.

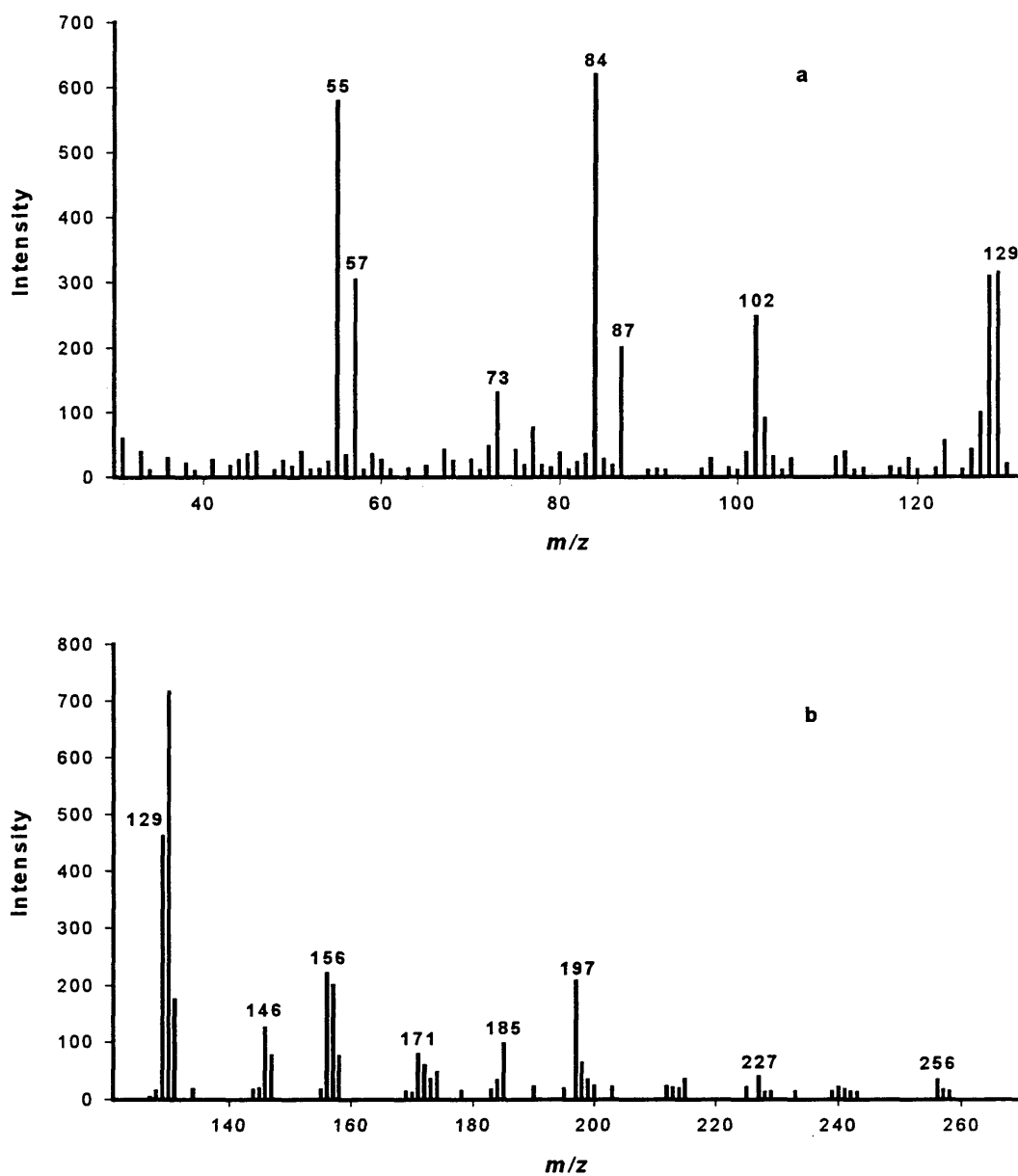


Figure 1.26. Pyrolysis (a) product ion mass spectrum of  $m/z$  129 and (b) precursor ion mass spectrum of  $m/z$  129 from *Brucella neotomae*.

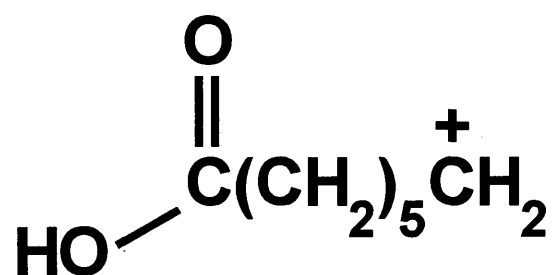


Figure 1.27. A proposed structure for biomarker ion 129.

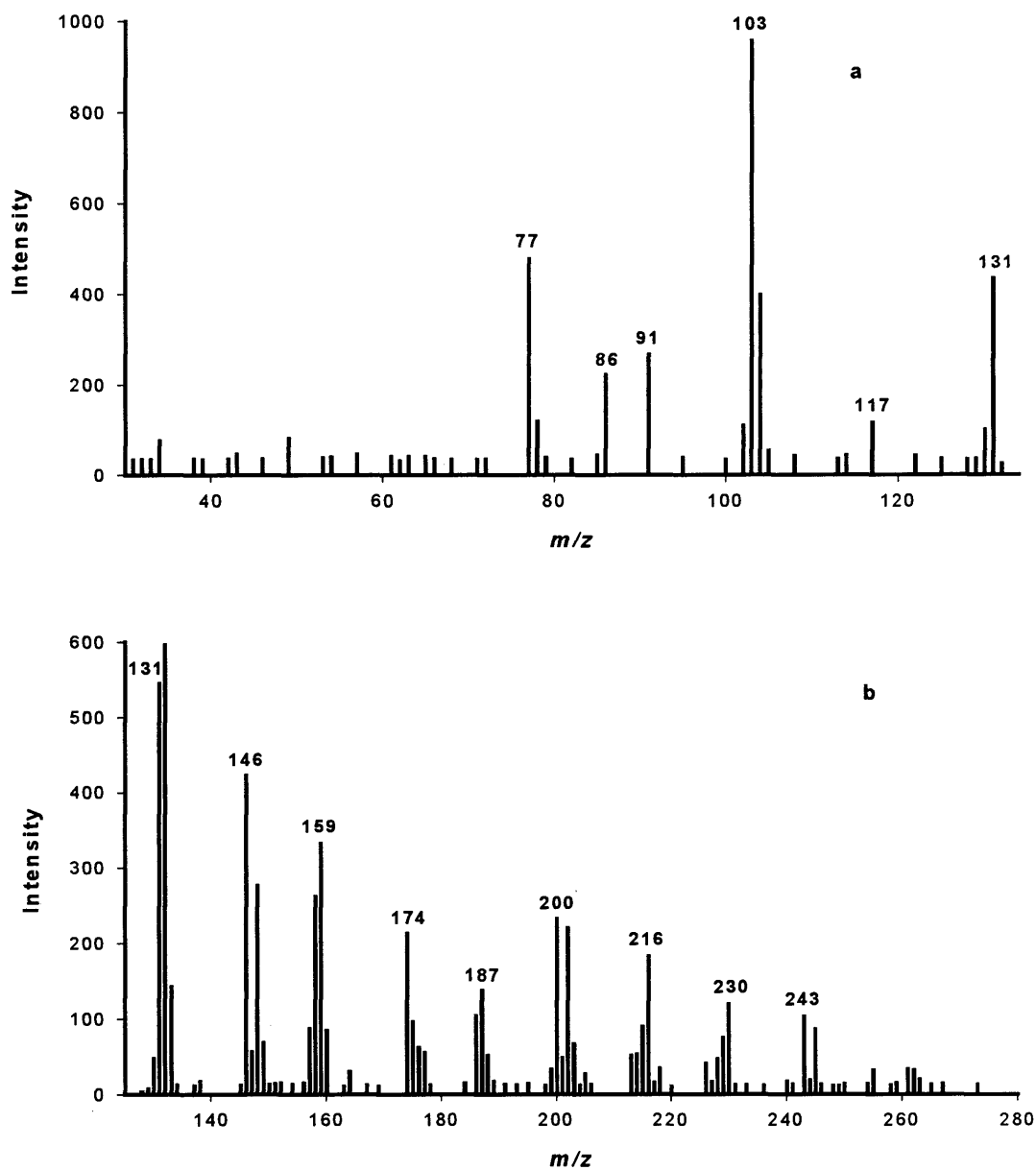


Figure 1.28. Pyrolysis (a) product ion mass spectrum of  $m/z$  131 and (b) precursor ion mass spectrum of  $m/z$  131 from *Brucella neotomae*.

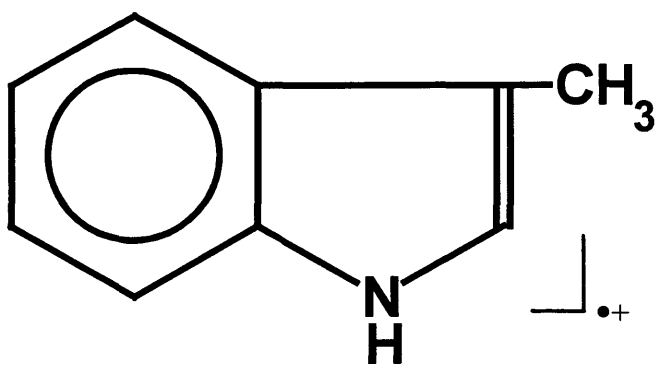


Figure 1.29. A proposed structure for biomarker ion 131.

Furthermore,  $m/z$  186 in the whole cell microorganism fragmented to  $m/z$  131 and 117. Ion 243, observed in the precursor-ion scan of  $m/z$  131, may be the DKP of glycyl-tryptophan (14). This DKP readily fragments to  $m/z$  131, 130 and 117 (14). A fragmentation pathway for  $m/z$  131 based on tryptophan is given in Figure 1.30. Tryptophan is suggested as one source of  $m/z$  131.

## CONCLUSIONS

Low-resolution pyrolysis mass spectrometry/mass spectrometry (MS/MS) is one approach to biomarker identification. As shown in Table 1.2, the biomarker ions of statistical and biological importance are a collection of fragments of nucleic acids, proteins, carbohydrates and lipids. Most of these ions have been assigned a proposed structure and composition based on product- and precursor-ion scans and existing literature. Yet, identification of the chemical species that produced each biomarker was extremely difficult due to the low-resolution nature of the analysis and the large number of common peaks. The knowledge that each nominal mass peak in a bacterium may result from one or more biochemical class of species has been realized by performing the previously described experiments. Furthermore, as most nominal mass peaks in the spectrum of a complex sample (whole bacterial cells) are a consortium of ions, a more strenuous technique must be employed to make clear the most common source of the nominal mass peak. Finally, when the fragmentation products are logically related to starting material the potential of pyrolysis is recognized.

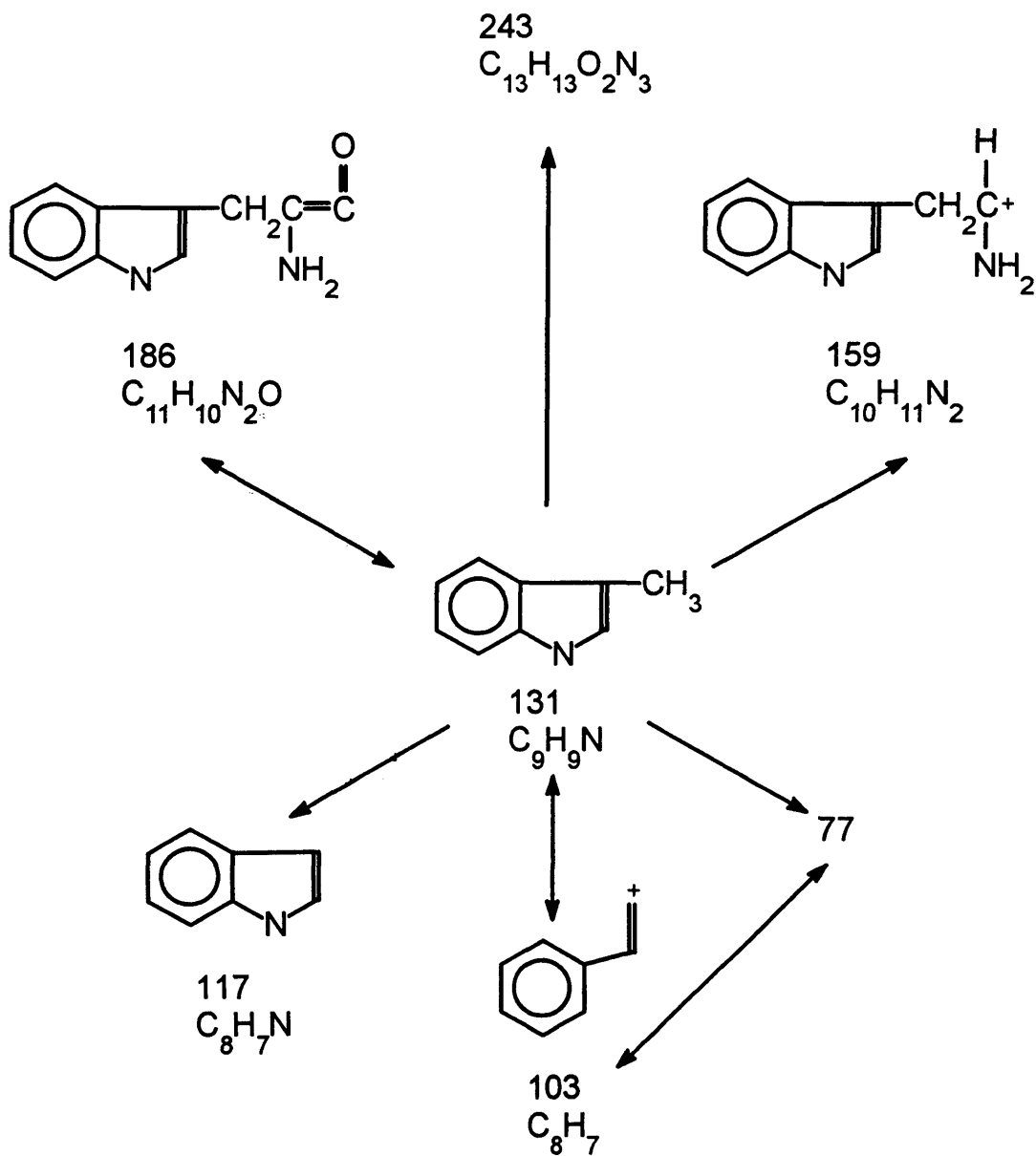


Figure 1.30. A proposed fragmentation pathway with tryptophan origins for biomarker ion 131.

Table 1.2. Proposed biochemical origins of the selected biomarker ions.

Biomarker Ion	Protein	Nucleic Acid	Carbohydrate	Lipid
67	X	X	X	
81		X	X	
89	X			
91	X			
95		X	X	
102	X			
103	X			
115	X			
117	X			
128	X			
129				X
131	X			

**REFERENCES**

- (1) Voorhees, K. J.; Basile, F.; Beverly, M. B.; Abbas-Hawks, C.; Hendricker, A.; Cody, R. B.; Hadfield, T. L. *J. Anal. Appl. Pyrolysis* **1997**, *40,41*, 111-134.
- (2) Mavrovouniotis, M. L.; Harper, A. M.; Ifarraguerri, A. I. ; Edgewood Research and Technology: Aberdeen Proving Ground, 1994.
- (3) DeLuca, S.; Sarver, E. W.; Harrington, P.; Voorhees, K. J. *Anal. Chem.* **1990**, *62*, 1465.
- (4) Noguerola, A. S. Ph.D. dissertation, Colorado School of Mines, Golden, CO, 1992.
- (5) Meuzelaar, H. L. C.; Haverkamp, J.; Hileman, F. D. *Pyrolysis-Mass Spectrometry of Recent and Fossil Biomaterials: Compendium and Atlas*; Elsevier: Amsterdam, 1982.
- (6) Merritt, M. A. J.; Robertson, D. H. *J. Gas Chrom.* **1967**, *5*, 96.
- (7) Ratcliff, M. A. J.; Medley, E. E.; Simmonds, P. G. *J. Org. Chem.* **1974**, *39*, 1481.
- (8) Rice, J. M.; Dudek, G. O.; Barber, M. *J. Am. Chem. Soc.* **1965**, *87*, 4569.
- (9) Helleur, R. J.; Budgell, D. R.; Hayes, E. R. *Anal. Chim. Acta* **1987**, *192*, 243.
- (10) Rice, J. M.; Dudek, G. O. *J. Am. Chem. Soc.* **1967**, *89*, 2719.
- (11) Wiebers, J. L. *Nucleic Acids Res.* **1976**, *3*, 2959.
- (12) Shulman, G. P.; Simmonds, P. G. *Chem. Common.* **1968**, 1040.
- (13) Schulten, H. R.; Bahr, U.; Gortz, W. *J. Anal. Appl. Pyrolysis* **1981/1982**, *3*, 229.
- (14) Hendricker, A. D. Ph.D. Dissertation, Colorado School of Mines, Golden, CO, 1998.
- (15) Svec, H. J.; Junk, G. A. *J. Am. Chem. Soc.* **1964**, *86*, 2278.
- (16) Biemann, K. *Mass Spectrometry: Organic Chemical Applications*; McGraw-Hill Book Company, Inc.: New York, 1962.
- (17) Murphy, R. C. *Mass Spectrometry of Lipids, Handbook of Lipid Research*; Plenum Press: New York, 1993.

## Chapter 2

# IDENTIFICATION OF BIOMARKERS IN THE DESORPTION ELECTRON IONIZATION-HIGH RESOLUTION MASS SPECTRUM OF *BRUCELLA NEOTOMAE*

## ABSTRACT

Desorption electron ionization-high resolution-mass spectrometry (DEI-HR-MS) has been used to simultaneously analyze whole bacterial cells and standards to elucidate the species of several biomarker ions originating from carbohydrates, nucleic acids, proteins and lipids. DEI-HR-MS is a powerful technique for examining biomarker ions in a complex mixture, since most nominal masses are composed of several contributing species. HR-MS provides the capability to identify the composition of a low resolution mass spectral peak. It is of fundamental interest to define the site of origin of pyrolysis products in the macromolecular structure of a microorganism. The identification of ions by DEI-HR-MS facilitates the goal of understanding biomarker ion origins.

## INTRODUCTION

As stated in Chapter 1, the major classes of substances common in living systems are carbohydrates, nucleic acids, proteins and lipids. Carbohydrates (sugars) are organic compounds containing carbon, hydrogen, and oxygen corresponding to the formula  $C_n(H_2O)_m$ . In addition, replacing one or more of the hydroxyl groups with other chemical species can form derivatives of carbohydrates. For example, peptidoglycan (bacterial cell wall polymer) contains the glucose derivatives N-acetylglucosamine and muramic acid.

The most biologically relevant carbohydrates are those containing four, five, six and seven carbon atoms. Pentoses (C<sub>5</sub> sugars) are significant in the specialized derivatives of carbohydrates which are nucleic acids. Hexoses (C<sub>6</sub> sugars) are the monomeric constituents of cell wall polymers and energy reserves. Polysaccharides (long chain of monosaccharides) can also combine with other classes of macromolecules, such as lipid or protein, to form glycolipids or glycoproteins. Glycolipids constitute a major portion of the cell wall of Gram-negative bacteria.

Monosaccharides have been characterized by electron ionization (EI) (1, 2), field desorption (FD) (3-5), chemical ionization (CI) (1, 2), and fast atom bombardment (FAB) (6) mass spectrometry. Application of desorption chemical ionization (DCI) to glycosides has also been described (7-11). Two classes of compounds formed from rapid pyrolysis of carbohydrates are anhydrosugars and furan derivatives. Pyrolysis-gas chromatography of polysaccharides has shown that anhydrosugars are produced through a depolymerization transglycosidation mechanism involving nucleophilic displacement of the glycosidic groups by one of the free hydroxyl or amine groups of the sugar molecule (12). Upon further heating, anhydrosugars dehydrate and decompose. Therefore, many of the pyrolysis products identified from sugars are common to all saccharides.

Nucleic acids are specialized derivatives of carbohydrates. DNA (deoxyribonucleic acid) and RNA (ribonucleic acid) are polymers of monomers called nucleotides. Each nucleotide is composed of three separate units; a five carbon sugar, either ribose (in RNA) or deoxyribose (in DNA), a nitrogen base, and a molecule of phosphate, PO<sub>4</sub><sup>3-</sup>.

Nucleic acids have been studied by several mass spectrometric (MS) techniques including electrospray (ESI-MS) (13-16), matrix-assisted laser desorption/ionization (MALDI-MS) (16-20), EI-MS and Py-MS (21-25). Primary fragmentation of any polydeoxyribonucleotide upon pyrolysis involves cleavage at the phosphodiester bonds linking the nucleotide residues. Subsequent EI<sup>+</sup> fragmentation result in ions which are

diagnostic for the common nucleotide components of the polynucleotide (23-27), including intact bases or even more or less severely dehydrated nucleosides.

Proteins constitute 70% of the dry weight of a bacterial cell (28) and play key roles in cell function; catalytic and structural. They are the organic chemicals of life. Proteins are polymers of various lengths containing defined sequences of amino acids covalently bonded by peptide linkages. While several hundred different amino acids are known to occur naturally (29), biochemists and chemists recognize twenty of these amino acids as common, Table 2.1. These are the amino acids that are normally present in proteins. The chemical variety intrinsic to the side chains of these amino acids is sufficiently great to allow for the chemical variance necessary to make proteins with widely different biochemical properties.

Proteins have been analyzed by numerous analytical methods including gas chromatography (GC), high performance liquid chromatography (HPLC), and several mass spectrometric (MS) techniques (30-39). The studies made by Simmonds *et al.* (37-39) on the thermal degradation of amino acids by pyrolysis-gas chromatography/mass spectrometry (Py-GC/MS) showed that common fragmentation mechanisms existed including simple decarboxylation, single dehydration, double dehydration yielding first a dipeptide and subsequently a diketopiperazine (DKP), deamination, or chain homolysis. More recently, Chiavari and Galletti (40) employed Py-GC/MS to analyze nineteen  $\alpha$ -amino acids and proposed pyrolytic fragmentation pathways to identify diagnostic fragments for the recognition of selected amino acids in protein materials.

Fatty acids are the main constituents of lipids and are important for bacterial identification (28). Simple lipids consist of three fatty acids bonded to the C<sub>3</sub> alcohol glycerol and are often referred to as triglycerides. The hydrolysis of lipids yields glycerol and long-chain fatty acids. Complex lipids are simple lipids that contain additional elements such as sulfur, phosphate or nitrogen. Phospholipids are an important class of complex lipids since they play a major role in the cytoplasmic membrane

Table 2.1. Standards used to represent the cellular content of proteins.

Glycine (G)
Alanine (A)
Serine (S)
Threonine (T)
Aspartic acid (D)
Asparagine (N)
Glutamic acid (E)
Glutamine (Q)
Cysteine (C)
Tyrosine (Y)
Lysine (K)
Arginine (R)
Histidine (H)
Proline (P)
Valine (V)
Leucine (L)
Isoleucine (I)
Methionine (M)
Phenylalanine (F)
Tryptophan (W)
Albumin

structure. Due to the dual properties of hydrophobicity and hydrophilicity, lipids are the ideal structural components of membranes.

Gas chromatography is frequently used for the chemotaxonomic classification of bacteria based on fatty acid methyl esters (FAMES) (41). Fatty acids and fatty acid derivatives were the first lipid substances studied in detail by mass spectrometry (42). Moreover, mass spectrometry has been employed to analyze FAMES of extremely pathogenic microorganisms (43). Py-MS (44, 45) has also been utilized to differentiate microorganism based on glyceride profiles.

As described in Chapter 1, the US Army has selected biomarker detection by pyrolysis-mass spectrometry (Py-MS) as the basis of one of their biological detectors. The instrumentation has been previously described (46). The ability to differentiate between pathogenic microorganisms and background material is critical to the success of the program. The Py-mass spectra of various biological samples (whole bacterial cells) defined biomarker peaks ( $m/z$  67, 76, 79, 89, 93, 95, 103, 105, 115, 117, 129 and 131) that could be used for differentiation of microorganisms based upon taxonomic significance (47). The selection of these ions was based on multivariate statistical analysis of a large quantity of data with some knowledge of the biomarkers (46, 47). This list of ions was refined and modified from those listed in Chapter 1. As a result, a series of rules was formulated to classify biological materials based on these peaks. However, the use of product- and precursor-ion scans employing a triple quadrupole mass spectrometer was insufficient in identifying the actual source of the biomarkers. In an attempt to elucidate the source and composition of these biomarkers, whole bacterial cells and pure standards were analyzed by desorption electron ionization-high resolution-mass spectrometry (DEI-HR-MS). A numerical expression of resolution can be obtained from the ratio  $m/\Delta m$ , where  $m$  is the  $m/z$  value of a peak in the mass spectrum and  $\Delta m$  is the difference between two adjacent peaks in the mass spectrum,  $m_1/(|m_1 - m_2|)$ . For low resolution analysis,  $\Delta m$  will be equal to 1 (unit resolution) and  $\Delta m$  may be equal to 0.010

for high resolution analysis. High resolution ( $R \geq 10,000$ ) allows the determination of molecular composition by exact mass measurement. Every isotope of every element (except carbon, which is assigned exactly 12.00000 Da) has a unique, non-integer mass. Exact mass measurements thus allow for the determination of chemical composition and therefore a characteristic “mass defect”. Moreover, the mass of an ion identifies its isotopic and elemental composition. A comprehensive study, including product- and precursor- ion scans, of carbohydrate, nucleic acid, protein and lipid related biomarkers is the subject of the present investigation. Fragmentation pathways (thermal and/or EI) are proposed, and the origins of the biomarker ions have been established.

## **EXPERIMENTAL**

### *Reagents*

Solutions of adenosine 5'-monophosphate (AMP), thymidine 5'-monophosphate (TMP), guanosine 5'-monophosphate (GMP), cytidine 5'-monophosphate (CMP), uridine 5'-monophosphate (UMP), adenine, thymine, guanine, cytosine, uracil, ribose, glucose, muramic acid, N-acetylglucosamine, a polysaccharide, and a lipopolysaccharide were prepared in distilled water (1 mg/ml) and were used as cellular content standards to represent carbohydrates and nucleic acids. Solutions of albumin (essentially fatty acid free) and the L-amino acids glycine (G), alanine (A), serine (S), threonine (T), aspartic acid (D), asparagine (N), glutamic acid (E), glutamine (Q), cysteine (C), tyrosine (Y), lysine (K), arginine (R), histidine (H) and proline (P) were prepared in distilled water (1 mg/ml). Solutions of the nonpolar side-chain L-amino acids valine (V), leucine (L), isoleucine (I), methionine (M), phenylalanine (F) and tryptophan (W) were prepared in a 1:1 hexane-isopropyl alcohol mixture (1mg/ml). The amino acid standards and albumin standards represent the cellular constituents of proteins. The cellular content of lipids was represented by fatty acids (C14:0, C16:0, C16:1, cycC17:0, C18:0, C18:1, cycC19:0 and

C19:0), glycerides (tripalmitin and phosphatidylglycerol), diphosphatidylglycerol (phosphatidylethanolamine and phosphatidyl-choline) and sphingomyelin. These standards were also prepared in distilled water (1mg/ml). All standards were purchased from Sigma.

### *Bacterial Samples*

Cultures of *Brucella neotomae* obtained from the Armed Forces Institute of Pathology (Washington, D.C.) were grown at 37°C with shaking (225 rpm) in Brucella broth for four days. Cultures were harvested by high speed centrifugation, washed twice with saline solution and resuspended in distilled water. Cells were gamma killed in a cobalt radiation source. The samples used for this work had an initial cell concentration of  $1 \times 10^{10}$  CFU (colony forming units)/ml (in H<sub>2</sub>O). *B. neotomae* is a Gram-negative biological agent simulant. The bacterial sample of *B. anthracis* was obtained as gamma-killed freeze-dried cells from the Armed Forces Institute of Pathology (Washington, D.C.) and was prepared as a 10 mg/ml water suspension.

### *Protein Extracts*

Protein extracts of *Brucella neotomae* were obtained by two methods. A modified acetone precipitation reaction (48) was employed to selectively precipitate water-soluble proteins. *B. neotomae*, suspended in 10mM Tris (tris[hydroxymethyl] aminomethane) buffer, were broken by sonication and centrifuged to remove cell debris. The supernatant liquid was chilled to 0°C and a ten-fold excess of acetone was added to precipitate the water-soluble proteins. The protein was obtained by centrifugation and then reconstituted in Tris buffer. A classical *n*-butanol extraction method (49) was used to isolate all the proteins of the bacterium. The whole cells of *B. neotomae* were suspended in phosphate-buffered saline (pH 7.4) and were sonicated. Four parts of cold *n*-butanol were added to the suspension and the mixture was stirred in an ice-bath. After

1 hour, the mixture was centrifuged and the aqueous phase was carefully removed for analysis. Both extracts were analyzed directly without further purification.

### *Lipid Extract*

A modified extraction procedure (50) for lipids from a biological matrix was successfully employed to provide a representative sample of total lipids in *Brucella neotomae*. The wet cell paste of *B. neotomae* was diluted to 1 ml with water. To the suspension, 3.75 ml of methanol-chloroform (2:1, v/v) was added; the mixture was shaken and left at room temperature for 1-2 hours with intermittent shaking. After centrifugation, the supernatant was removed and the residue was resuspended in 4.75 ml of methanol-chloroform-water (2:1:0.8, v/v); the mixture was then shaken and centrifuged. 2.5 ml each of chloroform and water were added to the combined supernatant extracts; the mixture was centrifuged. The lower chloroform phase was withdrawn, diluted with benzene and brought to dryness. The lipid residue was dissolved in chloroform-methanol (1:1). The positive result of the extraction procedure was confirmed by FAB-MS, where the presence of lipids was observed.

### *Instrumental*

A JEOL four sector high resolution mass spectrometer (MStation JMS-700T) equipped with a desorption ionization probe was used for the direct analysis of all samples. To overcome restrictions of volatility, nonvolatile samples are analyzed from the platinum wire that is exposed directly to the ion beam. Each analyzer (mass spectrometer) of the MStation employs the QQBQE-type double focusing optics, Figure 2.1. The optics are named this way because its components are arranged in the order QQBQE as viewed from the ion source. The Q lens is represented by Q (Q lenses diverge or converge ions along the center axis of the ion path), B represents the magnetic field (directional focusing) and E denotes the electric field (energy focusing). Microbial suspension or standard solutions in the amount of 1  $\mu$ L were applied to the desorption

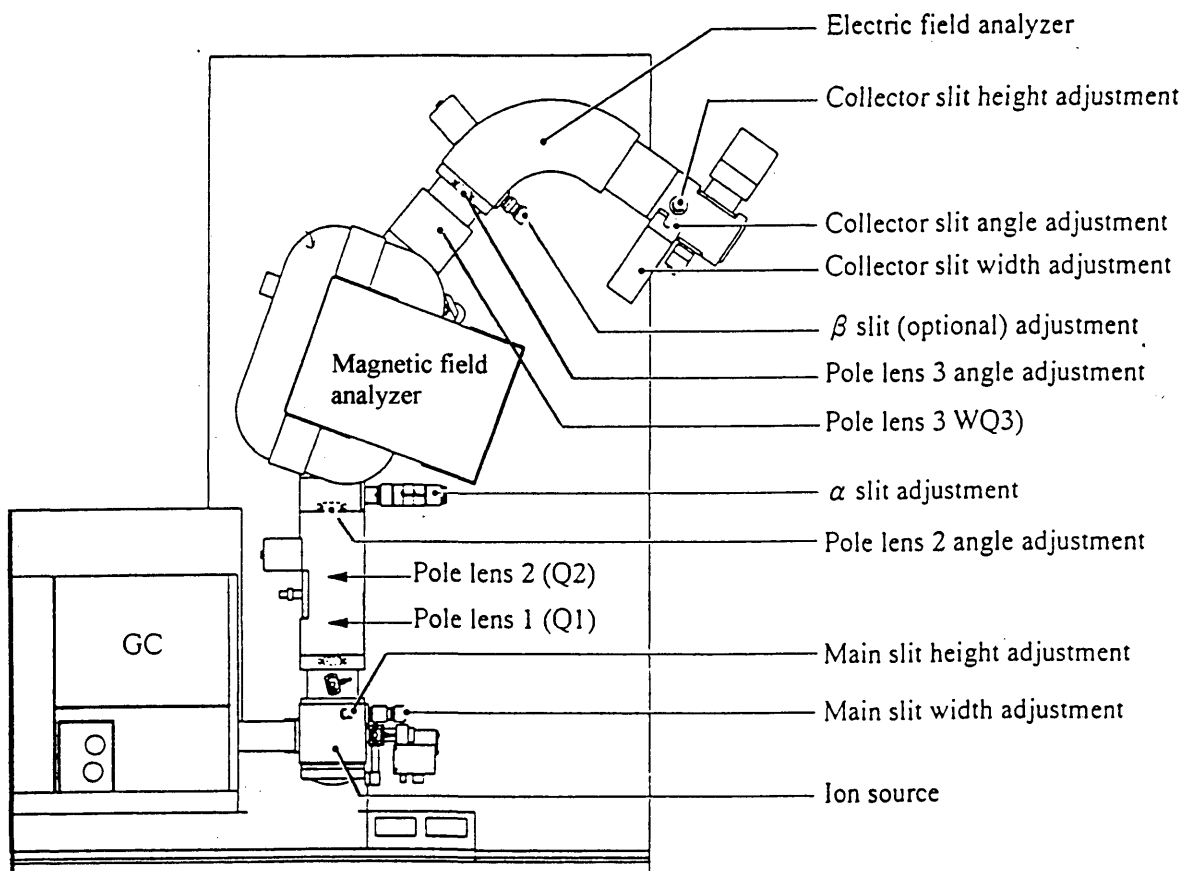


Figure 2.1. A schematic of an analyzer from the JEOL MStation JMS-700T. The MStation consists of two of these analyzers interfaced by a collision cell.

(Reprinted with permission from JEOL).

probe and brought to dryness. The platinum wire probe was heated to 1 ampere (A) at a rate of 1 A/min. The acceleration voltage used for normal scan was 8 kV. Normal spectra were obtained at resolutions of 10,000 and 30,000. All DEI+ spectra were obtained at 70 eV ionization energy and the ion source temperature was maintained at 200°C. Twenty scans were averaged to produce a reproducible mass spectrum. The results were acquired and processed by the Hewlett Packard Model 715/100XC workstation.

The MStation consists of a pair of double-focusing mass spectrometers (analyzers), MS1 and MS2 (both are identical to the one shown in Figure 2.1). The combination of the two analyzers constitutes a BEBE geometry. By scanning both the magnetic and electric fields while keeping the B/E ratio constant (linked scan), tandem mass spectrometry is realized. MS1 and MS2 are interfaced by a collision cell. The role of the MS/MS interface (collision cell) is to fragment precursor ions that have passed through the first mass analyzer by colliding them with collision gas, and to lead the generated product ions into the second analyzer efficiently. The acceleration voltage used for product scans was 8 kV, 10 kV for precursor scans. Helium was used as the collision gas with the collision cell voltage of 3 kV for product scan and 9.8 kV for precursor scan. All product scans were obtained at a resolution of 10,000, while precursor scans were obtained at a resolution of 1,000. Again, the spectra were obtained at 70 eV ionization energy.

For FAB analysis, a portion of the lipid extract was mixed with 3-nitrobenzylalcohol (NBA) in a 1:1 ratio (sample/matrix, v:v) and transferred to the tip of the FAB probe. An atom bombardment energy of 6kV, at an emission current of 100μA, was used during the FAB ionization process while the accelerating voltage was maintained at 10kV.

## RESULTS AND DISCUSSION

To represent the contents of whole bacterial cells, a collection of standards including sugars, nucleic acid building blocks, proteins and lipids were studied. These standards were analyzed using the same conditions as in the analysis of the whole cell microorganism, yet to be discussed. The peaks observed in the standards were compared to those found in the whole bacterial cells and cell extracts to determine biomarker origins. Using accurate mass data together with unsaturation counts (rings plus double bonds,  $R+DB$ ), the chemical formula for particular contributors of each peak was calculated. The list of possible structures includes all elemental compositions having masses that fall within a specified error tolerance of the measured mass. The fragmentation pathways that are presented are postulated. For the pathways, the double-ended arrows confirm the ion in the precursor- and product-ion scans. The single-ended arrows confirm the ion in the precursor- or product-ion scan. Where possible, individual pyrolysis fragments are identified by comparing their mass spectra with published spectra. Structures of the various peaks are not drawn (unless supported by literature) due to the fact that a large number of isomeric structures could be used to represent each peak and the structures have not been exhaustively analyzed via labeled studies; a task beyond the goal of this work. However, empirical formulas are used in the face of this ambiguity and these formulas are shown to be common to those found in pure standards.

High resolution ( $R=10,000$  or  $30,000$ ) DEI+ spectra of *B. neotomae* biomarker ions 67, 76, 79, 89, 93, 95, 103, 105, 115, 117, 129 and 131 were obtained in order to determine the major contributing ions of each peak cluster and are shown in Figures 2.2-2.13. The biomarker ions in *B. neotomae* will be discussed in detail according to the biochemical class which gave rise to each ion: carbohydrate/nucleic acid, protein, and lipid. Only the biomarker ions observed in the spectra of both *B. neotomae* and the standards will be discussed. Ions observed in the spectrum of *B. neotomae*, but not in the spectra of the standards, will forego discussion as their origins can not be unambiguously

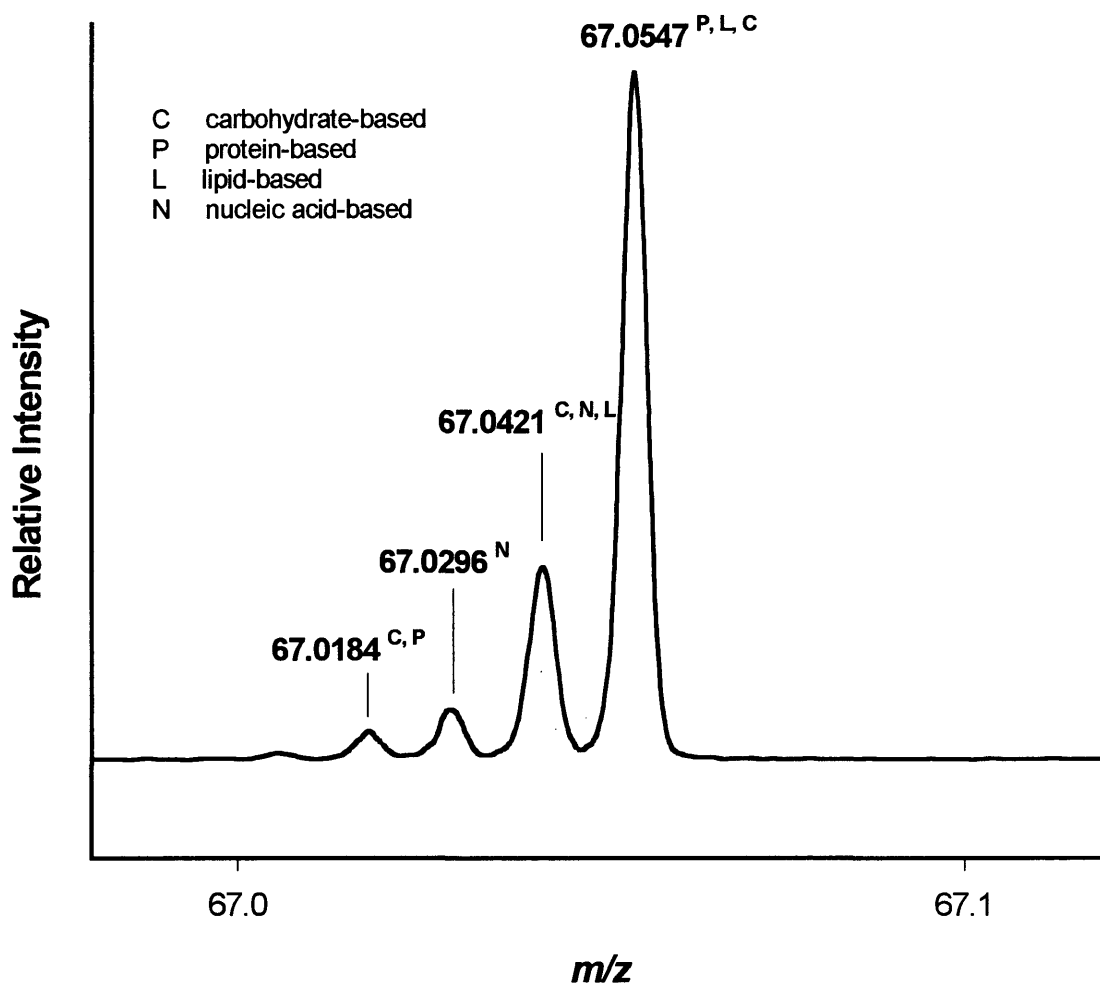


Figure 2.2. HR-DEI (R=10,000) mass spectrum of *m/z* 67 from *Brucella neotomae*.

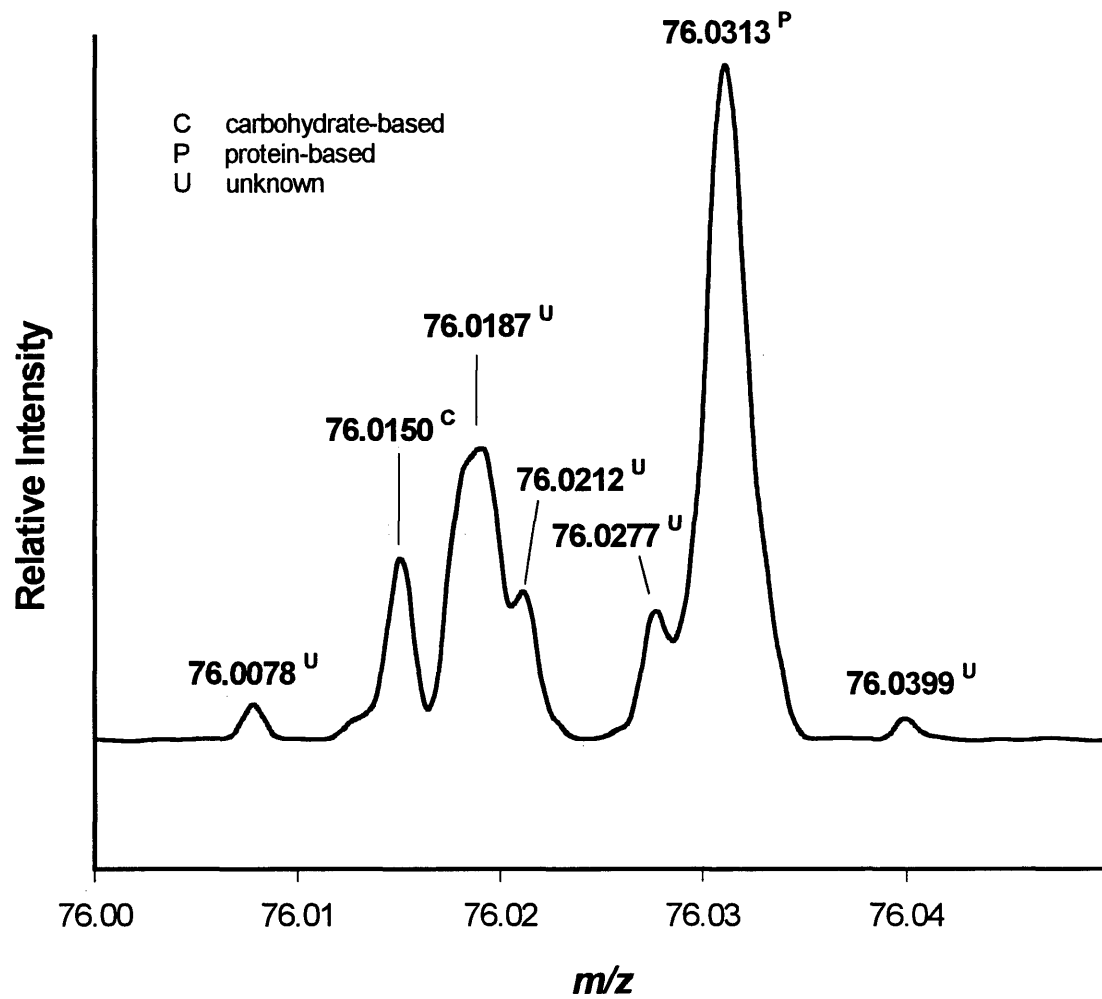


Figure 2.3. HR-DEI (R=30,000) mass spectrum of  $m/z$  76 from *Brucella neotomae*.

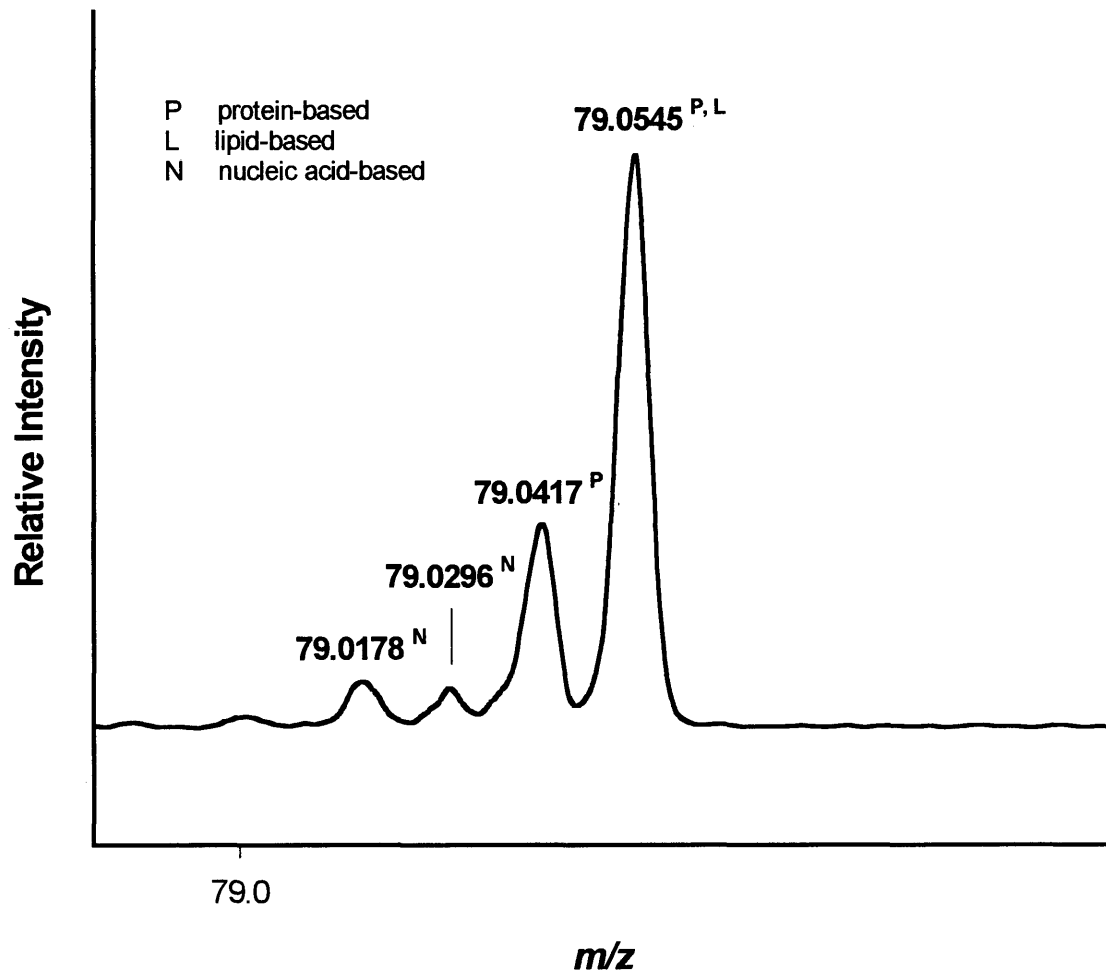


Figure 2.4. HR-DEI (R=10,000) mass spectrum of *m/z* 79 from *Brucella neotomae*.

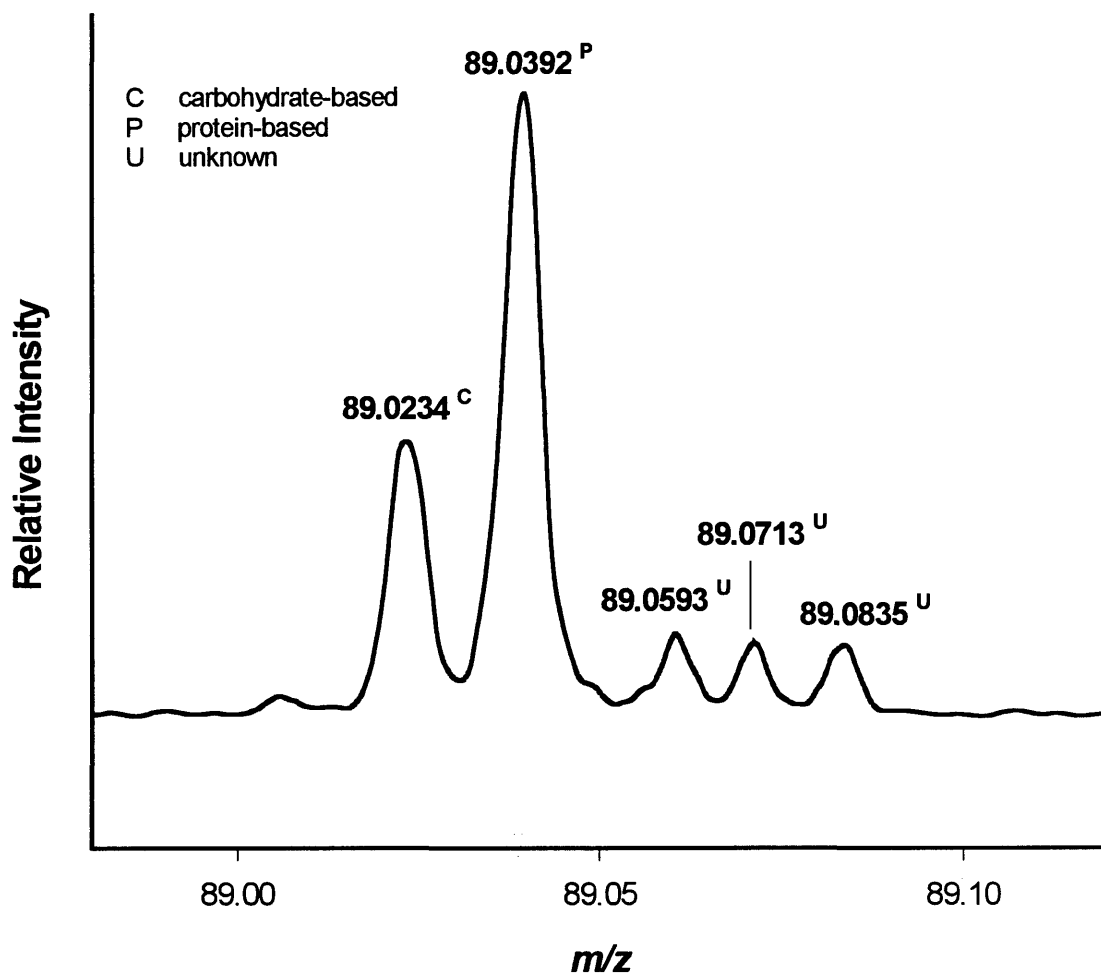


Figure 2.5. HR-DEI ( $R=10,000$ ) mass spectrum of  $m/z$  89 from *Brucella neotomae*.

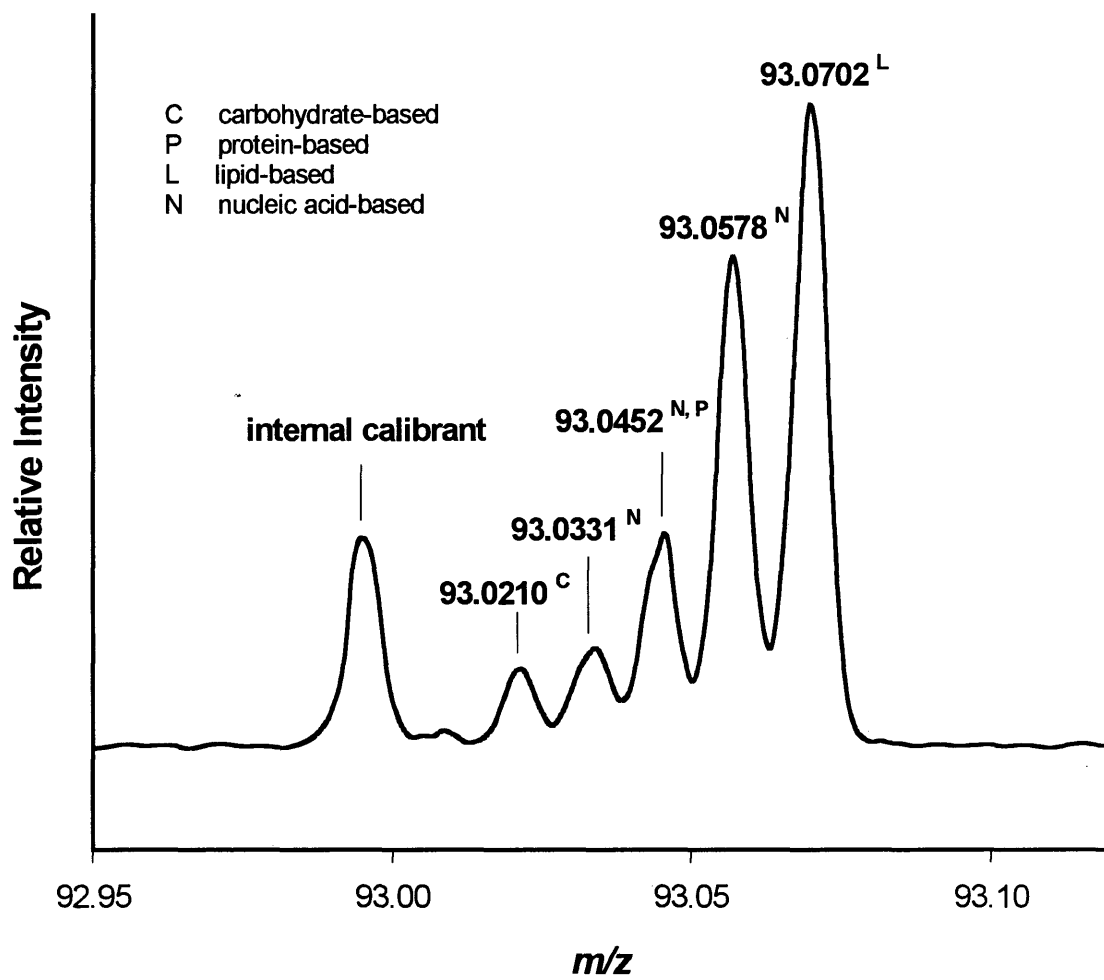


Figure 2.6. HR-DEI (R=10,000) mass spectrum of *m/z* 93 from *Brucella neotomae*.

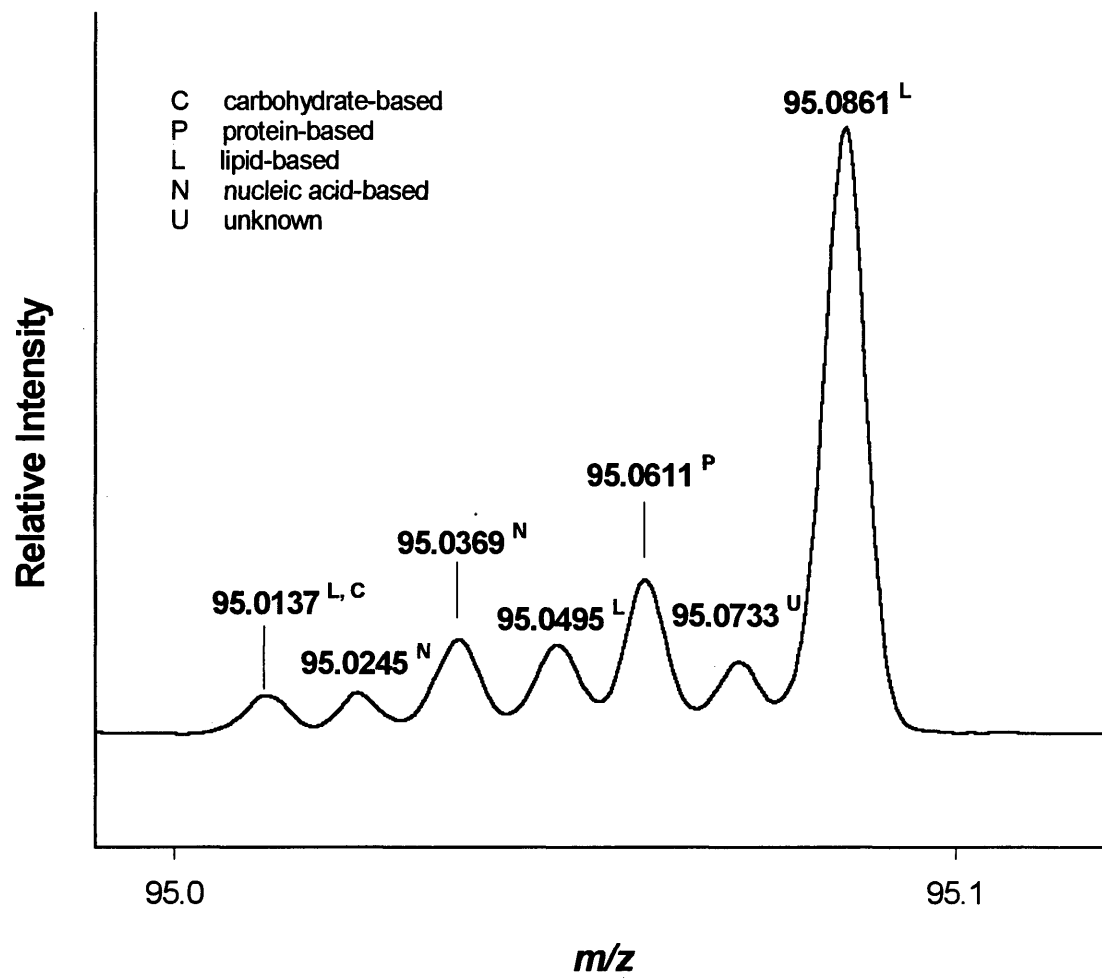


Figure 2.7. HR-DEI (R=10,000) mass spectrum of  $m/z$  95 from *Brucella neotomae*.

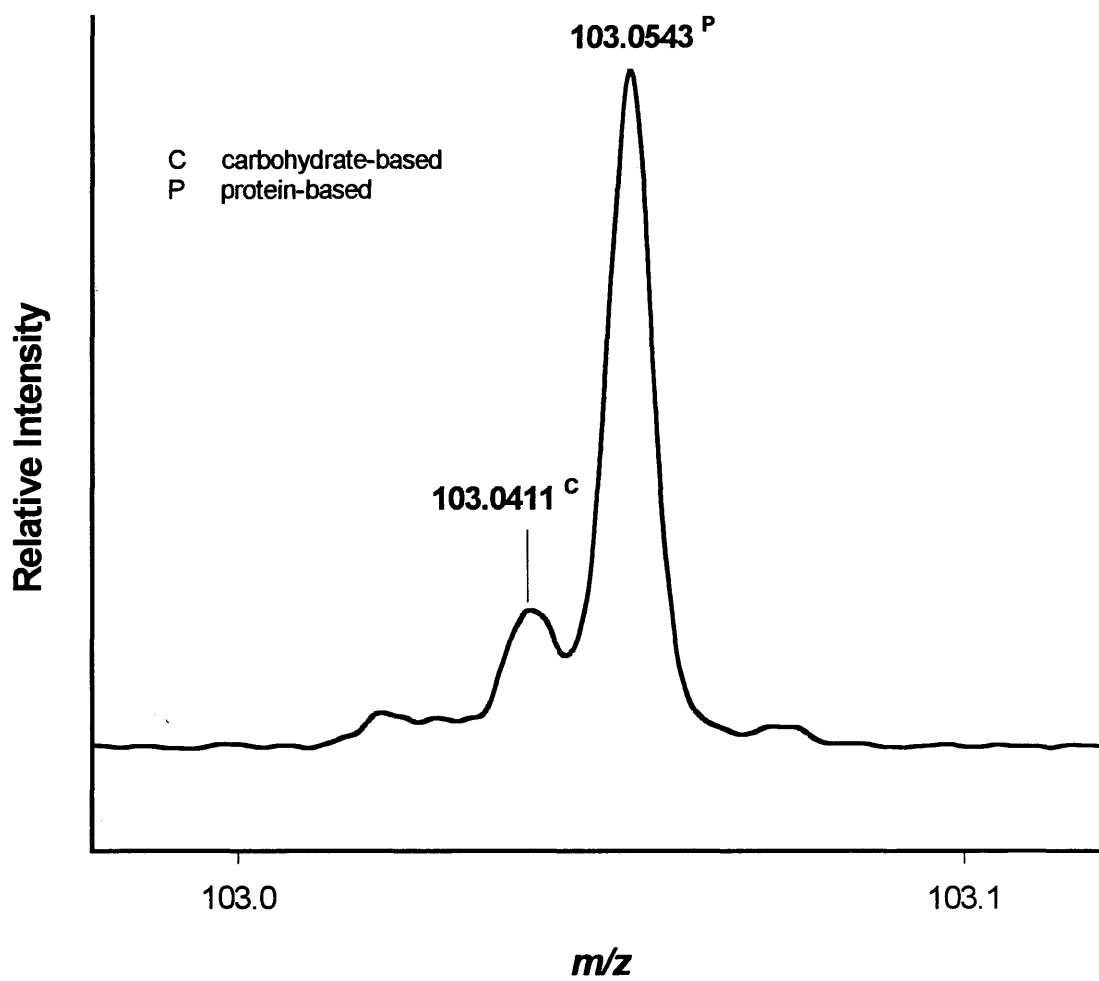


Figure 2.8. HR-DEI (R=10,000) mass spectrum of m/z 103 from *Brucella neotomae*.

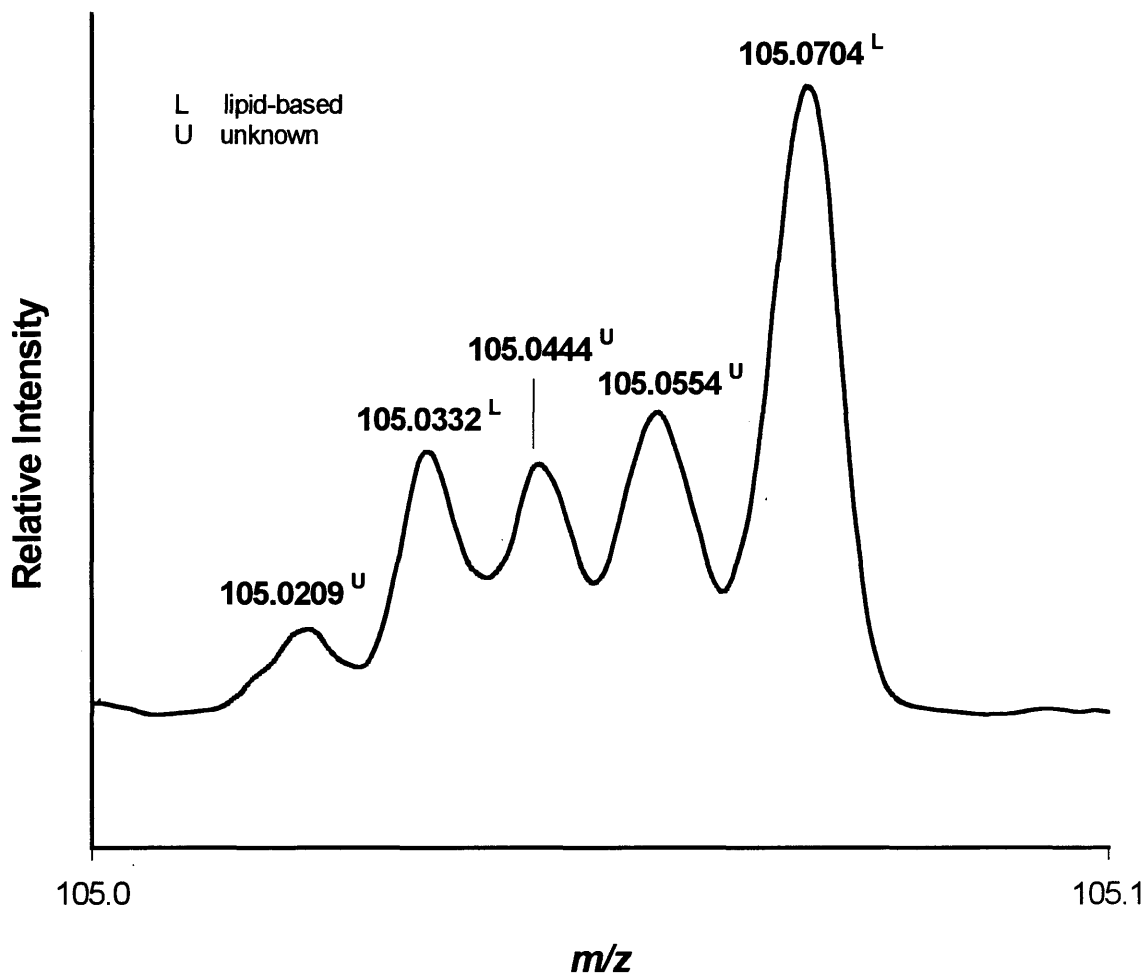


Figure 2.9. HR-DEI (R=10,000) mass spectrum of  $m/z$  105 from *Brucella neotomae*.

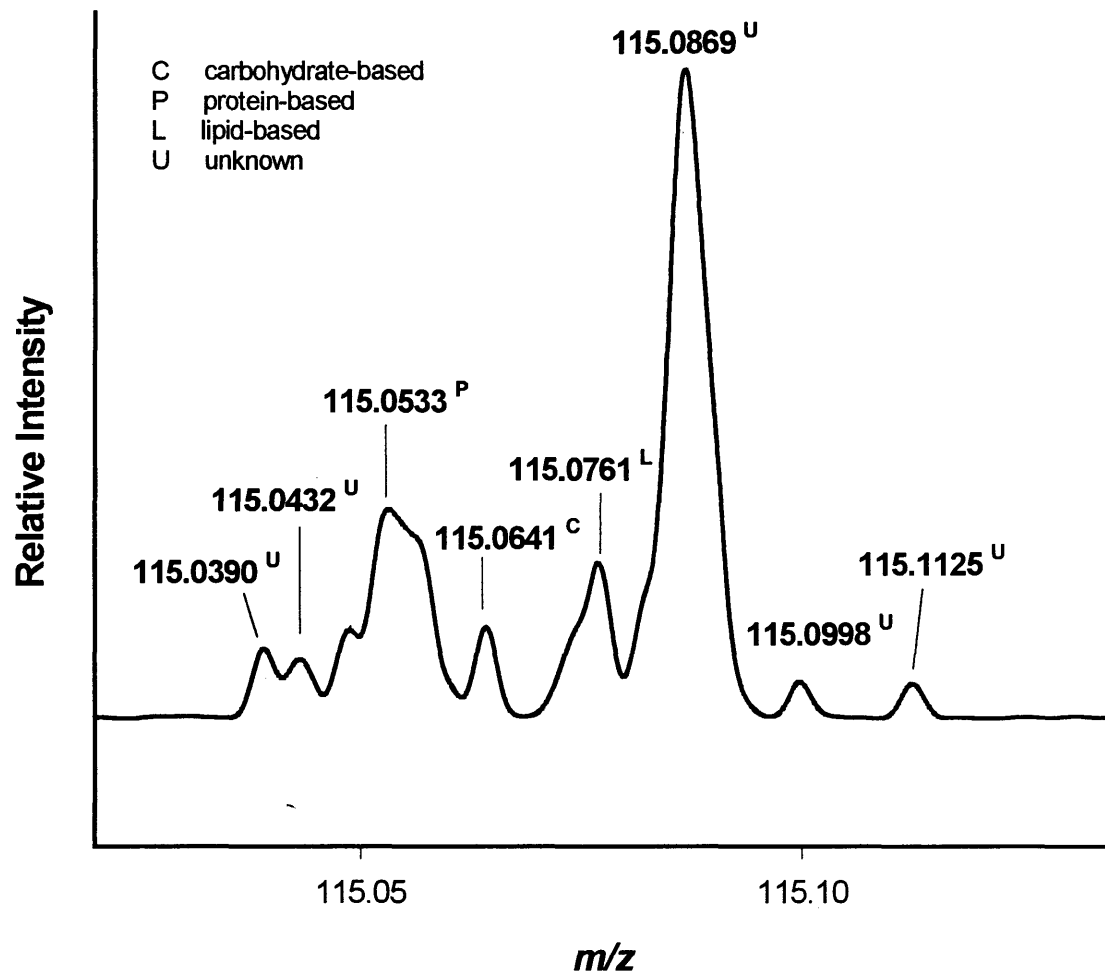


Figure 2.10. HR-DEI (R=30,000) mass spectrum of *m/z* 115 from *Brucella neotomae*.

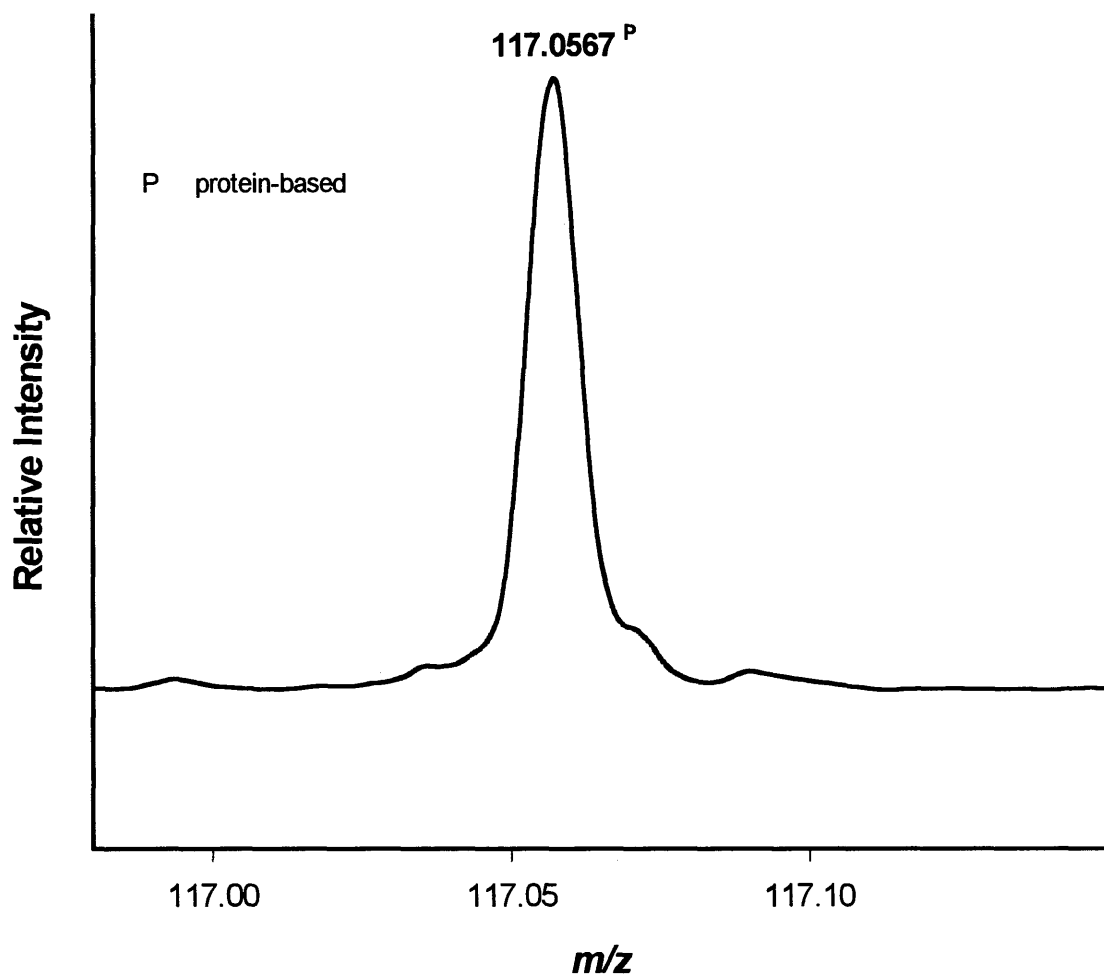


Figure 2.11. HR-DEI (R=10,000) mass spectrum of m/z 117 from *Brucella neotomae*.

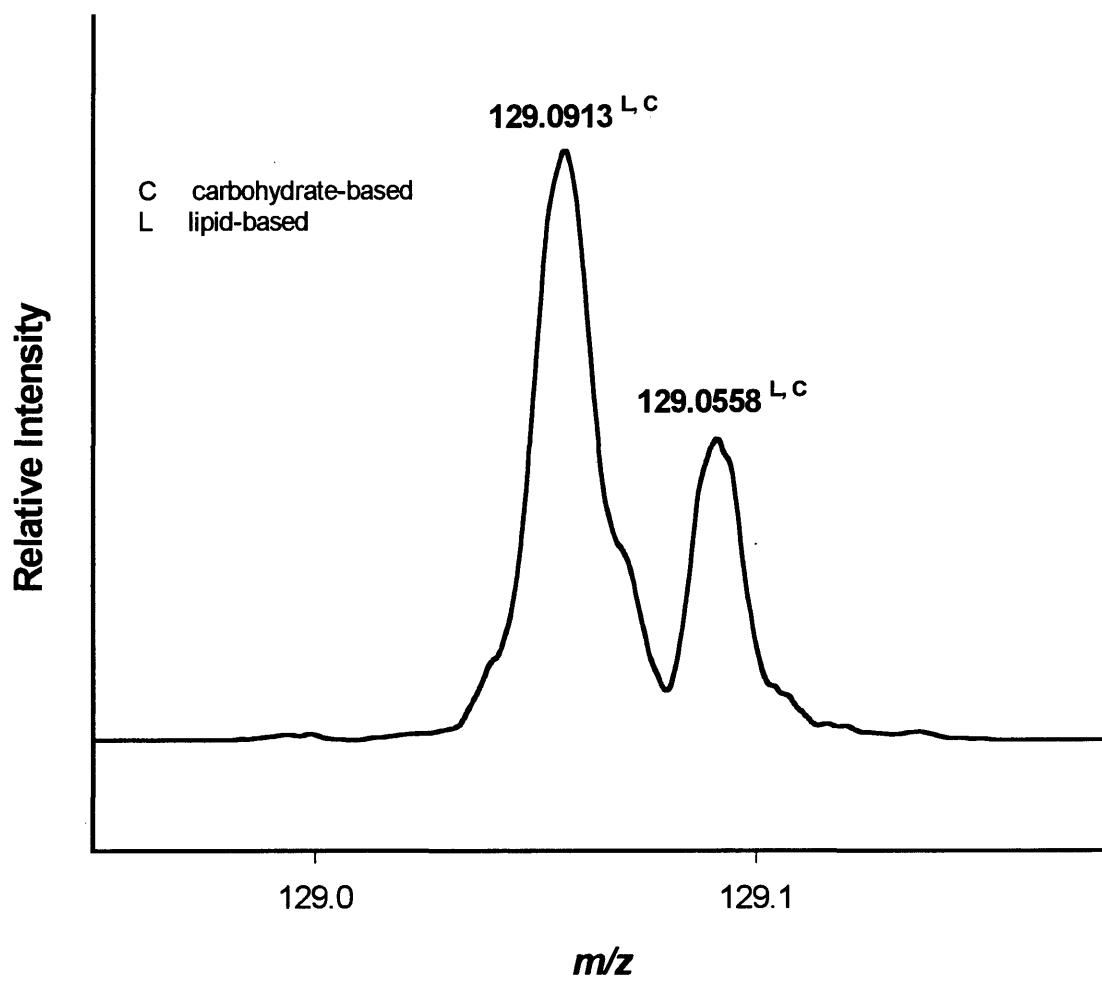


Figure 2.12. HR-DEI (R=10,000) mass spectrum of m/z 129 from *Brucella neotomae*.

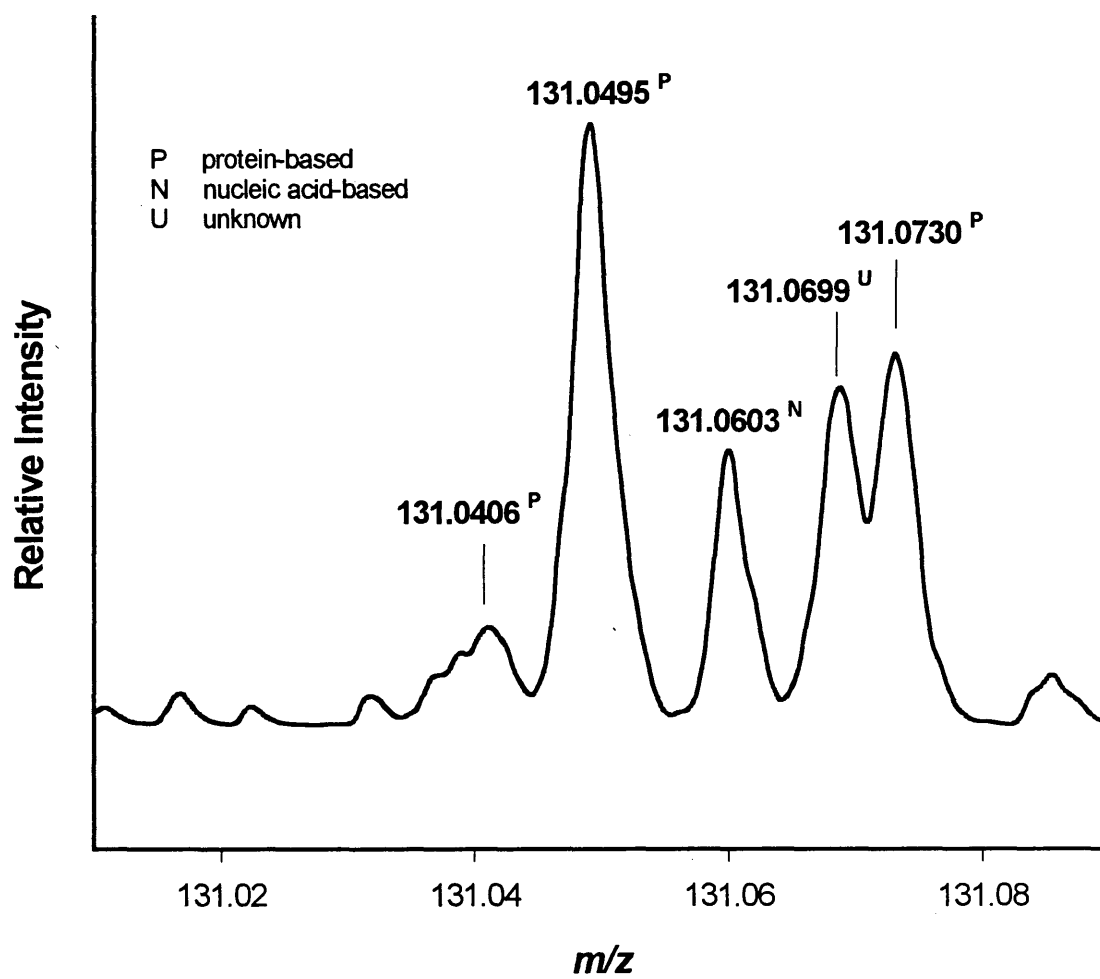


Figure 2.13. HR-DEI (R=30,000) mass spectrum of *m/z* 131 from *Brucella neotomae*.

assigned at this time. Upon review of the spectrum of each standard, only the standards that exhibited the biomarker ion under discussion will be listed. Therefore, if the standard is not listed, the biomarker ion was not observed in the spectrum of that standard, although all standards were analyzed for each biomarker ion. The product- and precursor-ion scans of the biomarker ions in *B. neotomae* are given in the Appendix.

### **Carbohydrate/Nucleic Acid –Based Biomarker Ions**

Pure (no trace of cellular constituents) carbohydrate or nucleic acid extracts are difficult to obtain from whole bacterial cells. Therefore, a collection of standards was chosen for analysis that represented the cellular content of sugars and nucleic acids. These standards (Table 2.2) were analyzed using the same conditions as in the analysis of the whole cell microorganism, and the peaks were compared to those found in the whole bacterial cells to determine biomarker origins. Table 2.3 summarizes the biomarker ions with proposed carbohydrate and/or nucleic acid origins.

#### **Biomarker m/z 67**

The peak cluster with nominal mass m/z 67 (Figure 2.2) is composed of four major contributing ions. In the spectra of standards listed in Table 2.2, all four ions were observed: m/z 67.0547 (C<sub>5</sub>H<sub>7</sub>), 67.0421 (C<sub>4</sub>H<sub>5</sub>N), 67.0296 (C<sub>3</sub>H<sub>3</sub>N<sub>2</sub>) and 67.0184 (C<sub>4</sub>H<sub>3</sub>O). M/z 67.0547 (C<sub>5</sub>H<sub>7</sub>) occurred predominantly in the spectrum of the lipopolysaccharide standard with minor contributions in the polysaccharide and muramic acid spectra. Fragmentation observed for m/z 67.0547 in the bacterium using HR-product-ion scan (R=10,000) produced product ions at m/z 41, 39 and 27. A typical product-ion scan is given in Figure 2.14. The origin of the m/z 67.0547 ion of the bacterium was examined using a precursor-ion scan, Figure 2.15. Figure 2.15 represents a typical precursor-ion scan. Major precursor ions included m/z 82, 94, 95, 96, 109, 110, 121, 123, 136, 137, 138, 150 and 151. This data, however, represents the origins of all of

Table 2.2. Standards used to represent the cellular content of nucleic acids and carbohydrates.

Nucleic Acid Standards	Carbohydrate Standards
Adenosine 5'-monophosphate (AMP) Thymidine 5'-monophosphate (TMP) Guanosine 5'-monophosphate (GMP) Cytidine 5'-monophosphate (CMP) Uridine 5'-monophosphate (UMP) Adenine Thymine Guanine Cytosine Uracil	Ribose Glucose Muramic acid N-acetylglucosamine Polysaccharide Lipopolysaccharide

Table 2.3. Biomarker ions with proposed carbohydrate and/or nucleic acid origins.

Nominal Mass	Empirical Formula	Calculated Mass	Measured Mass	Error (MMU)	(R+DB)
67	C <sub>5</sub> H <sub>7</sub>	67.0548	67.0547	-0.1	2.5
67	C <sub>4</sub> H <sub>5</sub> N	67.0422	67.0421	-0.1	3.0
67	C <sub>3</sub> H <sub>3</sub> N <sub>2</sub>	67.0296	67.0296	+0.0	3.5
67	C <sub>4</sub> H <sub>3</sub> O	67.0184	67.0184	+0.0	3.5
76	C <sub>2</sub> H <sub>4</sub> O <sub>3</sub>	76.0160	76.0150	-1.0	1.0
79	C <sub>4</sub> H <sub>3</sub> N <sub>2</sub>	79.0296	79.0296	+0.0	4.5
79	C <sub>3</sub> HN <sub>3</sub>	79.0170	79.0178	+0.8	5.0
89	C <sub>3</sub> H <sub>5</sub> O <sub>3</sub>	89.0239	89.0234	-0.5	1.5
93	C <sub>6</sub> H <sub>7</sub> N	93.0578	93.0578	+0.0	4.0
93	C <sub>5</sub> H <sub>5</sub> N <sub>2</sub>	93.0453	93.0452	-0.1	4.5
93	C <sub>4</sub> H <sub>3</sub> N <sub>3</sub>	93.0327	93.0331	+0.4	5.0
93	C <sub>5</sub> H <sub>3</sub> ON	93.0215	93.0210	-0.5	5.0
95	C <sub>5</sub> H <sub>5</sub> ON	95.0371	95.0369	-0.2	4.0
95	C <sub>4</sub> H <sub>3</sub> ON <sub>2</sub>	95.0245	95.0245	+0.0	4.5
95	C <sub>5</sub> H <sub>3</sub> O <sub>2</sub>	95.0133	95.0137	+0.4	4.5
103	C <sub>4</sub> H <sub>7</sub> O <sub>3</sub>	103.0395	103.0411	+1.6	1.5
115	C <sub>5</sub> H <sub>9</sub> O <sub>2</sub> N	115.0633	115.0641	+0.8	2.0
129	C <sub>7</sub> H <sub>13</sub> O <sub>2</sub>	129.0916	129.0913	-0.3	1.5
129	C <sub>6</sub> H <sub>9</sub> O <sub>3</sub>	129.0552	129.0558	+0.6	2.5
131	C <sub>8</sub> H <sub>7</sub> N <sub>2</sub>	131.0609	131.0603	-0.6	6.5

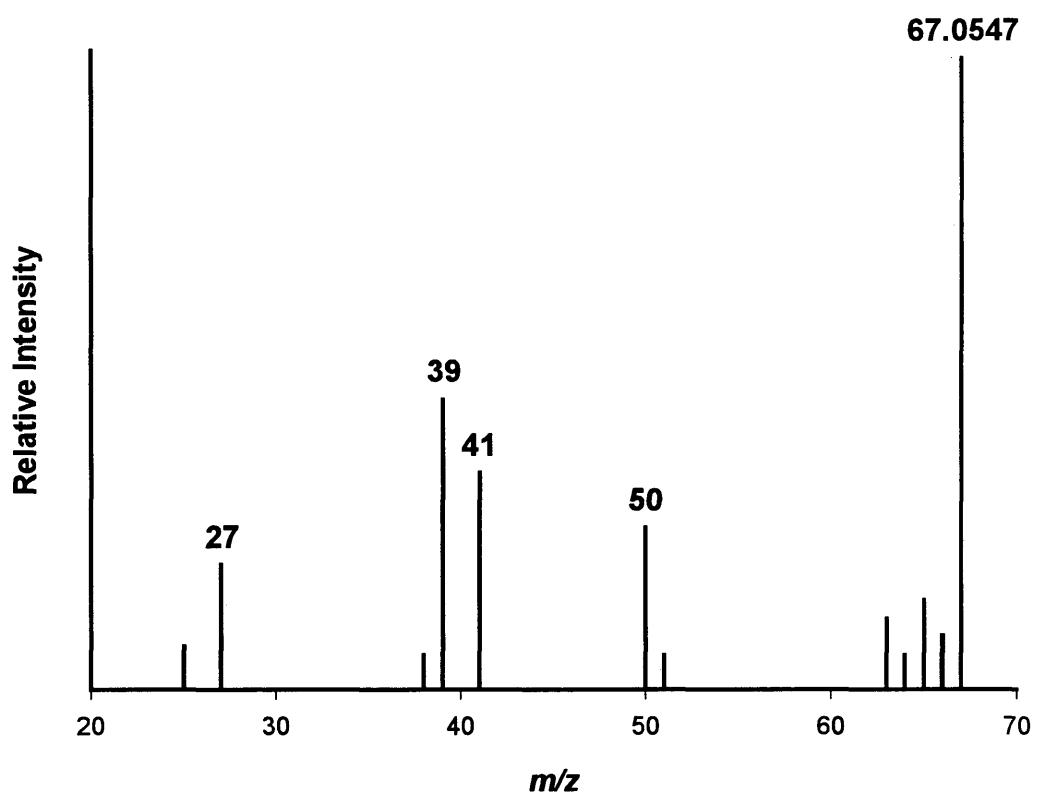


Figure 2.14. HR-DEI product ion mass spectrum of m/z 67.0547 from *Brucella neotomae*.

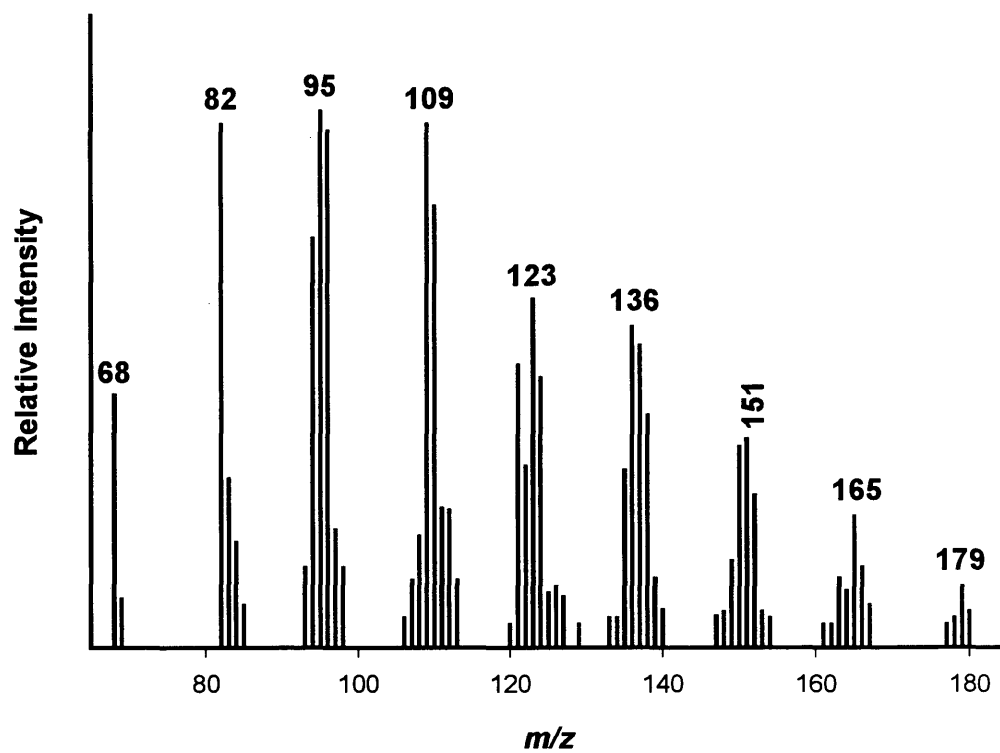


Figure 2.15. DEI precursor ion mass spectrum of  $m/z$  67 from *Brucella neotomae*.

the peaks in the  $m/z$  67 cluster due to the low resolution character of the precursor-ion scan. Attention has, for this reason, been focused on the ions with hydrocarbon origins as observed in pure standards (*i.e.* lipopolysaccharides). The precursor ion of  $m/z$  67.0547 in *B. neotomae* was found to be 95.0861 ( $C_7H_{11}$ ). The proposed pathway for hydrocarbon contributors of 67.0547 is given in Figure 2.16.

$M/z$  67.0421 ( $C_4H_5N$ ) shows similar fragmentation to  $m/z$  67.0547, with an additional fragment at  $m/z$  52. The molecule contains a nitrogen atom. The precursor ions of  $m/z$  67.0421 in the bacterium were found to be  $m/z$  95.0369 ( $C_5H_5ON$ ), which had precursors at  $m/z$  149.0586 ( $C_7H_7ON_3$ ),  $m/z$  163.0500 ( $C_8H_7O_2N_2$ ),  $m/z$  175.0508 ( $C_7H_5ON_5$ ) and  $m/z$  177.0640 ( $C_9H_9O_2N_2$ ).  $M/z$  149.0586 was identified as cytosine attached to a  $C_3H_2$  sugar fragment (51). This ion fragments further to  $m/z$  135.0432 ( $C_6H_5ON_3$ ) (52). Ions 163.0500 and 177.0640 are the bases uracil and thymine, respectively, attached to a  $C_4H_4$  sugar fragment (53).  $M/z$  177.0640 further decomposes to  $m/z$  150.0434 ( $C_7H_6O_2N_2$ ) and  $m/z$  83.0373 ( $C_4H_5ON$ ).  $M/z$  150.0434 was identified as thymine attached to a two carbon fragment from the sugar moiety and  $m/z$  83.0373 is a fragment of thymine (23). Guanine attached to a two carbon fragment from the sugar moiety has an exact mass of 175.0508 (51). This ion favorably decomposes to  $m/z$  151.0499 ( $C_5H_5ON_5$ ) (23). The assignment of the afore mentioned ions was based on exact mass measurements of both the standards and the whole cell microorganism correlated to existing literature values. That is, exact mass measurements for precursor ions were obtained by comparing ion masses of the bacterium with the standard. Subsequent product-ion scans confirmed the sameness of the ions (identical fragmentation pattern). Another precursor ion of  $m/z$  67.0421 was found to be  $m/z$  137.0703 ( $C_4H_{11}O_4N$ ).  $M/z$  137.0703 exists as a fragment of muramic acid as shown in Figure 2.17b. The proposed correlation map indicating the relationship among fragment ions in the DEI mass spectrum for nucleotides and muramic acid contributors of  $m/z$  67.0421 is given in Figure 2.18.

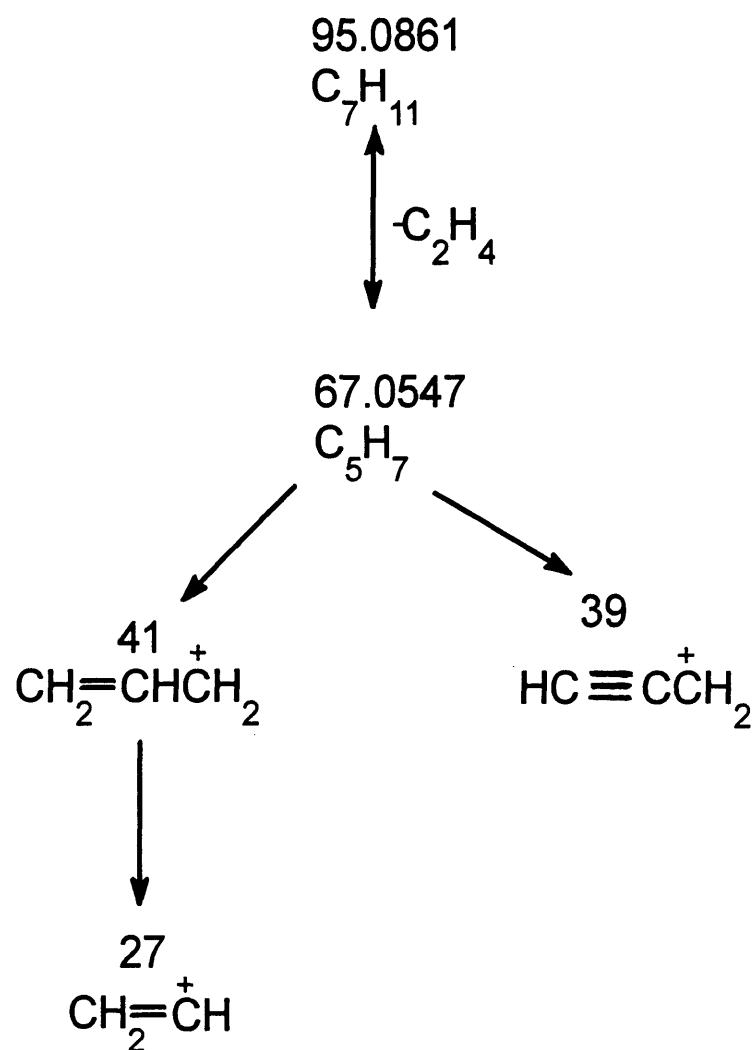


Figure 2.16. Proposed fragmentation pathway of m/z 67.0547 and m/z 95.0861.

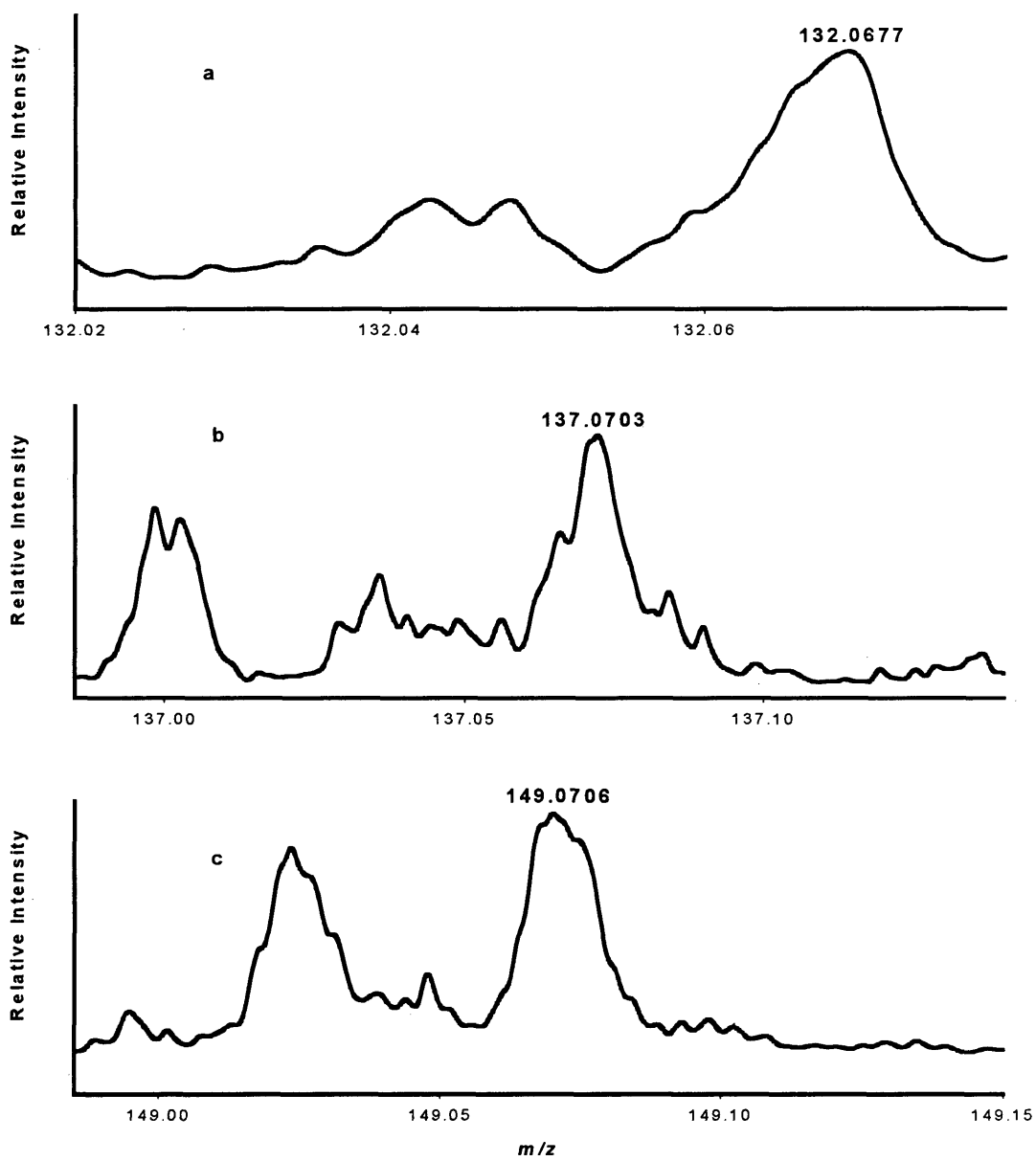


Figure 2.17. HR-DEI ( $R=10,000$ ) mass spectra of (a)  $m/z$  132, (b)  $m/z$  137 and (c)  $m/z$  149 from muramic acid.

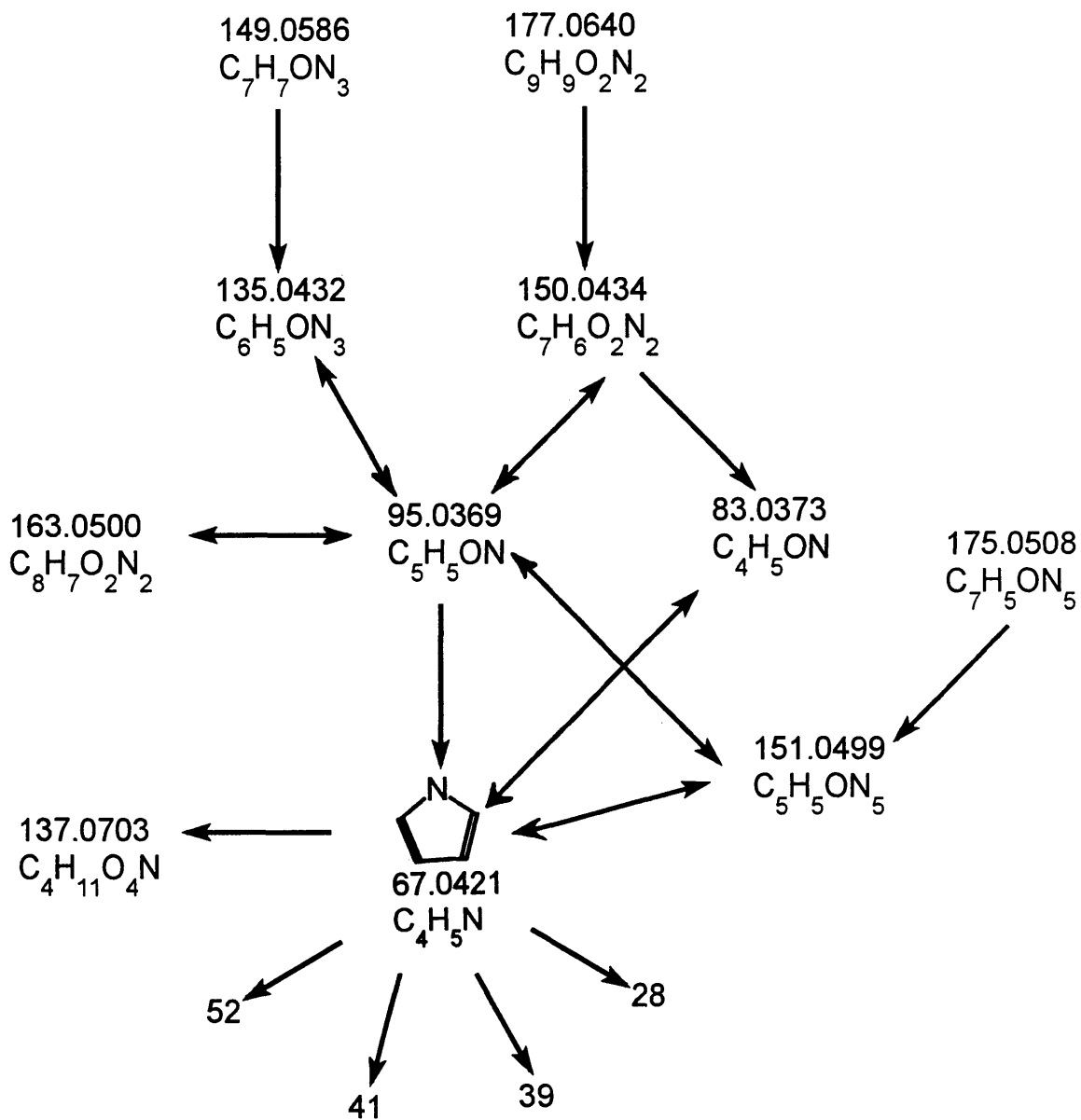


Figure 2.18. Proposed fragmentation pathway of  $m/z$  67.0421 and  $m/z$  95.0369.

Product ions of  $m/z$  67.0296 ( $C_3H_3N_2$ ) in *B. neotomae* were  $m/z$  40, 39, 38 and 28. The prominent peak at  $m/z$  40 indicates a HCN loss from  $m/z$  67.0296. A precursor ion was identified as  $m/z$  95.0245 ( $C_4H_3ON_2$ ), which has a precursor at  $m/z$  111.0436 ( $C_4H_5ON_3$ ). These two ions are due to the nitrogen base cytosine.  $M/z$  111.0436 is the molecular ion ( $M^+$ ) and  $m/z$  95.0245 is a decomposition product (loss of  $-NH_2$ ) (23). Additional precursor ions include  $m/z$  135.0544 ( $C_5H_5N_5$ ) and  $m/z$  108.0444 ( $C_4H_4N_4$ ) from the nitrogen base adenine,  $M^+$  and a decomposition product (loss of  $-HCN$ ), respectively (23). The assignment of these ions was based on exact mass measurements of cytosine, adenine and the bacterium. Proposed fragmentation patterns are shown in Figure 2.19.

Product ions at  $m/z$  39, 38 and 37 were observed for  $m/z$  67.0184 ( $C_4H_3O$ ) in *B. neotomae*.  $M/z$  67.0184 was significant in the mass spectrum of the polysaccharide standard with minor contributions in the spectra of the other carbohydrate and nucleotide standards. It was not, however, produced by the fragmentation of any nitrogen base standards. The precursor ions of  $m/z$  67.0184 in the whole cell microorganism were found to be  $m/z$  95.0137 ( $C_5H_3O_2$ ) and  $m/z$  96.0201 ( $C_5H_4O_2$ ), furfural. Ion 95.0137 is furfural minus a proton ( $M^+ - H$ ). Furfural is a furan derivative formed by rapid pyrolysis of carbohydrates (11).  $M/z$  110.0361, methyl furfural ( $C_6H_6O_2$ ) is another precursor ion of  $m/z$  67.0184. Sugars dehydrate and decompose to low mass ions making the assignment of higher mass origins difficult. Proposed structures and fragmentation patterns are shown in Figure 2.20.

### **Biomarker $m/z$ 76**

The  $m/z$  76 cluster (Figure 2.3) contains only one ion that was found in the ribose standard:  $m/z$  76.0150 ( $C_2H_4O_3$ ). The proposed fragmentation pathway given in Figure 2.21 for  $m/z$  76.0150 shows precursor ions that are observed in the NIST spectra of ribose;  $m/z$  132.0450 ( $C_5H_8O_4$ ),  $m/z$  119.0337 ( $C_4H_7O_4$ ),  $m/z$  103.0411 ( $C_4H_7O_3$ ) and 89.0234 ( $C_3H_5O_3$ ).

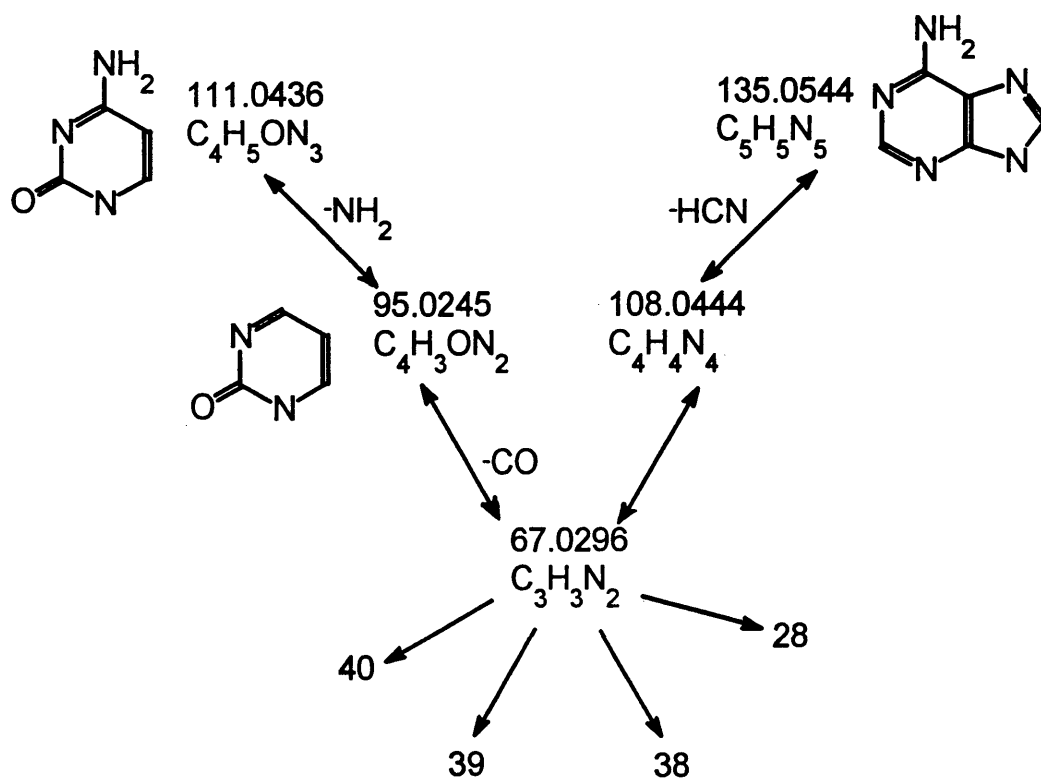


Figure 2.19. Proposed fragmentation pathway of  $m/z$  67.0296 and  $m/z$  95.0245.

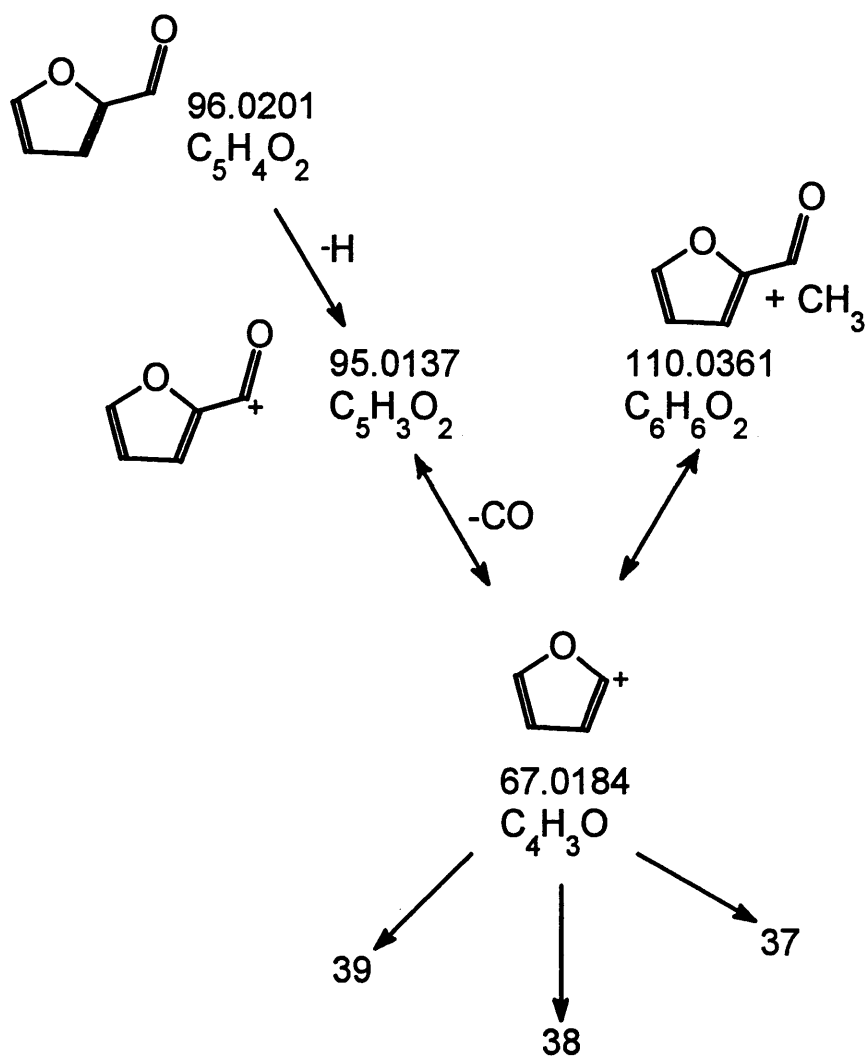


Figure 2.20. Proposed fragmentation pathway of m/z 67.0184 and m/z 95.0137.

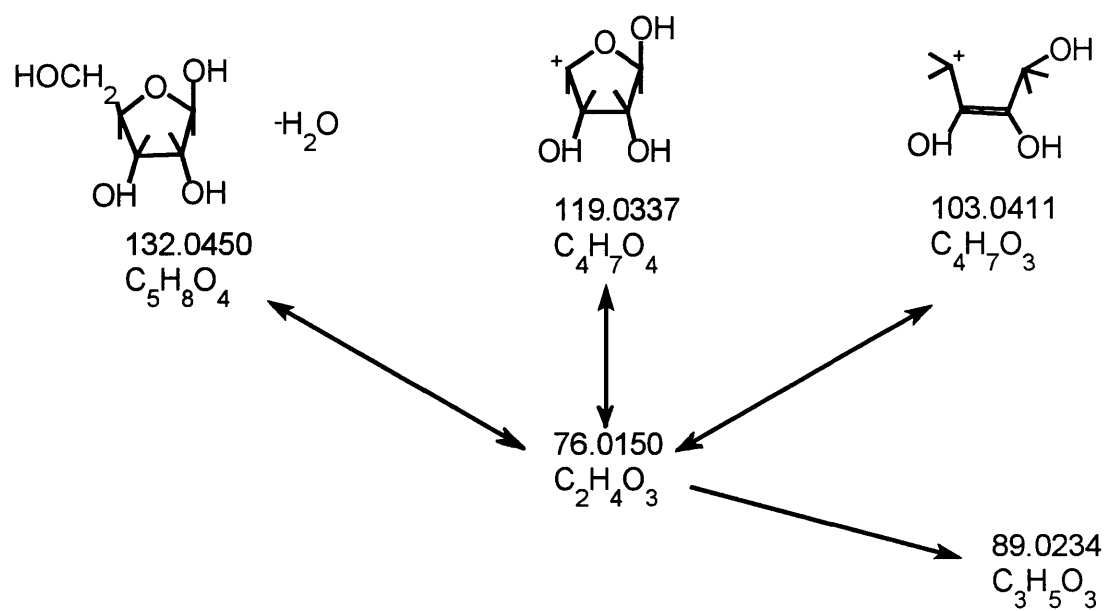


Figure 2.21. Proposed fragmentation pathway of m/z 76.0150, m/z 103.0411 and m/z 89.0234.

### Biomarker m/z 79

The peak cluster at m/z 79 (Figure 2.4) shows four distinguished peaks, two of which were observed in the spectra of the nucleic acid standards: m/z 79.0296 ( $C_4H_3N_2$ ) and 79.0178 ( $C_3HN_3$ ). M/z 79.0296 ( $C_4H_3N_2$ ) was identified as a fragment of CMP. Fragmentation of m/z 79.0296 in *B. neotomae* indicated product ions at m/z 53, 52, 51, 37 and 26. Precursor ions at m/z 191.0703 ( $C_9H_9O_2N_3$ ), m/z 162.0661 ( $C_8H_8ON_3$ ), m/z 149.0586 ( $C_7H_7ON_3$ ), m/z 148.0511 ( $C_7H_6ON_3$ ) and m/z 95.0245 ( $C_4H_3ON_2$ ) were observed for m/z 79.0296. All of these ions originate from CMP in the bacterium. Ion 191.0703 was identified as the base cytosine plus the sugar moiety, while m/z 162.0661, m/z 149.0586 and m/z 148.0511 were identified as cytosine attached to sugar fragments (23, 51, 53). The assignment of these ions was based on exact mass measurements of CMP and the whole cell microorganism. The proposed decomposition pattern of m/z 79.0296 is given in Figure 2.22.

The product spectra of m/z 79.0178 ( $C_3HN_3$ ) in *B. neotomae* shows fragmentation to m/z 53, 51, 50, 49 and 48 with m/z 51 being the most intense. M/z 79.0178 was predominant in the spectrum of the guanine standard, but was not observed in the spectra of the other standards listed in Table 2.2. M/z 151.0499 ( $C_5H_5ON_5$ ), m/z 135.0318 ( $C_5H_3ON_4$ ) and m/z 108.0444 ( $C_4H_4N_4$ ) were observed in the precursor-ion scan of m/z 79.0178 for *B. neotomae*. These precursor ions support guanine origins for m/z 79.0178 (23) and are shown in Figure 2.23. Once again, the assignment of these ions was based on exact mass measurements of guanine and the whole cell microorganism.

### Biomarker m/z 89

The m/z 89 cluster contains five peaks (Figure 2.5), of which one was found in the spectra of all the carbohydrate standards, particularly ribose: m/z 89.0234 ( $C_3H_5O_3$ ). The four other peaks were not produced by the fragmentation of any of the standards listed in Table 2.2 and will therefore forego discussion. The precursor ions of m/z 89.0234 in *B. neotomae* were found to be m/z 103.0411 ( $C_4H_7O_3$ ) and m/z 117.0567

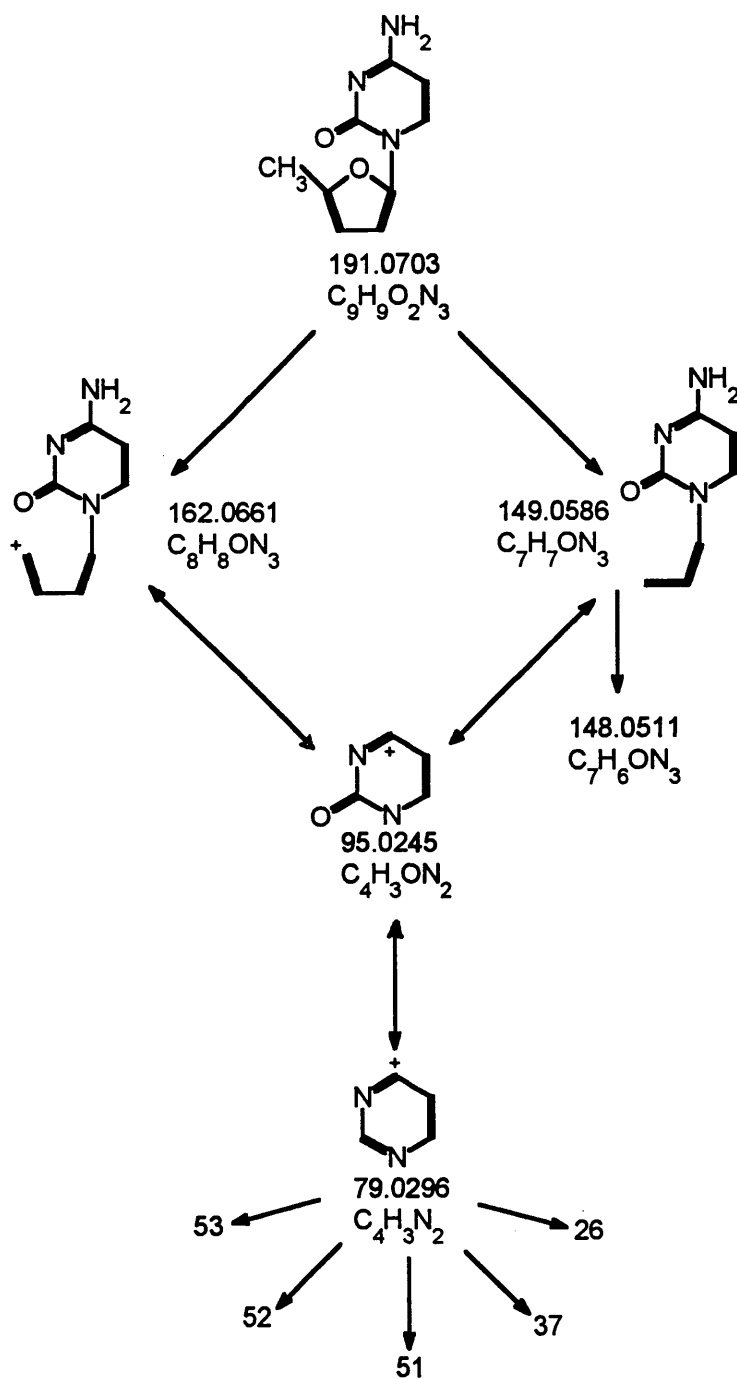


Figure 2.22. Proposed fragmentation pathway of  $m/z$  79.0296 and  $m/z$  95.0245.

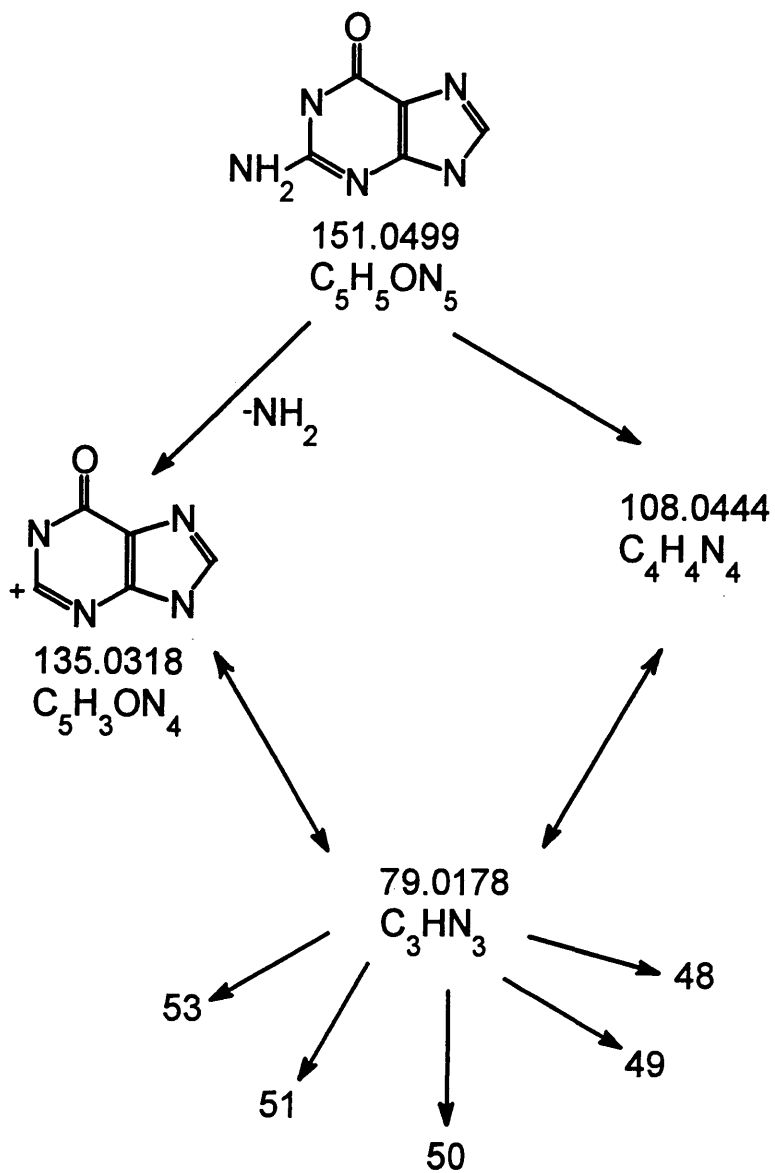


Figure 2.23. Proposed fragmentation pathway of  $m/z$  79.0178.

(C<sub>5</sub>H<sub>9</sub>O<sub>3</sub>), common sugar fragments. The lack of other precursor ions in the spectrum strongly supports carbohydrate origins for m/z 89.0234.

### **Biomarker m/z 93**

The peak profile pictured in Figure 2.6 shows five major contributors to the nominal mass 93. The peak at m/z 92.9953 is an internal calibrant peak. In the spectra of the nucleic acid and carbohydrate standards listed in Table 2.2, four of these peaks were observed: m/z 93.0578 (C<sub>6</sub>H<sub>7</sub>N), 93.0452 (C<sub>5</sub>H<sub>5</sub>N<sub>2</sub>), 93.0331 (C<sub>4</sub>H<sub>3</sub>N<sub>3</sub>) and 93.0210 (C<sub>5</sub>H<sub>3</sub>ON). The fragmentation observed for m/z 93.0578 (C<sub>6</sub>H<sub>7</sub>N) in the bacterium indicated product ions at m/z 78, 65, 64, 52, 51, 50, 39 and 38. The precursor ions of m/z 93.0578 were found to be m/z 162.0661 (C<sub>8</sub>H<sub>8</sub>ON<sub>3</sub>) and m/z 191.0703 (C<sub>9</sub>H<sub>9</sub>O<sub>2</sub>N<sub>3</sub>). These ions originated from CMP (53) as discussed previously. Another precursor ion of m/z 93.0578 was m/z 163.0500 (C<sub>8</sub>H<sub>7</sub>O<sub>2</sub>N<sub>2</sub>), the base uracil attached to a C<sub>4</sub>H<sub>4</sub> sugar fragment (51). M/z 93.0578 was produced by the fragmentation of CMP and UMP. It was not produced by the fragmentation of the other standards listed in Table 2.2. Therefore, the assignment of precursor ions was based on exact mass measurements of CMP, UMP and the whole cell microorganism. A proposed decomposition pattern of m/z 93.0578 is shown in Figure 2.24.

The fragmentation of m/z 93.0452 (C<sub>5</sub>H<sub>5</sub>N<sub>2</sub>) in *B. neotomae* was markedly different than the fragmentation of m/z 93.0578. Fragment ions of m/z 93.0452 included m/z 79, 66 and 39. Precursor ions at m/z 191.0703 (C<sub>9</sub>H<sub>9</sub>O<sub>2</sub>N<sub>3</sub>), m/z 162.0661 (C<sub>8</sub>H<sub>8</sub>ON<sub>3</sub>), m/z 149.0586 (C<sub>7</sub>H<sub>7</sub>ON<sub>3</sub>) and m/z 148.0511 (C<sub>7</sub>H<sub>6</sub>ON<sub>3</sub>) were observed for m/z 93.0452 in *B. neotomae*. These ions originate from CMP (23, 52, 53) in the bacterium. M/z 93.0452 was produced by the fragmentation of CMP, and was not produced by the fragmentation of the other standards listed in Table 2.2. Since CMP fragments by several mechanisms, two ions at nominal mass 93 are associated with CMP.

The nitrogen base adenine is suggested as being the predominant source of m/z 93.0331 (C<sub>4</sub>H<sub>3</sub>N<sub>3</sub>), since this ion was not observed in the spectra of the other standards

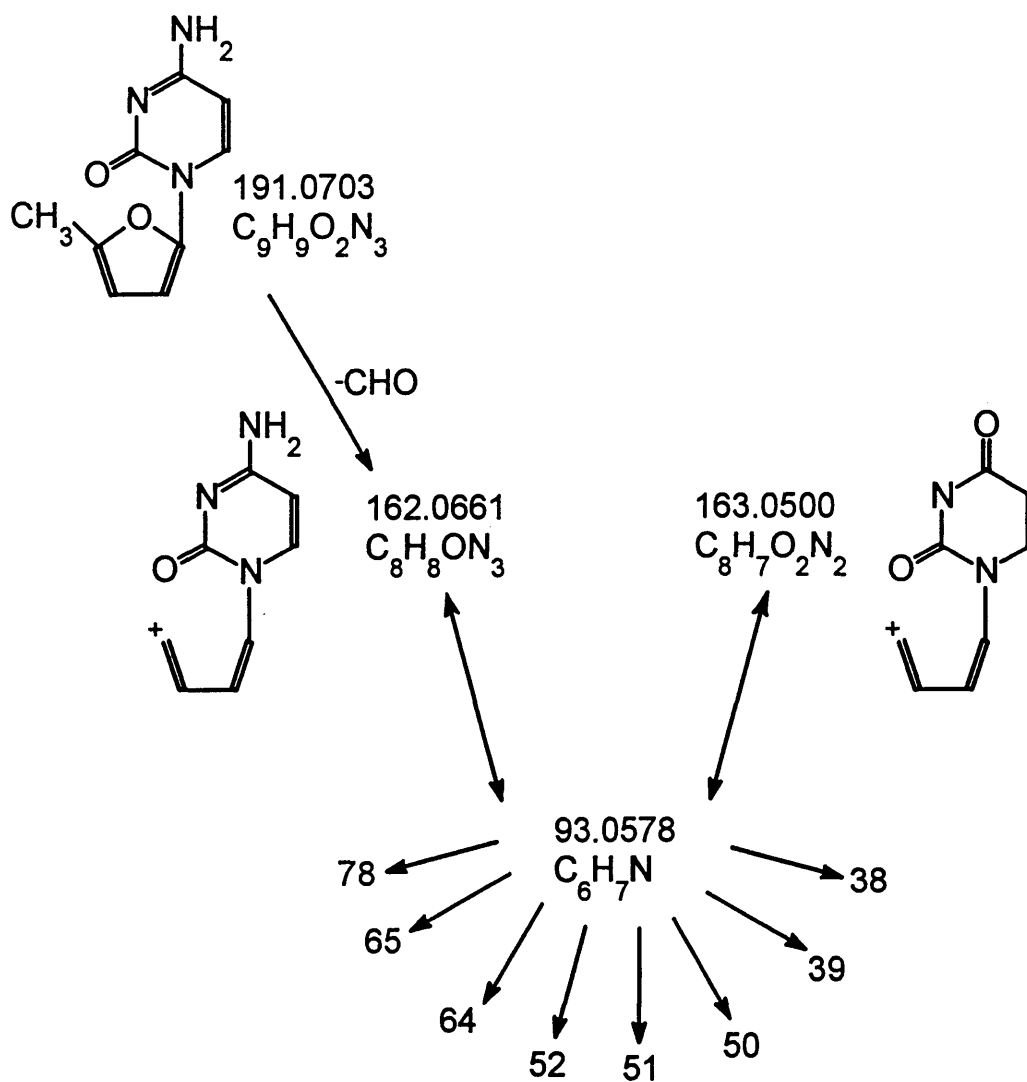


Figure 2.24. Proposed fragmentation pathway of  $m/z$  93.0578.

listed in Table 2.2. Fragment ions of  $m/z$  93.0331 include  $m/z$  66, 65 and 39, with  $m/z$  65 being the most intense (sequential loss of H and HCN). Intense precursor ions in *B. neotomae* at  $m/z$  135.0544 ( $C_5H_5N_5$ ) and  $m/z$  108.0444 ( $C_4H_4N_4$ ), which are reported as adenine ions, support adenine origins (23). Since  $m/z$  93.0331 was produced solely by the fragmentation of adenine, the assignment of precursor ions was based on exact mass measurements of adenine and the whole cell microorganism data.

Product ions at  $m/z$  79, 65, 64, 49 and 38 were observed for  $m/z$  93.0210 ( $C_5H_3ON$ ) in *B. neotomae*. This ion was observed in the muramic acid standard, but was not seen in the spectra of the other standards listed in Table 2.2. The precursor ions of  $m/z$  93.0210 in *B. neotomae* were found to be  $m/z$  149.0706 ( $C_5H_{11}O_4N$ ) and  $m/z$  132.0677 ( $C_5H_{10}O_3N$ ). These ions were observed previously in the HR-DEI spectrum of muramic acid as shown in Figure 2.17a and Figure 2.17c.

### **Biomarker $m/z$ 95**

The peak cluster with nominal mass  $m/z$  95 (Figure 2.7) is composed of seven major contributing peaks, three of which are present in the nucleic acid and/or carbohydrate standards:  $m/z$  95.0369 ( $C_5H_5ON$ ), 95.0245 ( $C_4H_3ON_2$ ) and 95.0137 ( $C_5H_3O_2$ ).  $m/z$  95.0369 ( $C_5H_5ON$ ) was significant in the mass spectra of CMP and GMP with minor contributions in the spectra of UMP, TMP, AMP and muramic acid. Fragment ions of  $m/z$  95.0369 in the bacterium include  $m/z$  67, 52, 39 and 38. The precursor ions of  $m/z$  95.0369 in *B. neotomae* along with a fragmentation map indicating the relationship among the nucleotide ions has been discussed and is presented in Figure 2.18.

Product ions of  $m/z$  95.0245 ( $C_4H_3ON_2$ ) in the whole cell microorganism include 69, 68, 67, 54, 40 and 27. Prominent peaks at  $m/z$  69 and 68 indicate a CN and HCN loss, respectively. The origin of the  $m/z$  95.0245 ion was examined using a precursor-ion scan. The precursor ion was found to be  $m/z$  111.0436 ( $C_4H_5ON_3$ ). Furthermore, ion 95.0245 was observed exclusively in the spectrum of the cytosine and CMP standards;

evidence that  $m/z$  95.0245 originates from cytosine (23, 51).  $M/z$  95.0245 was not produced by the fragmentation of the other standards listed in Table 2.2, therefore, the assignment of the precursor ion was based on exact mass measurements of cytosine, CMP and the bacterium. The fragmentation has been shown in Figures 2.19 and 2.22.

The HR product-ion scan of  $m/z$  95.0137 ( $C_5H_3O_2$ ) in *B. neotomae* indicated fragment ions of  $m/z$  67, 66, 53, 39, 38 and 37. This ion was produced by the fragmentation of all the carbohydrate standards listed in Table 2.2, but was not produced by the fragmentation of any of the nucleic acid standards.  $M/z$  95.0137 is furfural minus a hydrogen atom ( $M^+ - H$ ). As stated previously, furfural is a furan derivative formed by rapid pyrolysis of carbohydrates (11). The fragmentation pathway was previously shown in Figure 2.20.

### **Biomarker $m/z$ 103**

The spectrum of  $m/z$  103 (Figure 2.8) shows a cluster of two major contributors. In the spectra of all carbohydrate standards, one peak was always observed:  $m/z$  103.0411 ( $C_4H_7O_3$ ). Product ions at  $m/z$  89, 88, 76, 75, 74, 73, 52 and 50 were observed for  $m/z$  103.0411 in *B. neotomae*. Precursor ions include the sugar peaks at  $m/z$  132.0450 ( $C_5H_8O_4$ ) and  $m/z$  119.0337 ( $C_4H_7O_4$ ) (33).  $M/z$  103.0411 was not observed in the spectra of the nucleic acid standards listed in Table 2.2. Therefore, the assignment of precursor ions was based on exact mass measurements of the carbohydrate standards and the whole cell microorganism data. The proposed fragmentation pattern has been shown in Figure 2.21.

### **Biomarker $m/z$ 115**

Of the peaks found in the  $m/z$  115 cluster shown in Figure 2.10, only the peak at  $m/z$  115.0641 ( $C_5H_9O_2N$ ) was observed in the carbohydrate standard, N-acetylglucosamine. The precursor ions of  $m/z$  115.0641 in *B. neotomae* include  $m/z$  143.0598 ( $C_6H_9O_3N$ ),  $m/z$  185.0711 ( $C_8H_{11}O_4N$ ) and  $m/z$  186.0788 ( $C_8H_{12}O_4N$ ). These

ions are fragments of N-acetylglucosamine (NAG) as measured from the pure standard (Figure 2.25). The decomposition of NAG ( $C_8H_{15}O_6N$ ) under DEI conditions involves the loss of water to produce fragments  $m/z$  185.0711 and  $m/z$  186.0788 followed by further fragmentation to  $m/z$  143.0598.

### **Biomarker $m/z$ 129**

The  $m/z$  129 cluster (Figure 2.12) contains two peaks: 129.0913 ( $C_7H_{13}O_2$ ) and 129.0558 ( $C_6H_9O_3$ ), both of which were observed in the lipopolysaccharide standard. Neither of these ions was produced by the fragmentation of any of the other standards listed in Table 2.2. Product ions of  $m/z$  129.0913 in the bacterium include  $m/z$  95, 87, 86, 67, 55, 54, 43, 41, 39 and 27.  $M/z$  129.0913 was, however, observed in fatty acid standards; therefore, it must originate from the fatty acid portion of the lipopolysaccharide. The presence of acylium ions  $[RCO]^+$  and acylium ion adducts  $[RCO+74]^+$  as precursor ions support this assignment. The mechanism of formation of acylium ions and their adducts has been previously described (42).

$M/z$  129.0558 ( $C_6H_9O_3$ ) showed similar fragmentation, with intense fragments at  $m/z$  112, 84, and 44. Again, this ion was observed in fatty acid standards. As fatty acids undergo several fragmentation mechanisms, the precursor ions of  $m/z$  129.0558 were also found to be  $m/z$  338.2801 ( $C_{21}H_{38}O_3$  from C18:1) and  $m/z$  352.2972 ( $C_{22}H_{40}O_3$  from C19:1). The assignment of the afore mentioned ions was based on exact mass measurements of both the lipopolysaccharide standard and *B. neotomae* data.

### **Biomarker $m/z$ 131**

Of the peaks found in the  $m/z$  131 cluster shown in Figure 2.13, only the peak at  $m/z$  131.0603 ( $C_8H_7N_2$ ) was observed in the spectra of the standards listed in Table 2.2.  $M/z$  131.0603 ( $C_8H_7N_2$ ) was produced by the fragmentation of CMP and UMP. Precursor ions of  $m/z$  131.0603 in the whole cell microorganism include  $m/z$  148.0632 ( $C_8H_8ON_2$ ), which has a precursor at  $m/z$  191.0703 ( $C_9H_9O_2N_3$ ).  $M/z$ s 148.0632 and

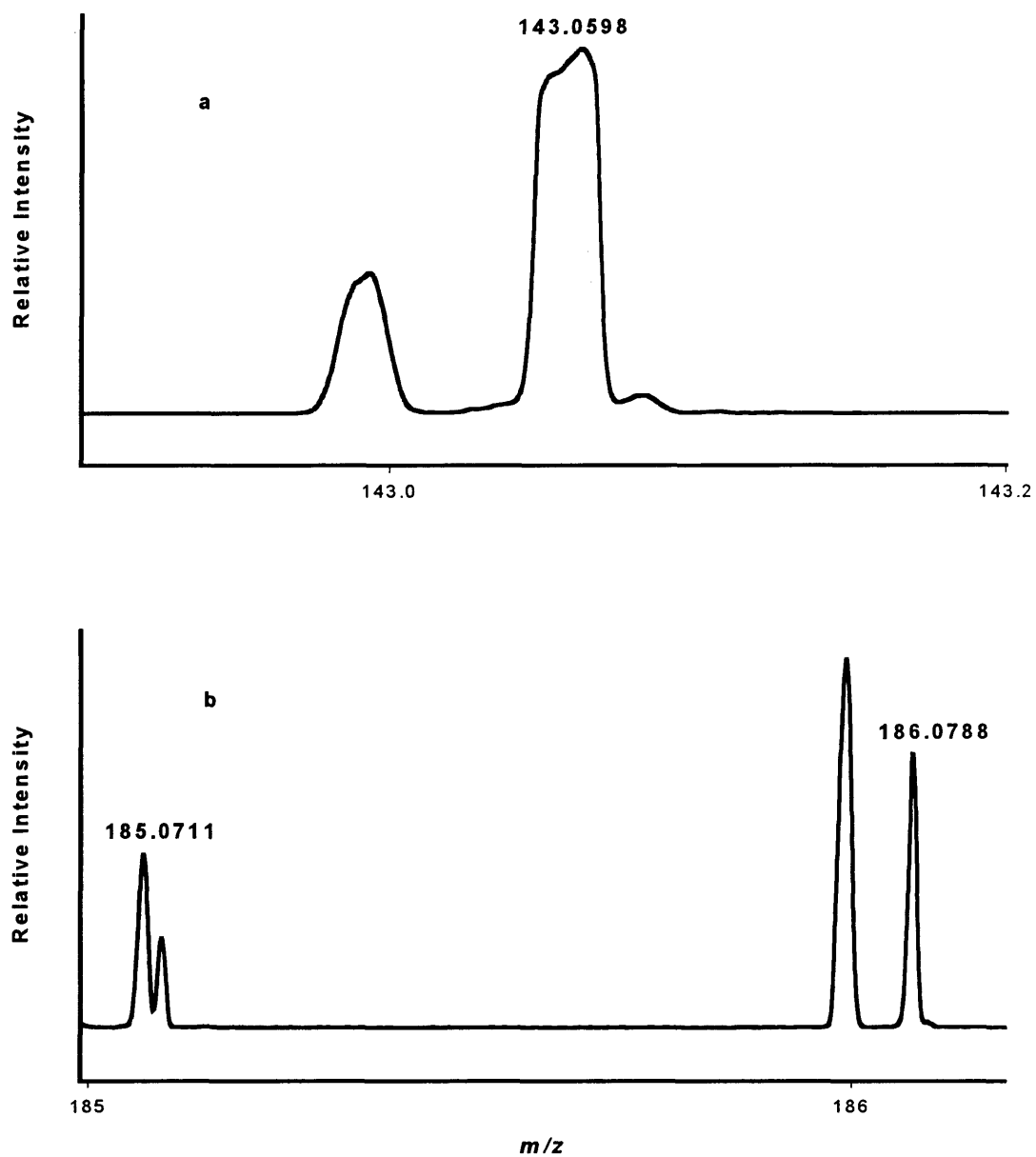


Figure 2.25. HR-DEI ( $R=10,000$ ) mass spectra of (a)  $m/z$  143 and (b)  $m/z$  185 and  $m/z$  186 from N-acetylglucosamine (NAG).

191.0703 are ions associated with CMP (23, 53). Another precursor ion of  $m/z$  131.0603 in *B. neotomae* was found to be  $m/z$  192.0537 ( $C_9H_8O_3N_2$ ). This ion is the base uracil attached to a dehydrated sugar moiety (23). As  $m/z$  131.0603 was produced solely by the fragmentation of CMP and UMP, the assignment of the precursor ions was based on exact mass measurements of CMP, UMP and the bacterium.

### **Protein-Based Biomarker Ions**

Protein extracts were obtained from *B. neotomae*. These extracts were not pure (*i.e.* they contained small fractions of other cellular constituents). Therefore, the twenty common amino acids listed in Table 2.1 were analyzed as was a pure (essentially fatty acid free) albumin sample. The albumin sample was used in an attempt to simulate the common fragmentation mechanism of diketopiperazine (DKP) formation (37-39). The standards and protein extracts were analyzed using the same conditions as in the analysis of the whole cell microorganism, and the peaks were compared to those found in the bacterium to determine biomarker origins. Table 2.4 summarizes the biomarker ions with proposed protein origins.

#### **Biomarker $m/z$ 67**

The peak cluster with nominal mass  $m/z$  67 (Figure 2.2) is composed of four major contributing ions. In the spectra of the protein extracts and standards, two ions were observed:  $m/z$  67.0547 ( $C_5H_7$ ) and  $m/z$  67.0184 ( $C_4H_3O$ ). An ion signal was detected for  $m/z$  67.0547 ( $C_5H_7$ ) in the spectra of the protein extracts, albumin and lysine standards. Fragmentation for  $m/z$  67.0547 in the bacterium using a HR-product-ion scan ( $R=10,000$ ) produced product ions at  $m/z$  41, 39 and 27. This typical product-ion scan was given in Figure 2.14. The origin of the  $m/z$  67.0547 ion in *B. neotomae* was examined using a precursor-ion scan, Figure 2.15. Major precursor ions included  $m/z$  82, 94, 95, 96, 109, 110, 121, 123, 136, 137, 138, 150 and 151. This data, as stated

Table 2.4. Biomarker ions with proposed protein origins.

<b>Nominal Mass</b>	<b>Empirical Formula</b>	<b>Calculated Mass</b>	<b>Measured Mass</b>	<b>Error (MMU)</b>	<b>R+DB</b>
67	C <sub>5</sub> H <sub>7</sub>	67.0548	67.0547	-0.1	2.5
67	C <sub>4</sub> H <sub>3</sub> O	67.0184	67.0184	+0.0	3.5
76	C <sub>6</sub> H <sub>4</sub>	76.0313	76.0313	+0.0	5.0
79	C <sub>6</sub> H <sub>7</sub>	79.0548	79.0545	-0.3	3.5
79	C <sub>5</sub> H <sub>5</sub> N	79.0422	79.0417	-0.5	4.0
89	C <sub>7</sub> H <sub>5</sub>	89.0391	89.0392	+0.1	5.5
93	C <sub>5</sub> H <sub>5</sub> N <sub>2</sub>	93.0453	93.0452	-0.1	4.5
95	C <sub>5</sub> H <sub>7</sub> N <sub>2</sub>	95.0609	95.0611	+0.2	3.5
103	C <sub>8</sub> H <sub>7</sub>	103.0548	103.0543	-0.5	5.5
115	C <sub>9</sub> H <sub>7</sub>	115.0548	115.0533	-1.5	6.5
117	C <sub>8</sub> H <sub>7</sub> N	117.0578	117.0567	-1.1	6.0
131	C <sub>9</sub> H <sub>9</sub> N	131.0735	131.0730	-0.5	6.0
131	C <sub>9</sub> H <sub>7</sub> O	131.0497	131.0495	-0.2	6.5
131	C <sub>5</sub> H <sub>9</sub> ONS	131.0405	131.0406	+0.1	2.0

previously, represents the origins of all of the peaks in the  $m/z$  67 cluster due to the low resolution character of the precursor-ion scan. Attention has, for this reason, been focused on the ions with lysine origins as observed in pure standards and protein extracts. The precursor ion of  $m/z$  67.0547 in the bacterium was found to be  $m/z$  83.0733 ( $C_5H_9N$ ). This ion is a fragment ion of lysine (40, 54).

Proline is suggested to be the predominant amino acid source of  $m/z$  67.0184 ( $C_4H_3O$ ), since this ion was not observed in the spectra of the other amino acids listed in Table 2.1. Fragment ions include  $m/z$  39, 38 and 37. The precursor ion in *B. neotomae* at  $m/z$  97.0519 ( $C_5H_7ON$ ), which is reported as a proline ion (55), supports proline origins. Since  $m/z$  67.0184 was produced by the fragmentation of proline, the assignment of the precursor ion was based on exact mass measurements of proline, albumin, protein extracts and the whole cell microorganism.

### **Biomarker $m/z$ 76**

The  $m/z$  76 cluster (Figure 2.3) contains one ion that was found in the protein extracts, albumin and tryptophan standards:  $m/z$  76.0313 ( $C_6H_4$ ). The fragmentation observed for  $m/z$  76.0313 ( $C_6H_4$ ) of *B. neotomae* indicated product ions at  $m/z$  50, 49, 39, 38 and 37. The precursor ions of  $m/z$  76.0313 in the bacterium were found to be  $m/z$  186.0795 ( $C_{11}H_{10}ON_2$ ),  $m/z$  160.1001 ( $C_{10}H_{12}N_2$ ),  $m/z$  131.0730 ( $C_9H_9N$ ),  $m/z$  130.0652 ( $C_9H_8N$ ),  $m/z$  117.0567 ( $C_8H_7N$ ) and  $m/z$  103.0543 ( $C_8H_7$ ) all originating from tryptophan (54).  $M/z$ s 186.0795 and 160.1001 are fragment ions of tryptophan, a dehydration product (55) and a decarboxylation product (37-40), respectively. The assignment of these ions was based on exact mass measurements of tryptophan, albumin, protein extracts and *B. neotomae*. The proposed pathway for tryptophan contributions to  $m/z$  76.0313 is given in Figure 2.26.

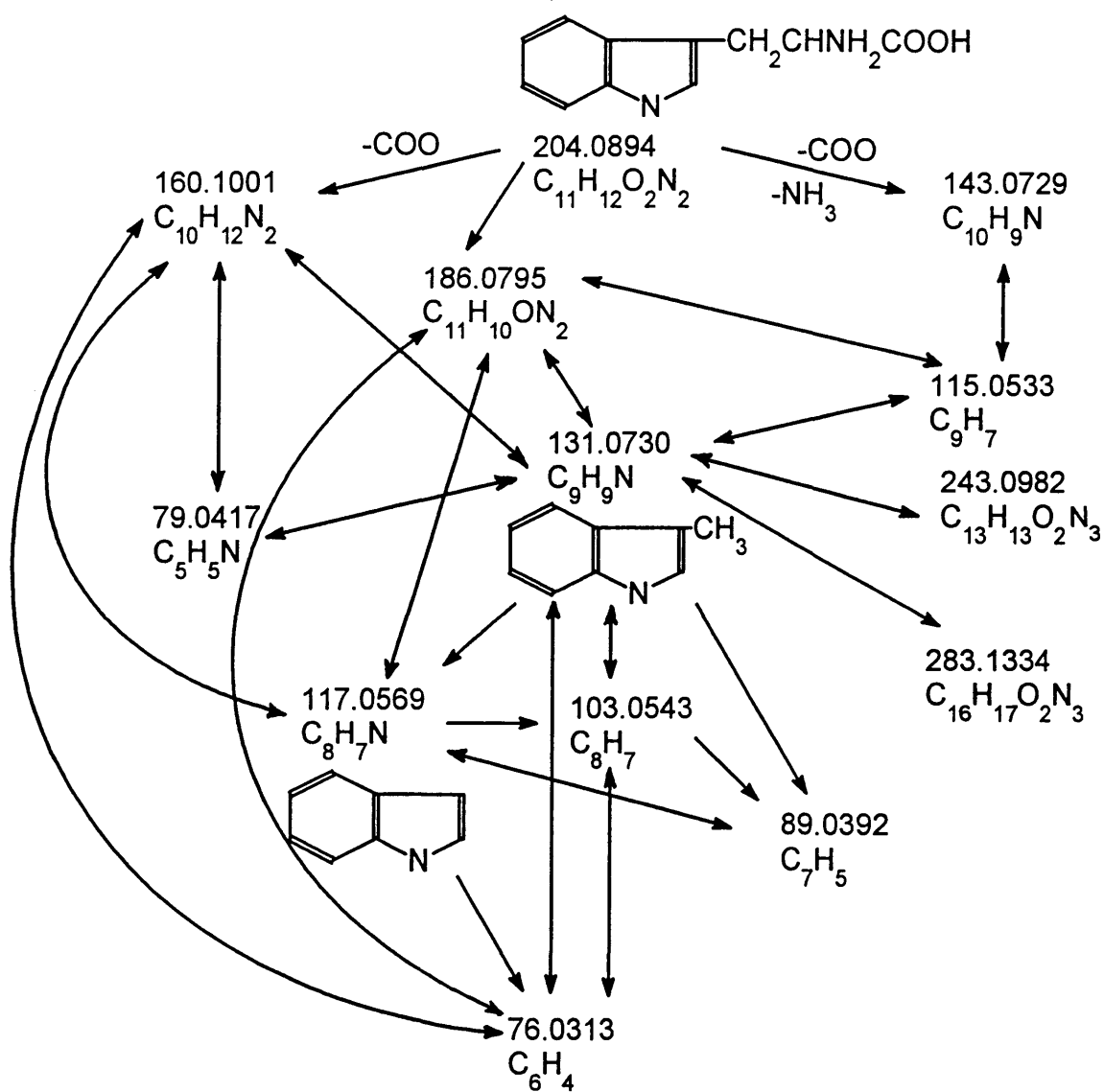


Figure 2.26. Proposed fragmentation pathway of m/z 76.0313, m/z 79.0417, m/z 89.0392, m/z 103.0543, m/z 115.0533, m/z 117.0567 and m/z 131.0730.

### Biomarker m/z 79

The m/z 79 cluster contains four peaks (Figure 2.4), of which two were found in the spectra of the protein standards and extracts: m/z 79.0545 (C<sub>6</sub>H<sub>7</sub>) and m/z 79.0417 (C<sub>5</sub>H<sub>5</sub>N). The fragmentation observed for m/z 79.0545 (C<sub>6</sub>H<sub>7</sub>) in the bacterium indicated product ions at m/z 63, 51, 39, 36 and 27. Precursor ions at m/z 163.0614 (C<sub>9</sub>H<sub>9</sub>O<sub>2</sub>N), m/z 136.0763 (C<sub>8</sub>H<sub>10</sub>ON) and m/z 108.0566 (C<sub>7</sub>H<sub>8</sub>O) were observed for m/z 79.0545. These ions are all fragment ions of tyrosine (54-56). Other precursor ions of m/z 79.0545 include DKPs of tyrosine: m/z 220.0845 (C<sub>11</sub>H<sub>12</sub>O<sub>3</sub>N<sub>2</sub>, Y-G), m/z 234.1014 (C<sub>12</sub>H<sub>14</sub>O<sub>3</sub>N<sub>2</sub>, Y-A), m/z 262.1307 (C<sub>14</sub>H<sub>18</sub>O<sub>3</sub>N<sub>2</sub>, Y-V), m/z 264.1095 (C<sub>13</sub>H<sub>16</sub>O<sub>4</sub>N<sub>2</sub>, Y-T) and m/z 278.0926 (C<sub>13</sub>H<sub>14</sub>O<sub>5</sub>N<sub>2</sub>, Y-D). M/z 79.0545 was produced by the fragmentation of tyrosine (54). It was not produced by the fragmentation of the other amino acids listed in Table 2.1. Therefore, the assignment of precursor ions was based on exact mass measurements of tyrosine, albumin, protein extracts and the whole cell microorganism data. A proposed fragmentation pathway of m/z 79.0545 is shown in Figure 2.27.

M/z 79.0417 (C<sub>5</sub>H<sub>5</sub>N) of *B. neotomae* was produced by the fragmentation of tryptophan. Fragmentation observed for m/z 79.0417 in the bacterium indicated product ions at m/z 61, 52, 51, 50, 41, 39 and 37. The precursor ion of m/z 79.0417 in the bacterium was found to be m/z 160.1001 (C<sub>10</sub>H<sub>12</sub>N<sub>2</sub>). As shown in Figure 2.26, m/z 160.1001 is the decarboxylation residue of tryptophan. The assignment of this ion was based on exact mass measurements of tryptophan, albumin, protein extracts and *B. neotomae*.

### Biomarker m/z 89

The peak profile presented in Figure 2.5 shows five contributors to nominal mass 89. In the spectra of tryptophan, albumin and the protein extracts, one of these peaks was observed: m/z 89.0392 (C<sub>7</sub>H<sub>5</sub>). The precursor ion of m/z 89.0392 in *B. neotomae* was found to be m/z 117.0567 (C<sub>8</sub>H<sub>7</sub>N), indole. This ion is a tryptophan fragment. The fragmentation pathway has been shown in Figure 2.26.

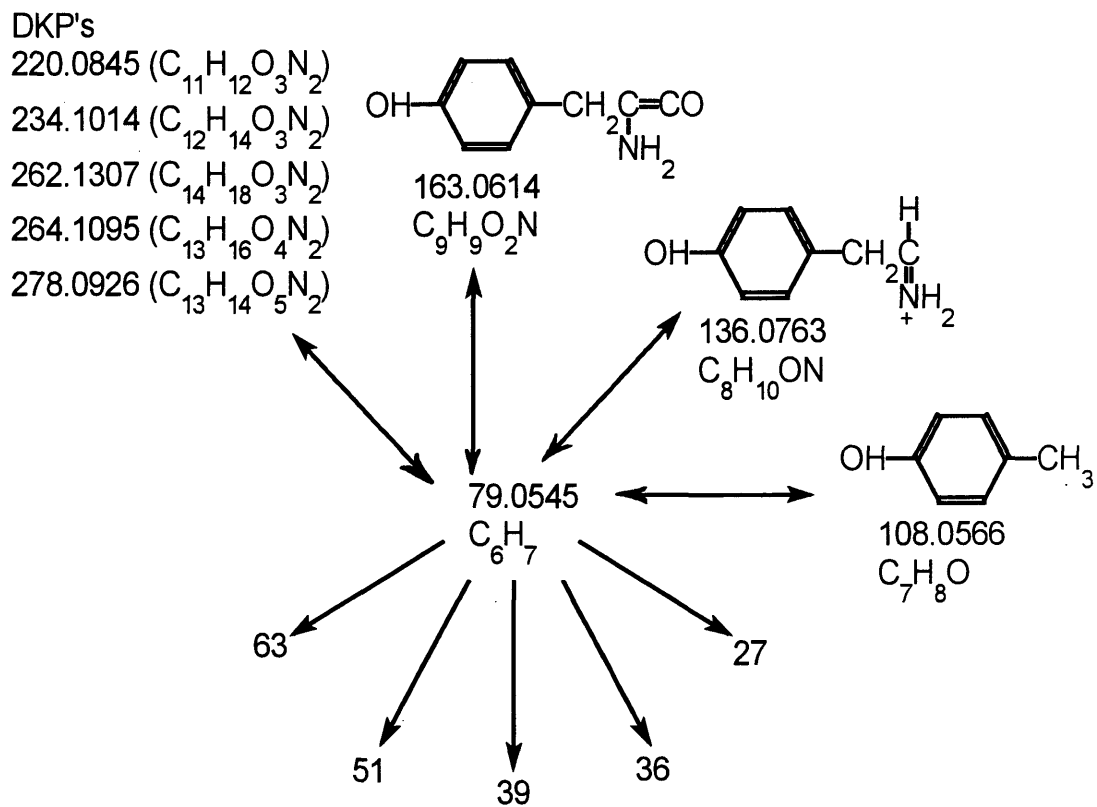


Figure 2.27. Proposed fragmentation pathway of m/z 79.0545.

### **Biomarker m/z 93**

The peak cluster for nominal mass m/z 93 (Figure 2.6) is composed of five major contributing peaks, one of which was also observed in the protein standards and extracts: m/z 93.0452 (C<sub>5</sub>H<sub>5</sub>N<sub>2</sub>). The peak at m/z 92.9953 is an internal calibrant peak. M/z 93.0452 (C<sub>5</sub>H<sub>5</sub>N<sub>2</sub>) was significant in the mass spectrum of histidine. Fragment ions of m/z 93.0452 in *B. neotomae* include m/z 79, 66 and 39. The origin of m/z 93.0452 was examined using a precursor-ion scan. Precursor ions were found to be m/z 111.0802 (C<sub>5</sub>H<sub>9</sub>N<sub>3</sub>) and m/z 137.0581 (C<sub>6</sub>H<sub>7</sub>ON<sub>3</sub>). These ions are associated with histidine. Ions 111.0802 and 137.0581 are a decarboxylation residue (54) and a dehydration residue (55), respectively.

### **Biomarker m/z 95**

The HR-spectrum of m/z 95 (Figure 2.7) shows a cluster of seven major contributors. In the spectra of the amino acids, albumin and protein extracts, only one peak was consistently observed: m/z 95.0611 (C<sub>5</sub>H<sub>7</sub>N<sub>2</sub>). Product ions at m/z 80, 68, 67, 54, 53, 52, 41 and 39 were observed for m/z 95.0611 (C<sub>5</sub>H<sub>7</sub>N<sub>2</sub>) in *B. neotomae*. Precursor ions include histidine peaks at m/z 111.0802 (C<sub>5</sub>H<sub>9</sub>N<sub>3</sub>), m/z 137.0581 (C<sub>6</sub>H<sub>7</sub>ON<sub>3</sub>), m/z 155.0661 (C<sub>6</sub>H<sub>9</sub>O<sub>2</sub>N<sub>3</sub>) and m/z 194.0796 (C<sub>8</sub>H<sub>10</sub>O<sub>2</sub>N<sub>4</sub>). M/z 155.0661 is the molecular ion (M<sup>+</sup>) of histidine. M/z 137.0581 and 111.0802 have previously been discussed. M/z 194.0796 is the DKP of histidine and glycine. However, no other histidine DKP's were observed. An ion signal was detected at m/z 95.0611 in the spectra of arginine. However, no precursor ions associated with arginine were observed in the precursor-ion scan of m/z 95 in the whole cell microorganism. M/z 95.0611 of *B. neotomae* was produced by the fragmentation of histidine and arginine.

### **Biomarker m/z 103**

The m/z 103 cluster contains two peaks (Figure 2.8), of which one was found in all of the spectra of the protein standards and extracts: m/z 103.0543 (C<sub>8</sub>H<sub>7</sub>). The fragmentation observed for biomarker m/z 103.0543 (C<sub>8</sub>H<sub>7</sub>) in *B. neotomae* indicated product ions at m/z 89, 77, 76, 63, 51, 50 and 39. Precursor ions at m/z 120.0817 (C<sub>8</sub>H<sub>10</sub>N), m/z 130.0652 (C<sub>9</sub>H<sub>8</sub>N) and m/z 131.0730 (C<sub>9</sub>H<sub>9</sub>N) were observed for m/z 103.0543 in *B. neotomae*. M/z 120.0817 was identified as a decarboxylation product of phenylalanine; m/z 130.0652 and m/z 131.0730 are fragment ions of tryptophan (54). The ion at m/z 103.0543 was produced by the fragmentation of phenylalanine and tryptophan and was not produced by the fragmentation of the other 19 amino acids listed in Table 2.1. Therefore, the assignment of precursor ions was based on exact mass measurements of phenylalanine, tryptophan, albumin, protein extracts and the whole cell microorganism data. A proposed decomposition pattern of m/z 103.0543 is shown in Figure 2.28.

### **Biomarker m/z 115**

Of the peaks found in the m/z 115 cluster shown in Figure 2.10, only the peak at m/z 115.0533 (C<sub>9</sub>H<sub>7</sub>) was observed in the protein extracts, albumin, and tryptophan standards. The precursor ions of m/z 115.0533 in the bacterium include m/z 143.0729 (C<sub>10</sub>H<sub>9</sub>N) and m/z 186.0795 (C<sub>11</sub>H<sub>10</sub>ON<sub>2</sub>). M/z 143.0729 is a fragment of tryptophan (decarboxylation followed by deamination) (54), and m/z 186.0795 is a dehydration residue of tryptophan as shown in Figure 2.26 (55). The assignment of precursor ions was based on exact mass measurements of the protein extracts, *B. neotomae*, albumin and tryptophan standards.

### **Biomarker m/z 117**

The HR peak profile pictured in Figure 2.11 shows one contributor to nominal mass 117: m/z 117.0567 (C<sub>8</sub>H<sub>7</sub>N). Ion 117.0567 was observed in the spectra of

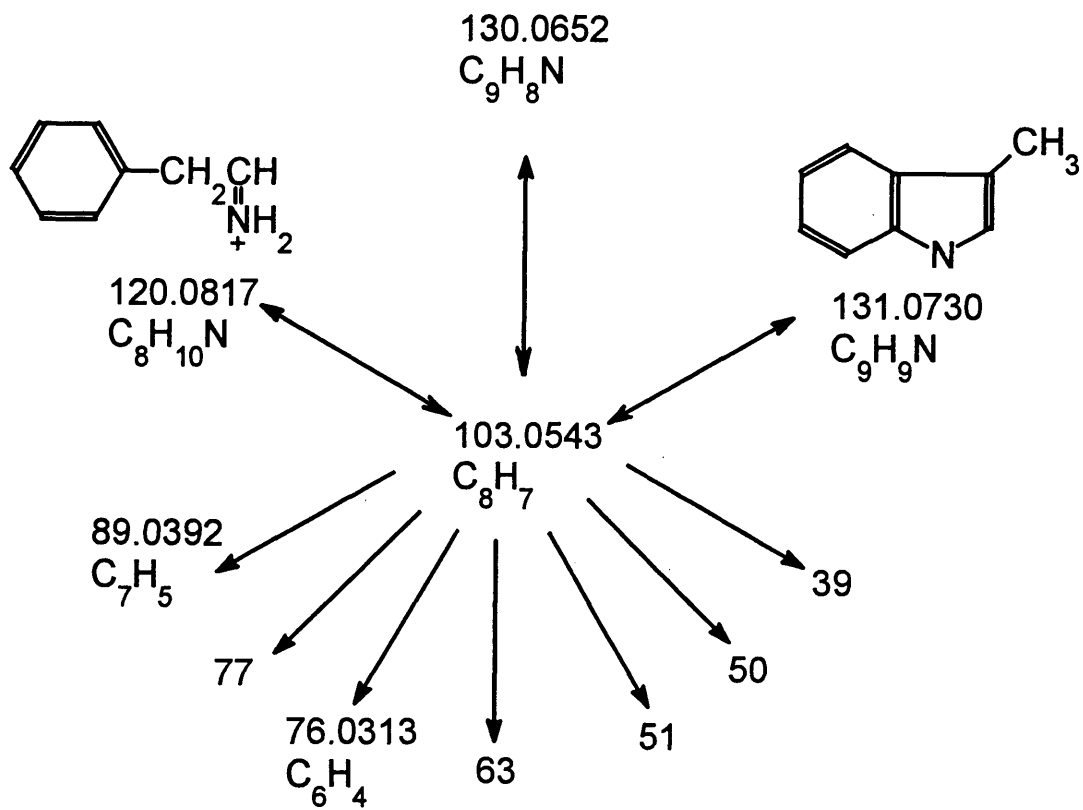


Figure 2.28. Proposed fragmentation pathway of  $m/z$  76.0313 and  $m/z$  103.0543.

tryptophan, albumin and the protein extracts, but was not observed in any of the other amino acids listed in Table 2.1. Fragmentation observed for the ion at  $m/z$  117.0567 of the bacterium indicated product ions at  $m/z$  103, 102, 99, 91, 89, 76, 75, 63, 51 and 39. The precursor ions were found to be  $m/z$  160.1001 ( $C_{10}H_{12}N_2$ ) and  $m/z$  186.0795 ( $C_{11}H_{10}ON_2$ ). These ions are fragments of tryptophan and have been discussed previously. Therefore,  $m/z$  117.0567 was assigned as the organic product indole (54). The proposed fragmentation pattern has been shown in Figure 2.26.

### **Biomarker $m/z$ 131**

The peak cluster with nominal mass  $m/z$  131 (Figure 2.13) is composed of several contributing ions. In the spectra of the protein extracts and standards, three ions were observed:  $m/z$  131.0730 ( $C_9H_9N$ ),  $m/z$  131.0495 ( $C_9H_7O$ ) and  $m/z$  131.0406 ( $C_5H_9ONS$ ). An ion signal was detected for  $m/z$  131.0730 ( $C_9H_9N$ ) predominantly in the spectra of the tryptophan standard and the n-butanol protein extract. Fragmentation observed for ion 131.0730 in *B. neotomae* using HR-product-ion scan ( $R=10,000$ ) produced product ions at  $m/z$  117, 115, 104, 103, 91, 89, 79, 77, 76, 64, 51 and 39. The origin of the  $m/z$  103.0730 ion of the whole cell microorganism was examined using a precursor-ion scan. The precursor ions of  $m/z$  131.0730 were found to be  $m/z$  160.1001 ( $C_{10}H_{12}N_2$ ),  $m/z$  186.0795 ( $C_{11}H_{10}ON_2$ ),  $m/z$  204.0894 ( $C_{11}H_{12}O_2N_2$ ),  $m/z$  243.0982 ( $C_{13}H_{13}O_2N_3$ ) and  $m/z$  283.1334 ( $C_{16}H_{17}O_2N_3$ ).  $M/z$  204.0894 is the amino acid tryptophan ( $M^+$ ).  $M/z$ s 160.1001 and 186.0795 are fragment ions of  $m/z$  204.0894, a decarboxylation product and a dehydration product, respectively, as discussed previously.  $M/z$  243.0982 is the DKP of tryptophan and glycine, while  $m/z$  283.1334 is the DKP of tryptophan and proline. The assignment of the afore mentioned ions was based on exact mass measurements of the standards, extracts and the bacterium correlated to existing literature values. The proposed decomposition pathway for tryptophan contributions to  $m/z$  131.0730 was given in Figure 2.26.

M/z 131.0495 ( $C_9H_7O$ ) shows similar fragmentation to m/z 131.0730. However, m/z 131.0495 contains an oxygen atom. A precursor ion of m/z 131.0495 in *B. neotomae* was found to be m/z 147.0673 ( $C_9H_9ON$ ). M/z 147.0673 is a dehydration residue of phenylalanine ( $C_9H_{11}O_2N$ ) (55). Other precursor ions of m/z 131.0495 include DKPs of phenylalanine: m/z 244.1230 ( $C_{14}H_{16}O_2N_2$ , F-P), m/z 261.1124 ( $C_{13}H_{15}O_3N_3$ , F-N), m/z 276.1123 ( $C_{14}H_{16}O_4N_2$ , F-E), m/z 278.1096 ( $C_{14}H_{18}O_2N_2S$ , F-M) and m/z 284.1265 ( $C_{15}H_{16}O_2N_4$ , F-H). The assignment of these ions was based on exact mass measurements of phenylalanine, the protein extracts, albumin and the whole cell microorganism. Proposed fragmentation patterns are shown in Figure 2.29.

M/z 131.0406 ( $C_5H_9ONS$ ) was produced by the dehydration of methionine (55). Precursor ions at m/z 149.0483 ( $C_5H_{11}O_2NS$ ), m/z 188.0595 ( $C_7H_{12}O_2N_2S$ ), m/z 202.0750 ( $C_8H_{14}O_2N_2S$ ), m/z 230.1059 ( $C_{10}H_{18}O_2N_2S$ ), m/z 245.0818 ( $C_9H_{15}O_3N_3S$ ) and m/z 278.1096 ( $C_{14}H_{18}O_2N_2S$ ) were observed for m/z 131.0406 in *B. neotomae*. M/z 149.0483 is the amino acid methionine ( $M^+$ ). M/zs 188.0595, 202.0750, 230.1059, 245.0818 and 278.1096 are DKP ions of methionine with G, A, V, N and F, respectively. As m/z 131.0406 was produced solely by the fragmentation of methionine, the assignment of the precursor ions was based on exact mass measurements of methionine, albumin, protein extracts and the bacterium.

### **Lipid-Based Biomarker Ions**

The bacterial lipid extract used in this phase was from *B. neotomae*. Along with the lipid extract, several common lipid standards listed in Table 2.5 were also analyzed. The standards and lipid extract were analyzed using the same conditions as in the analysis of the whole cell microorganism, and the peaks were compared to those from the whole cell microorganism data to determine biomarker origins. Table 2.6 summarizes the biomarker ions with proposed lipid origins. These ions will be discussed in detail.

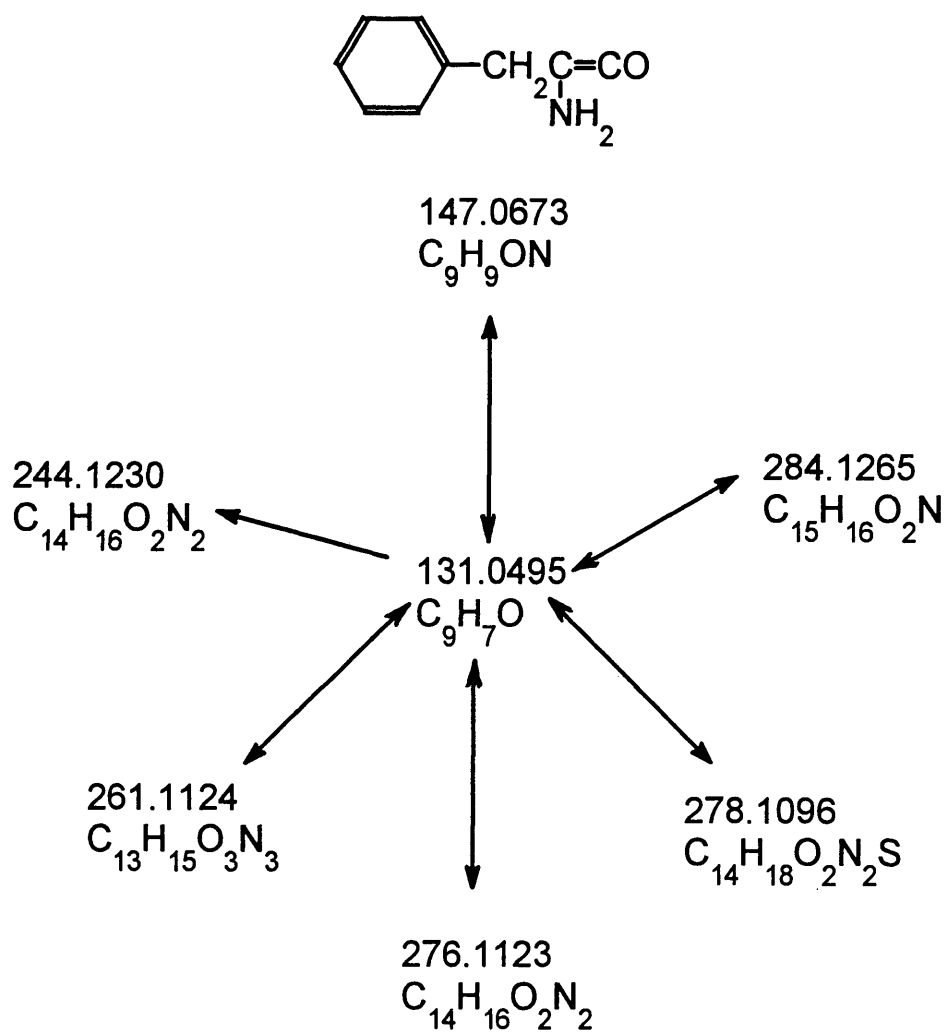


Figure 2.29. Proposed fragmentation pathway of m/z 131.0495.

Table 2.5. Standards used to represent the cellular content of lipids.

C14:0
C16:0
C16:1
Cyclo C17:0
C18:0
C18:1
Cyclo C19:0
C19:0
Tripalmitin
Phosphatidylglycerol
Phosphatidylethanolamine
Phosphatidyl-choline
Sphingomyelin

Table 2.6. Biomarker ions with proposed lipid origins.

<b>Nominal Mass</b>	<b>Empirical Formula</b>	<b>Calculated Mass</b>	<b>Measured Mass</b>	<b>Error (MMU)</b>	<b>(R+DB)</b>
67	C <sub>5</sub> H <sub>7</sub>	67.0548	67.0547	-0.1	2.5
67	C <sub>4</sub> H <sub>5</sub> N	67.0422	67.0421	-0.1	3.0
79	C <sub>6</sub> H <sub>7</sub>	79.0548	79.0545	-0.3	3.5
93	C <sub>7</sub> H <sub>9</sub>	93.0704	93.0702	-0.2	3.5
95	C <sub>7</sub> H <sub>11</sub>	95.0861	95.0861	+0.0	2.5
95	C <sub>6</sub> H <sub>7</sub> O	95.0497	95.0495	-0.2	3.5
95	C <sub>5</sub> H <sub>3</sub> O <sub>2</sub>	95.0133	95.0137	+0.4	4.5
105	C <sub>8</sub> H <sub>9</sub>	105.0704	105.0704	+0.0	4.5
105	C <sub>7</sub> H <sub>5</sub> O	105.0340	105.0332	-0.8	5.5
115	C <sub>6</sub> H <sub>11</sub> O <sub>2</sub>	115.0759	115.0761	+0.2	1.5
129	C <sub>7</sub> H <sub>13</sub> O <sub>2</sub>	129.0916	129.0913	-0.3	1.5
129	C <sub>6</sub> H <sub>9</sub> O <sub>3</sub>	129.0552	129.0558	+0.6	2.5

**Biomarker m/z 67**

The peak cluster with nominal mass  $m/z$  67 is composed of four major contributing peaks at  $R=10,000$  (Figure 2.2). Only two of these peaks were observed in the spectra of the lipid extract and the standards listed in Table 2.5:  $m/z$  67.0547 ( $C_5H_7$ ) and  $m/z$  67.0421 ( $C_4H_5N$ ).  $M/z$  67.0547 ( $C_5H_7$ ) was observed in the spectra of all standards listed in Table 2.5. Using a high resolution product-ion scan analysis ( $R=10,000$ ), the fragmentation observed for  $m/z$  67.0547 in the bacterium was found to be characteristic of an unsaturated hydrocarbon chain. The prominent product ions were  $m/z$  41, 39 and 27 (Figure 2.16). The origin of the  $m/z$  67.0547 ion was examined using a precursor-ion scan, as shown in Figure 2.15. It was found to have multiple origins. This data, as stated previously, represents the origins of all of the peaks in the  $m/z$  67 cluster due to the low resolution character of the precursor-ion scan. Attention has, for this reason, been focused only on ions with lipid origins as observed in pure standards and the lipid extract. Furthermore, the precursor ion spectrum of  $m/z$  67 indicates the presence of a homologous series of fatty acid based ions separated by 14 amu.  $M/z$  95.0861 ( $C_7H_{11}$ ) was identified as a precursor of  $m/z$  67.0547 in the bacterium studies. Since  $m/z$  67.0547 was observed in all the standards listed in Table 2.5, it must originate from the side chain portion of the fatty acid.

The ion at  $m/z$  67.0421 ( $C_4H_5N$ ) was observed exclusively in the phospholipid standards. The presence of this peak in both the lipid extract and intact bacterial cell pyrolysis spectra, suggests that a precursor of this peak must be a phospholipid type compound. The elemental composition and unsaturation counts along with the product ions of  $m/z$  67.0421 in the bacterium ( $m/z$  52, 41, 39 and 28) suggests a pyrrole type structure (Figure 2.30) which has been previously proposed for this ion (57).

**Biomarker m/z 79**

The HR profile of the  $m/z$  79 cluster (Figure 2.3) contains only one ion which was found in the lipid extract and the standards listed in Table 2.5:  $m/z$  79.0545 ( $C_6H_7$ ).

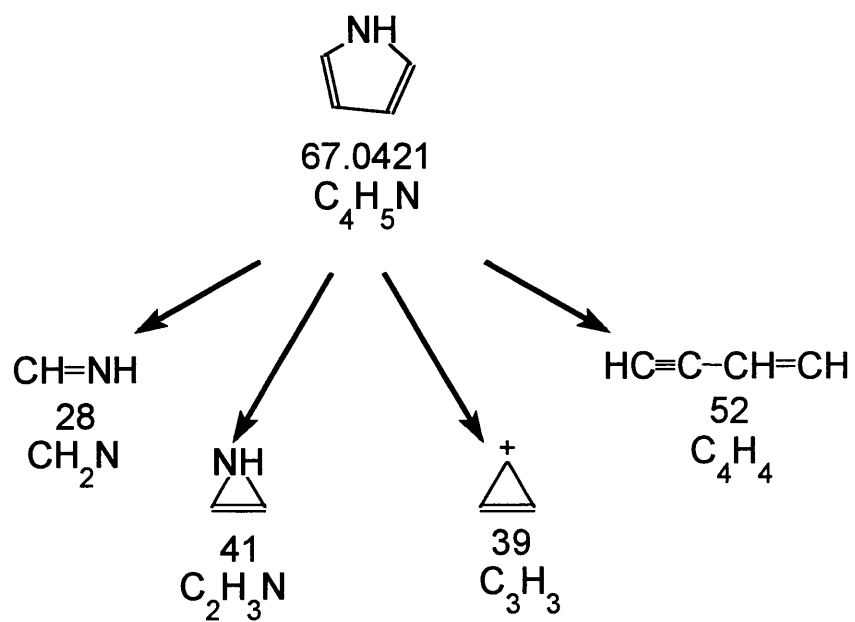


Figure 2.30. Proposed fragmentation pathway of m/z 67.0421.

Since  $m/z$  79.0545 was not observed in the spectra of the fatty acids, but was observed in the spectra of the other standards listed in Table 2.5, it must originate from glycerol and the ceramide backbone of the lipid molecule not from the fatty acid side-chain. The product ions of  $m/z$  79.0545 include  $m/z$  77, 63, 51, 39 and 27. A precursor-ion scan shows  $m/z$  123 to be a major precursor of the  $m/z$  79 peak. Using HR product-ion scans and HR normal-ion scans of *B. neotomae* and the standards,  $m/z$  123.1173 ( $C_9H_{15}$ ) was confirmed as a precursor of  $m/z$  79.0545. A pathway for the formation and decomposition of  $m/z$  79.0545, based on the precursor- and product-ion scans, is shown in Figure 2.31.

### **Biomarker $m/z$ 93**

Five significant peaks are observed in the  $m/z$  93 cluster (Figure 2.6). The peak at  $m/z$  92.9953 is an internal calibrant peak. The largest peak in the cluster,  $m/z$  93.0702 ( $C_7H_9$ ) was observed in all the analyzed standards listed in Table 2.5 as well as in the lipid extract. In the product-ion spectrum of  $m/z$  93.0702 of *B. neotomae*, the fragmentation of this molecule is characterized by  $m/z$  77, 65, 50 and 39. The precursor-ion spectrum of  $m/z$  93.0702 of the bacterium is dominated by the following peaks: 192, 220, 234, 278, 311, 339 and 354, of which 220.2187 ( $C_{16}H_{28}$ ), 311.2590 ( $C_{19}H_{35}O_3$ ) and 339.2880 ( $C_{21}H_{39}O_3$ ) were found in the lipid extract, tripalmitin and the fatty acid standards. The presence of  $m/z$  93.0702 in all the standards listed in Table 2.5 indicates the origin as being from the fatty acid chain. The data from the precursor-ion scan confirms these origins. The proposed pathway is given in Figure 2.32.

### **Biomarker $m/z$ 95**

The peak cluster at  $m/z$  95 (Figure 2.7) shows seven distinguished peaks, three of which are present in the spectra of the lipid extract and the standards of Table 2.5:  $m/z$  95.0861 ( $C_7H_{11}$ ),  $m/z$  95.0495 ( $C_6H_7O$ ) and  $m/z$  95.0137 ( $C_5H_3O_2$ ). The precursor and product-ion scan data of  $m/z$  95.0861 ( $C_7H_{11}$ ) closely resembles that of ion 67.0547;

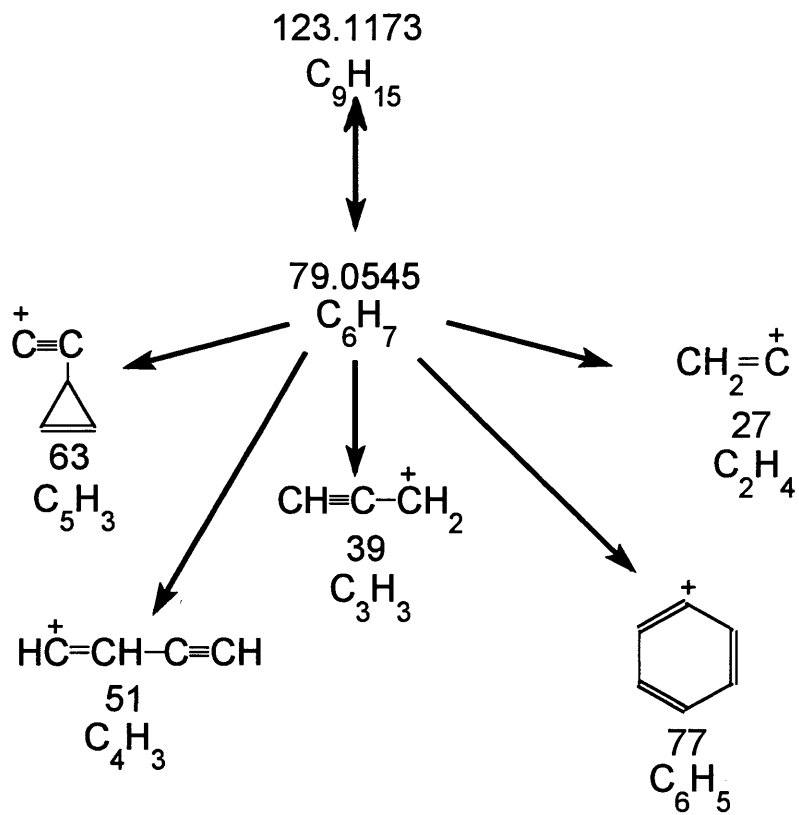


Figure 2.31. Proposed fragmentation pathway of  $m/z$  79.0545.

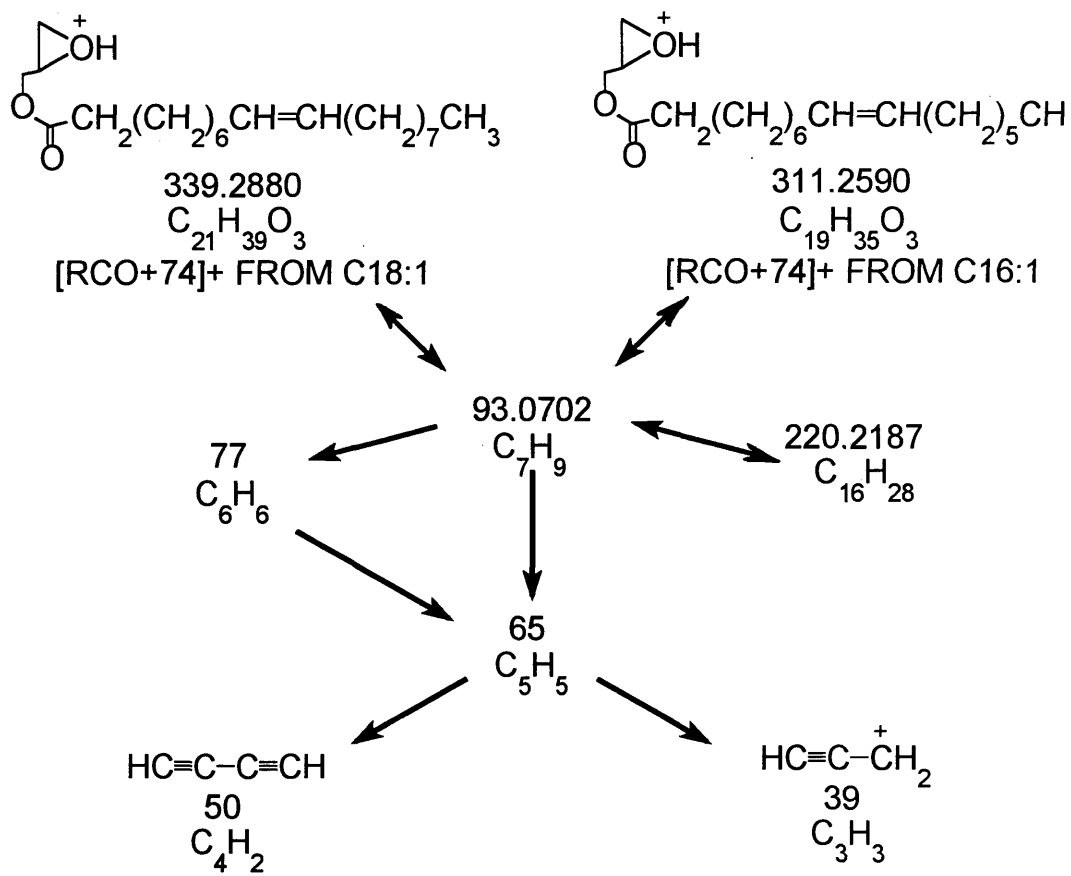


Figure 2.32. Proposed fragmentation pathway of  $m/z$  93.0702.

therefore, it is very likely that the  $m/z$  95.0861 peak is part of the pathway for  $m/z$  67.0547, as shown in Figure 2.16. The precursor-ion scan of  $m/z$  95.0861 in *B. neotomae* indicates the presence of a large number of products characteristic of long-chain fatty acids, as described by Murphy (42). The proposed fragmentation pathway leading to  $m/z$  95.0861 is given in Figure 2.33. However, the structures of  $m/z$  95.0495 ( $C_6H_7O$ ) and 95.0137 ( $C_5H_3O_2$ ) could not be unambiguously assigned.

### **Biomarker $m/z$ 105**

The HR ion cluster at mass  $m/z$  105 contains five separate peaks (Figure 2.9), two of which were observed in the spectra of the triglyceride standards and the lipid extract:  $m/z$  105.0704 ( $C_8H_9$ ) and  $m/z$  105.0332 ( $C_7H_5O$ ). A strong fragment ion at  $m/z$  77 in the high resolution product spectra of both of these ions suggests the presence of a benzene ring. The precursor-ion scan data, and the high resolution mass measurements, indicate that the precursor ions originate from homologs of the  $m/z$  105.0704 specie that are separated by 14 amu:  $m/z$  133.1018 ( $C_{10}H_{13}$ ),  $m/z$  147.1174 ( $C_{11}H_{15}$ ) and 161.1340 ( $C_{12}H_{17}$ ). A fragmentation pathway for the  $C_8H_9$  and  $C_7H_5O$  species is shown in Figure 2.34.

### **Biomarker $m/z$ 115**

The  $m/z$  115 cluster provides a complex pattern which can be resolved only with  $R=30,000$  and higher, Figure 2.10.  $M/z$  115.0761 ( $C_6H_{11}O_2$ ) has been observed in the spectra of tripalmitin, phosphatidylglycerol and the lipid extract. The product-ion scan, which was performed at  $R=20,000$ , did not provide sufficient resolution to permit observation of the product ions of the lipid-based peaks. With increased resolution, the signal from the two peaks was no longer detectable due to their low intensity. The following peaks were observed in the precursor-ion scan:  $m/z$  143, 185, 256, 351, 378 and 397.  $M/z$  143.1089 ( $C_8H_{15}O_2$ ) was linked to  $m/z$  115.0761 ( $C_6H_{11}O_2$ ) via logical loss

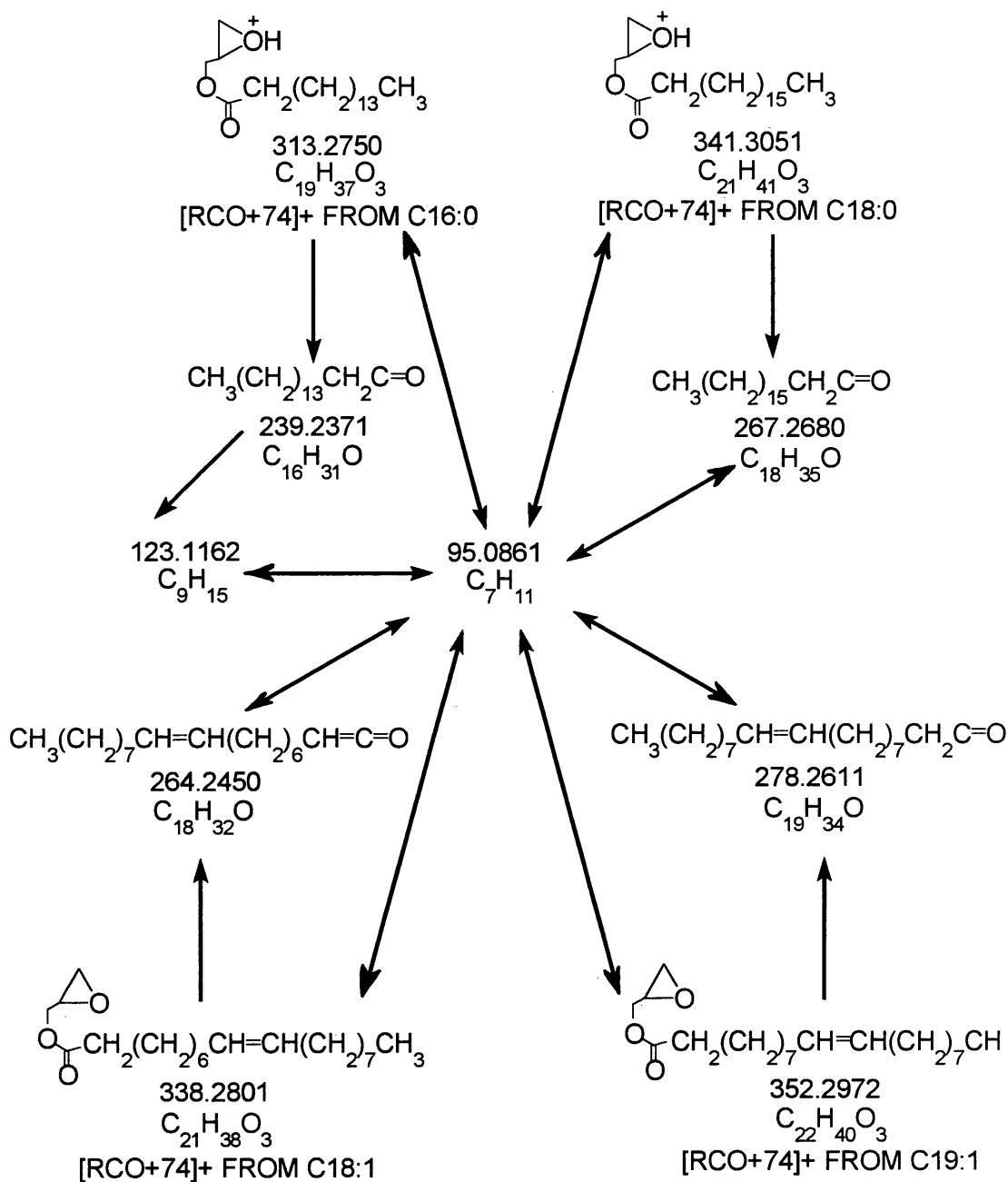


Figure 2.33. Proposed fragmentation pathway of  $m/z$  95.0861.

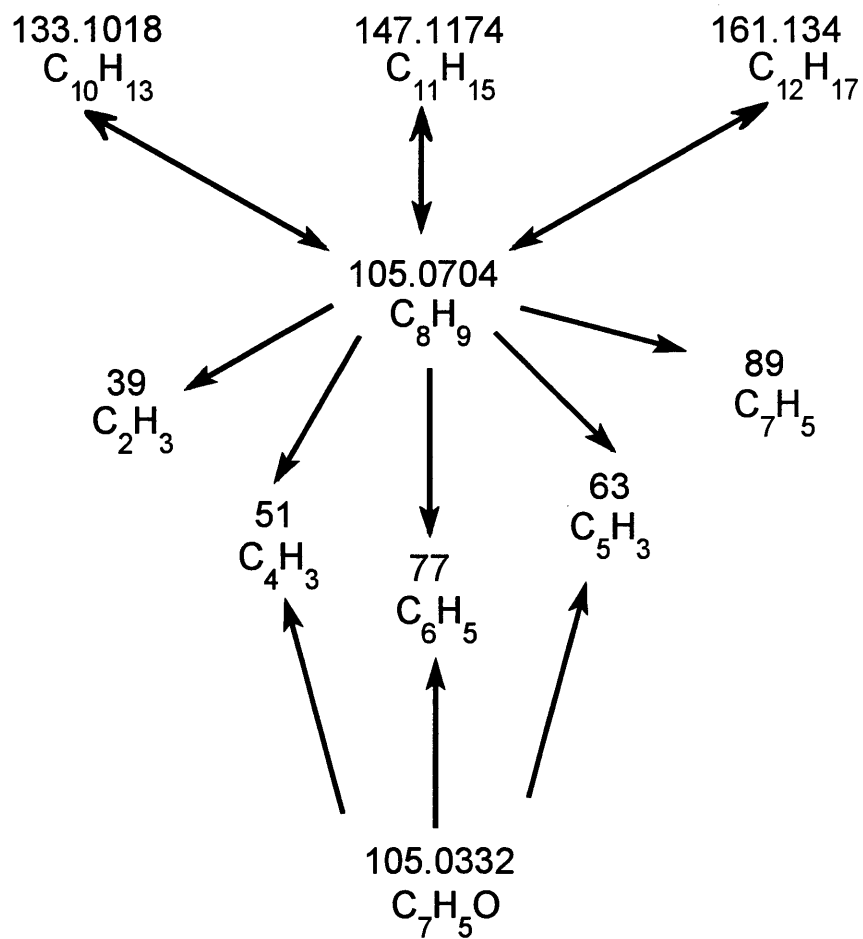


Figure 2.34. Proposed fragmentation pathway of  $m/z$  105.0704 and  $m/z$  105.0332.

of  $C_2H_4$ . The other ions observed in the precursor-ion scan most likely arise from the non-lipid-based peaks in the  $m/z$  115 cluster.

### **Biomarker $m/z$ 129**

Two major peaks are detected in the  $m/z$  129 cluster,  $m/z$  129.0913 ( $C_7H_{13}O_2$ ) and  $m/z$  129.0558 ( $C_6H_9O_3$ ) (Figure 2.12), both of which were observed in the lipid extract and all of the standards listed in Table 2.5. A product-ion scan of  $m/z$  129.0913 reveals ions which were observed in previously described pathways, i.e.  $m/z$  27, 39 and 41. The precursor-ion scan indicates the origin of  $m/z$  129.0913 as being the fatty acid portion of the glyceride molecules. The presence of acylium ions  $[RCO]^+$  and acylium ion adducts  $[RCO + 74]^+$  characteristic of the fragmentation of glycerides in the precursor-ion scan supports fatty acid origins. The mechanism of formation of acylium ions and their adducts was previously described in literature (42). The formation of fragment ions associated with  $m/z$  129.0913 in *B. neotomae* is shown in Figure 2.35.

$M/z$  129.0558 ( $C_6H_9O_3$ ) also originates from the glyceride molecule. The major precursors of  $m/z$  129.0558 are  $m/z$  338.0281 ( $C_{21}H_{38}O_3$ ) and  $m/z$  352.2972 ( $C_{22}H_{40}O_3$ ). The product-ion scan of  $m/z$  129.0558 provided the following ions:  $m/z$  112, 85, 84 and 27. The fragmentation is shown in Figure 2.36.

### **Biomarker Ions in Gram-positive bacteria**

Thus far, the entire discussion of biomarker ions has centered on whole bacterial cells of *B. neotomae*, a Gram-negative biological agent simulant. To validate the use of the biomarker ions for the differentiation and identification of other bacteria, a species of *Bacillus anthracis* was examined. *B. anthracis* is a highly pathogenic Gram-positive bacterium. High resolution profiles for each biomarker ion were obtained from the *B. anthracis* sample and they were compared to the HR biomarker ion profiles of *B. neotomae*. Figure 2.37 demonstrates the differences observed in the profiles of  $m/z$  95

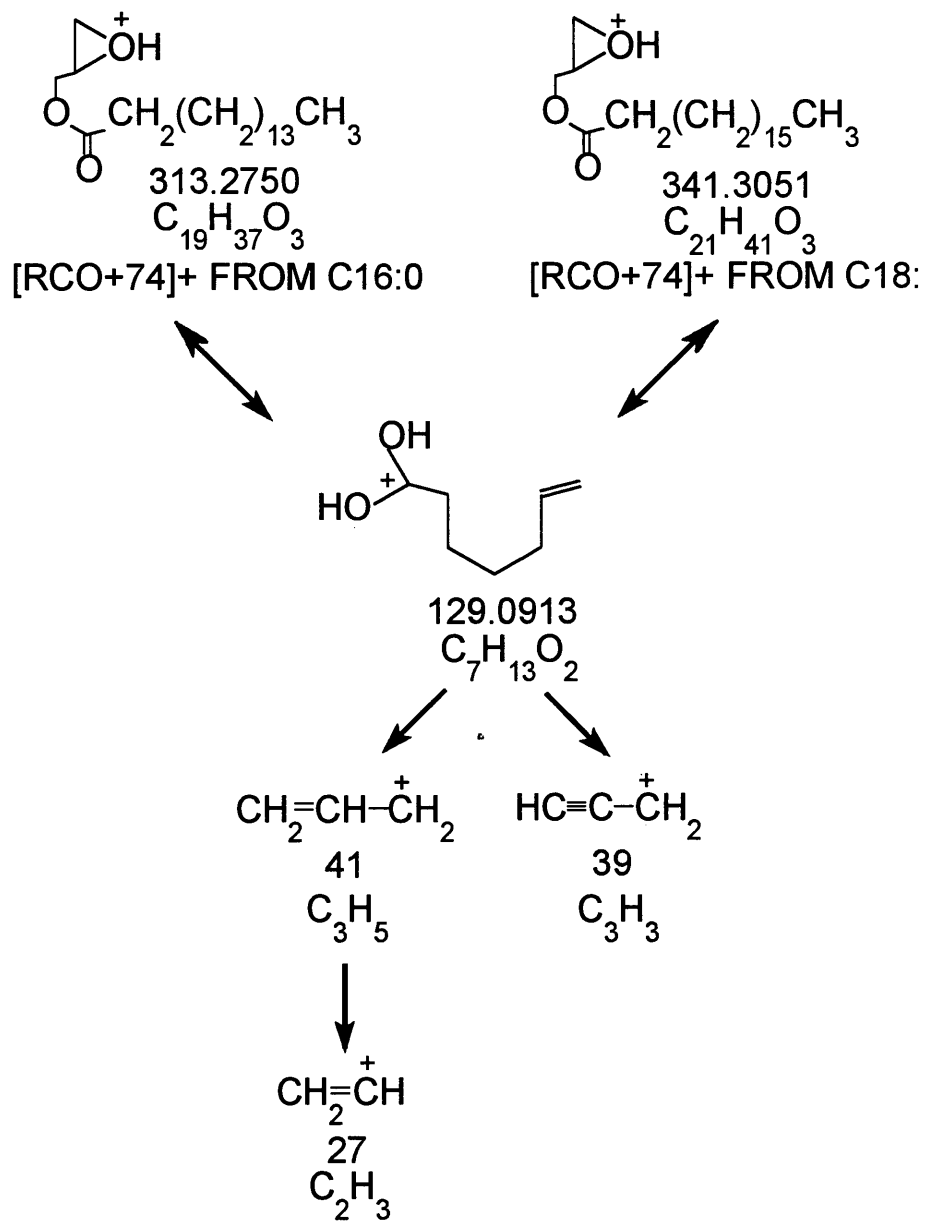


Figure 2.35. Proposed fragmentation pathway of m/z 129.0913.

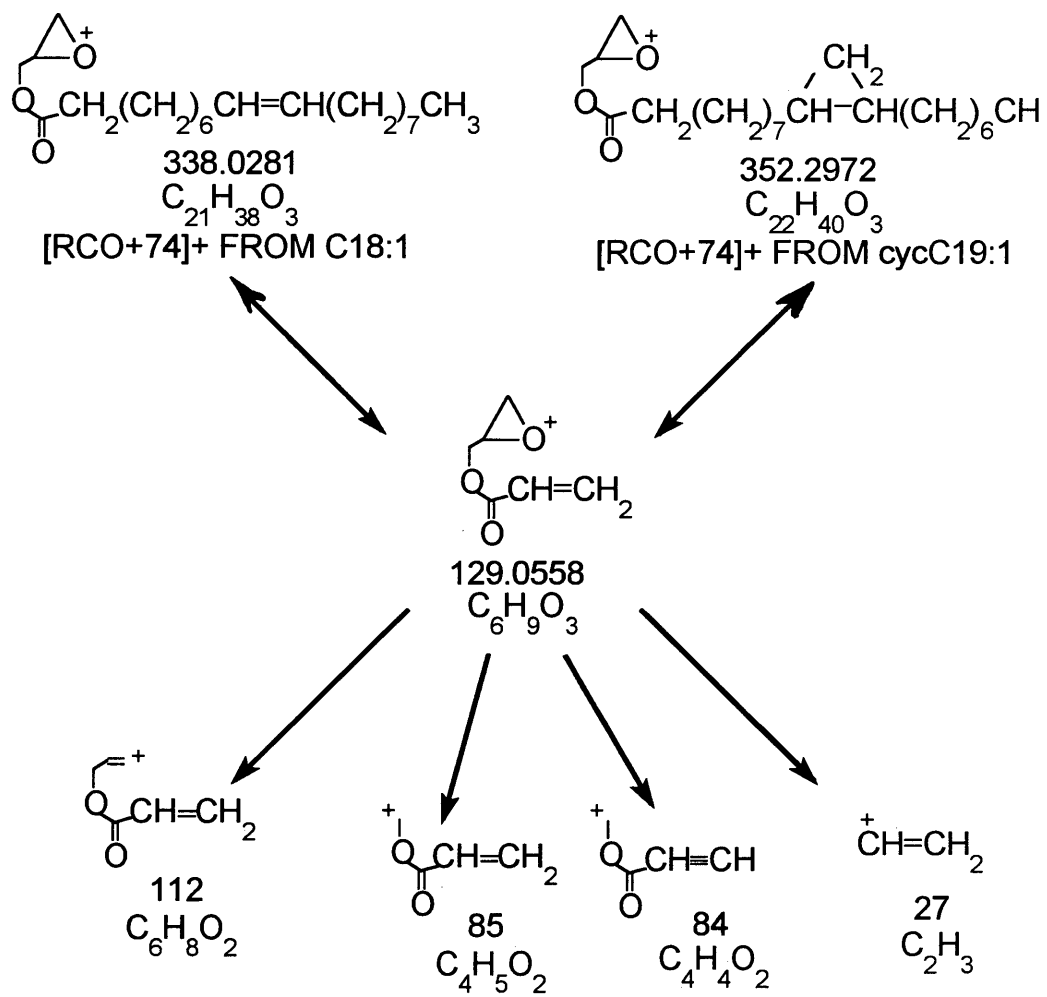


Figure 2.36. Proposed fragmentation pathway of m/z 129.0558.

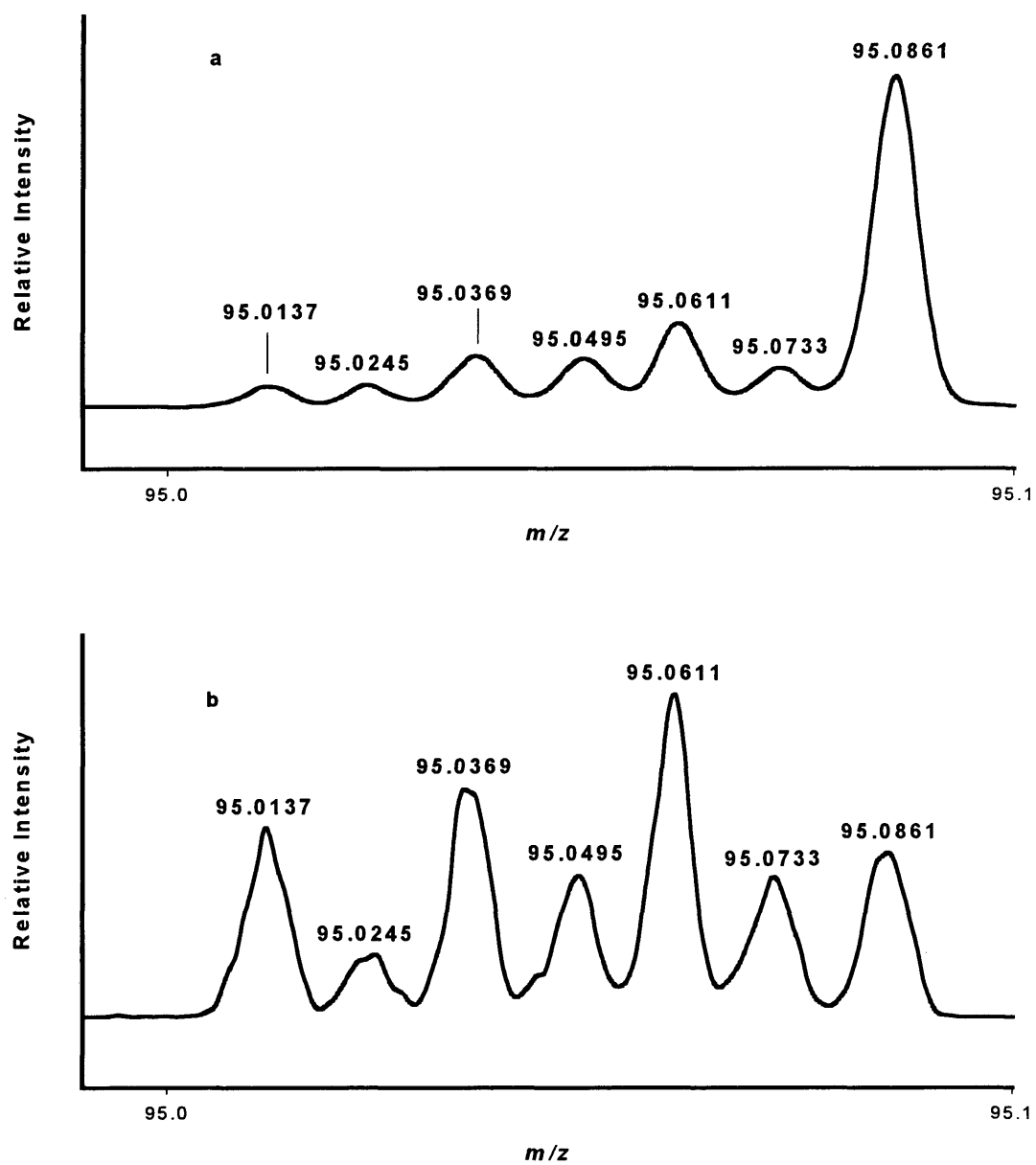


Figure 2.37. HR-DEI ( $R=10,000$ ) mass spectra of  $m/z$  95 from (a) *Brucella neotomae* and (b) *Bacillus anthracis*.

for the different bacterial species. Although differences in ion intensities between the profiles were observed, the  $m/z$  95 cluster had the same ions for both bacteria. A similar trend is observed for the other biomarker ions. The changes in the HR peak profiles observed in the different bacterial species are hypothesized to be a result of Gram-type. In Gram-negative bacteria, the cell wall consists of two double layers of phospholipids found in the outer membrane and in the plasma membrane. The contribution of the lipid based peaks is therefore higher than in the Gram-positive species, which contain only one double layer of phospholipids in the plasma membrane. Therefore, lipid-based peaks will tend to have higher intensities in Gram-negative bacteria as compared to Gram-positive bacteria.

## CONCLUSIONS

The ability to use DEI-HR-MS/MS to elucidate the source and composition of biomarker ions has been shown. As most nominal mass peaks in the spectrum of a complex sample (i.e. whole bacterial cells) are a consortium of peaks, DEI-HR-MS provides the capability to identify the components of the mass spectral cluster and characterize the components according to the biochemical class that gave rise to each. This information will aid in the process of differentiating microorganisms based on taxonomically significant ions. Ten peaks were found to carry carbohydrate/nucleic acid components:  $m/z$  67, 76, 79, 89, 93, 95, 103, 115, 129 and 131. Ten peaks were also found to carry protein components:  $m/z$  67, 76, 79, 89, 93, 95, 103, 115, 117 and 131. Furthermore, seven peaks were found to carry lipid components:  $m/z$  67, 79, 93, 95, 105, 115 and 129. These results are summarized in Table 2.7. The most intense ion for most of the clusters was either protein or lipid-based. Therefore, the use of carbohydrate and nucleic acid based peaks for the identification of bacteria using low mass ions 67, 76, 79, 89, 93, 95, 103, 105, 115, 117, 129 and 131 are less relevant than either fatty acid or

Table 2.7. Proposed origins of biomarker ions.

<b>Biomarker Ion</b>	<b>Carbohydrate Based</b>	<b>Nucleic Acid Based</b>	<b>Protein Based</b>	<b>Lipid Based</b>
67.0547	X		X	X
67.0421	X	X		X
67.0296		X		
67.0184	X		X	
76.0313			X	
76.0150	X			
79.0545			X	X
79.0417			X	
79.0296		X		
79.0178		X		
89.0392			X	
89.0234	X			
93.0702				X
93.0578		X		
93.0452		X	X	
93.0331		X		
93.0210	X			
95.0861				X
95.0611			X	
95.0495				X
95.0369		X		
95.0245		X		
95.0137	X			X
103.0543			X	
103.0411	X			
105.0704				X
105.0332				X
115.0761				X
115.0641	X			
115.0533			X	
117.0567			X	
129.0913	X			X
129.0558	X			X
131.0730			X	
131.0603		X		
131.0495			X	
131.0406			X	

protein based peaks in the cluster. The peaks that are labeled as unknown in Figures 2.2 – 2.13 were not observed in any of the standards or extracts that were analyzed. Therefore, no assignment of biochemical origins was appointed. The lack of pure standards for all possible pyrolysis products produced from biomaterials limits origin assignments. The present findings will aid in refining the selection process of ions used as biomarker ions specific for bacteria and in understanding the origins of these ions as arising from specific biochemical classes.

**REFERENCES**

- (1) Bowser, D. V.; Teece, R. G.; Somani, S. M. *Biomed. Mass Spectrom.* **1978**, *5*, 627.
- (2) Kulkarni, P. S.; Kulkarni, S. Y.; Pansare, V. S. *Org. Mass Spectrom.* **1986**, *21*, 23.
- (3) Cerny, R. L.; Tomer, K. B.; Gross, M. L. *Org. Mass Spectrom.* **1986**, *21*, 655.
- (4) Rollgen, F. W.; Giessmann, U.; Borchers, F.; Levsen, K. *Org. Mass Spectrom.* **1978**, *13*, 459.
- (5) Puzo, G.; Prome, J. C. *Adv. Mass Spectrom.* **1980**, *8*, 1003.
- (6) Fournie, J. J.; Puzo, G. *Anal. Chem.* **1985**, *57*, 2287.
- (7) Bruins, A. P. *Anal. Chem.* **1980**, *52*, 605.
- (8) Hostettmann, K.; Doumas, J.; Hardy, M. *Helv. Chim. Acta* **1981**, *64*, 297.
- (9) Bruins, A. P. *Biomed. Mass Spectrom.* **1981**, *8*, 31.
- (10) Rapp, U.; Dielmann, G.; Games, D. E.; Gower, J. L.; Lewis, E. *Adv. Mass Spectrom.* **1980**, *8B*, 1660.
- (11) Helleur, R. J.; Budgell, D. R.; Hayes, E. R. *Anal. Chim. Acta* **1987**, *192*, 243.
- (12) Shafizadeh, F. *J. Anal. Appl. Pyrolysis* **1982**, *3*, 283.
- (13) Potier, N.; Van Dorsselaer, A.; Bischoff, R. *Nucleic Acids Res.* **1994**, *22*, 3895.
- (14) Reddy, D. M.; Iden, C. R. *Nucleosides Nucleotides* **1993**, *12*, 815.
- (15) Wampler, F. M.; Blades, A. T.; Kebarle, P. *J. Am. Soc. Mass Spectrom.* **1993**, *4*, 289.
- (16) Buchanan, M. V.; Hettich, R. L. *Anal. Chem.* **1993**, *65*, 245A.
- (17) Fitzgerald, M. C.; Smith, L. M. *Annu. Rev. Biophys. Biomol.* **1995**, *24*, 117.
- (18) Kirpekar, F.; Nordhoff, E.; Hillenkamp, F. *Nucleic Acids Res.* **1994**, *22*, 3866.
- (19) Pieves, U.; Zurcher, W.; Schar, M. *Nucleic Acids Res.* **1993**, *21*, 3191.
- (20) Christian, N. P.; Colby, S. M.; Reilly, J. P. *Rapid Commun. Mass Spectrom.* **1995**, *9*, 1061.
- (21) Charnock, G. A.; Loo, J. L. *Anal. Biochem.* **1970**, *37*, 81.

- (22) Wiebers, J. L. *Anal. Biochem.* **1973**, *51*, 542.
- (23) Wiebers, J. L.; Shapiro, J. A. *Biochemistry* **1977**, *16*, 1044.
- (24) Burgard, D. R.; Perone, S. P.; Wiebers, J. L. *Biochemistry* **1977**, *16*, 1051.
- (25) Wiebers, J. L. *Nucleic Acids Res.* **1976**, *3*, 2959.
- (26) Rice, J. M.; Dudek, G. O.; Barber, M. *J. Am. Chem. Soc.* **1965**, *87*, 4569.
- (27) Rice, J. M.; Dudek, G. O. *J. Am. Chem. Soc.* **1967**, *89*, 2719.
- (28) Tournabene, T. G. ; Edgewood Research Development and Engineering Center: Aberdeen Proving Grounds, 1995.
- (29) Brock, T. D.; Madigan, M. T. *Biology of Microorganisms*, sixth ed.; Prentice Hall: Englewood Cliffs, 1991.
- (30) McBride, W. J.; Klingman, J. D. *Anal. Biochem.* **1968**, *25*, 109.
- (31) Frauk, G.; Strubert, W. *Chromatographia* **1973**, *6*, 522.
- (32) Husek, P.; Sweeley, C. C. *J. High Res. Chrom.* **1991**, *14*, 751.
- (33) Karas, M.; Hillenkamp, F. *Anal. Chem.* **1988**, *60*, 2299.
- (34) Tanaka, K.; Waki, H.; Ido, Y.; Akita, S.; Yoshida, Y.; Yoshida, T. *Rapid Commun. Mass Spectrom.* **1988**, *8*, 151.
- (35) Loo, J. A.; Udseth, H. R.; Smith, R. D. *Anal. Biochem.* **1989**, *179*, 404.
- (36) Blemann, K.; Martin, S. A. *Mass Spectrom. Rev.* **1987**, *6*, 1.
- (37) Shulman, G. P.; Simmonds, P. G. *Chem. Common.* **1968**, 1040.
- (38) Simmonds, P. G.; Medley, E. E.; Ratcliff, M. A. J.; Shulman, G. P. *Anal. Chem.* **1972**, *44*, 2060.
- (39) Ratcliff, M. A. J.; Medley, E. E.; Simmonds, P. G. *J. Org. Chem.* **1974**, *39*, 1481.
- (40) Chiavari, G.; Galletti, G. C. *J. Anal. Appl. Pyrolysis* **1992**, *24*, 123.
- (41) *Microbial Identification System operating manual*; Microbial ID: Newark, Del., 1993.
- (42) Murphy, R. C. *Mass Spectrometry of Lipids, Handbook of Lipid Research*; Plenum Press: New York, 1993.

- (43) Basile, F.; Beverly, M. B.; Hadfield, T. L.; Voorhees, K. J. *TrAC, Trends Anal. Chem.* **1998**, *17*, 95-109.
- (44) Anhalt, J. P.; Fenselau, C. *Anal. Chem.* **1975**, *47*, 219-225.
- (45) DeLuca, S. J.; Sarver, E. W.; Voorhees, K. J. *J. Anal. Appl. Pyrolysis* **1992**, *23*, 1-14.
- (46) Voorhees, K. J.; Basile, F.; Beverly, M. B.; Abbas-Hawks, C.; Hendricker, A.; Cody, R. B.; Hadfield, T. L. *J. Anal. Appl. Pyrolysis* **1997**, *40,41*, 111-134.
- (47) Mavrovouniotis, M. L.; Harper, A. M.; Ifarraguerri, A. I. ; Edgewood Research and Technology: Aberdeen Proving Ground, 1994.
- (48) Liang, X.; Zheng, K.; Qian, M. G.; Ludman, D. M. *Rapid Commun. Mass Spectrom.* **1990**, *10*, 1219.
- (49) Gondolf, K. B.; Batsford, S. R.; Vogt, A. *J. Chrom.* **1990**, *521*, 325.
- (50) Folch, J.; Lees, M.; Sloane-Stanley, G. H. *J. Biol. Chem.* **1957**, *226*, 497-509.
- (51) Jankowski, K. *Recent Developments in Mass Spectrometry in Biochemistry, Medicine and Environmental Research*; Elsevier Scientific Publishing Company: Amsterdam, 1983.
- (52) Schulten, H. R.; Bahr, U.; Gortz, W. *J. Anal. Appl. Pyrolysis* **1981/1982**, *3*, 229.
- (53) Gross, M. L.; Lyon, P. A.; Dasgupta, A.; Gupta, N. K. *Nucleic Acids Res.* **1978**, *5*, 2695.
- (54) Hendricker, A. D. Ph.D. Dissertation, Colorado School of Mines, Golden, CO, 1998.
- (55) Biemann, K. *Methods in Enzymology*; Academic Press: San Diego, 1990.
- (56) Noguerola, A. S. Ph.D. dissertation, Colorado School of Mines, Golden, CO, 1992.
- (57) Budzikiewicz, H.; Djerassi, C.; Williams, D. H. *Interpretation of Mass Spectra of Organic Compounds*; Holden-Day, Inc.: San Francisco, 1964.

### Chapter 3

## ***IN SITU* METHYLATION OF NUCLEIC ACIDS USING PYROLYSIS/MASS SPECTROMETRY**

### **ABSTRACT**

Curie-point pyrolysis/tandem mass spectrometry (Py/MS/MS) has been used with tetramethylammonium hydroxide (TMAH) to conduct *in situ* methylation of nucleic acid bases. Nitrogen bases in free nucleotides, oligonucleotides, calf thymus DNA and whole bacterial cells reacted *in situ* during pyrolysis with TMAH to form the methylated bases. Derivatization increased the volatility of the nitrogen bases and the mass of the diagnostic base peaks, thereby removing them from the positions of lower-mass background peaks. Each nitrogen base can be methylated to varying degrees according to the number of acidic hydrogens. The degree of methylation as a function of TMAH concentration for the oligonucleotide, calf thymus DNA, and the whole bacteria samples was determined and found to correlate with the nature (double-stranded, pure, free nucleotides, etc.) of DNA. The methylated bases were identified by their positive-ion electron ionization fragmentation patterns and confirmed with tandem mass spectrometry. The detection of the methylated bases by Py/MS/MS facilitates the goal of identifying the nucleic acids in a complex mixture (i.e. whole bacterial cells) without prior extraction and derivatization.

## INTRODUCTION

Traditionally, analysis of nucleic acids has presented an experimental challenge to mass spectroscopists due to the high polarity of nucleosides and nucleotides (1). Today, however, nucleic acids are studied extensively by several mass spectroscopic techniques including electrospray-mass spectrometry (ESI-MS) (2-5) and matrix-assisted laser desorption/ionization-mass spectrometry (MALDI-MS) (5-9). Developments in ESI-MS and MALDI-MS have redirected the analysis of nucleic acids away from more traditional techniques such as electron ionization (EI-MS), GC (gas chromatography)/EI-MS and pyrolysis mass spectrometry (Py-MS) (10-14). However, recent efforts by the U.S. Army to develop an automated biological detector has renewed interest in traditional sample pre-treatment and volatilization methods, like pyrolysis, prior to mass analysis of the resulting biomarkers (15). Derivatization of nucleic acids with a methylating agent prior to analysis can overcome the problem of low volatility. Furthermore, derivatization may serve to prevent thermal degradation of samples, and in many cases it may also produce spectra with more structural information (16,17). Enhancing the detection of nitrogen bases for mass spectrometric analysis is important in the differentiation between living matter and inorganic matter, and can provide some general bacteriological taxonomic information through the measurement of mole percent guanine plus cytosine (mol % G + C) of DNA (18).

The use of tetramethylammonium hydroxide (TMAH) for the *in situ* methylation of nucleic acid bases using pyrolysis/tandem mass spectrometry (Py/MS/MS) has not been previously reported. Past studies involving Py/MS and nucleic acids have focused on the identification and detection of minor nucleotides (14), sequence analysis of oligodeoxyribonucleotides (12,13), discrimination between closely similar oligonucleotides (19), quantification of the percentages of nitrogen bases (18) and structural characterization of natural nucleosides (1). However, all of these applications focused on pure standards or extracted DNA. The following study presents a sensitive

and rapid detection of nucleic acids, following thermal, *in situ* derivatization without the need for extraction or prior derivatization, from whole bacterial cells with subsequent MS/MS analysis. This approach uses the methylated nitrogen bases as biomarkers.

## EXPERIMENTAL

### *Reagents*

A 2 mg/ml solution of adenosine 5'-monophosphate (AMP), an 8 mg/ml solution of thymidine 5'-monophosphate (TMP), a 4 mg/ml solution of guanosine 5'-monophosphate (GMP) and a 4 mg/ml solution of cytidine 5'-monophosphate (CMP) were prepared in distilled water and were used as free nucleotide standards. A calf thymus DNA standard solution was prepared in distilled water at 1 mg/ml. A 1.0 M tetramethylammonium hydroxide stock solution in methanol (HPLC grade) was used for the *in situ* methylation reactions. Other TMAH concentrations were prepared by serial dilution of the stock solution. All reagents were purchased from Sigma.

### *Oligonucleotides*

A single-strand oligodeoxyribonucleotide of the sequence ACG TAA CCG CTT ACG T was synthesized in an ABI Model 392 DNA Synthesizer by the Armed Forces Institute of Pathology, Washington, DC.

### *Bacterial sample*

The bacterial sample, *Brucella neotomae*, was described in Chapter 1.

### *Instrumental*

Pyrolysis mass spectra were obtained using an Extrel Model ELQ-400 triple quadrupole tandem mass spectrometer fitted with a Fisher Model 0310 (1 kW) rf-

generator to supply power to a Curie-point pyrolysis coil. The instrument and operating parameters have been described in the Experimental Section of Chapter 1.

### *Sample preparation*

The sample preparation used has also been described in the Experimental Section of Chapter 1. However, for *in situ* methylation experiments, a 5  $\mu\text{L}$  aliquot of specified TMAH concentration was added onto the sample-coated Curie-point wire. The resulting mixture of TMAH and analyte was then evaporated to dryness. All samples were analyzed in triplicate.

## **RESULTS AND DISCUSSION**

### **Free nucleotides**

To characterize the *in situ* methylation of nitrogen bases, standards of AMP, TMP, CMP and GMP were subjected to pyrolysis with and without TMAH and subsequently analyzed by EI-MS. The pyrolysis mass spectra of the standards without methylation and with *in situ* methylation by TMAH are shown in Figure 3.1 and Figure 3.2, respectively. The spectra of the standards exhibit major peaks at the molecular ions for the pyrimidine and purine bases, that is at  $m/z$  111, 126, 135 and 151 for cytosine (C), thymine (T), adenine (A) and guanine (G), respectively along with their EI+ fragment ions. The higher-mass peaks in Figure 3.1d are due to fragmentation of the dimerized compound. No pyrolytic degradation product, other than the free bases, is observed. Characteristic C peaks are  $m/z$  111 ( $M^+$ ), 83 ( $M^+ - \text{CO}$ ), 69 ( $M^+ - \text{NCO}$ ) and 68 ( $M^+ - \text{HNCO}$  or  $M^+$  after sequential losses of  $-\text{NH}_2$  and  $-\text{HCN}$ ). Thymine fragments are  $m/z$  126 ( $M^+$ ), 83 ( $M^+ - \text{HNCO}$ ) and 55 (sequential losses of  $-\text{HNCO}$  followed by  $-\text{CO}$ ). The major EI+ fragments associated with A include  $m/z$  135 ( $M^+$ ), 108 ( $M^+ - \text{HCN}$ ) and 81 (two sequential losses of  $-\text{HCN}$ ). Characteristic G peaks include  $m/z$  151 ( $M^+$ ),

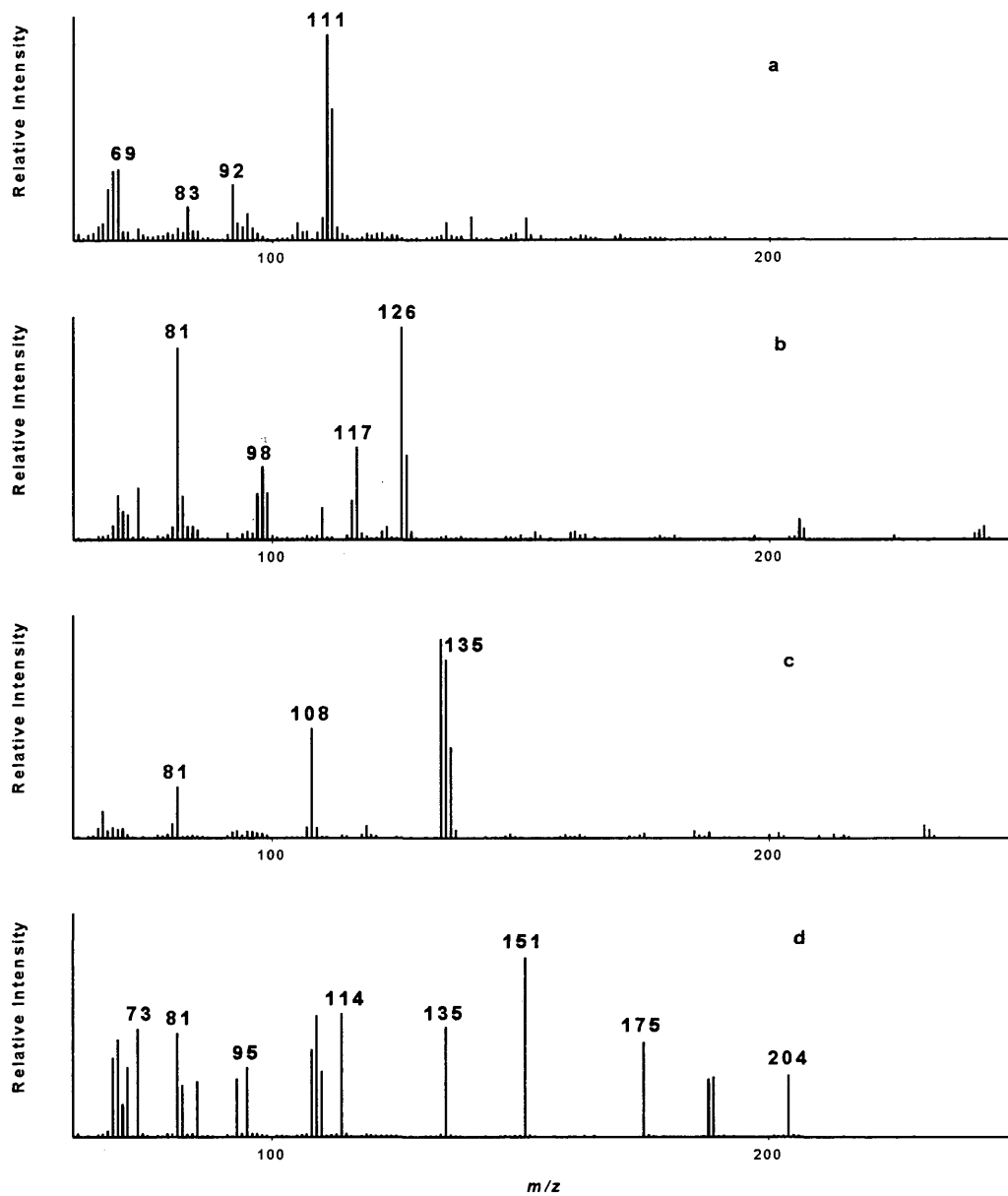


Figure 3.1. Pyrolysis mass spectra of the standards  
(a) CMP, (b) TMP, (c) AMP and (d) GMP.

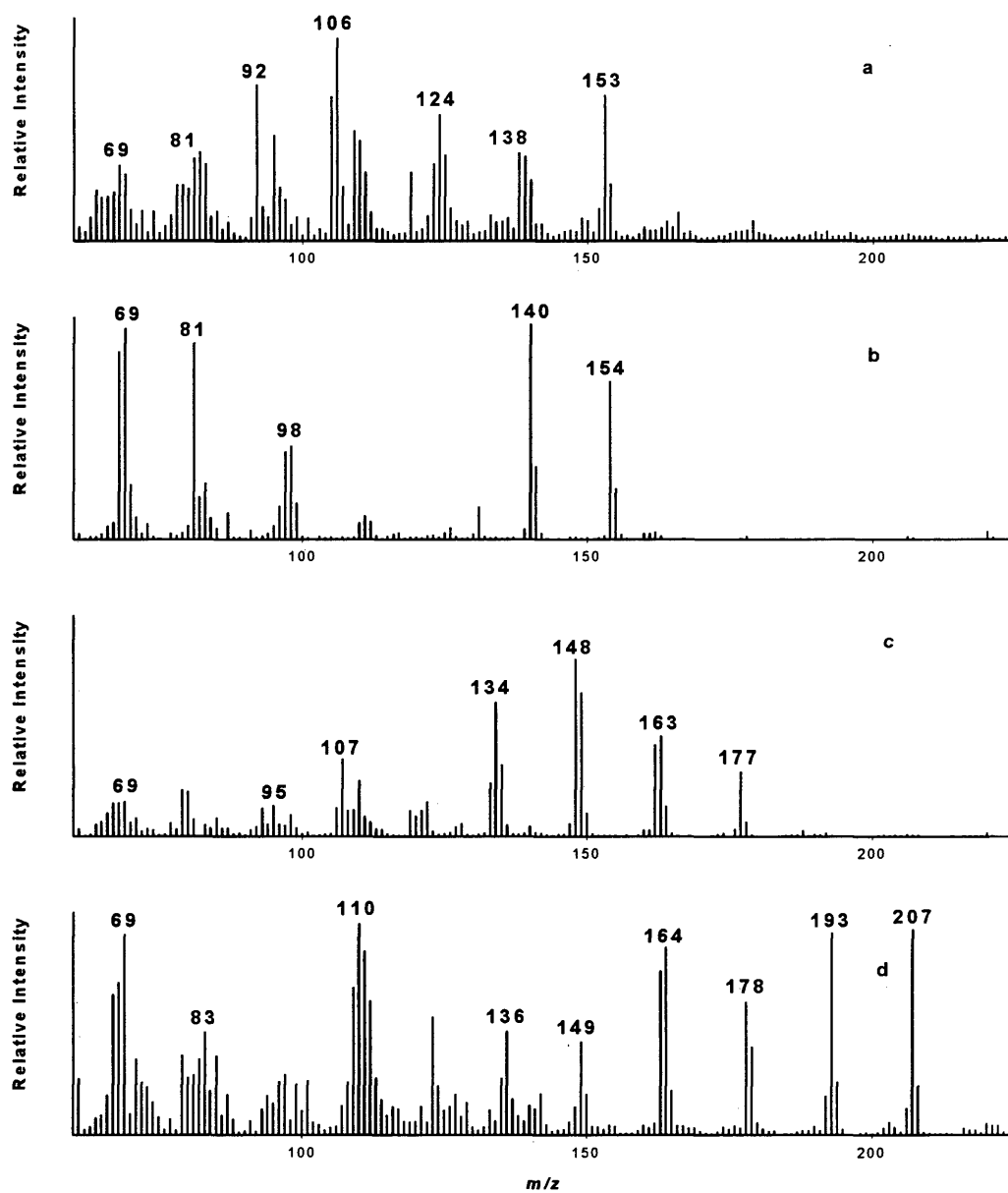


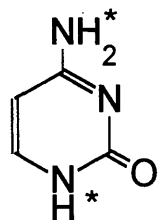
Figure 3.2. Pyrolysis mass spectra showing the *in situ* methylated standards of (a) CMP + 0.3M TMAH, (b) TMP + 0.03M TMAH, (c) AMP + 0.03M TMAH and (d) GMP + 0.05M TMAH.

135 ( $M^+ - NH_2$ ), 110 ( $M^+ - CHN_2$ ), 109 ( $M^+ - CH_2N_2$ ) and 108 ( $M^+ - HNCO$ ). The EI+ fragmentation pattern of each nucleotide has been published elsewhere (14, 20, 21).

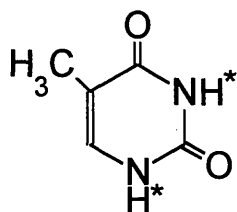
The pyrolysis mass spectra of *in situ* methylated standards with TMAH show distinct ions in comparison to those of the unmethylated standards. Each nitrogen base can be methylated to varying degrees according to the number of acidic hydrogens and, as mentioned later, TMAH concentration. There are four possible methylation sites in G, three sites in C and A and two sites in T (Figure 3.3). A list of these ions is given in Table 3.1. Along with the methylated base peaks, EI+ fragment ions at m/z 124 and 138 for C, m/z 148 and 162 for A, and m/z 164 and 178 for G were also observed. These ions are produced by losses of  $\cdot CH_3$  or  $\cdot NCH_3$ . These losses were confirmed by *in situ* thermal methylation with deuterated TMAH followed by MS/MS. Product-ion spectra of m/z 153 (C, with three methylations), m/z 154 (T, with two methylations), m/z 177 (A, with three methylations) and m/z 193 (G, with three methylations) are shown in Figure 3.4. Other major ions present in these spectra are the EI+ fragment ions associated with each base (14, 20, 21) plus the methyl group. Thymine fragments to m/z 97 ( $M^+ - CH_3NCO$ ) and 69 (sequential losses of  $-CH_3NCO$  followed by  $-CO$ ). These losses, too, were verified by a study using deuterated TMAH.

It was noted during the analysis of the free nucleotides that the concentration of TMAH had an effect on the extent of *in situ* methylation of the nitrogen bases (the number of acidic sites methylated in a base). Generally, the highest degree of methylation for CMP (3 methyl groups, ratio of m/z 153 / m/z 111) occurred with higher concentrations of TMAH, while single methylation (ratio of m/z 125 / m/z 111) occurred with lower concentrations of TMAH. Similar results were observed for TMP and AMP. GMP, however, did not follow this trend and at this time the discrepancy cannot be explained, but may be due to sample preparation on the pyrolysis wire.

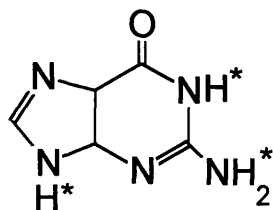
The information generated from the methylation and subsequent EI+ fragmentation of the nitrogen bases of the standards was used to provide a basis to



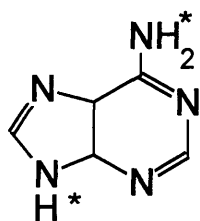
Cytosine  
MW 111  
Derivative masses 125, 139, 153



Thymine  
MW 126  
Derivative masses 140, 154



Guanine  
MW 151  
Derivative masses 165, 179, 193, 207



Adenine  
MW 135  
Derivative masses 149, 163, 177

\* acidic hydrogen(s): site for *in situ* methylation

Figure 3.3. DNA bases and their methyl derivatives.

Table 3.1. M/z values of the methylated nitrogen base peaks.

---

<b>Nitrogen base</b>	<b>Number of methylations</b>			
	<b>1</b>	<b>2</b>	<b>3</b>	<b>4</b>
Cytosine	125	139	153	
Thymine	140	154	-	
Adenine	149	163	177	-
Guanine	165	179	193	207

---

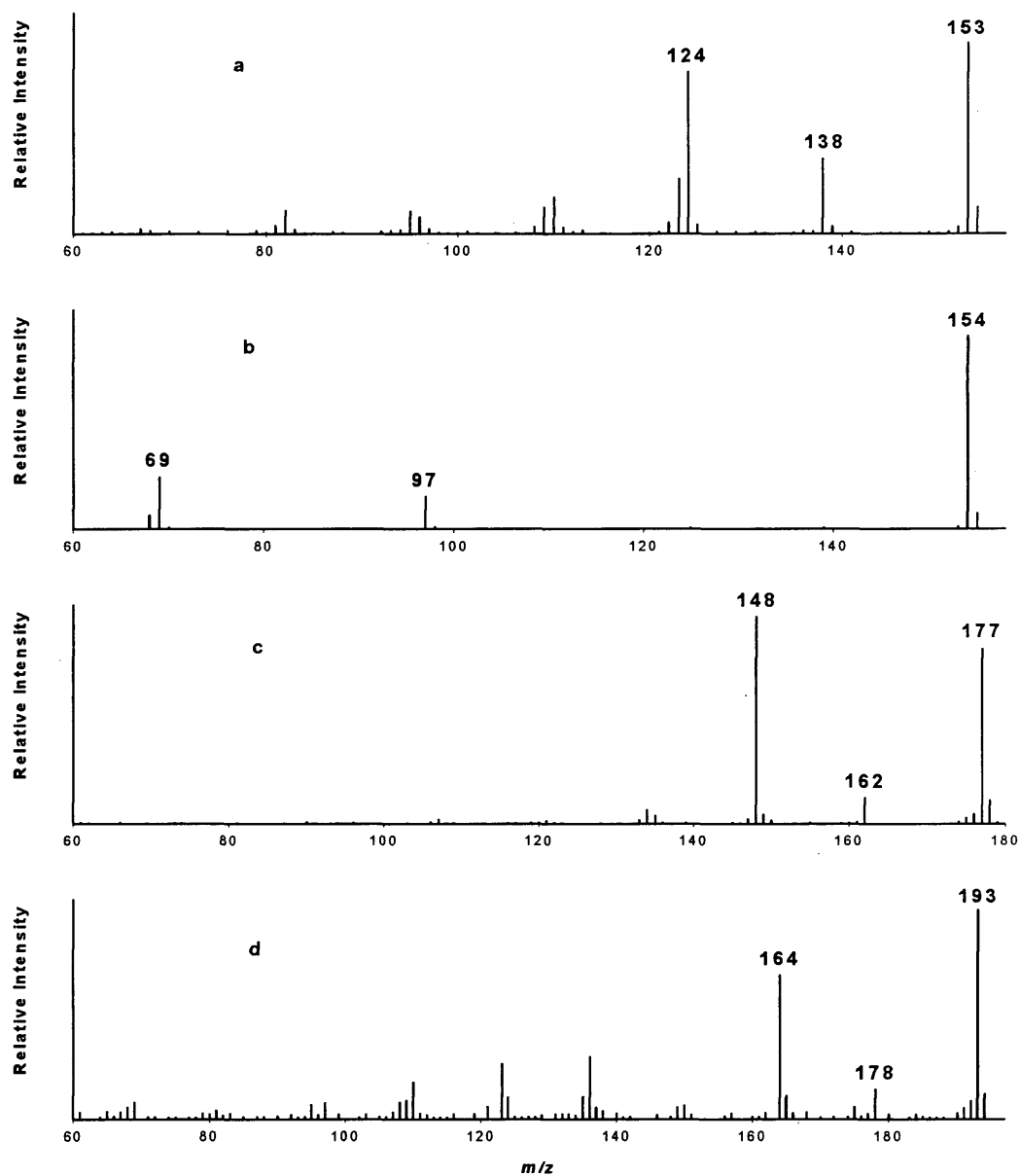


Figure 3.4. Pyrolysis product-ion spectra of (a)  $m/z$  153 from *in situ* methylated CMP with 0.01M TMAH, (b)  $m/z$  154 from TMP with 0.01M TMAH, (c)  $m/z$  177 from AMP with 0.01M TMAH and (d)  $m/z$  193 from GMP with 0.01M TMAH.

understand the *in situ* methylation of more complex samples: oligonucleotides, calf thymus DNA and DNA in whole bacterial cells.

### Oligonucleotide

The oligonucleotide was analyzed under the same Py/MS conditions as previously discussed. Primary fragmentation of any polydeoxyribonucleotide upon pyrolysis involves cleavage at the phosphodiester bonds linking the nucleotide residues. Subsequent EI<sup>+</sup> fragmentations result in ions that are diagnostic for the common nucleotide components of the polynucleotide (12-14), namely  $m/z$  111, 126, 135 and 151 as mentioned previously. The pyrolysis mass spectrum of the oligonucleotide is given in Figure 3.5a. Major ions are common nucleotide components. While this oligonucleotide has equal amounts of each nitrogen base, only the molecular ions of T ( $m/z$  126) and A ( $m/z$  135) were observed. Cytosine fragmented to  $m/z$  69 and G to  $m/z$  135 and  $m/z$  108. The ion at  $m/z$  215 is due to A plus the sugar moiety. The spectrum in Figure 3.5b is that of the *in situ* methylated oligonucleotide with TMAH. The ions observed in the spectrum are those listed in Table 3.1. The other major ions present in the spectrum are the EI<sup>+</sup> fragment ions associated with each methylated base.

Spectra of the oligonucleotide obtained with varying TMAH concentrations were similar to the spectrum given in Figure 3.5b. However, the absolute intensity of the methylated nitrogen base peaks (ions presented in Table 3.1) varied according to TMAH concentration. A comparison of TMAH concentration versus ion intensity ratio (ion with highest degree of methylation to ion with no methylation) for each base was performed. The maximum degree of methylation in each base was observed at a different TMAH concentration even though the bases were present in equal amounts. This difference in reactivity may be attributed to the structural differences of the bases (purine versus pyrimidine) or to their overall volatility. However, a 0.03M TMAH concentration was found to give the most useful profile for all of the bases (i.e. the spectra where most of the ions listed in Table 3.1 were above noise levels or had the highest intensity).

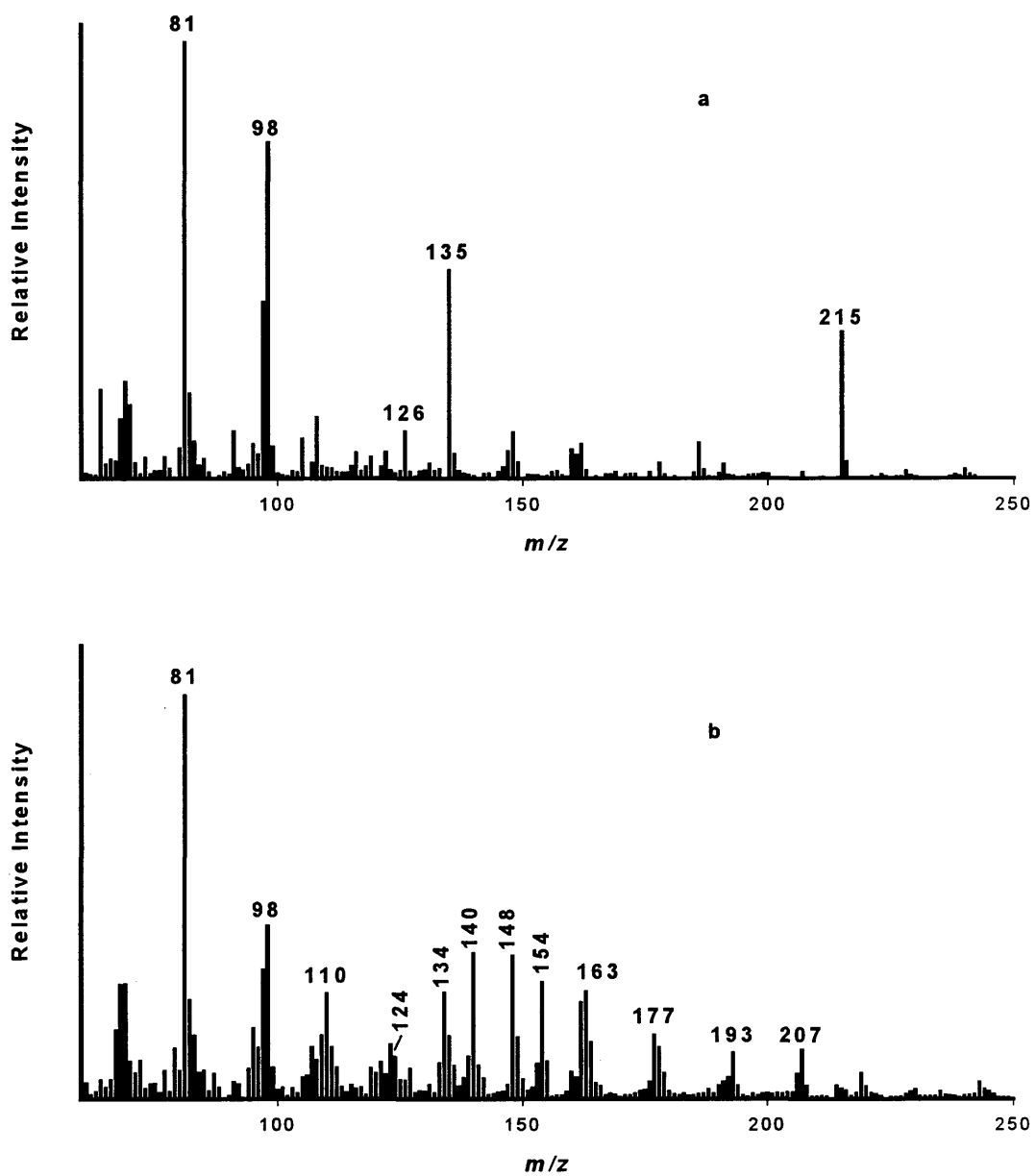


Figure 3.5. Pyrolysis mass spectra of the oligonucleotide (a) without and (b) with *in situ* methylation using 0.03M TMAH.

### **Calf thymus DNA**

To further investigate the TMAH concentration dependence of thermal *in situ* methylation of nitrogen bases, a pure extracted nucleic acid (calf thymus DNA) was studied. Pyrolysis mass spectra of calf thymus DNA without and with TMAH are shown in Figure 3.6. Spectra obtained using different TMAH concentrations had a similar profile to the spectrum in Figure 3.6b. Figure 3.7 presents the thermal *in situ* methylated product-ion scans of  $m/z$  153,  $m/z$  154,  $m/z$  177 and  $m/z$  193 for calf thymus DNA. Comparison of the calf thymus DNA Py/MS/MS spectra (Figure 3.7) with those of the free nucleotide (Figure 3.4) shows that peak ratios in the spectra are unaffected by the nature of the sample (free nucleotides vs. pure DNA). However, as with the oligonucleotide, each of the bases required a different TMAH concentration for maximum methylation.

### **Bacterial whole cells**

Figure 3.8a and 3.8b are representative spectra from the whole cell (*B. neotomae*) without and with pyrolytic *in situ* methylation, respectively. Even though the calf thymus DNA data indicated that a 0.03M TMAH concentration gave the most useful profile or best results for that sample, a 0.05M TMAH concentration gave the most useful profile with the best signal-to-noise ratio, for the whole bacterial cell. The difference in TMAH concentration requirements between bacterial whole cells and pure calf thymus DNA may be attributed to the bacterial whole cell being much more complex, consisting of DNA, RNA, proteins and fatty acids, all of which can be derivatized during *in situ* methylation. Also, bacteria may require stronger conditions for thermal methylation to occur.

The optimal biomarkers for DNA bases in whole cells, by *in situ* methylation Py/MS/MS, were determined (see Table 3.2). Figure 3.9 shows product spectra of  $m/z$  153, 154, 177 and 193 for a whole bacterial cell sample. All the MS/MS spectra, except that of  $m/z$  154, matched the Py/MS/MS spectra obtained from the pure nucleotide

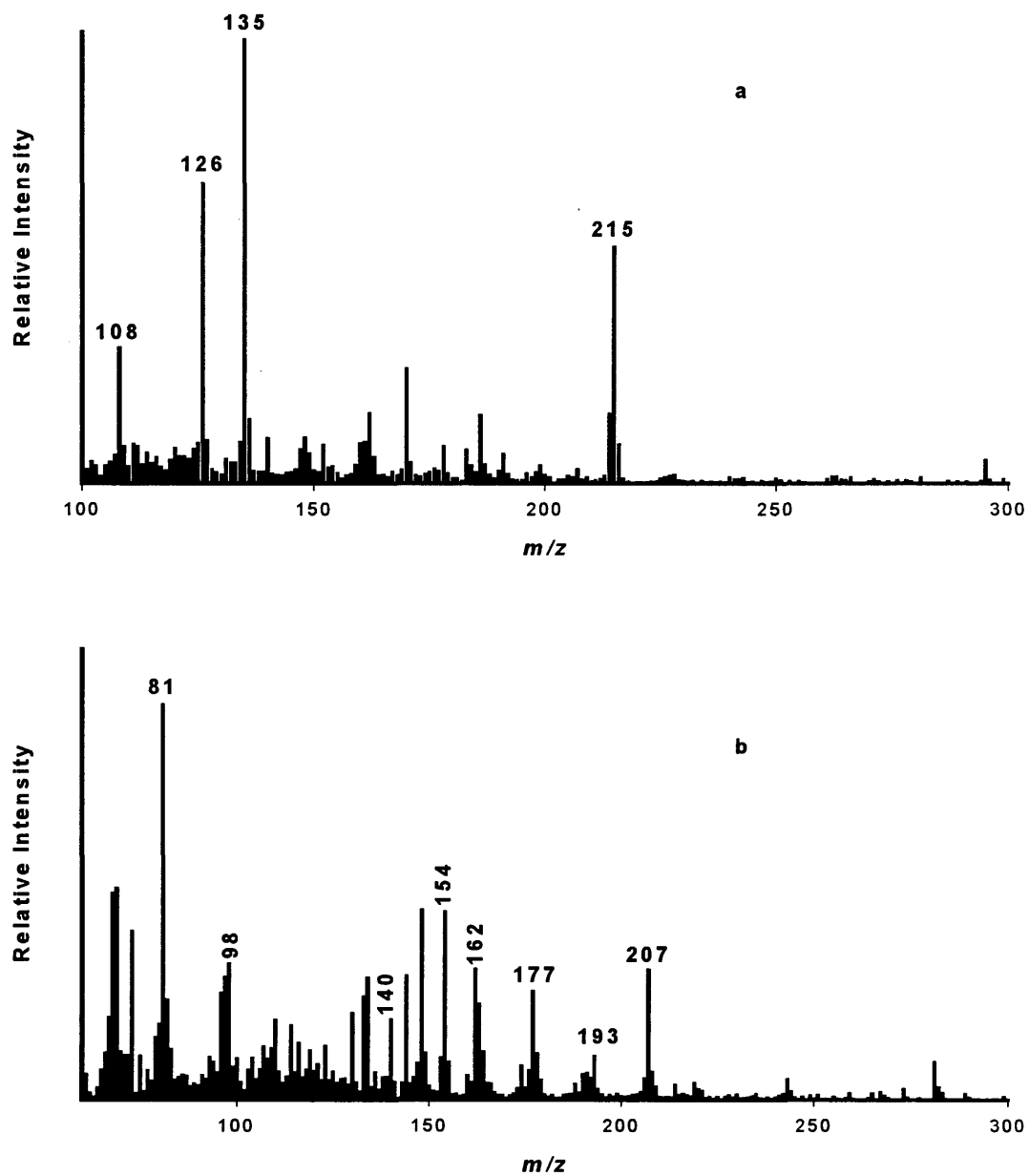


Figure 3.6. Pyrolysis mass spectra of calf thymus DNA (a) without and (b) with *in situ* methylation using 0.03M TMAH.

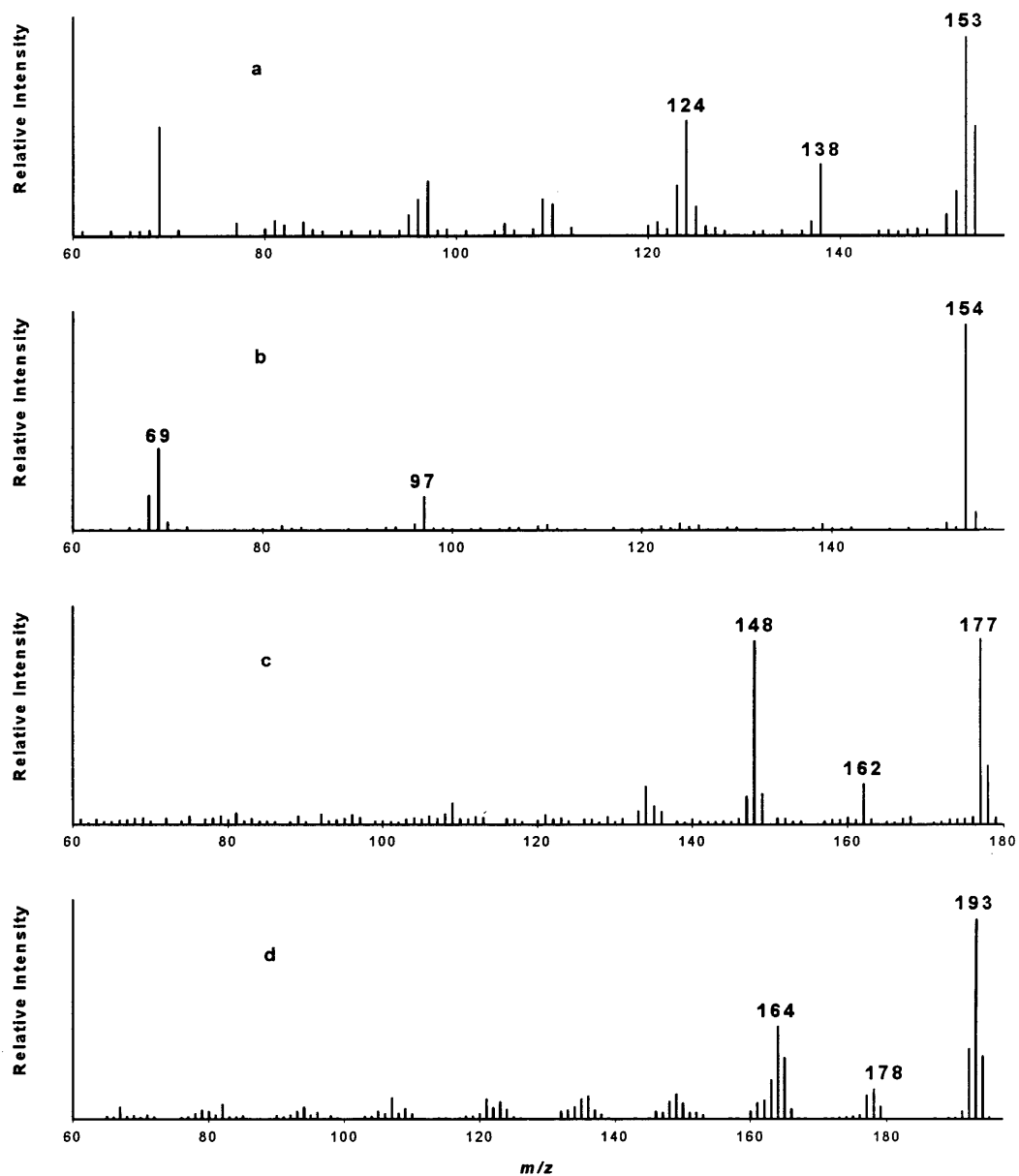


Figure 3.7. Pyrolysis product-ion spectra from *in situ* methylated calf thymus DNA with 0.1M TMAH of (a)  $m/z$  153, (b)  $m/z$  154, (c)  $m/z$  177 and (d)  $m/z$  193.

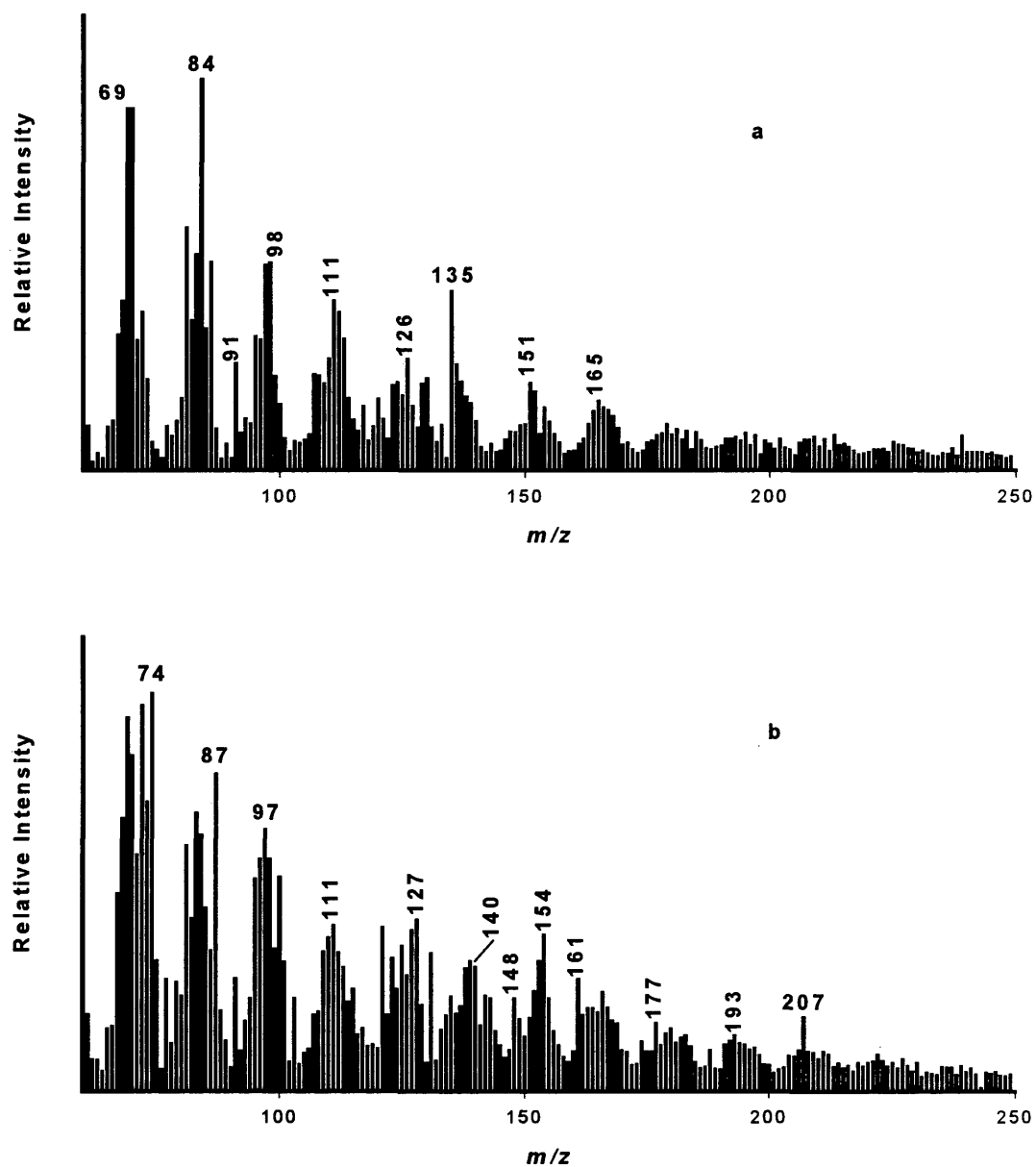


Figure 3.8. Pyrolysis mass spectra of *B. neotomae* whole cells (a) without and (b) with *in situ* methylation using 0.05M TMAH.

Table 3.2. Nucleic acid biomarker ions for the whole cell, *B. neotomae*.

---

<b>Nitrogen base</b>	<b>Biomarker ion</b>
Cytosine	m/z 153, three methylation sites
Adenine	m/z 177, three methylation sites
Guanine	m/z 193, three methylation sites

---

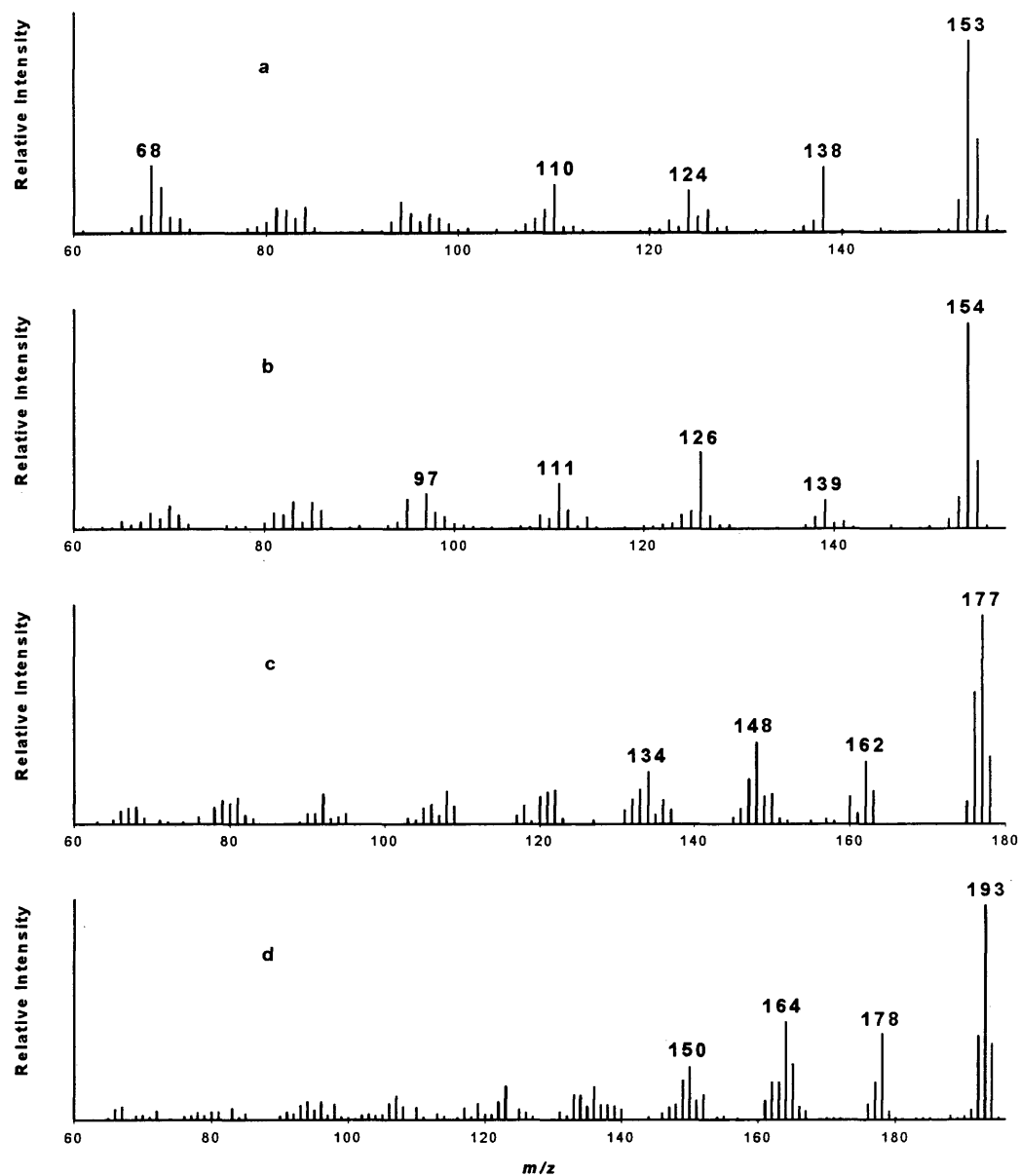


Figure 3.9. Pyrolysis product-ion spectra from *in situ* methylated *B. neotomae* whole cells with 0.05M TMAH of (a)  $m/z$  153 for cytosine, (b)  $m/z$  154 for thymine, (c)  $m/z$  177 for adenine and (d)  $m/z$  193 for guanine.

standards (Figure 3.4). The ion at  $m/z$  154 has other structural isomers associated with it, as indicated by the fragment peaks at  $m/z$  139, 126 and 111 (Figure 3.9). The presence of other species at  $m/z$  154 is shown in the high resolution mass spectrum from *B. neotomae*, Figure 3.10. Therefore, its use as a biomarker, solely for the nitrogen base thymine, may not be useful. Other methylated ion peaks may also be used as biomarkers (e.g.  $m/z$  163 for two methylations of adenine) in addition to those listed in Table 3.2. The best biomarker for each base varies according to the degree of methylation.

## CONCLUSIONS

The ability to use Curie-point pyrolysis mass spectrometry for *in situ* methylation of nitrogen bases, including those present in whole bacterial cells, has been shown to give increased structural information. Rather than observing only a few nitrogen base peaks at lower masses, *in situ* methylation increases the masses and volatility of the nitrogen base peaks and allows identification of more ions representative of DNA bases. Additionally, *in situ* methylation is a rapid technique (total time for analysis is less than 10 minutes) that affords no appreciable sample loss, and allows the routine detection of cytosine and guanine which are difficult to detect otherwise. Based on these results, *in situ* methylated nitrogen bases can be successfully used as biomarkers for identifying DNA components in a broad spectrum of samples ranging from purified DNA to whole cells. The data generated with this approach has been evaluated for its use in determining mol % G + C content of DNA in bacteria, and it will be discussed in the following chapter.

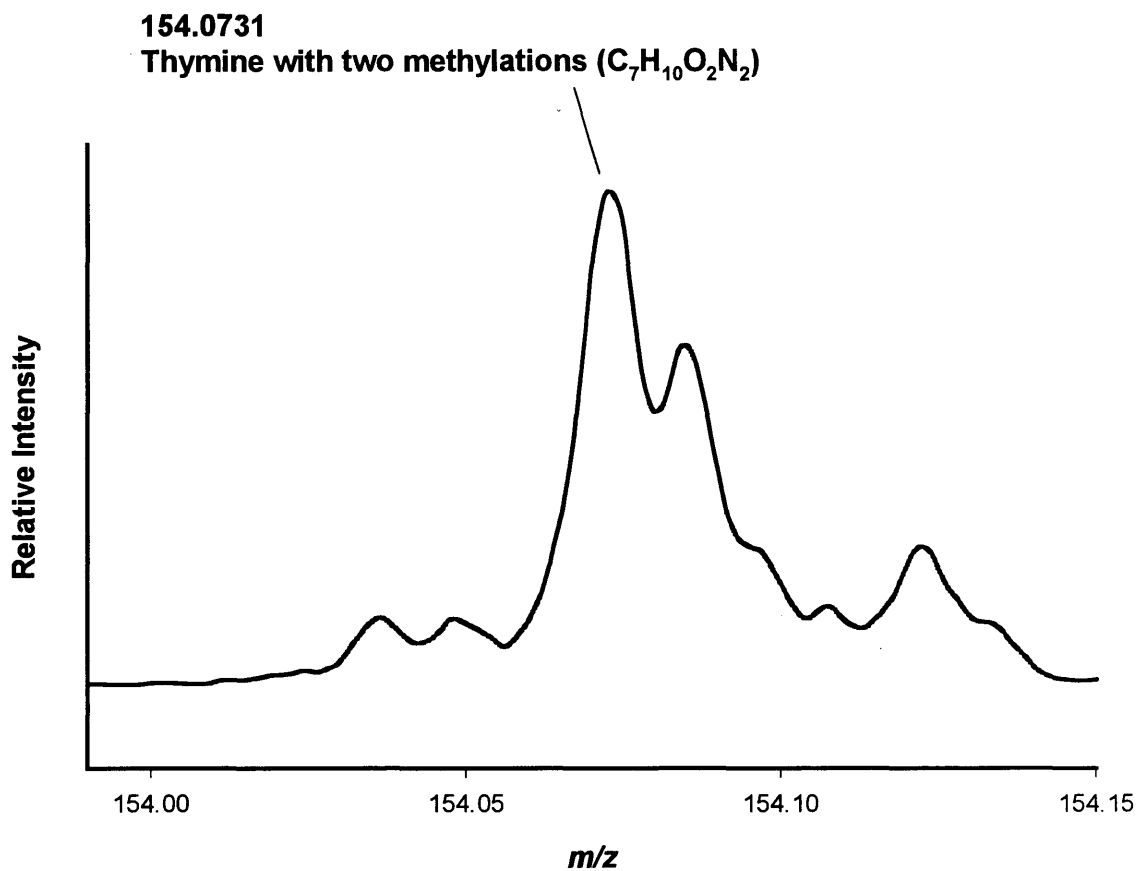


Figure 3.10. HR-DEI ( $R=10,000$ ) mass spectrum of  $m/z$  154 from *in situ* methylated *Brucella neotomae*.

## REFERENCES

- (1) McCloskey, J. A. *Acc. Chem. Res.* **1991**, *24*, 81.
- (2) Potier, N.; Van Dorsselaer, A.; Bischoff, R. *Nucleic Acids Res.* **1994**, *22*, 3895.
- (3) Reddy, D. M.; Iden, C. R. *Nucleosides Nucleotides* **1993**, *12*, 815.
- (4) Wampler, F. M.; Blades, A. T.; Kebarle, P. *J. Am. Soc. Mass Spectrom.* **1993**, *4*, 289.
- (5) Buchanan, M. V.; Hettich, R. L. *Anal. Chem.* **1993**, *65*, 245A.
- (6) Fitzgerald, M. C.; Smith, L. M. *Annu. Rev. Biophys. Biomol.* **1995**, *24*, 117.
- (7) Kirpekar, F.; Nordhoff, E.; Hillenkamp, F. *Nucleic Acids Res.* **1994**, *22*, 3866.
- (8) Pieves, U.; Zurcher, W.; Schar, M. *Nucleic Acids Res.* **1993**, *21*, 3191.
- (9) Christian, N. P.; Colby, S. M.; Reilly, J. P. *Rapid Commun. Mass Spectrom.* **1995**, *9*, 1061.
- (10) Charnock, G. A.; Loo, J. L. *Anal. Biochem.* **1970**, *37*, 81.
- (11) Wiebers, J. L. *Anal. Biochem.* **1973**, *51*, 542.
- (12) Wiebers, J. L.; Shapiro, J. A. *Biochemistry* **1977**, *16*, 1044.
- (13) Burgard, D. R.; Perone, S. P.; Wiebers, J. L. *Biochemistry* **1977**, *16*, 1051.
- (14) Wiebers, J. L. *Nucleic Acids Res.* **1976**, *3*, 2959.
- (15) Snyder, A. P.; Smith, P. B. W.; Dworzanski, J. P.; Meuzelaar, H. L. C. *Pyrolysis-Gas Chromatography-Mass Spectrometry: Detection of Biological Warfare Agents*; American Chemical Society: Washington, 1994.
- (16) Knapp, D. R. *Methods Enzymol.* **1990**, *193*, 314.
- (17) Beverly, M. B.; Basile, F.; Voorhees, K. J.; Hadfield, T. L. *Rapid Commun. Mass Spectrom.* **1996**, *10*, 455-58.
- (18) Hawley, D. M.; Wiebers, J. L. *Nucleic Acids Research* **1978**, *5*, 4949.
- (19) Freeman, R.; Wheeler, J.; Sisson, P. R.; Ward, A. C.; Robertson, H.; Lightfoot, N. *F. J. Anal. Appl. Pyrolysis* **1994**, *28*, 39.
- (20) Rice, J. M.; Dudek, G. O.; Barber, M. *J. Am. Chem. Soc.* **1965**, *87*, 4569.

- (21) Rice, J. M.; Dudek, G. O. *J. Am. Chem. Soc.* **1967**, *89*, 2719.

## Chapter 4

### NITROGEN BASE COMPOSITION ESTIMATION BY MASS SPECTROMETRY

#### ABSTRACT

Mass spectrometry with *in situ* methylation has been used to analyze nucleotide solutions, pure DNA and whole bacterial cells for the purpose of determining nitrogen base content. Standard curves were constructed for each class of samples (i.e. nucleotide solutions, pure DNA and whole bacterial cells) based on the observation that a direct correlation existed between the percent relative intensity of diagnostic peaks ( $m/z$  111, 125, 139, 153 from cytosine, 126, 140, 154 from thymine, 135, 149, 163, 177 from adenine and 151, 165, 179, 193, 207 from guanine) from each nitrogen base in the mass spectrum and the known percent composition of the samples. The mole percent guanine plus cytosine (mol % G+C) content of unknowns was calculated using the calibration curves. The construction of the calibration curves and the analysis of the unknowns are presented.

#### INTRODUCTION

An observation made by E. Chargaff in the late 1940's, stated that certain regularities could be seen in the percentages of heterocyclic (nitrogen) bases obtained from the DNA of a variety of species. The deoxyribonucleic acid (DNA) of most organisms contains the purine bases adenine (A) and guanine (G) and the pyrimidine

bases thymine (T) and cytosine (C). Chargaff noted that the ratio  $(\%A+\%T)/(\%G+\%C)$  varied from species to species. Later, 1953, Watson and Crick proposed the secondary structure of DNA as a double helix. The DNA in eukaryotic and prokaryotic organisms consists of double strands with specific base pairs (A+T) or (G+C) located along complementary strands. Due to the observation that the ratio of A+T to G+C base pairs may differ from one organism to the next and that the ratio in a given organism, usually expressed as mole percentage G+C (mol % G+C), is relatively constant, the mol % G+C content has been used for the comparative characterization of organisms. A DNA base ratio expressed as mole percent guanine plus cytosine (mol % G+C) and given by the expression,

$$\{[(G+C)/(A+T+G+C)] \times 100\}$$

is a unique feature of DNA that has taxonomic significance. Among the bacteria, the mol % G+C content range from approximately 25-75% and the value is constant for a given organism. Often, bacteria that are closely related have similar mol % G+C content. However, mol % G+C content is an exclusionary determinant rather than a supportive one in the characterization of bacteria because the mol % G+C content does not take into account the linear arrangement of the nucleotides in the DNA.

Initially, the mol % G+C content was determined by acid hydrolysis of the DNA, followed by separation of the nucleotide bases by paper chromatography and then elution and quantification of the individual bases spectrophotometrically (1). Also, the thermal denaturation ( $T_m$ ) and buoyant density ( $B_d$ ) methods have been employed to determine mol % G+C (2). These are traditional analysis techniques that measure indirectly the mol % G+C. During the controlled heating of double-stranded DNA in an UV spectrophotometer, the absorbance increases. The temperature at the midpoint of the curve obtained by plotting temperature versus absorbance is called the “melting temperature” or  $T_m$ . The higher the  $T_m$ , the higher the mol % G+C of the DNA (2).

Similarly, when DNA is exposed to centrifugation in a cesium chloride (CsCl) density gradient, the DNA will become located in the form of a band at a position where its density exactly matches that of the CsCl solution (2). The density of DNA in CsCl increases linearly with the mol % G+C (3). Although these methods are widely used, problems do arise due to contamination and/or excessive fragmentation of the DNA during its purification. Therefore, high pressure liquid chromatography (HPLC) methods have been employed to eliminate these problems (4 - 6). Yet, HPLC analysis requires a time-consuming nuclease digest of the DNA. A more recent approach to estimating the mol % G+C has been double-staining bacterial cells with the fluorescent dyes chromomycin A3 and Hoechst 33258. Chromomycin binds preferentially to DNA rich in G+C and Hoechst 33258 binds preferentially to DNA rich in A+T. The cells are then analyzed in a dual-beam flow cytometer (7).

The capabilities of mass spectrometry in biochemistry are well established. This technique offers high sensitivity, detailed structural information and rapid analysis. Nucleic acids are among the biopolymers commonly analyzed. Hawley and Wiebers (8), Jankowski (9) and Soler (10) all used pyrolysis mass spectrometry (Py-MS) to quantify the common components of DNA. They found that a direct measurement of the diagnostic ions,  $m/z$  111 (C), 126 (T), 135 (A) and 151 (G) reflected the amount of nitrogen base present. Standard curves for each nitrogen base were constructed based on the observation that a direct correlation existed between the percent deflection of diagnostic peaks from each nitrogen base in the mass spectrum and the known percent composition of pure standards. The percent deflection was defined as the peak height of a given base divided by the total peak heights of all the bases. An example of this calculation for cytosine follows:

$$\% \text{ deflection for cytosine} = [(PH \text{ of } 111 / \Sigma PH \text{ of } 111, 126, 135, 151) \times 100]$$

$$PH = \text{peak height (cm)}$$

The relationship between the percent deflection and the percent composition was shown by regression analysis to be linear. This work was based on pure DNA extracts.

As described in Chapter 3, the premise for using tetramethylammonium hydroxide (TMAH) with pyrolysis mass spectrometry (Py-MS) for the *in situ* methylation and analysis of nitrogen bases, has been to obtain quantitative compositional information of DNA. This quantitative data (mol % G+C) is essential for determining the unrelatedness of two organisms. An increase in nitrogen base volatility is realized when these bases are methylated at the N-H and O-H groups. The present study involves the estimation of mol % G+C for free nucleotide solutions, pure DNA and whole bacterial cells using Py-MS with *in situ* methylation. Several mass spectrometers were employed to verify the validity of this technique. This approach uses the methylated nitrogen bases as diagnostic peaks.

## **EXPERIMENTAL**

### *Reagents*

Equimolar (0.1M) solutions of adenosine 5'-monophosphate (AMP), thymidine 5'-monophosphate (TMP), guanosine 5'-monophosphate (GMP) and cytidine 5'-monophosphate (CMP) were prepared separately in distilled water. These equimolar solutions were then mixed to give the samples listed in Table 4.1. Pure DNA standard solutions of calf thymus, *E. coli*, *M. luteus*, and salmon sperm were prepared in distilled water at 1 mg/ml. A 1.0 M tetramethylammonium hydroxide stock solution in methanol (HPLC grade) was used for the *in situ* methylation reactions. Other TMAH concentrations were prepared by serial dilution of the stock solution. All reagents were obtained from Sigma.

Table 4.1. Free nucleotide solutions used for the construction of a standard curve for calculating % composition of nitrogen bases.

<b>Standard Solution</b>	<b>μL of 0.1M CMP</b>	<b>μL of 0.1M TMP</b>	<b>μL of 0.1M AMP</b>	<b>μL of 0.1M GMP</b>
27% G+C	130	360	370	140
35% G+C	180	325	325	170
40% G+C	200	290	310	200
51% G+C	250	240	250	260
63% G+C	300	190	180	330
72% G+C	370	140	140	350

### *Bacterial Samples*

The bacterial samples listed in Table 4.2 were obtained as gamma-killed freeze-dried cells from the Armed Forces Institute of Pathology (Washington, DC). The bacterial samples listed in Table 4.3 were grown at 35<sup>0</sup>C with shaking (225 rpm) in tryptic soy broth for four days. Cultures were harvested by centrifugation, washed twice with saline solution and lyophilized. All bacterial samples were prepared as 10 mg/ml water suspensions.

### *Instrumental*

The Extrel Model ELQ-400 triple quadrupole mass spectrometer, used for the analysis of the free nucleotide solutions, has been described in the Experimental Section of Chapter 1. The sample preparation for analysis was also outlined in the Experimental Sections of Chapters 1 and 3. A 0.1M TMAH solution was used for *in situ* methylation reactions of the free nucleotides.

The JEOL four sector high resolution mass spectrometer (MStation JMS-700T) equipped with a desorption ionization probe was used for the direct DEI<sup>+</sup> analysis of the pure DNA standards and has been described in the Experimental Section of Chapter 2. The sample preparation has also been described in the Experimental Section of Chapter 2. However, for *in situ* methylation experiments, a 1  $\mu$ L aliquot of 0.1M TMAH was added onto the sample-coated desorption wire. The resulting mixture of TMAH and analyte was then evaporated to dryness. This instrument was also used for the analysis of whole bacterial cells using chemical ionization. The acceleration voltage used for normal desorption chemical ionization (DCI<sup>+</sup>) scans was 8 kV. Isobutane (C<sub>4</sub>H<sub>10</sub>) was used as the CI reagent gas and was maintained at a pressure of  $9.0 \times 10^{-4}$  pascals. All DCI<sup>+</sup> spectra were obtained at 200 eV ionization energy and the ion source temperature was maintained at 200<sup>0</sup>C. Sample preparation for DCI<sup>+</sup> analysis was the same as that for DEI<sup>+</sup> analysis except 0.5M TMAH was employed.

Table 4.2. Bacterial samples received from the Armed Forces Institute of Pathology.

Sample number	Organism-Strain	Media	Growth Stage
1	<i>B. anthracis-Vollum</i>	LD	½ log
2	<i>B. anthracis-Vollum</i>	CAD	½ log
3	<i>B. anthracis-Vollum</i>	CAD	Spore
4	<i>B. anthracis-Zimbabwe</i>	LD	½ log
5	<i>B. anthracis-Zimbabwe</i>	LD	Spore
6	<i>B. anthracis-Zimbabwe</i>	CAD	Spore
7	<i>B. anthracis-Ames</i>	LD	Spore
8	<i>B. anthracis-Ames</i>	CAD	½ log
9	<i>B. anthracis-Ames</i>	CAD	Spore
10	<i>B. anthracis-Sternes</i>	LD	½ log
11	<i>B. anthracis-Sternes</i>	LD	Spore
12	<i>B. anthracis-Sternes</i>	CAD	Spore
13	<i>F. tularensis-TypeA/Utah</i>	IVCHO	Log
14	<i>F. tularensis-TypeA/Utah</i>	MHA	Stationary
15	<i>F. tularensis-Palaeartica</i>	MHB	Log
16	<i>F. tularensis-Palaeartica</i>	MHA	Log
17	<i>F. tularensis-LVS</i>	MHB	Stationary
18	<i>F. tularensis-LVS</i>	MHA	Log
19	<i>Y. pestis-195/P India</i>	blood	Top
20	<i>Y. pestis-195/P India</i>	TSB	Top
21	<i>Y. pestis-La Paz</i>	blood	Top
22	<i>Y. pestis-Nair Kenya</i>	blood	Top
23	<i>Y. pestis-EV76</i>	blood	Top
24	<i>Y. pestis-EV76</i>	TSB	½ log
25	<i>Y. pestis-EV76</i>	TSB	Top
26	<i>B. melitensis-melitensis/WILD</i>	BA	Top
27	<i>B. melitensis-melitensis/WILD</i>	BB	½ log
28	<i>B. melitensis-melitensis/WILD</i>	BB	Top
29	<i>B. melitensis-melitensis/REV-1</i>	BA	Top
30	<i>B. melitensis-melitensis/REV-1</i>	BB	Top
31	<i>B. melitensis-Suis</i>	BA	Top
32	<i>B. melitensis-Suis</i>	BB	Top
33	<i>B. melitensis-abortus/WILD</i>	BB	½ log
34	<i>B. melitensis-abortus/WILD</i>	BB	Top
35	<i>B. melitensis-abortus/S19vac</i>	BA	Top
36	<i>B. melitensis-abortus/S19vac</i>	BB	½ log

Leighton-Doi (LD), Casein acid digest (CAD), Brucella broth (BB), Brucella agar (BA), Trypticase Soy broth (TSB), Trypticase Soy agar (TSA), IsoVitalax Chocolate (IVCHOC), Muller-Hinton broth (MHB) and Muller-Hinton agar (MHA)

Table 4.3. Bacterial samples used for the construction of standard curves for calculating % composition of nitrogen bases in DNA of whole cells.

<b>Microorganism</b>	<b>Published* mol % G+C content</b>
<i>Staphylococcus epidermidis</i>	30.0 – 37.0 (T <sub>m</sub> )
<i>Bacillus thuringiensis</i>	33.5 – 40.1 (T <sub>m</sub> )
<i>Listeria monocytogenes</i>	37.0 – 39.0 (T <sub>m</sub> )
<i>Bacillus lichenformis</i>	42.9 – 49.9 (T <sub>m</sub> )
<i>Serratia marcescens</i>	57.5 – 60.0 (T <sub>m</sub> )
<i>Pseudomonas stutzeri</i>	60.7 – 66.3
<i>Proteus mirabilis</i>	39.3 (T <sub>m</sub> )
<i>Bacillus subtilis</i>	42.9 (T <sub>m</sub> )
<i>Enterobacter aerogenes</i>	53.0 – 54.0 (B <sub>d</sub> )

T<sub>m</sub> – thermal melting profile

B<sub>d</sub> – buoyant density

\* - *Bergey's Manual of Systematic Bacteriology*, N.R. Krieg, Ed., Williams & Wilkins, Baltimore 1984.

A Bruker air buffered quadrupole ion trap mass spectrometer (CBMS, chemical/biological mass spectrometer) fitted with an infrared pyrolyzer was used for the direct analysis of whole bacterial cells. An instrument diagram of the field-portable MS is shown in Figure 4.1. For mass spectral analysis, 15  $\mu\text{L}$  bacterial suspensions were coinjected with 5  $\mu\text{L}$  of 1M TMAH in water, immediately prior to pyrolysis. The pyrolyzer was maintained at 180 $^{\circ}\text{C}$  during sample introduction and reached a final temperature of 450 $^{\circ}\text{C}$  during pyrolysis. The total cycle time (sample collection, pyrolysis and cleaning cycle) was 240 seconds. Pyrolysis began at 50 seconds and ended at 115 seconds. The samples were injected via a syringe at 45 seconds. Pyrolysates were transferred into the ion trap mass spectrometer by use of air as the carrier gas at a flow rate of 1.5 L/min. through a three-meter (32  $\mu\text{m}$  I.D.) deactivated fused silica capillary transfer line, held at 200 $^{\circ}\text{C}$ . A silicone membrane (180 $^{\circ}\text{C}$ ) was used to interface the transfer line and the mass spectrometer. The quadrupole ion trap pressure was maintained at  $5 \times 10^{-5}$  torr and an ion cooling time of 50  $\mu\text{sec}$  was used. Positive electron ionization (70 eV) was employed with ionization times from 50  $\mu\text{sec}$  to 20 msec. A mass range of 145 – 400 Da was scanned for each analysis (11).

#### *Data Analysis*

The method of least squares was used to generate the calibration curves and they were constructed as follows: from the mass spectrum, the peak intensities of the diagnostic peaks (Table 4.4) were obtained. These values were summed and the combined peak intensities of guanine and cytosine were divided by this total to calculate the percent relative intensity (i.e. % deflection). An example of a typical calculation is as follows:

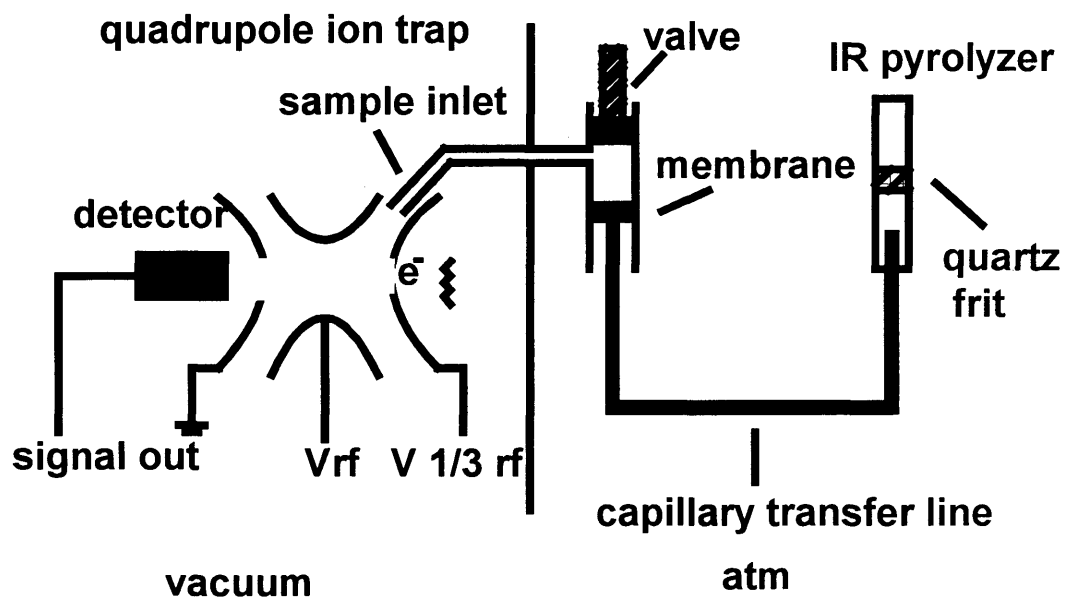


Figure 4.1. Instrument diagram of the field-portable mass spectrometer (CBMS).

Table 4.4. M/z values of the methylated nitrogen bases used as diagnostic peaks for the calculation of percent relative intensity.

<b>Nitrogen Base</b>	<b>Number of methylations</b>				
	<b>0</b>	<b>1</b>	<b>2</b>	<b>3</b>	<b>4</b>
Cytosine	111	125	139	153	-
Thymine	126	140	154	-	-
Adenine	135	149	163	177	-
Guanine	151	165	179	193	207

$$\% \text{ relative intensity} = (I_G + I_C) / I_{\text{total}}$$

I = intensity obtained from the mass spectrum for a given ion

$$I_G = I_{207} + I_{193} + I_{179} + I_{165} + I_{151}$$

$$I_C = I_{153} + I_{139} + I_{125} + I_{111}$$

$$I_A = I_{177} + I_{163} + I_{149} + I_{135}$$

$$I_T = I_{154} + I_{140} + I_{126}$$

$$I_{\text{total}} = I_G + I_C + I_A + I_T$$

The calculated percent relative intensity values were plotted on the y axis and the mol % G+C content was plotted on the x axis. The mol % G+C content was either known (nucleotide solutions) or obtained from literature (pure DNA, whole cell microorganisms). The calibration plots were then used to calculate the mol % G+C of unknowns.

## RESULTS AND DISCUSSION

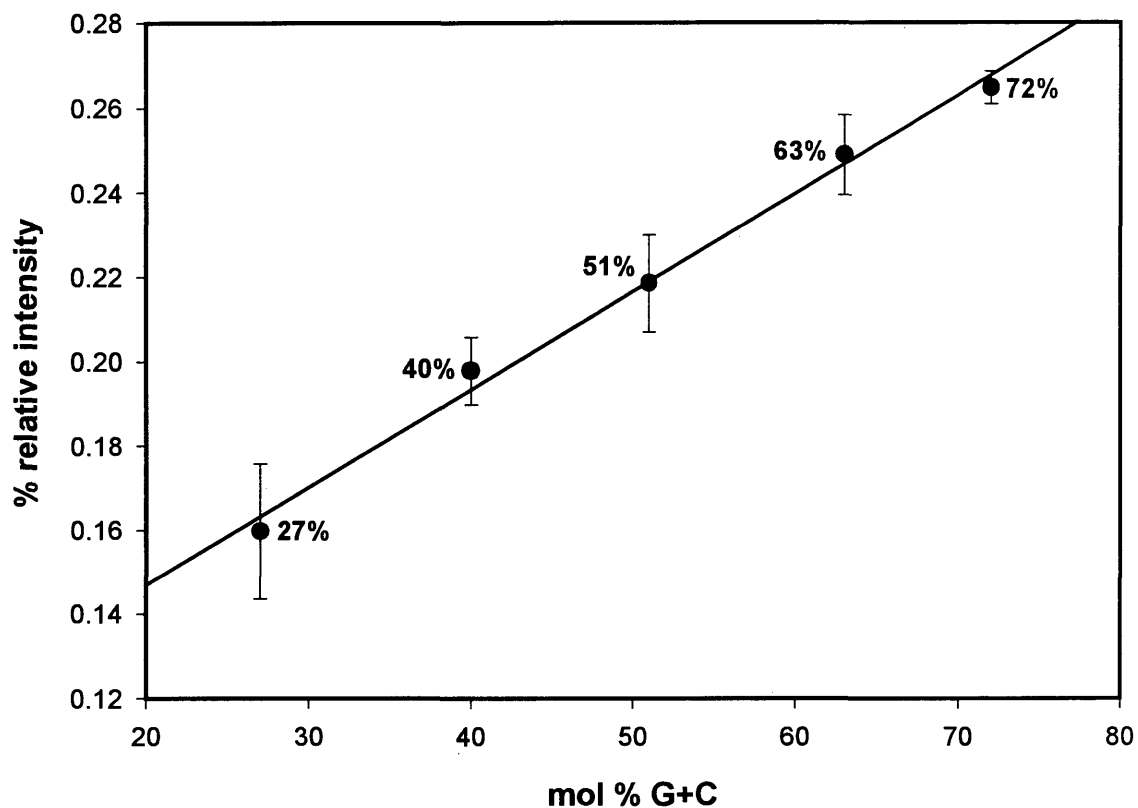
### *Nucleotide solutions*

As described by Hawley and Wiebers (8), a direct correlation exists between the percent deflection of a given nitrogen base and the percent composition of pure standards. To endorse this observation, a collection of solutions containing varying amounts of each nitrogen base were analyzed by Curie-point pyrolysis mass spectrometry with *in situ* methylation using an Extrel Model ELQ-400 triple quadrupole mass spectrometer. These solutions are listed in Table 4.1 and were analyzed in triplicate from 60 – 300 Da. The values are listed as  $\mu\text{L}$  of 0.1M solutions per 1 ml of total constituents. The biomarker ions used for the percent deflection calculation are given in Table 4.4. These ions have previously been described in Chapter 3. *In situ* methylation increases the number of

diagnostic peaks for each nitrogen base by replacing the acidic hydrogens with a methyl group. In addition, increased volatility of the bases is realized.

The calibration curve for the free nucleotides is given in Figure 4.2 plotting mol % G+C on the x axis and % relative intensity on the y axis. In constructing the calibration curve, the mol % G+C content was known since the standards were made with equimolar solutions of each nitrogen base. The method of least squares was used to generate the calibration curve and the mathematical relationship between x and y is given by  $y = 2.3 \times 10^{-3} (\pm 1.6 \times 10^{-4}) x + 0.10 (\pm 8.6 \times 10^{-3})$ . The linear correlation coefficient ( $r$ ) of the curve was found to be 0.97 and the standard deviation about regression ( $s_r$ ) is  $\pm 9.0 \times 10^{-3}$ . The plot was constructed using the 27%, 40%, 51%, 63% and 72% G+C standards listed in Table 4.1. The 35% G+C standard was also analyzed by mass spectrometry and was taken as an “unknown” to calculate the mol % G+C from the standard curve given in Figure 4.2. From the standard curve in Figure 4.2, the “unknown” was found to have a mol % G+C of 38. The standard deviation for the result obtained from the calibration curve ( $s_c$ ) is  $\pm 2.5$ .

As electron ionization (EI) gives rise to extensive molecular ion fragmentation, an attempt was made to account for the fragment ions in the percent relative intensity calculation. Under EI conditions, the nitrogen bases fragment as described in Chapter 3. Each molecular ion, listed in Table 4.4, has several fragment ions. By obtaining the EI spectrum for each species in Table 4.4 from either the NIST data base or by *in situ* methylation pyrolysis GC-MS analysis, fragment ions and their intensities were identified. This data was used to calculate a  $k$  value (correction factor) for each molecular ion listed in Table 4.4. The  $k$  values for each molecular ion are listed in Table 4.5. A sample calculation for obtaining the  $k$  value for  $m/z$  111 follows:



Each point represents the average percent relative intensity values from the analyses of 3 individual samples. The error bars are calculated at a 95% confidence limit.

$$y = 2.3 \times 10^{-3} (\pm 1.6 \times 10^{-4}) x + 0.10 (\pm 8.6 \times 10^{-3})$$

$$r = 0.97$$

Figure 4.2. Standard plot for quantification of nitrogen bases in free nucleotide solutions.

Table 4.5.  $k$  values calculated for each of the diagnostic peaks.

<b>Diagnostic peak</b>	<b>Calculated <math>k</math> value</b>
111	0.32
125	0.30
126	0.31
135	0.23
139	0.36
140	0.28
149	0.22
151	0.23
153	0.15
154	0.31
163	0.14
165	0.23
177	0.09
179	0.19
193	0.30
207	0.19

$$k_{m/z111} = I_{111}/I_{total}$$

I = ion intensities obtained from the spectrum

$I_{total}$  = the sum of all fragment ion intensities for m/z 111

The  $k$  values for ions 111 (C), 125 (C), 126 (T), 135 (A), 140 (T), 149 (A), 151 (G), 153 (C), 154 (T), 163 (A), 165 (G), 177 (A), and 179 (G) were obtained using the NIST data base spectrum of each analyte. The  $k$  values for ions 139 (C), 193 (G), and 207 (G) were obtained by Py-GC/MS analysis of the *in situ* methylation of cytosine and guanine. A sample calculation for obtaining the % relative intensity values employing the  $k$  values follows.

$$\% \text{ relative intensity}_k = (I_G + I_C) / I_{total}$$

I = the intensity obtained from the mass spectrum for a given ion

$$I_G = I_{207}/0.19 + I_{193}/0.30 + I_{179}/0.24 + I_{165}/0.30 + I_{151}/0.47$$

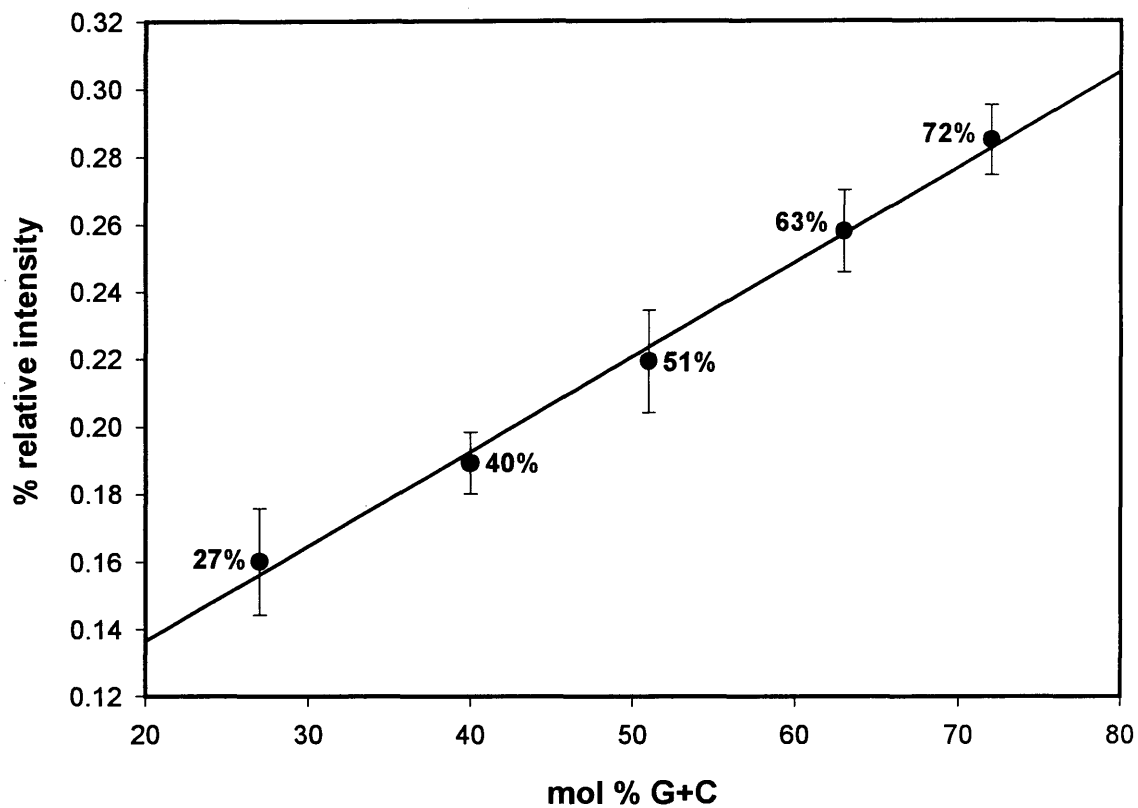
$$I_C = I_{153}/0.22 + I_{139}/0.42 + I_{125}/0.42 + I_{111}/0.50$$

$$I_A = I_{177}/0.12 + I_{163}/0.18 + I_{149}/0.28 + I_{135}/0.43$$

$$I_T = I_{154}/0.38 + I_{140}/0.40 + I_{126}/0.74$$

$$I_{total} = I_G + I_C + I_A + I_T$$

The newly generated % relative intensity values with  $k$  values included were used to construct a second calibration curve based on the method of least squares, Figure 4.3. The data corresponds to a straight line of the form  $y = 2.8 \times 10^{-3} (\pm 2.0 \times 10^{-4}) x + 0.08 (\pm 1.1 \times 10^{-2})$ . The linear correlation coefficient ( $r$ ) of the curve was 0.97 and  $s_r$  equals  $\pm 1.1 \times 10^{-2}$ . Again the plot was constructed using the 27%, 40%, 51%, 63% and 72% G+C standards and the “unknown” was the 35% standard. A mass spectrum of this sample is given in Figure 4.4. From the standard curve in Figure 4.3, the “unknown” was determined to have a mol % G+C of 36. The standard deviation for the result obtained from the calibration curve ( $s_c$ ) is  $\pm 2.5$ .



Each point represents the average percent relative intensity values from analyses of 3 individual samples. The error bars are calculated at a 95% confidence limit.

$$y = 2.8 \times 10^{-3} (\pm 2.0 \times 10^{-4}) x + 0.08 (\pm 1.1 \times 10^{-2})$$

$$r = 0.97$$

Figure 4.3. Standard plot for quantification of nitrogen bases in free nucleotide solutions ( $k$  values included in the % relative intensity calculation).

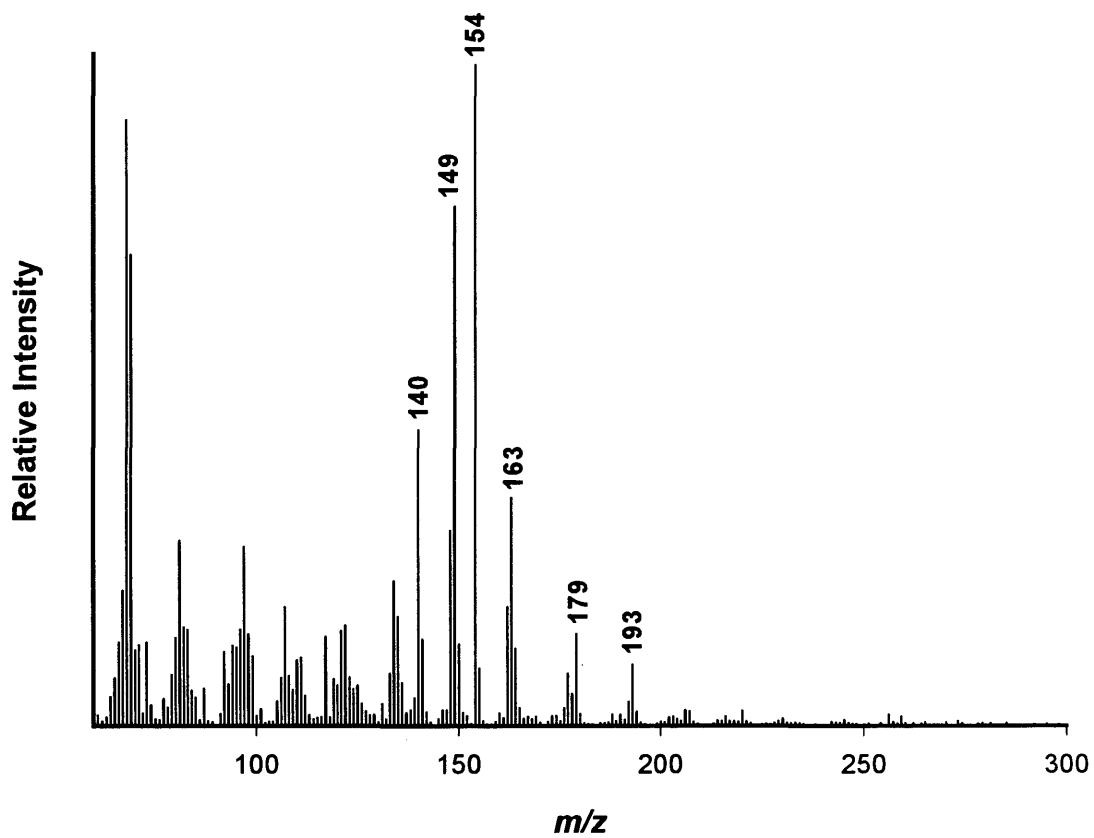


Figure 4.4. Py-mass spectrum of a 35% G+C standard solution with *in situ* methylation using 0.1 M TMAH.

Table 4.6 outlines the results obtained for the free nucleotide “unknown”. In both cases, the assessment from the mass spectral method for the determination of mol % G+C shows a strong correlation to the known value of 35%; 38 ( $\pm 2.5$ )% without  $k$  values included in the % relative intensity calculation and 36 ( $\pm 2.5$ )% with  $k$  values included in the % relative intensity calculation. The % relative intensity values calculated with the  $k$  values and used in the calibration curve (Figure 4.3); however, offer a result closer to the actual value of the “unknown”. In the case of free nucleotides, the inclusion of molecular ion fragmentation ions by  $k$  values is relevant and should be used.

#### *Pure DNA*

The pure DNA standards, Table 4.7, were analyzed in triplicate by desorption-electron ionization (DEI) mass spectrometry using a four-sector double focusing MS (JEOL MStation). The mass range used for this experiment was 145 – 400 Da. This mass range was chosen to emulate the range used in the analysis of whole bacterial cells, yet to be discussed. As the range started at  $m/z$  145, ions 111, 125, 126, 135, 139 and 140 were not used in the % relative intensity calculation as previously discussed. However the exclusion of the ion intensities for  $m/z$  111, 125, 126, 135, 139 and 140 in the % relative intensity calculation is justified as traditionally these ions are of low intensity compared to the other diagnostic ion peak intensities (Chapter 3).

A calibration curve for the pure DNA standards is shown in Figure 4.5. As discussed previously, the peak intensities of the diagnostic peaks ( $m/z$  207, 193, 179, 177, 165, 163, 154, 153 and 151) were obtained from the mass spectrum. Again, these values were summed and the combined peak intensities of guanine and cytosine were divided by this total to calculate the % relative intensity. The mol % G+C content used on the x axis of the calibration plot of the pure DNA standards was supplied by Sigma. The calibration curve was generated by means of the least squares method where

Table 4.6. Comparison of mass spectral quantitation method for mol % G+C in standard solutions with known values.

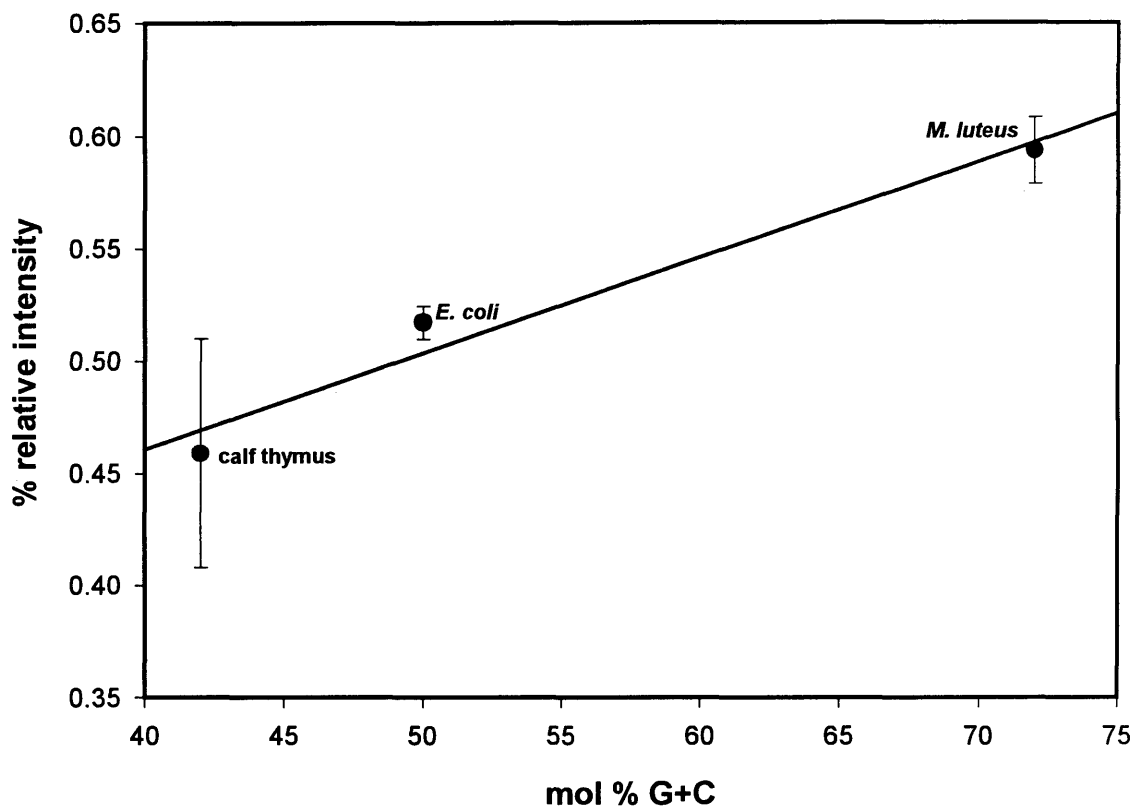
<b>Sample</b>	<b>Calculated mol % G+C</b>	<b>Calculated mol % G+C including <i>k</i> values</b>
35 % G+C	38 ( $\pm 2.5$ )	36 ( $\pm 2.5$ )

Table 4.7. Pure DNA standards used for the construction of a standard curve for calculating % composition of nitrogen bases.

<b>Pure DNA Sample</b>	<b>Published* mol % G+C content</b>
Calf thymus	42.0 (T <sub>m</sub> )
<i>Escherichia coli</i>	50.0 (T <sub>m</sub> )
<i>Micrococcus luteus</i>	72.0 (T <sub>m</sub> )

T<sub>m</sub> – thermal melting profile

\* - Value supplied by Sigma Chemical Company



Each point represents the average percent relative intensity values from analyses of 3 individual samples. The error bars are calculated at a 95% confidence limit.

$$y = 4.27 \times 10^{-3} (\pm 8.09 \times 10^{-4}) x + 0.290 (\pm 4.54 \times 10^{-2})$$

$$r = 0.894$$

Figure 4.5. Standard plot for quantification of nitrogen bases in pure DNA.

$y = 4.27 \times 10^{-3} (\pm 8.09 \times 10^{-4}) x + 0.290 (\pm 4.54 \times 10^{-2})$  and  $r$  equals 0.894. The standard deviation about regression ( $s_r$ ) was found to be  $\pm 3.07 \times 10^{-2}$ . The error associated with the calf thymus DNA sample is rather large (Figure 4.5). This may be attributed to different heating profiles caused by changes in the platinum wire of the DEI probe. Although the filament temperature increases in proportion to the filament current, actual filament temperature may slightly differ according to the shape and length of the filament.

A pure DNA standard (salmon sperm) was analyzed by the mass spectral method. A mass spectrum of the salmon sperm DNA is shown in Figure 4.6. The mol % G+C of salmon sperm was calculated from the standard curve shown in Figure 4.5 and was found to be 45.1 ( $\pm 4.81$ ). Table 4.8 summarizes the mol % G+C content obtained from the mass spectral method as compared with the value obtained by thermal melting profile. Also included in Table 4.8 is the mol % G+C content obtained for salmon sperm DNA from the calibration curve employing  $k$  values and it was found to be 44.2 ( $\pm 4.15$ ). The calibration curve for the pure DNA standards with  $k$  values is given in Figure 4.7. The linear correlation coefficient ( $r$ ) increased to 0.918,  $s_r$  was found to be  $\pm 2.59 \times 10^{-2}$ , and  $y = 4.16 \times 10^{-3} (\pm 6.81 \times 10^{-4}) x + 0.254 (\pm 3.82 \times 10^{-2})$ .

Again, as in the case of the free nucleotide solutions, the inclusion of  $k$  values improves the ability to correctly assign a mol % G+C content to an unknown. The linear correlation coefficient of the calibration curve employing the  $k$  values (Figure 4.7) also improved from 0.894 to 0.918. The evaluation of the mass spectral method for the determination of mol % G+C of pure DNA again shows a strong correlation to the thermal melting profile method traditionally used to determine mol % G+C content of DNA.

#### *Whole Bacterial Cells – Electron Ionization*

The logical progression of sample complexity leads to the analysis of whole bacterial cells. The determination of mol % G+C content of DNA of whole bacterial

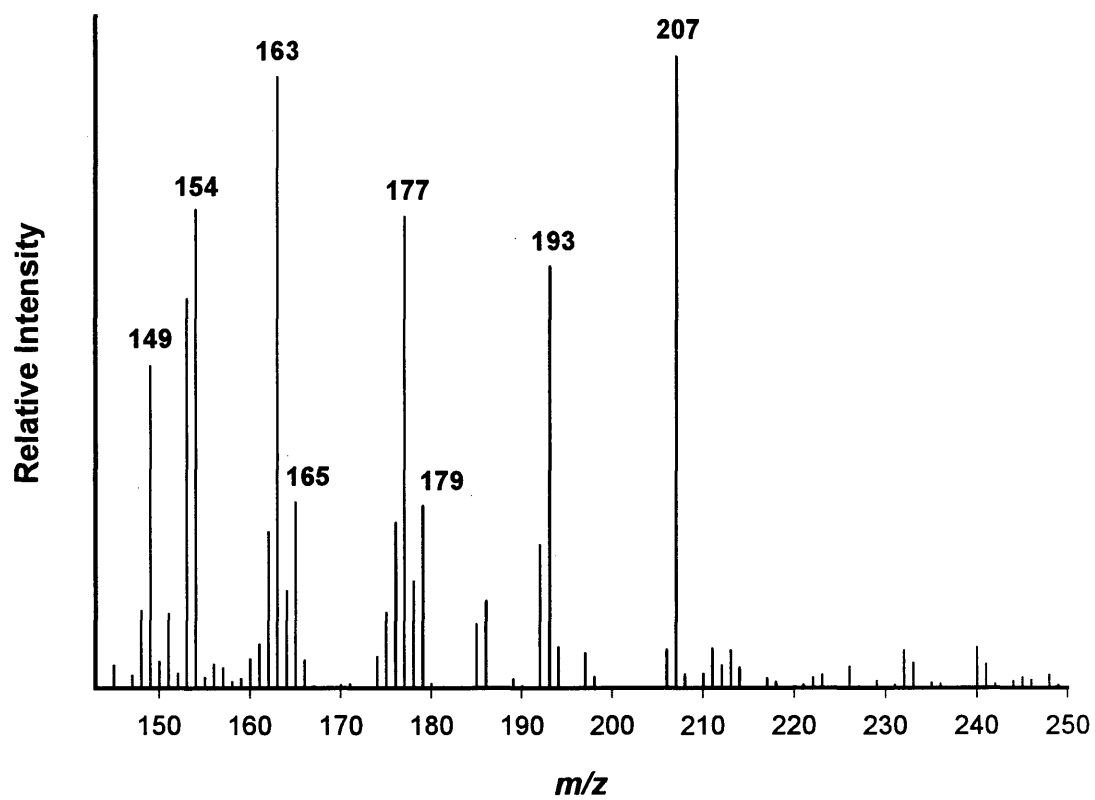


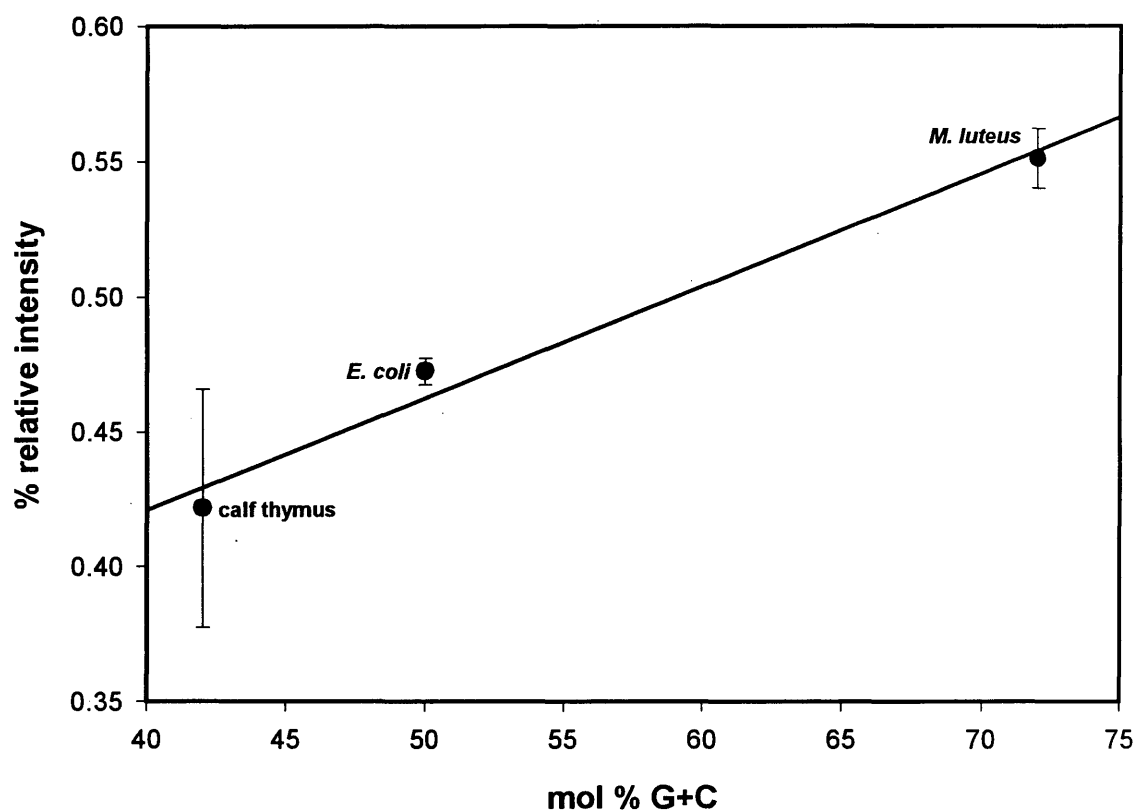
Figure 4.6. DEI mass spectrum of salmon sperm DNA with *in situ* methylation using 0.1 M TMAH.

Table 4.8. Comparison of mass spectral quantitation method for mol % G+C in pure DNA with known values.

<b>Sample</b>	<b>Published* mol % G+C</b>	<b>Calculated mol % G+C</b>	<b>Calculated mol % G+C including <i>k</i> values</b>
Salmon sperm DNA	44.0 (T <sub>m</sub> )	45.1 (± 4.81)	44.2 (± 4.15)

T<sub>m</sub> – thermal melting profile

\* - value supplied by Sigma Chemical Company



Each point represents the average percent relative intensity values from analyses of 3 individual samples. The error bars are calculated at a 95% confidence limit.

$$y = 4.16 \times 10^{-3} (\pm 6.81 \times 10^{-4}) x + 0.254 (\pm 3.82 \times 10^{-2})$$

$$r = 0.918$$

Figure 4.7. Standard plot for quantification of nitrogen bases in pure DNA  
( $k$  values included in the % relative intensity calculation).

cells is the ultimate goal of this project. The whole bacterial cells, *S. epidermidis*, *B. thuringiensis*, *L. monocytogenes*, *B. licheniformis*, *S. marcescens* and *P. stutzeri*, were analyzed in four replicates by pyrolysis positive electron ionization mass spectrometry with *in situ* methylation using an air buffered quadrupole ion trap MS fitted with an infrared pyrolyzer (Bruker). A typical mass spectrum of a whole cell microorganism (*B. licheniformis*) analyzed by this instrument is given in Figure 4.8. Bacterial samples were carefully selected as a representative sample population of bacteria having mol % content of 25-75%. The mass range used for this experiment was 145 – 400 Da. This mass range was chosen to avoid lower mass protein-derived peaks from dominating the spectrum, particularly  $m/z$  135 (12). Again, ions 111, 125, 126, 135, 139 and 140 were not used in the % relative intensity calculation.

The peak intensities of the diagnostic peaks listed in Table 4.4 were summed and used to divide the combined peak intensities of guanine and cytosine to calculate the % relative intensity. The mol % G+C content used on the x axis of the calibration plot for whole bacterial cells was taken from *Bergey's Manual of Systematic Bacteriology* (13). Since mol % G+C content is listed as a range, the mean of the range was used as the x value for the calibration plot. Using the method of least squares, a calibration curve was generated for the quantification of DNA in whole bacterial cells plotting known mol % G+C on the x axis and % relative intensity on the y axis, Figure 4.9. The regression line is given by  $y = 3.67 \times 10^{-3} (\pm 5.37 \times 10^{-4}) x + 0.412 (\pm 2.55 \times 10^{-2})$ ,  $r$  was found to be 0.824 and  $s_r$  is  $\pm 2.99 \times 10^{-2}$ .

Whole bacterial cells not used for the construction of the calibration plot, Table 4.2, were analyzed by the same methodology. The mol % G+C content was calculated from the curve shown in Figure 4.9 and was found to be 36.0 ( $\pm 2.15$ ) for *B. anthracis*, 40.2 ( $\pm 2.54$ ) for *F. tularensis*, 45.5 ( $\pm 2.43$ ) for *Y. pestis* and 54.6 ( $\pm 2.18$ ) for *B. melitensis*. Table 4.9 is a compilation of these values compared with the values determined by thermal melting profiles or buoyant density methods for these DNAs. The

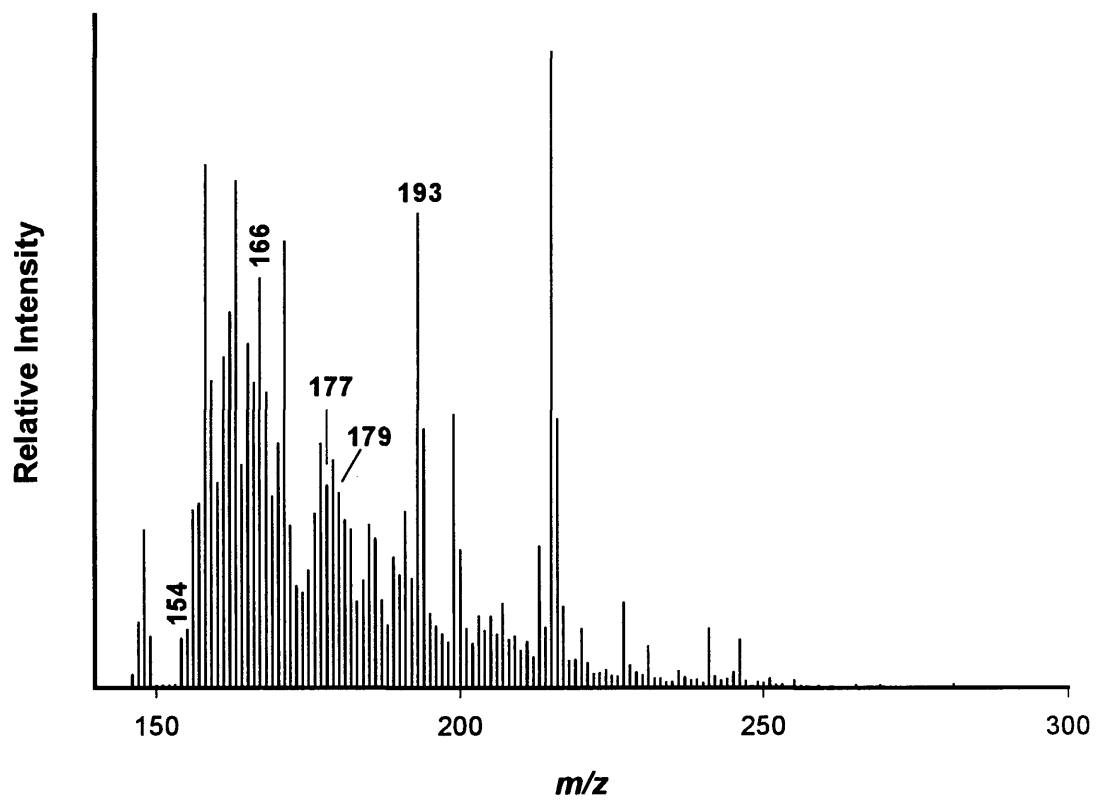
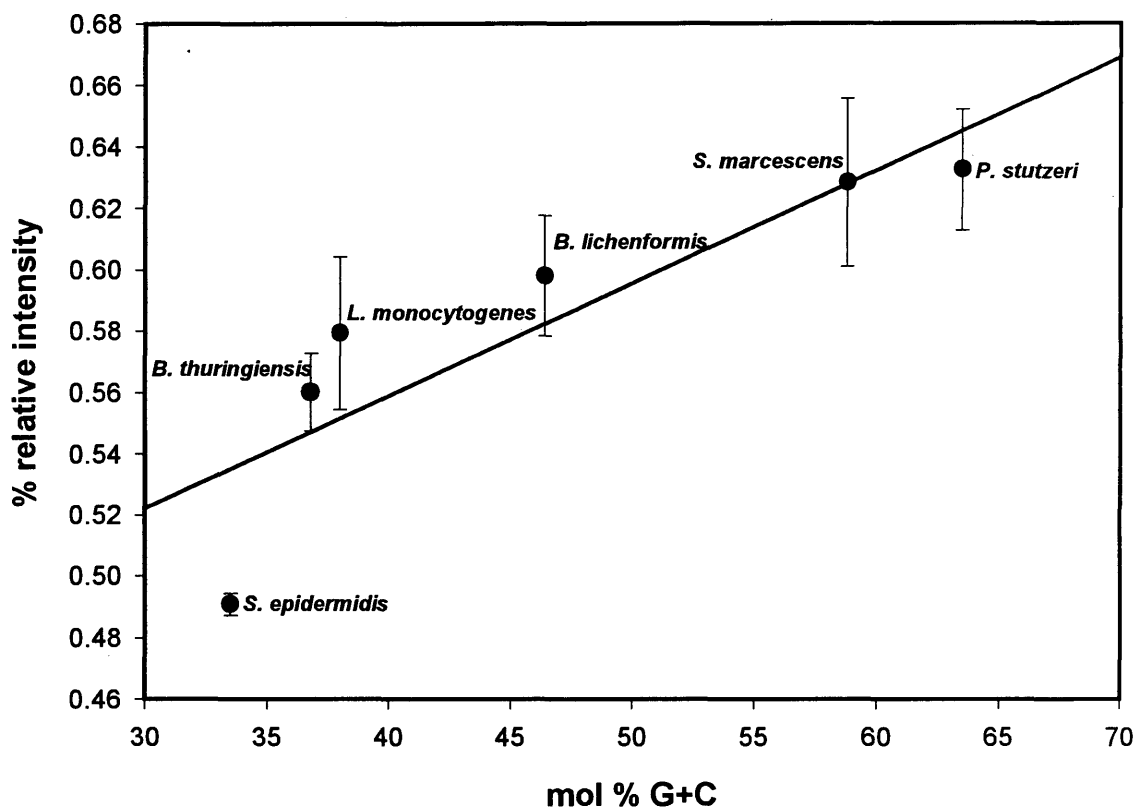


Figure 4.8. Py-mass spectrum of *B. lichenformis* with *in situ* methylation using 1.0 M TMAH.



Each point represents the average percent relative intensity values from analyses of 4 individual samples. The error bars are calculated at a 95% confidence limit.

$$y = 3.67 \times 10^{-3} (\pm 5.37 \times 10^{-4}) x + 0.412 (\pm 2.55 \times 10^{-2})$$

$$r = 0.824$$

Figure 4.9. Standard plot for quantification of nitrogen bases in whole bacterial cells.

Table 4.9. Comparison of mass spectral quantitation method for mol % G+C in whole cell bacteria with known values.

<b>Microorganism</b>	<b>Published* mol % G+C</b>	<b>Calculated mol % G+C</b>
<i>Bacillus anthracis</i>	32.2 – 33.9 (T <sub>m</sub> )	36.0 (± 2.15)
<i>Francisella tularensis</i>	33.0 – 36.0 (T <sub>m</sub> )	40.2 (± 2.54)
<i>Yersinia pestis</i>	46.0 (T <sub>m</sub> )	45.5 (± 2.43)
<i>Brucella melitensis</i>	58.0 (T <sub>m</sub> )	54.6 (± 2.18)

T<sub>m</sub> – thermal melting profile

\* - *Bergey's Manual of Systematic Bacteriology*, N.R. Krieg, Ed., Williams & Wilkins, Baltimore 1984.

36 replicates of *B. anthracis*, 18 replicates of *F. tularensis*, 21 replicates of *Y. pestis* and 33 replicates of *B. melitensis* were analyzed to calculate the mol % G+C content

measured values are listed with the standard deviation obtained from the calibration curve ( $s_c$ ).

Table 4.9 represents all the bacterial samples listed in Table 4.2. The *B. anthracis* samples were analyzed collectively to obtain the mol % G+C content as were the *F. tularensis* samples, *Y. pestis* samples and *B. melitensis* samples. Since several strains, growth media and growth stages were analyzed for each of the species, a mol % G+C was calculated for each individual sample listed in Table 4.2. These values are given in Table 4.10. From Table 4.10, the effect of growth media or growth stage has little effect on predicting the mol % G+C content (i.e. there are no clear trends observed). However, for the *B. anthracis* species, the effect of sporulation is noticeable in predicting mol % G+C. The sporulated samples generally showed a higher mol % G+C content. By excluding the sporulated samples, but collectively analyzing the vegetative *B. anthracis* species, a mol % G+C of  $35.8 (\pm 2.68)$  was obtained. DNA is present in lesser amounts in spores than that found in vegetative cells (14). Also, the net synthesis of DNA ceases during early sporulation and the cellular DNA level remains constant until lysis of the sporangium occurs. At this time, the DNA in the sporangium is released into the medium resulting in a decrease in cellular DNA (14).

The released DNA of the sporangium may explain the artificially high mol % G+C content predicted for the sporulated samples. If the sporulated samples were not exhaustively washed, the released DNA would remain in the growth medium. This DNA would be more accessible to methylation and analysis than the DNA bound in the cell or spore.

The mol % G+C content for bacterial DNA given in Table 4.9 and predicted by the mass spectral methodology is met with cautious optimism. The diagnostic peaks of guanine, adenine and cytosine are common to DNA and RNA. Both RNA and DNA are present in the metabolically inert spore and the vegetative cells (15). RNA content of vegetative cells and spores depends on species, the cell or spore volume, and the growth conditions (14). The RNA/DNA ratio ranges from 2 to 7 depending on the species (16).

Table 4.10. Individual species assessment of mol % G+C  
determined by mass spectral method.

Published mol % G+C	Calculated mol % G+C	Organism-Strain	Media	Growth Stage
32.2 – 33.9	42.6 (± 4.99)	<i>B. anthracis-Vollum</i>	LD	½ log
32.2 – 33.9	27.6 (± 4.99)	<i>B. anthracis-Vollum</i>	CAD	½ log
32.2 – 33.9	38.3 (± 4.99)	<i>B. anthracis-Vollum</i>	CAD	Spore
32.2 – 33.9	31.4 (± 4.99)	<i>B. anthracis-Zimbabwe</i>	LD	½ log
32.2 – 33.9	36.6 (± 4.99)	<i>B. anthracis-Zimbabwe</i>	LD	Spore
32.2 – 33.9	30.9 (± 4.99)	<i>B. anthracis-Zimbabwe</i>	CAD	Spore
32.2 – 33.9	41.1 (± 4.99)	<i>B. anthracis-Ames</i>	LD	Spore
32.2 – 33.9	37.9 (± 4.99)	<i>B. anthracis-Ames</i>	CAD	½ log
32.2 – 33.9	40.2 (± 4.99)	<i>B. anthracis-Ames</i>	CAD	Spore
32.2 – 33.9	39.6 (± 4.99)	<i>B. anthracis-Sternes</i>	LD	½ log
32.2 – 33.9	34.5 (± 4.99)	<i>B. anthracis-Sternes</i>	LD	Spore
32.2 – 33.9	31.7 (± 4.99)	<i>B. anthracis-Sternes</i>	CAD	Spore
33.0 – 36.0	40.8 (± 4.99)	<i>F. tularensis-TypeA/Utah</i>	IVCHO	Log
33.0 – 36.0	45.8 (± 4.99)	<i>F. tularensis-TypeA/Utah</i>	MHA	Stationary
33.0 – 36.0	44.4 (± 4.99)	<i>F. tularensis-Palaeartica</i>	MHB	Log
33.0 – 36.0	38.0 (± 4.99)	<i>F. tularensis-Palaeartica</i>	MHA	Log
33.0 – 36.0	35.6 (± 4.99)	<i>F. tularensis-LVS</i>	MHB	Stationary
33.0 – 36.0	36.8 (± 4.99)	<i>F. tularensis-LVS</i>	MHA	Log
46.0	45.9 (± 4.99)	<i>Y. pestis-195/P India</i>	blood	Top
46.0	46.1 (± 4.99)	<i>Y. pestis-195/P India</i>	TSB	Top
46.0	47.3 (± 4.99)	<i>Y. pestis-La Paz</i>	blood	Top
46.0	47.6 (± 4.99)	<i>Y. pestis-Nair Kenya</i>	blood	Top
46.0	45.6 (± 4.99)	<i>Y. pestis-EV76</i>	blood	Top
46.0	44.0 (± 4.99)	<i>Y. pestis-EV76</i>	TSB	½ log
46.0	42.8 (± 4.99)	<i>Y. pestis-EV76</i>	TSB	Top
58.0	52.0 (± 4.99)	<i>B. melitensis-melitensis/WILD</i>	BA	Top
58.0	59.8 (± 4.99)	<i>B. melitensis-melitensis/WILD</i>	BB	½ log
58.0	58.6 (± 4.99)	<i>B. melitensis-melitensis/WILD</i>	BB	Top
58.0	52.5 (± 4.99)	<i>B. melitensis-melitensis/REV-1</i>	BA	Top
58.0	50.8 (± 4.99)	<i>B. melitensis-melitensis/REV-1</i>	BB	Top
58.0	53.3 (± 4.99)	<i>B. melitensis-Suis</i>	BA	Top
58.0	56.9 (± 4.99)	<i>B. melitensis-Suis</i>	BB	Top
58.0	56.3 (± 4.99)	<i>B. melitensis-abortus/WILD</i>	BB	½ log
58.0	56.6 (± 4.99)	<i>B. melitensis-abortus/WILD</i>	BB	Top
58.0	51.3 (± 4.99)	<i>B. melitensis-abortus/S19vac</i>	BA	Top
58.0	52.1 (± 4.99)	<i>B. melitensis-abortus/S19vac</i>	BB	½ log

Leighton-Doi (LD), Casein acid digest (CAD), Brucella broth (BB), Brucella agar (BA), Trypticase Soy broth (TSB), Trypticase Soy agar (TSA), IsoVitalax Chocolate (IVCHOC), Muller-Hinton broth (MHB) and Muller-Hinton agar (MHA)

\* - *Bergey's Manual of Systematic Bacteriology*, N.R. Krieg, Ed., Williams & Wilkins, Baltimore 1984.

3 replicates of each organism were analyzed to calculate the mol % G+C

Within the same species, this ratio could vary by 60% depending on the growth condition. To what extent the guanine, adenine and cytosine of RNA contribute to the % relative intensity calculation, has not been determined. However, calculations were performed in an attempt to understand the extent of RNA contribution to the % relative intensity value calculated for whole bacterial cells. For example, the raw intensities of the diagnostic peaks for guanine, adenine and cytosine were divided first by two, then by three and finally by five in an attempt to estimate varying levels of RNA content in the whole bacterial cells. These fractional intensities were then used in the calculation of the % relative intensities. However, no significant change in the predictability of mol % G+C of unknowns was noted as shown by the results listed in Table 4.11. This may be attributed to the fact that the intensity of the thymine diagnostic peak ( $m/z$  154) is relatively low when compared to the diagnostic peaks of the other nitrogen bases as shown in Figure 4.8.

Future work might include an in-depth study of RNA contribution to the overall signals of guanine, adenine and cytosine. This may be accomplished by growing a given bacterial species with the precursors to labeled uracil. After several generations of growth, the cells would incorporate only labeled uracil. The mass shift observed for the labeled uracil would allow for the determination of RNA contribution. Without labeled uracil, the methylated peaks of uracil are  $m/z$  126 and 140, ions common to thymine and outside the scan range that is currently employed.

To account for the fragmentation associated with the diagnostic peaks under EI conditions, a calibration curve for the bacterial samples including the previously discussed  $k$  values was constructed and is shown in Figure 4.10. The linear correlation coefficient ( $r$ ) decreased to 0.796 and  $s_r$  was found to be  $\pm 3.01 \times 10^{-2}$ . The line is defined by the formula  $y = 3.34 \times 10^{-3} (\pm 9.05 \times 10^{-4}) x + 0.298 (\pm 2.57 \times 10^{-2})$ . From this curve, the mol % G+C of four highly pathogenic bacteria was predicted and the values were found

Table 4.11. Comparison of mass spectral quantitation method for mol % G+C in whole cell bacteria with known values.

Microbe	Published* mol % G+C	Calculated mol % G+C	Calculated mol % G+C (raw intensities of A, G, C divided by 2 in the % relative intensity calculation)	Calculated mol % G+C (raw intensities of A, G, C divided by 3 in the % relative intensity calculation)	Calculated Mol % G+C (raw intensities of A, G, C divided by 5 in the % relative intensity calculation)
<i>B. anthracis</i>	32.2-33.9 (T <sub>m</sub> )	36.0 (± 2.15)	37.1 (± 2.02)	38.1 (± 1.93)	39.6 (± 1.82)
<i>F. tularensis</i>	33.0-36.0 (T <sub>m</sub> )	40.2 (± 2.54)	40.6 (± 2.39)	41.0 (± 2.28)	41.6 (± 2.15)
<i>Y. pestis</i>	46.0 (T <sub>m</sub> )	45.5 (± 2.43)	45.8 (± 2.29)	46.1 (± 2.19)	46.6 (± 2.06)
<i>B. melitensis</i>	58.0 (T <sub>m</sub> )	54.6 (± 2.18)	54.5 (± 2.06)	54.5 (± 1.96)	54.4 (± 1.85)

T<sub>m</sub> – thermal melting profile

\* - *Bergey's Manual of Systematic Bacteriology*, N.R. Krieg, Ed., Williams & Wilkins, Baltimore 1984.

36 replicates of *B. anthracis*, 18 replicates of *F. tularensis*, 21 replicates of *Y. pestis* and 33 replicates of *B. melitensis* were analyzed to calculate the mol % G+C.

Formula of the calibration curve used to obtain the values in column 4;

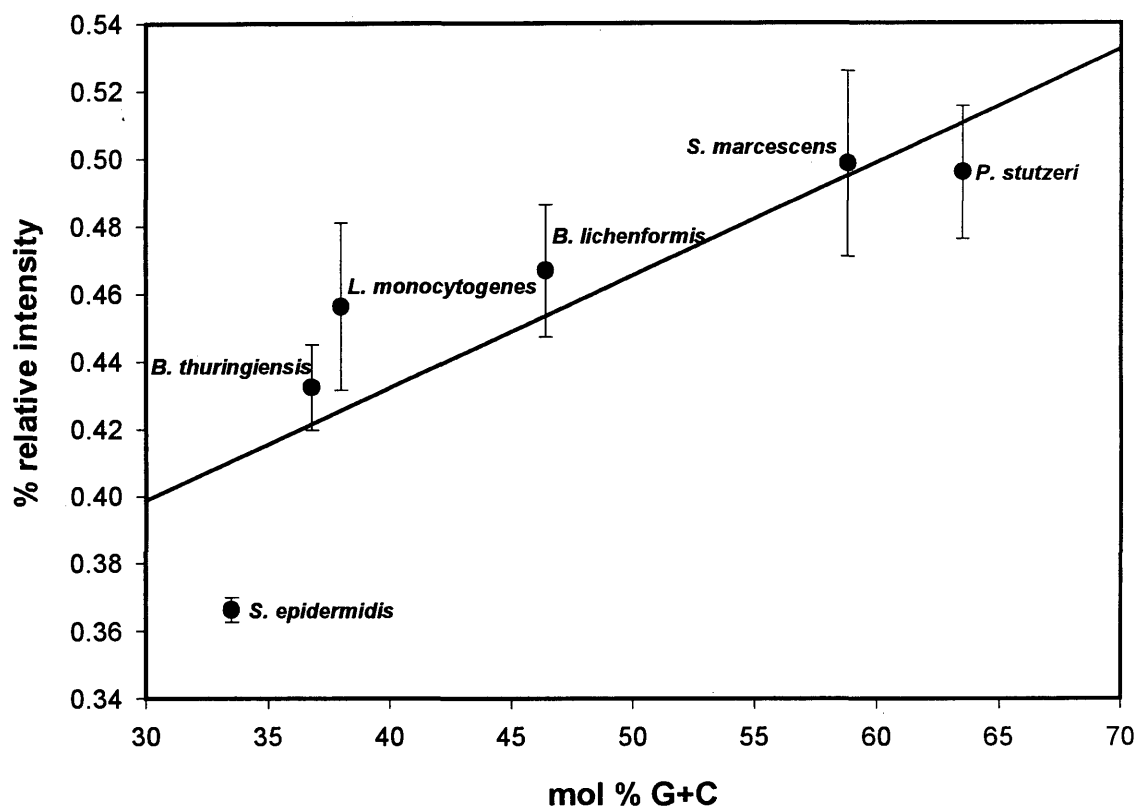
$$y = 3.81 \times 10^{-3} (\pm 5.25 \times 10^{-4}) x + 0.394 (\pm 2.49 \times 10^{-2}); r = 0.840; s_r = 2.92 \times 10^{-2}$$

Formula of the calibration curve used to obtain the values in column 5;

$$y = 3.93 \times 10^{-3} (\pm 5.17 \times 10^{-4}) x + 0.376 (\pm 2.46 \times 10^{-2}); r = 0.851; s_r = 2.88 \times 10^{-2}$$

Formula of the calibration curve used to obtain the values in column 6;

$$y = 4.14 \times 10^{-3} (\pm 5.14 \times 10^{-4}) x + 0.345 (\pm 2.44 \times 10^{-2}); r = 0.864; s_r = 2.86 \times 10^{-2}$$



Each point represents the average percent relative intensity values from analyses of 4 individual samples. The error bars are calculated at a 95% confidence limit.

$$y = 3.34 \times 10^{-3} (\pm 9.05 \times 10^{-4}) x + 0.298 (\pm 2.57 \times 10^{-2})$$

$$r = 0.796$$

Figure 4.10. Standard plot for quantification of nitrogen bases in whole bacterial cells (*k* values included in the % relative intensity calculation).

to be 36.0 ( $\pm 2.38$ ) for *B. anthracis*, 44.3 ( $\pm 2.81$ ) for *F. tularensis*, 47.5 ( $\pm 2.69$ ) for *Y. pestis* and 58.6 ( $\pm 2.42$ ) for *B. melitensis*, Table 4.12. These results are quite similar to those found when the *k* values were not employed. In the case of whole bacterial cells, the diagnostic peaks result from species other than the nitrogen bases of nucleic acids. For example, m/z 177 (A with 3 methylations) has two other ions associated with it, while m/z 165 (G with 1 methylation) and m/z 154 (T with 2 methylations) have even more complex high resolution Py-mass spectral profiles, Figure 4.11. Therefore, the *k* values have little effect in accounting for the nitrogen base fragmentation in whole bacterial cells.

As most mol % G+C content of microorganisms is published as a range, the evaluation of the measured values with the standard deviation are comparable with these published ranges. These results are encouraging, despite the fact that the contribution of RNA has not been fully accounted for in the calculation of the % relative intensity.

#### *Whole Bacterial Cells – Chemical Ionization*

The second phase of the Army's identification and classification of bacterial samples by field portable pyrolysis mass spectrometry may utilize chemical ionization rather than electron ionization. Chemical ionization is a "soft" ionization technique that affords less fragmentation of molecular ions. To understand how chemical ionization may affect the ability to determine mol % G+C content, a similar experiment to the one just discussed was performed. The whole bacterial cells, *S. epidermidis*, *P. mirabilis*, *B. subtilis*, *E. aerogenes* and *S. marcescens*, were analyzed in eight replicates by desorption-chemical ionization (DCI) mass spectrometry using a four-sector double focusing MS (JEOL MStation) with isobutane used as the reagent gas. The mass range used for this experiment was 80 – 400 Da. This mass range was chosen because it represents a possible range for future field applications. Since chemical ionization increases the molecular ion mass by one (addition of a proton), the diagnostic peaks of Table 4.4 are

Table 4.12. Comparison of mass spectral quantitation method (employing  $k$  values) for mol % G+C in whole cell bacteria with known values.

<b>Microorganism</b>	<b>Published* mol % G+C</b>	<b>Calculated mol % G+C including <math>k</math> values</b>
<i>Bacillus anthracis</i>	32.2 – 33.9 (T <sub>m</sub> )	36.0 (± 2.38)
<i>Francisella tularensis</i>	33.0 – 36.0 (T <sub>m</sub> )	44.3 (± 2.81)
<i>Yersinia pestis</i>	46.0 (T <sub>m</sub> )	47.5 (± 2.69)
<i>Brucella melitensis</i>	58.0 (T <sub>m</sub> )	58.6 (± 2.42)

T<sub>m</sub> – thermal melting profile

\* - *Bergey's Manual of Systematic Bacteriology*, N.R. Krieg, Ed., Williams & Wilkins, Baltimore 1984.

36 replicates of *B. anthracis*, 18 replicates of *F. tularensis*, 21 replicates of *Y. pestis* and 33 replicates of *B. melitensis* were analyzed to calculate the mol % G+C content

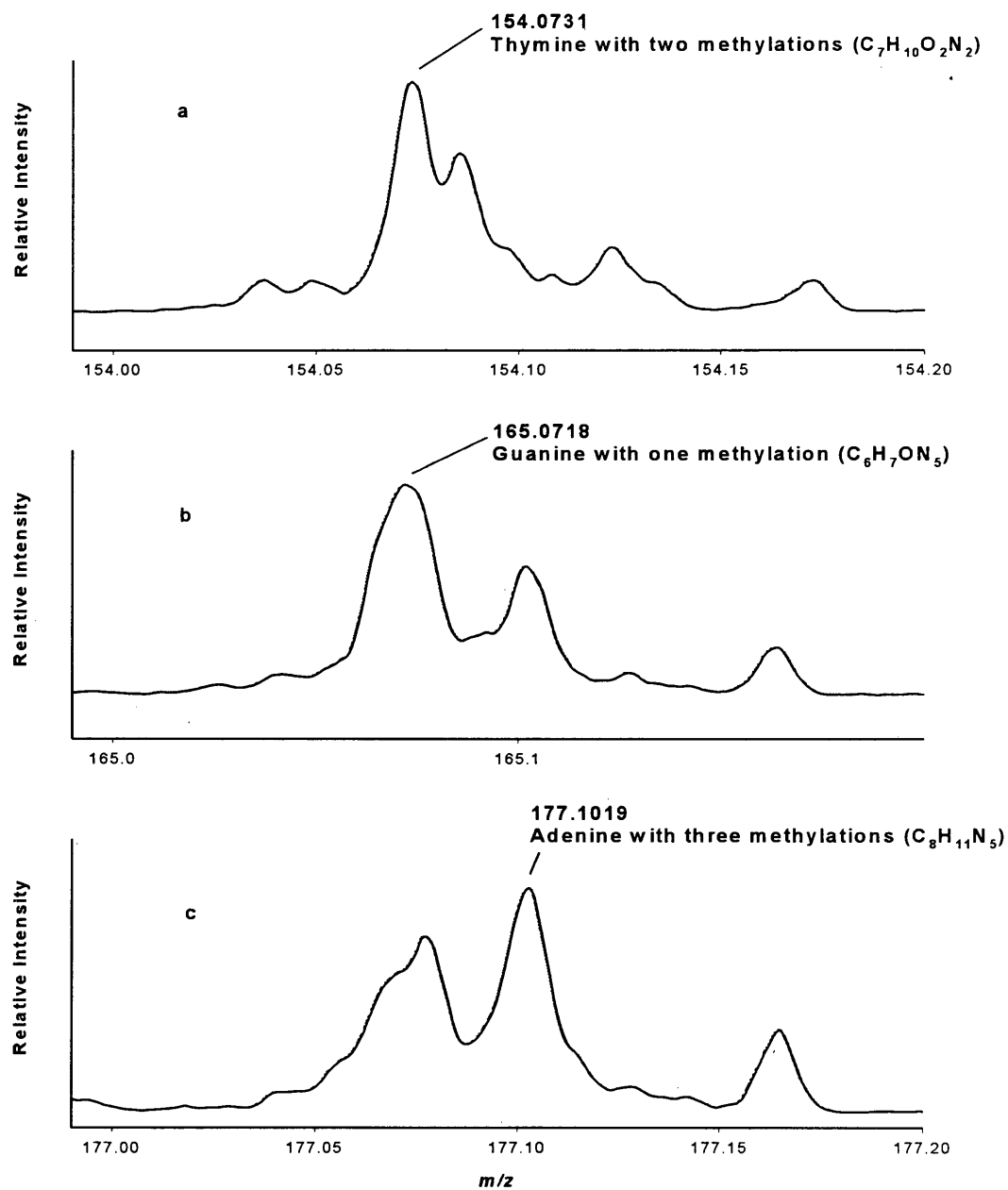


Figure 4.11. HR-DEI ( $R=10,000$ ) mass spectra of (a)  $m/z$  154, (b)  $m/z$  165 and (c)  $m/z$  177 from *Serratia marcescens*.

shifted up by one mass unit. In addition, during the *in situ* methylation of the whole bacterial cells under CI conditions, the nitrogen bases are methylated to the highest degree; little or no partial methylation was observed. That is, the base guanine is represented by m/z 208, adenine by m/z 178, thymine by m/z 155 and cytosine by m/z 154. The single, double and triple methylations are extremely small as shown in Figure 4.12. The explanation for this phenomenon is unclear, but has been noted by others (17). Therefore, only m/z 208, 178, 155 and 154 were used for the calculation of % relative intensity.

The calibration curve for the whole bacterial cells, analyzed by DCI-MS, is given in Figure 4.13. From the mass spectrum, the peak intensities of m/z 208 (G), 178 (A), 155 (T) and 154 (C) were summed and the combined peak intensities of guanine and cytosine were divided by this total to calculate the % relative intensity. Again, the mol % G+C content used on the x axis of the calibration plot for whole bacterial cells was taken from *Bergey's Manual of Systematic Bacteriology* (13). The data corresponds to a straight line of the form  $y = 6.91 \times 10^{-3} (\pm 6.22 \times 10^{-4}) x + 0.214 (\pm 2.90 \times 10^{-2})$ . The linear correlation coefficient ( $r$ ) of the curve was found to be 0.874 and  $s_r$  is  $\pm 3.65 \times 10^{-2}$ .

Whole bacterial cells, not used for the construction of the calibration plot (sample numbers 1, 3, 18, 24 and 31 of Table 4.2), were analyzed by DCI-MS and the mol % G+C was calculated from the curve shown in Figure 4.13. The results are compiled in Table 4.13 and were found to be 34.2 ( $\pm 2.50$ ) for *B. anthracis* (vegetative), 48.1 ( $\pm 2.77$ ) for *B. anthracis* (spores), 43.4 ( $\pm 2.77$ ) for *F. tularensis*, 47.9 ( $\pm 2.31$ ) for *Y. pestis* and 52.0 ( $\pm 2.50$ ) for *B. melitensis*. The measured values are listed with the standard deviation obtained from the calibration curve ( $s_c$ ). The measured values of *Y. pestis* and *B. anthracis* (vegetative) fall within the range of the published values. However, *F. tularensis*, *B. anthracis* (sporulated) and *B. melitensis* do not fall within published ranges. *F. tularensis* and *B. anthracis* (sporulated) were predicted with artificially high mol % G+C content and the mol % G+C predicted for *B. melitensis* was artificially low

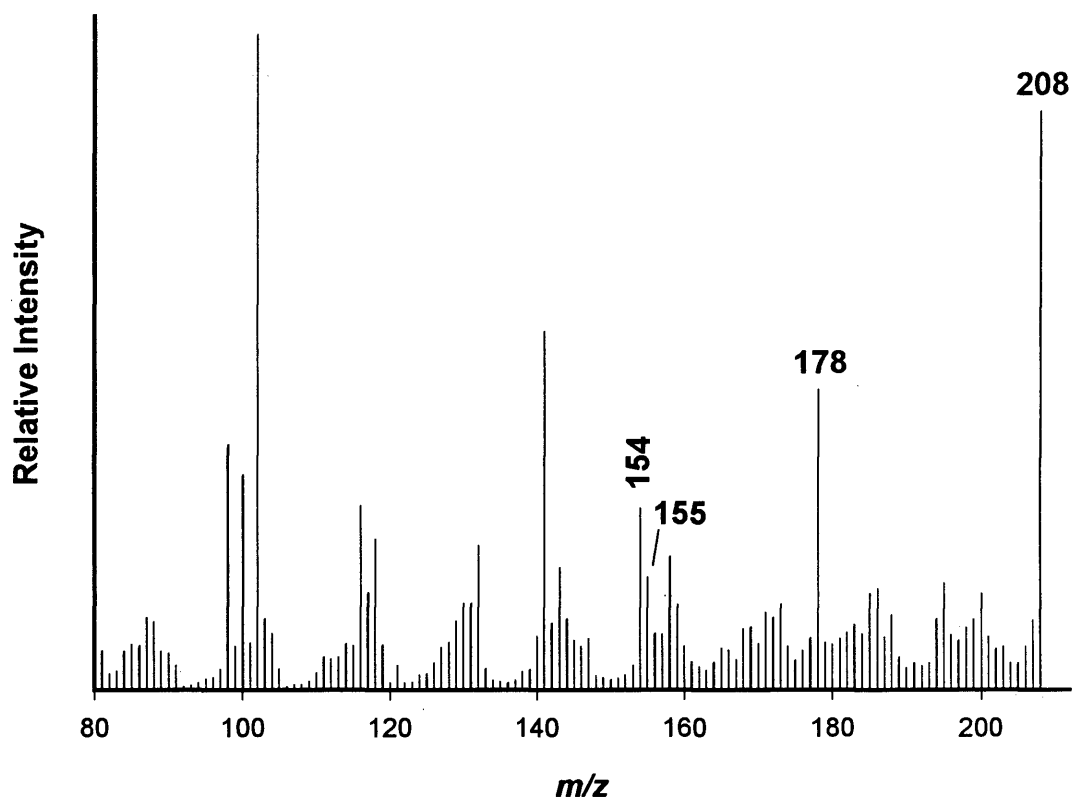
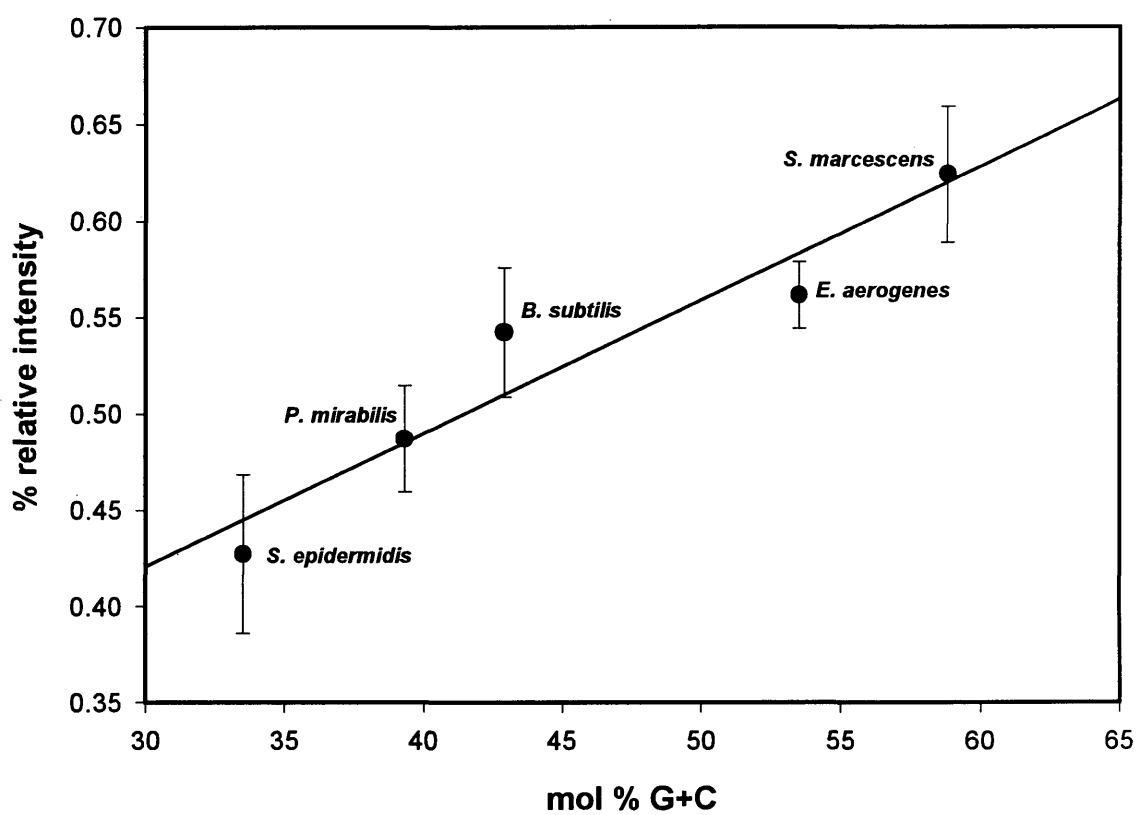


Figure 4.12. DCI mass spectrum of *S. marcescens* with *in situ* methylation using 0.5 M TMAH.



Each point represents the average percent relative intensity values from analyses of 8 individual samples. The error bars are calculated at a 95% confidence limit.

$$y = 6.91 \times 10^{-3} (\pm 6.22 \times 10^{-4}) x + 0.214 (\pm 2.90 \times 10^{-2})$$

$$r = 0.874$$

Figure 4.13. Standard plot for quantification of nitrogen bases in whole bacterial cells (chemical ionization methodology).

Table 4.13. Comparison of mass spectral quantitation method (chemical ionization) for mol % G+C in whole cell bacteria with known values.

<b>Microorganism</b>	<b>Published* mol % G+C</b>	<b>Calculated mol % G+C</b>
<i>Bacillus anthracis-Vollum</i> (vegetative)	32.2 – 33.9 (T <sub>m</sub> )	34.2 (± 2.50)
<i>Bacillus anthracis-Vollum</i> (spore)	32.2 – 33.9 (T <sub>m</sub> )	48.1 (± 2.77)
<i>Francisella tularensis</i> -LVS	33.0 – 36.0 (T <sub>m</sub> )	43.4 (± 2.77)
<i>Yersinia pestis</i> -EV76	46.0 (T <sub>m</sub> )	47.9 (± 2.31)
<i>Brucella melitensis</i> -Suis	58.0 (T <sub>m</sub> )	52.0 (± 2.50)

T<sub>m</sub> – thermal melting profile

\* - *Bergey's Manual of Systematic Bacteriology*, N.R. Krieg, Ed., Williams & Wilkins, Baltimore 1984.

5 replicates of *B. anthracis* (vegetative), 4 replicates of *B. anthracis* (spore), 4 replicates of *F. tularensis*, 6 replicates of *Y. pestis* and 5 replicates of *B. melitensis* were analyzed to calculate the mol % G+C content

when compared to published values. The discrepancy for the *B. anthracis* (sporulated) specie may be the amount of available DNA for methylation, as discussed previously. The discrepancies for the *F. tularinses* and *B. melintensis* samples can not be explained but may be a result of the sample itself. However, the knowledge that these samples are consistently predicted with either high or low mol % G+C content is invaluable. In addition, the methodology of CI analysis is simplified by using fewer diagnostic peaks in the % relative intensity calculation. Future work would involve the analysis of whole bacterial cells employing the field portable mass spectrometer with chemical ionization.

As discussed previously, the diagnostic peaks of guanine, adenine and cytosine are common to both DNA and RNA. Therefore, the results obtained from this analysis are again met with cautious optimism. To what extent these three nitrogen bases of RNA contribute to the % relative intensity values must be determined. Future work to resolve this question would be similar to that previously discussed.

## CONCLUSIONS

The work presented herein has shown that the mol % G+C content of free nucleotide solutions, pure DNA and whole bacterial cells can be determined by mass spectral analysis. The diagnostic peak intensities were obtained from the spectrum and were used to calculate the percent relative intensity. The calculated percent relative intensities were plotted versus the published mol % G+C content of a sample population. The method of least squares was used to construct a standard curve for the prediction of mol % G+C of unknowns.

For the free nucleotide solution and the pure DNA sample,  $k$  (correction) values were employed in the % relative intensity calculation. The  $k$  values were used in an attempt to correct for the fragmentation of molecular ions under EI conditions. The predictability of mol % G+C from the calibration curve was improved with the inclusion

of  $k$  values for these samples. However,  $k$  values did not improve the predictability of mol % G+C for whole bacterial cells under EI conditions. This may be due to the fact that the diagnostic peaks are shared among other chemical species.

Whole bacterial cells were analyzed by electron and chemical ionization mass spectrometry. The predictability of mol % G+C from the calibration curves (generated from the data collected by both mass spectral techniques) was good. However, to directly compare the effectiveness of EI over CI would be futile, since two different instruments were used for the analyses. However, the methodology of using diagnostic peaks from the mass spectrum to calculate % relative intensity is transferable between the two ionization techniques. The methodology for determining mol % G+C with mass spectrometry has, therefore, been soundly proven. Although the contribution of RNA has not been fully addressed, the results obtained herein are encouraging. Future work to address this situation has been previously discussed. This work would be a daunting task but worth exploration.

The DNA represents the genetic information contained within the cell or cells of an organism. There is little change in the mol % G+C content in the DNA from one generation to the next, and as a result, it is characteristic for a species. The mol % G+C content of DNA from the prokaryotes ranges from about 25 to 75% while for eukaryotes, it is in the mid-forties. Since there are many species of prokaryotes, it is obvious that a given G+C content is not the preserve of a single species. The importance of the G+C content in bacterial taxonomy is that it can be an excluding characteristic (2).

**REFERENCES**

- (1) Chargaff, E. *The Nucleic Acids*; Academic Press: New York, 1955.
- (2) Johnson, J. L. *Methods in Microbiology*; Academic Press: London, 1985.
- (3) Schildkraut, C. L.; Marmur, J.; Doty, P. *J. Mol. Biol.* **1962**, *4*, 430-443.
- (4) Ko, C. Y.; Johnson, J. L.; Barnett, L. B.; McNair, H. M.; Vercellotti, J. R. *Anal. Biochem.* **1977**, *80*, 183-192.
- (5) Katayama-Fujimura, Y. *Agric. Biol. Chem.* **1984**, *48*, 3169.
- (6) Sonoki, S.; Hisamatsu, S.; Kiuchi, A. *Nucleic Acids Research* **1993**, *21*, 2776.
- (7) Van Dilla, M. A.; Langlois, R. G.; Pinkel, D.; Yajko, D.; Hadley, W. K. *Science* **1983**, *220*, 620-623.
- (8) Hawley, D. M.; Wiebers, J. L. *Nucleic Acids Research* **1978**, *5*, 4949.
- (9) Jankowski, K. *Recent Developments in Mass Spectrometry in Biochemistry, Medicine and Environmental Research*; Elsevier Scientific Publishing Company: Amsterdam, 1983.
- (10) Soler, F.; Jankowski, K. *Eur. J. Mass Spec. Biochem., Medicine Environ. Res.* **1982**, *2*, 33.
- (11) Hendricker, A. D. Ph.D. Dissertation, Colorado School of Mines, Golden, CO, 1998.
- (12) Hendricker, A. D.; Basile, F.; Voorhees, K. J. *J. Anal. Appl. Pyrolysis* **1998**, *46*, 65-82.
- (13) *Bergey's Manual of Systematic Bacteriology*; Williams & Wilkins: Baltimore, 1984.
- (14) Gould, G. W.; Hurst, A. ; Academic Press Inc.: London, 1969.
- (15) Fitz-James, P. C. *Can. J. Microbiol.* **1955**, *1*, 502.
- (16) Fitz-James, P. C.; Young, I. E. *J. Bact.* **1959**, *78*, 743.
- (17) Barshick, S.-A. ,personal communication, 1997.

**APPENDIX**

**DEI PRODUCT-ION (R=20,000) AND PRECURSOR-ION (R=1,000)  
SCANS OF THE BIOMARKER IONS IN *B. NEOTOMAE*.**

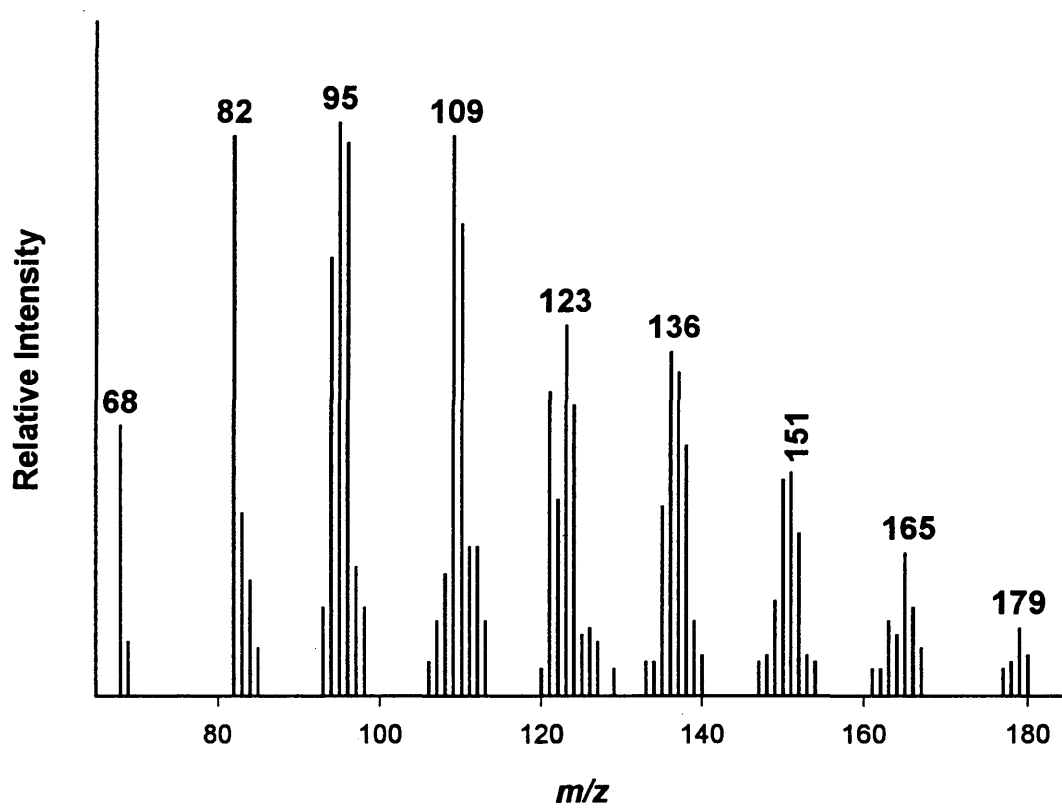


Figure A.1. DEI precursor ion mass spectrum of m/z 67 from *Brucella neotomae*.

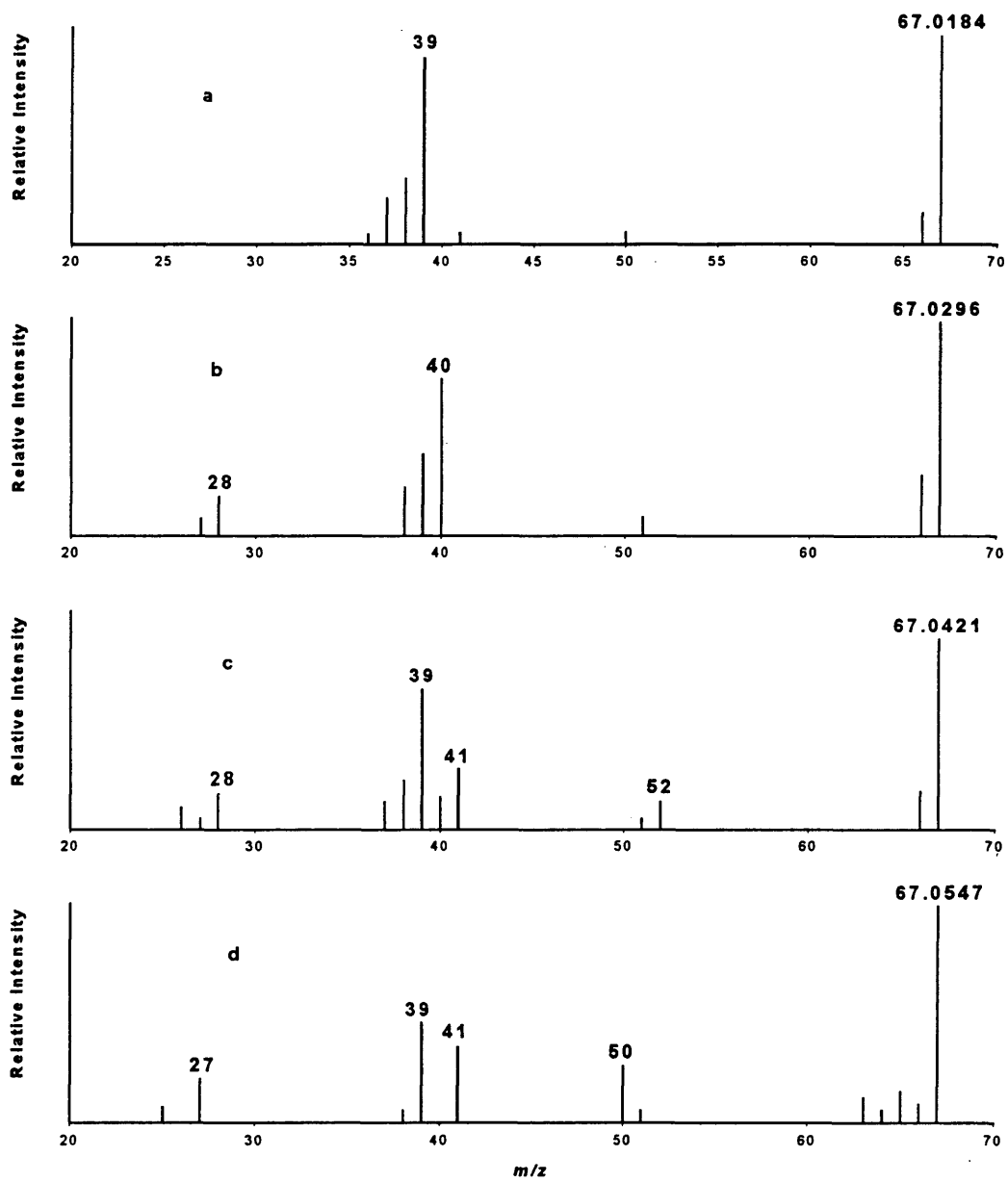


Figure A.2. HR-DEI product ion mass spectra of (a)  $m/z$  67.0184, (b)  $m/z$  67.0296, (c)  $m/z$  67.0421 and (d)  $m/z$  67.0547 from *Brucella neotomae*.

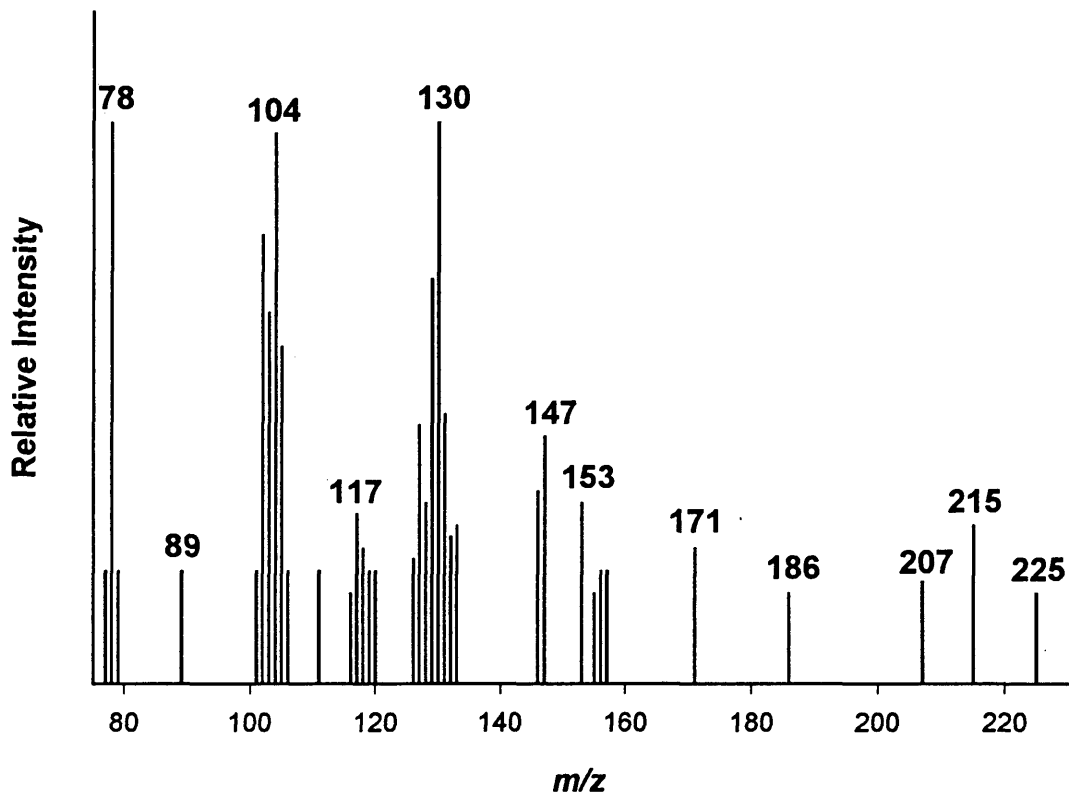


Figure A.3. DEI precursor ion mass spectrum of  $m/z$  76 from *Brucella neotomae*.

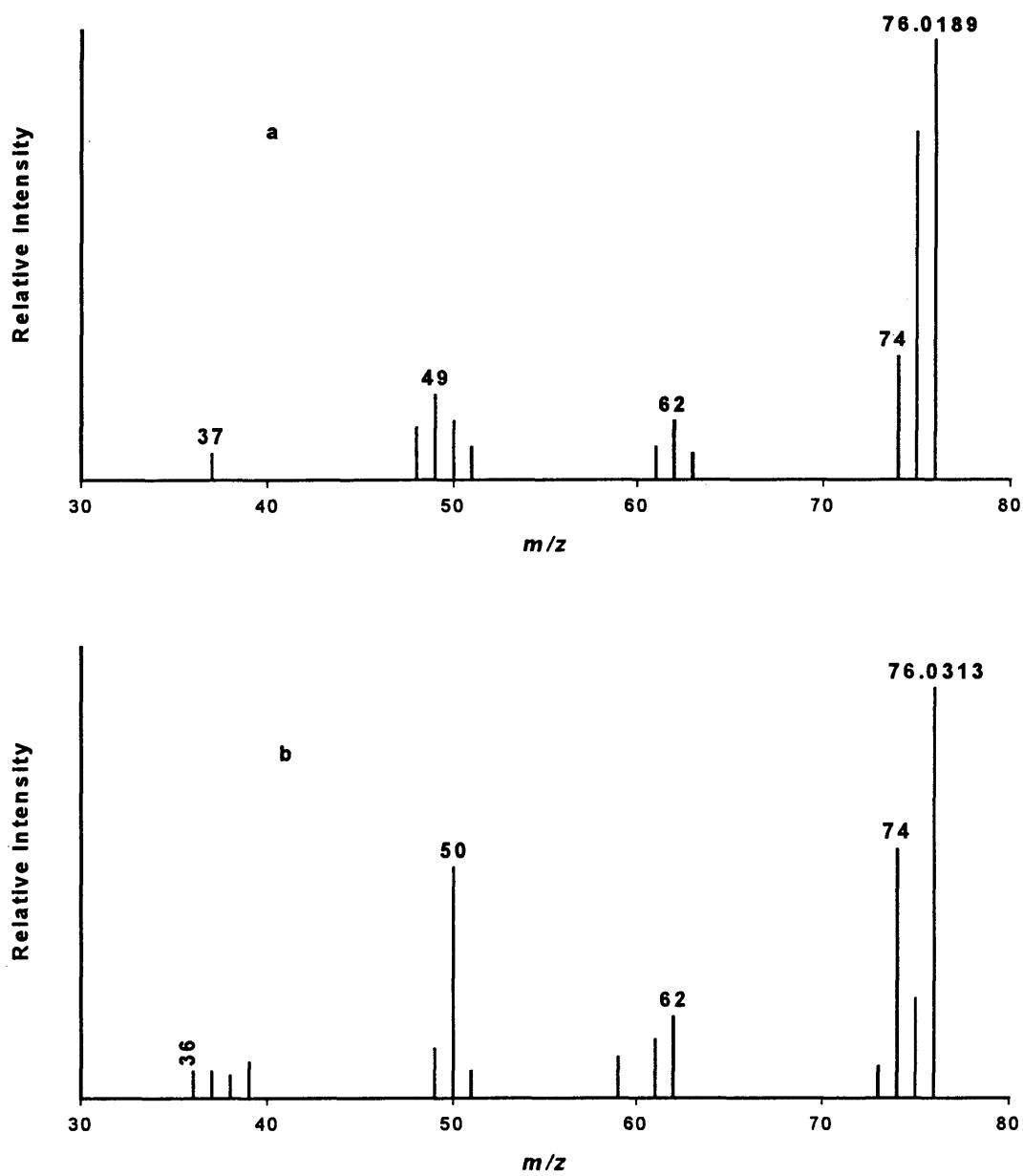


Figure A.4. HR-DEI product ion mass spectra of (a)  $m/z$  76.0189 and (b)  $m/z$  76.0313 from *Brucella neotomae*.

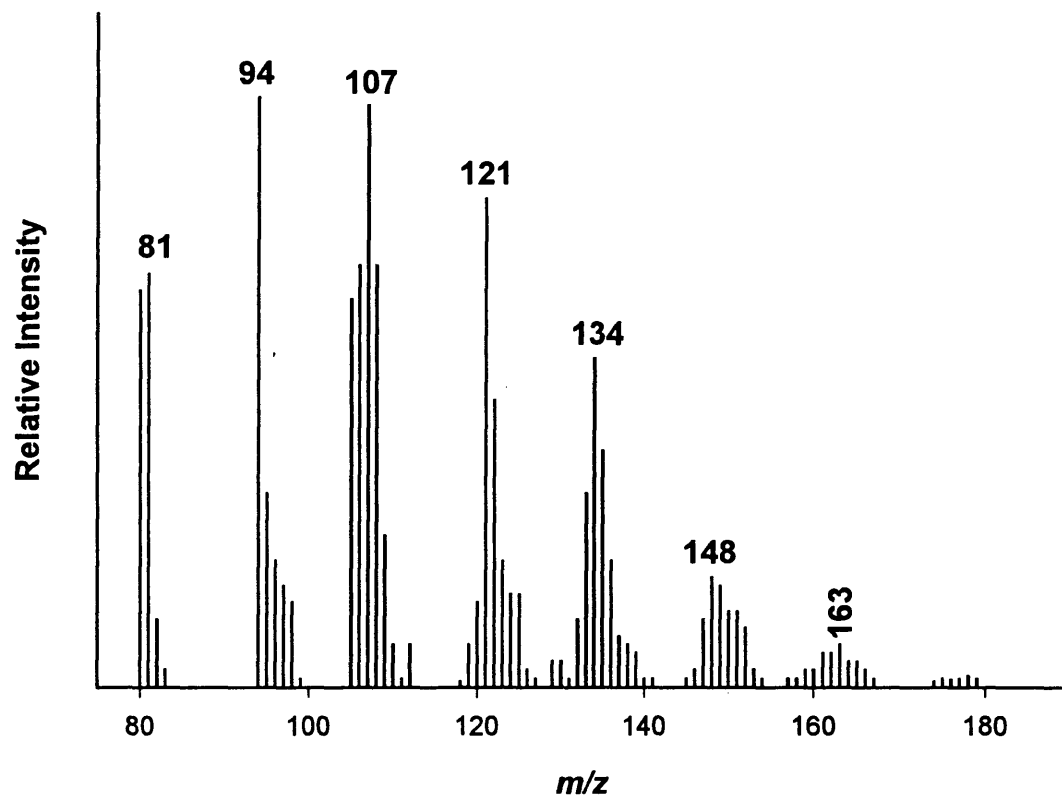


Figure A.5. DEI precursor ion mass spectrum of  $m/z$  79 from *Brucella neotomae*.

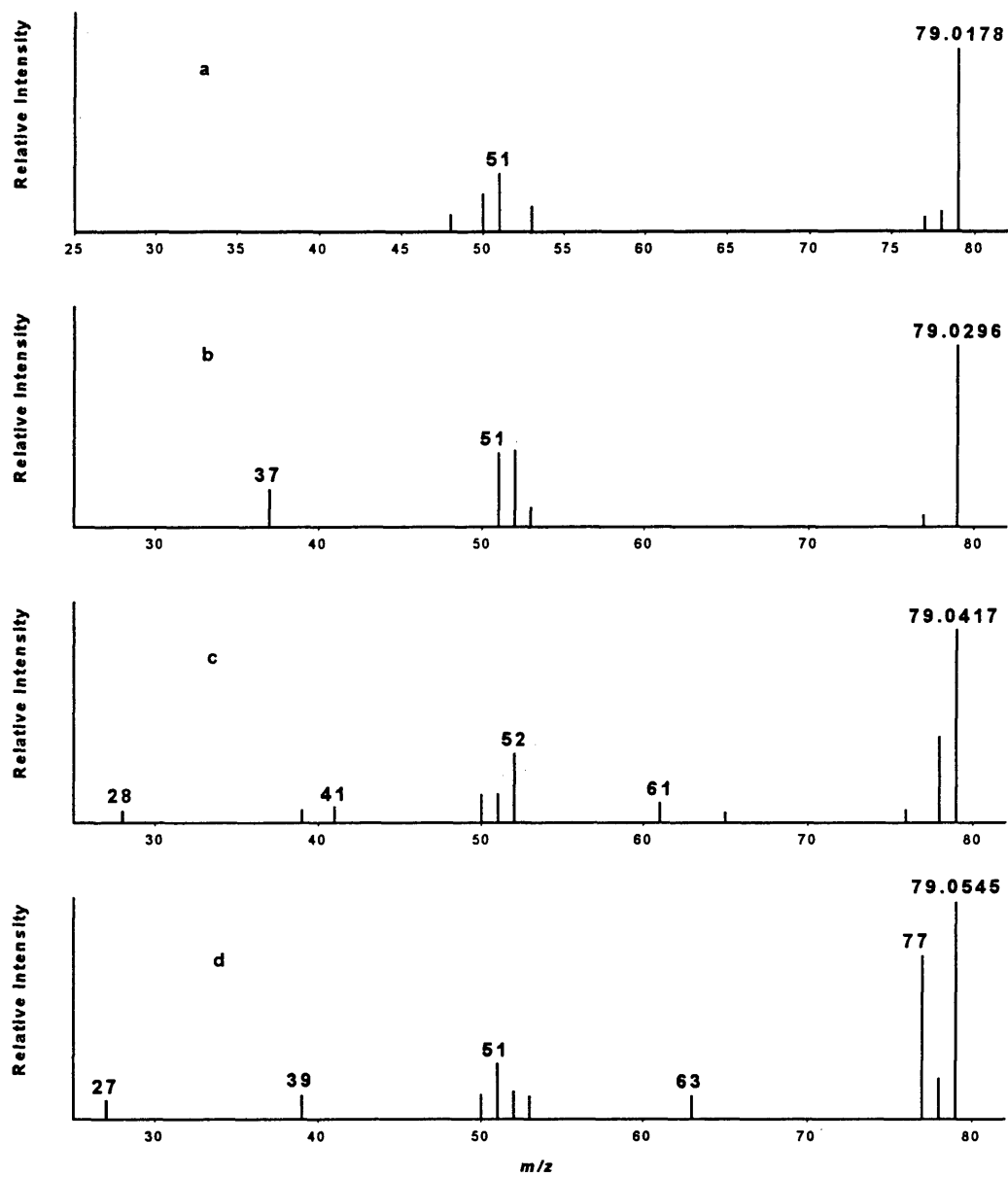


Figure A.6. HR-DEI product ion mass spectra of (a)  $m/z$  79.0178, (b)  $m/z$  79.0296, (c)  $m/z$  79.0417 and (d)  $m/z$  79.0545 from *Brucella neotomae*.

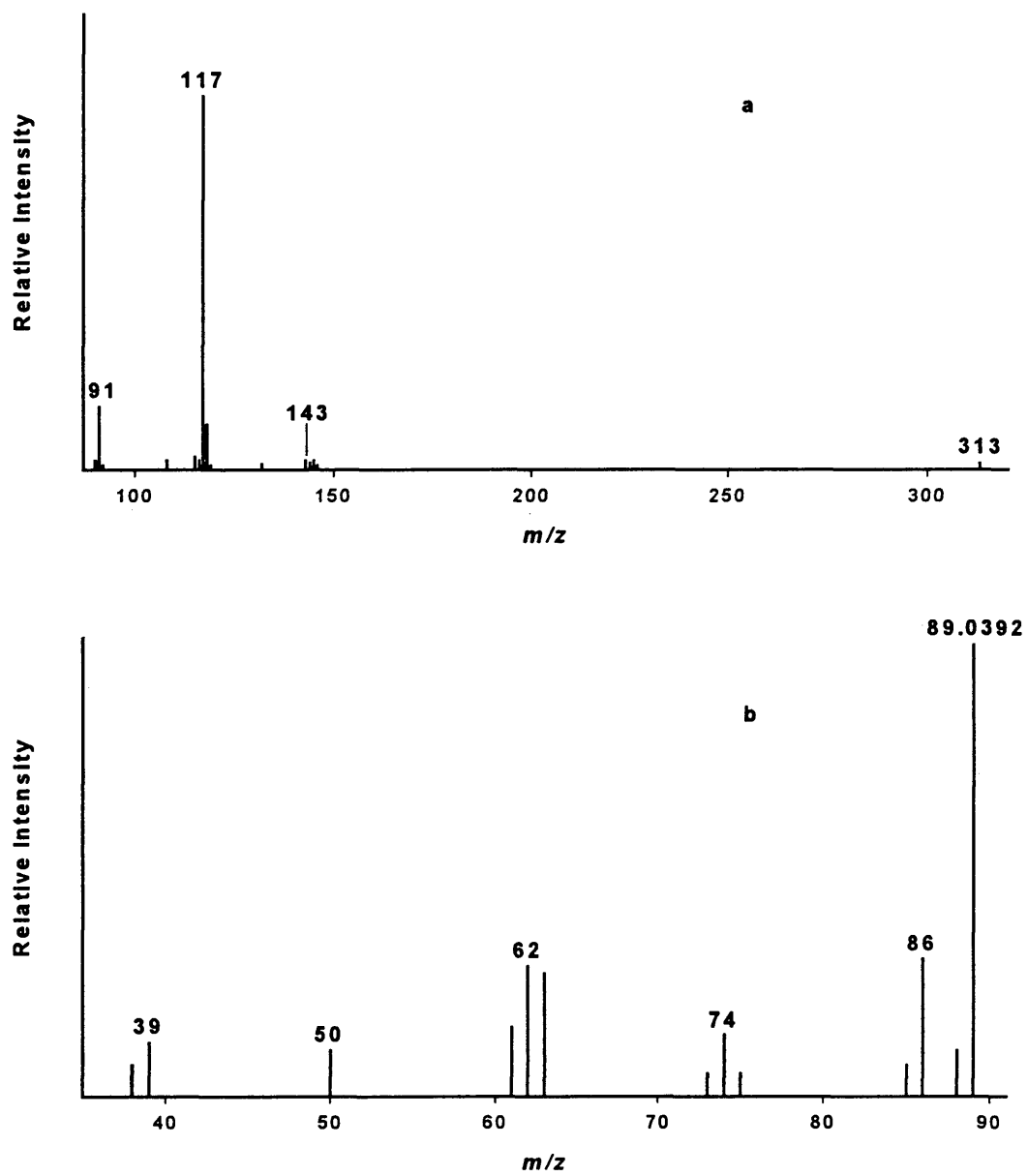


Figure A.7. DEI (a) precursor ion mass spectrum of  $m/z$  89 and (b) HR-DEI product ion mass spectrum of  $m/z$  89.0392 from *Brucella neotomae*.

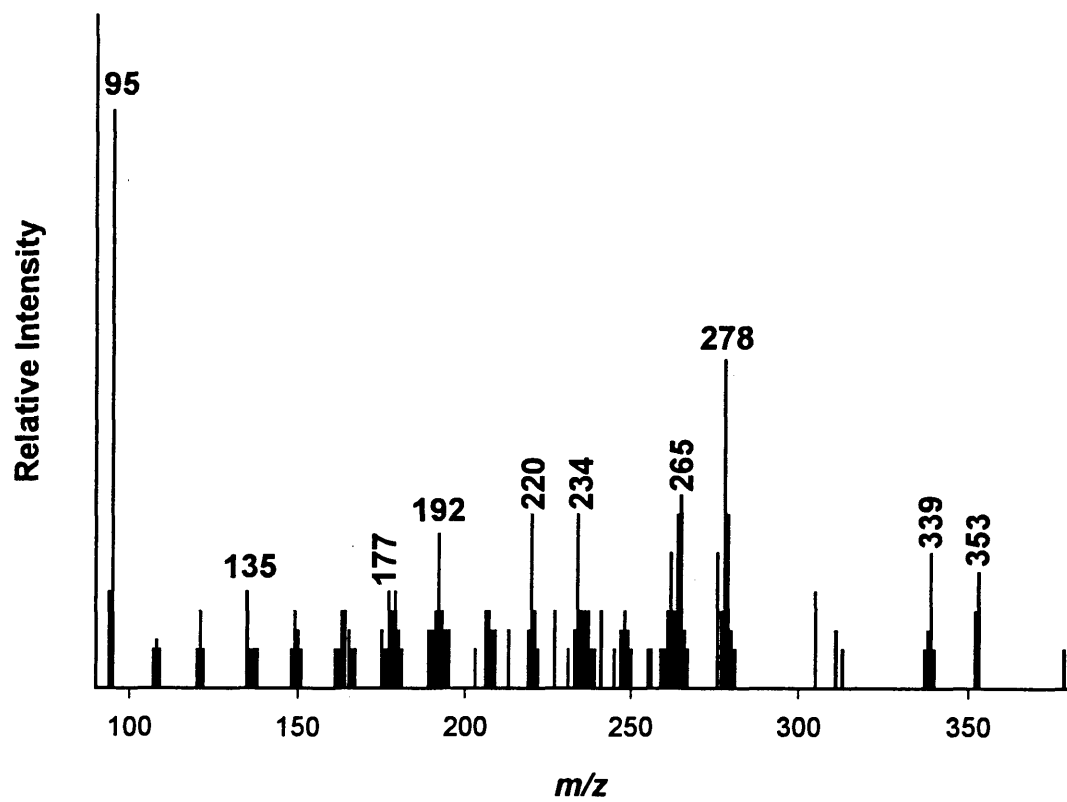


Figure A.8. DEI precursor ion mass spectrum of  $m/z$  93 from *Brucella neotomae*.

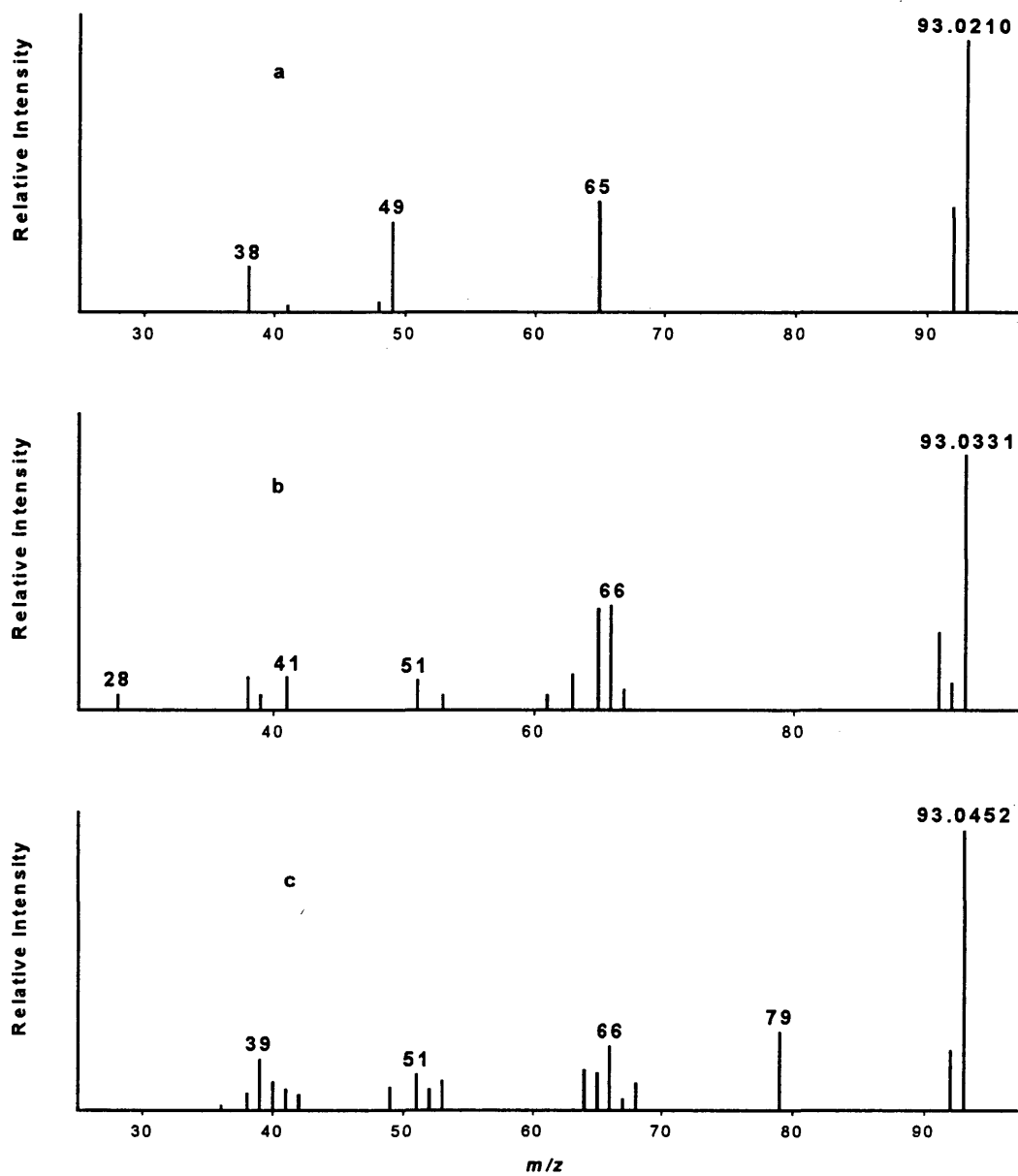


Figure A.9. HR-DEI product ion mass spectra of (a) m/z 93.0210, (b) m/z 93.0331 and (c) m/z 93.0452 from *Brucella neotomae*.

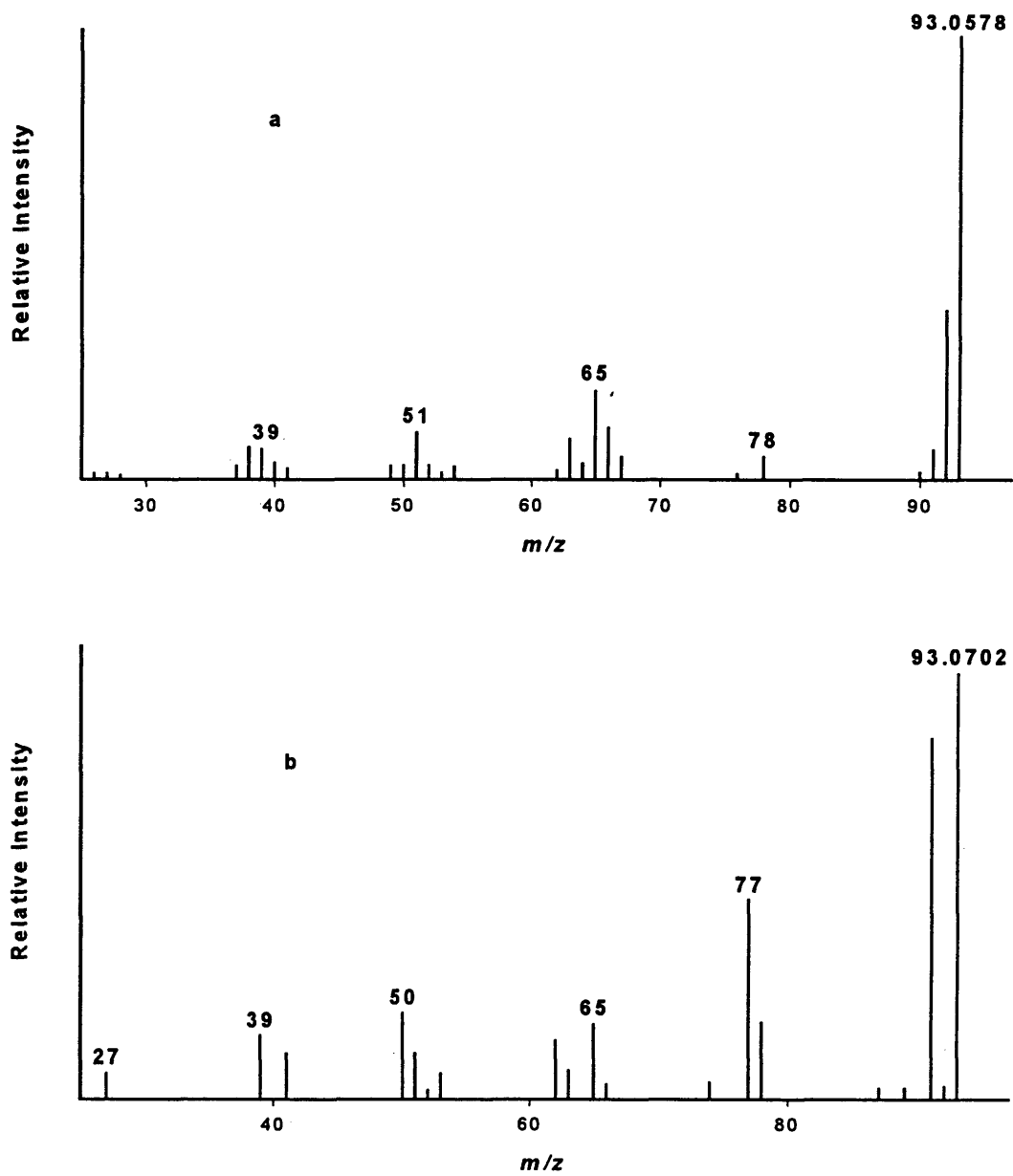


Figure A.10. HR-DEI product ion mass spectra of (a)  $m/z$  93.0578 and (b)  $m/z$  93.0702 from *Brucella neotomae*.

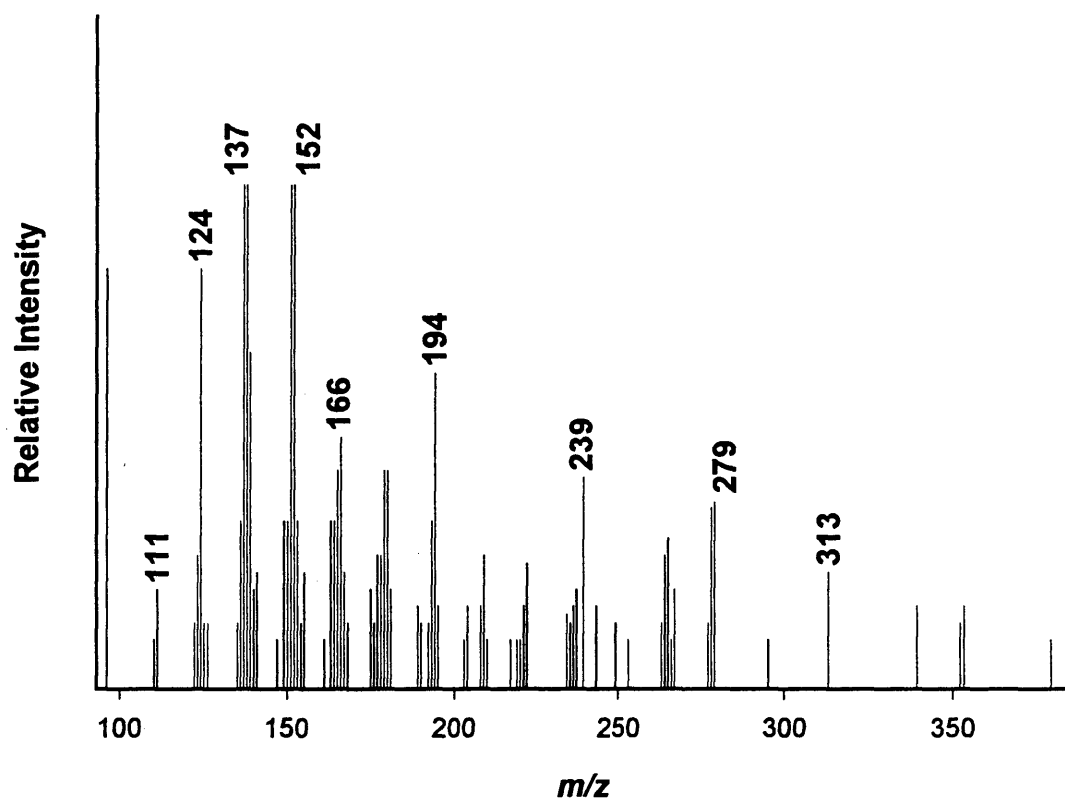


Figure A.11. DEI precursor ion mass spectrum of  $m/z$  95 from *Brucella neotomae*.

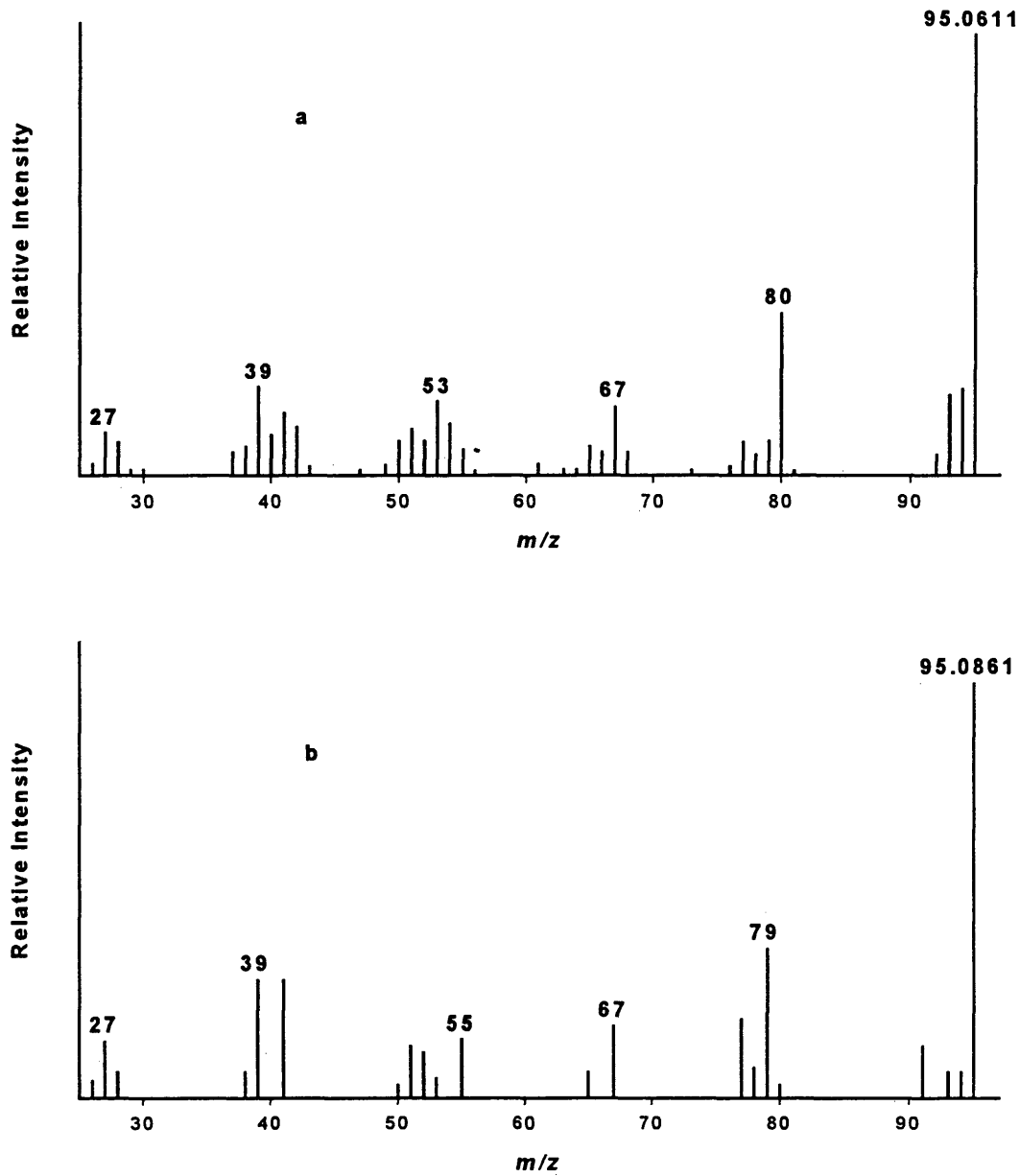


Figure A.12. HR-DEI product ion mass spectra of (a)  $m/z$  95.0611 and (b)  $m/z$  95.0861 from *Brucella neotomae*.

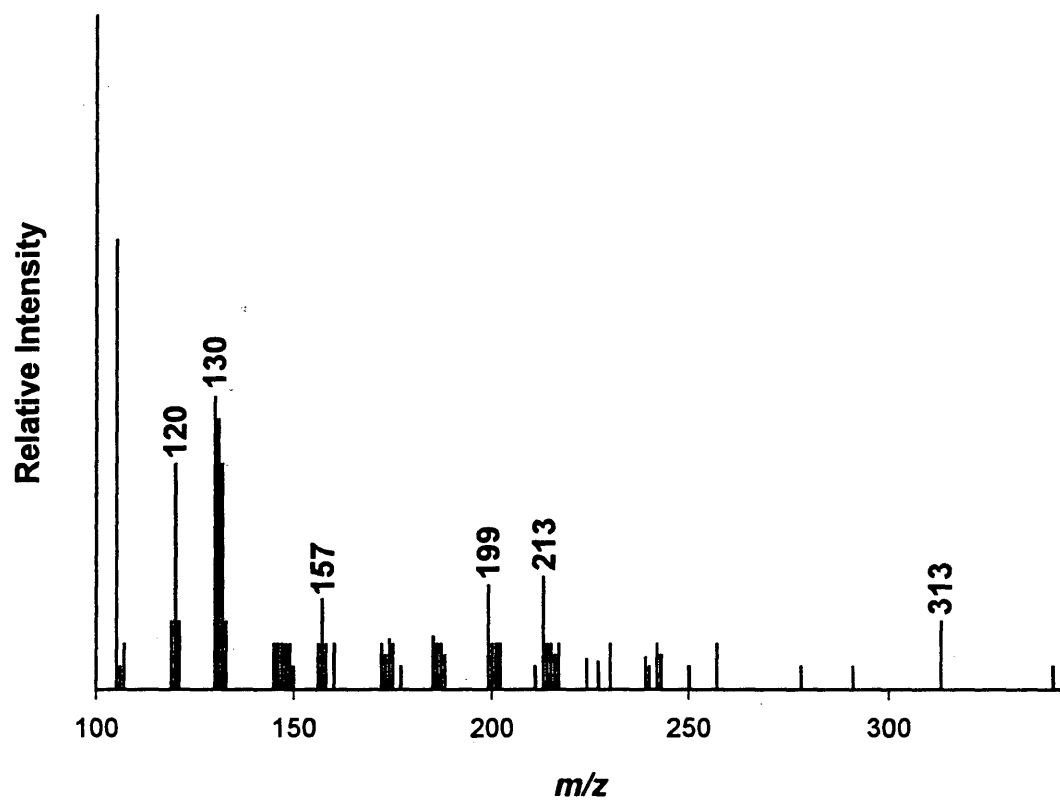


Figure A.13. DEI precursor ion mass spectrum of  $m/z$  103 from *Brucella neotomae*.

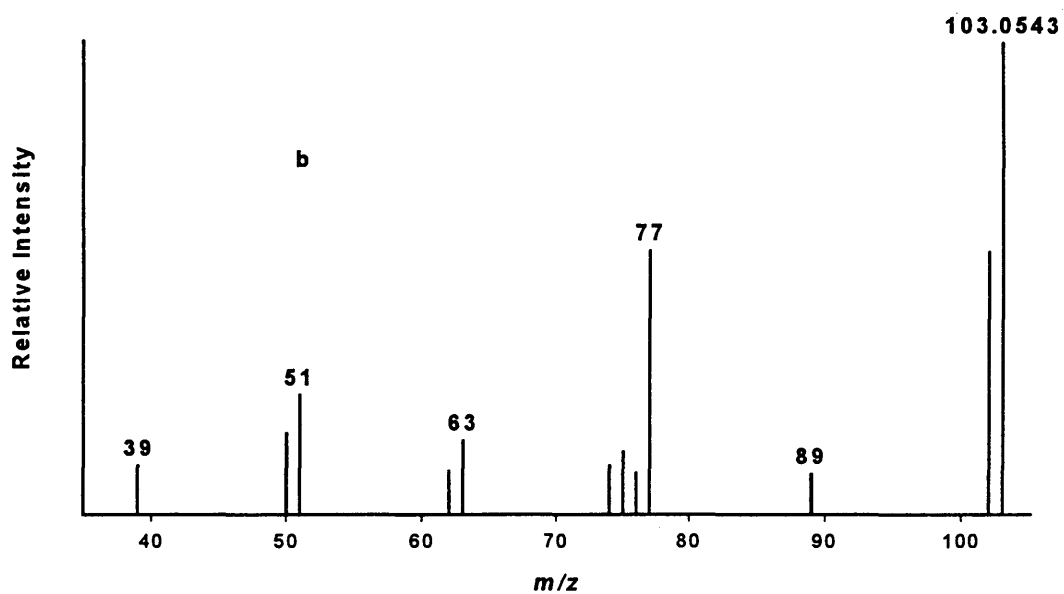
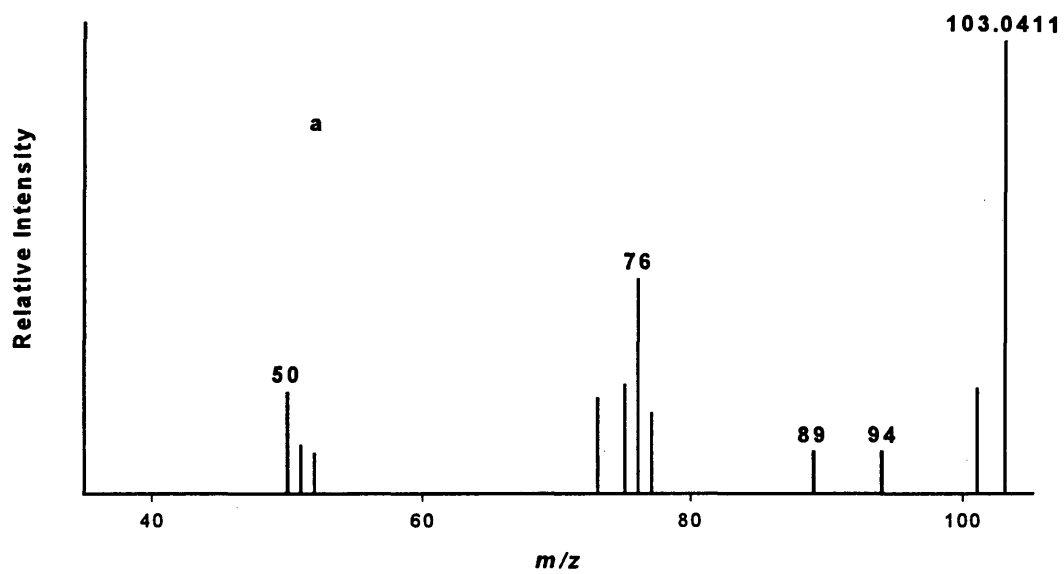


Figure A.14. HR-DEI product ion mass spectra of (a)  $m/z$  103.0411 and (b)  $m/z$  103.0543 from *Brucella neotomae*.

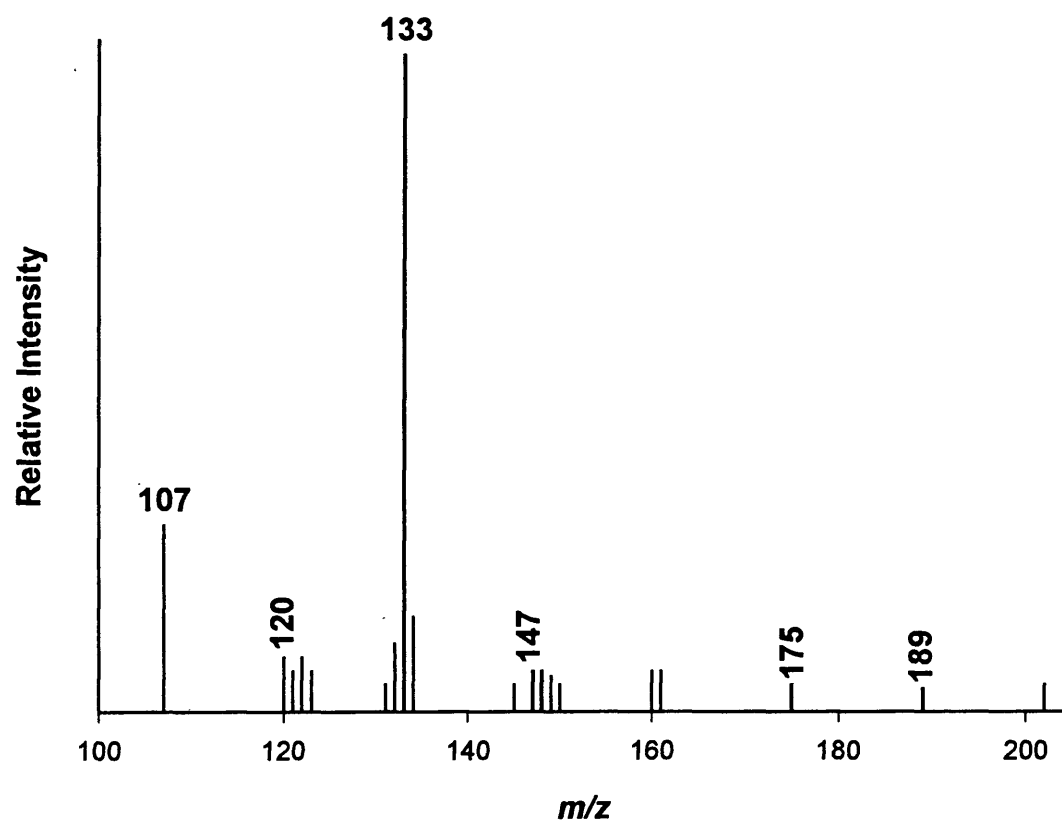


Figure A.15. DEI precursor ion mass spectrum of m/z 105 from *Brucella neotomae*.

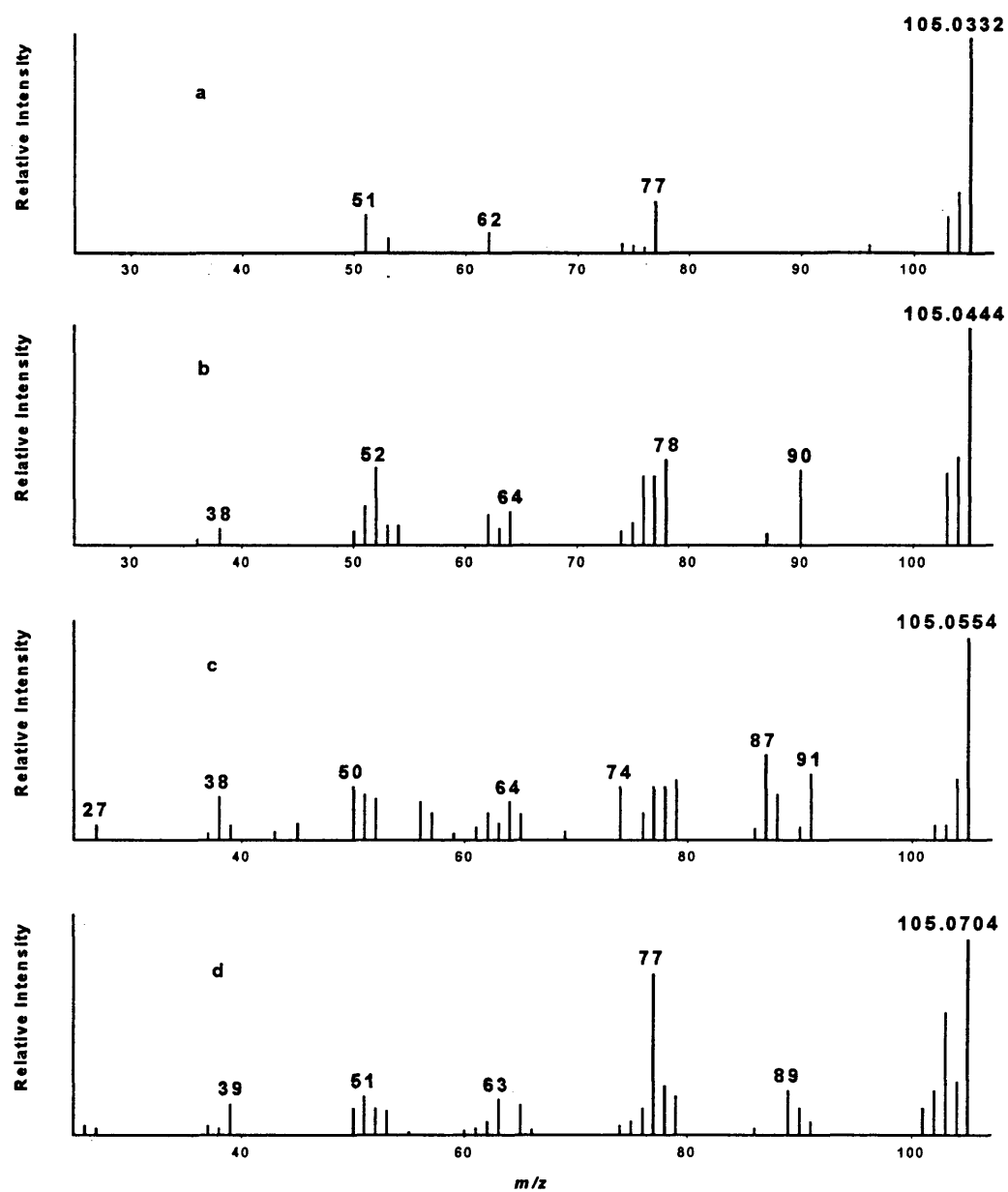


Figure A.16. HR-DEI product ion mass spectra of (a)  $m/z$  105.0332, (b)  $m/z$  105.0444, (c)  $m/z$  105.0554 and (d)  $m/z$  105.0704 from *Brucella neotomae*.

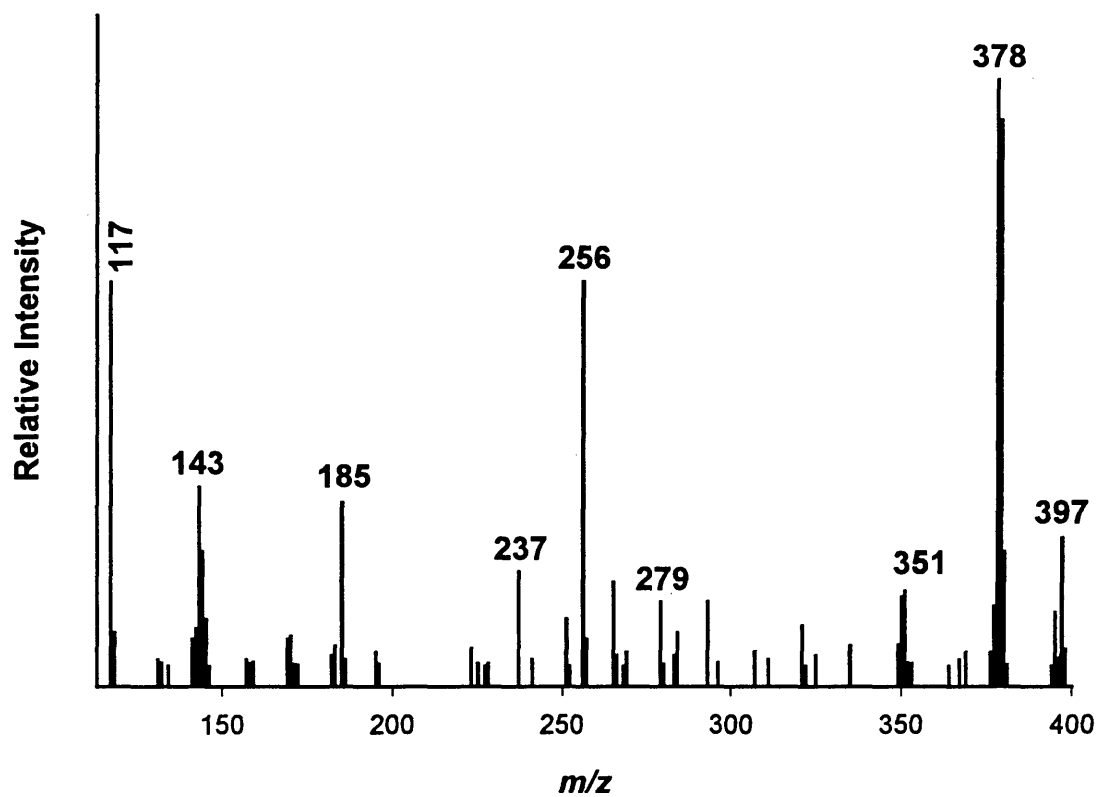


Figure A.17. DEI precursor ion mass spectrum of m/z 115 from *Brucella neotomae*.

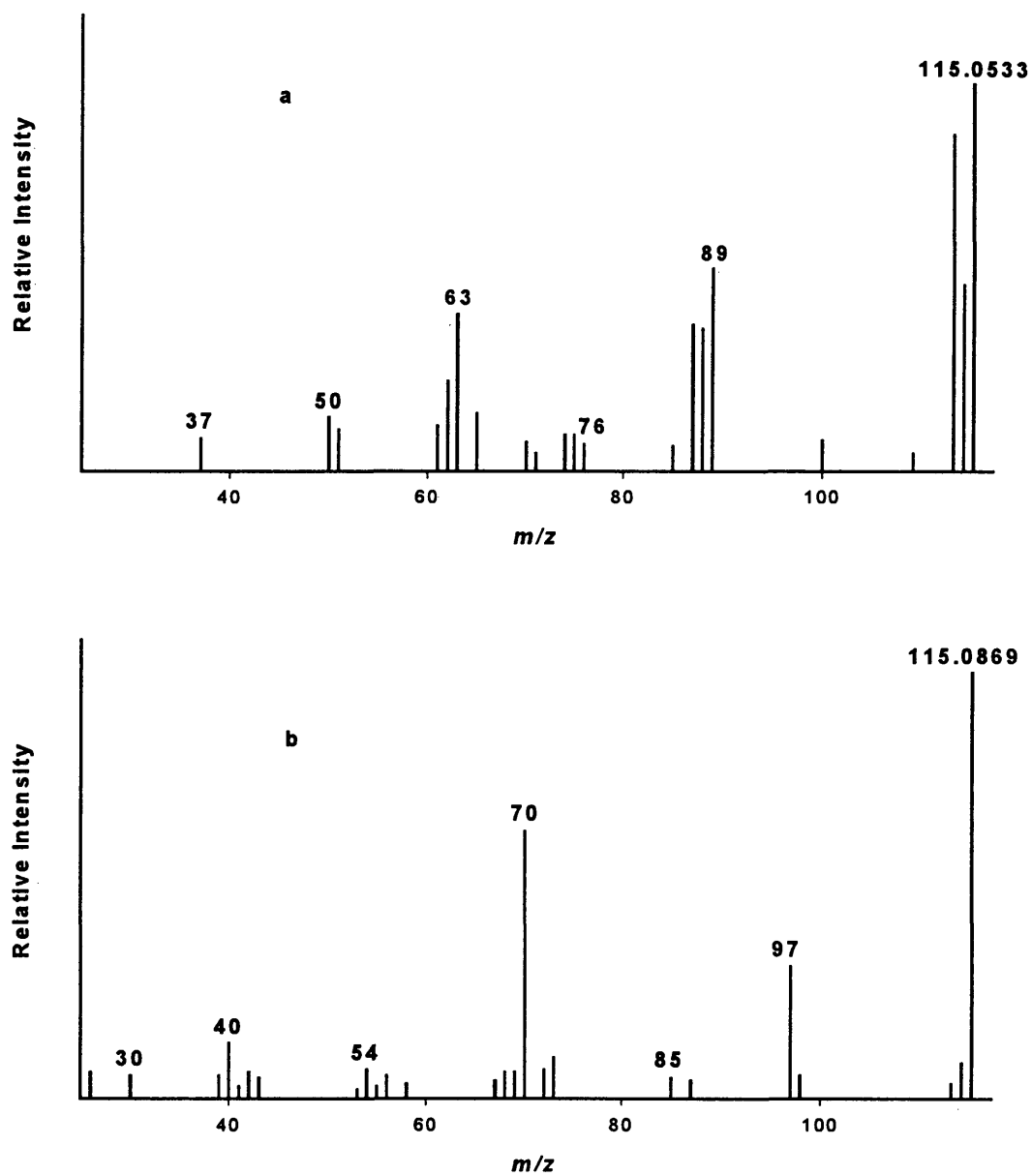


Figure A.18. HR-DEI product ion mass spectra of (a)  $m/z$  115.0533 and (b)  $m/z$  115.0869 from *Brucella neotomae*.

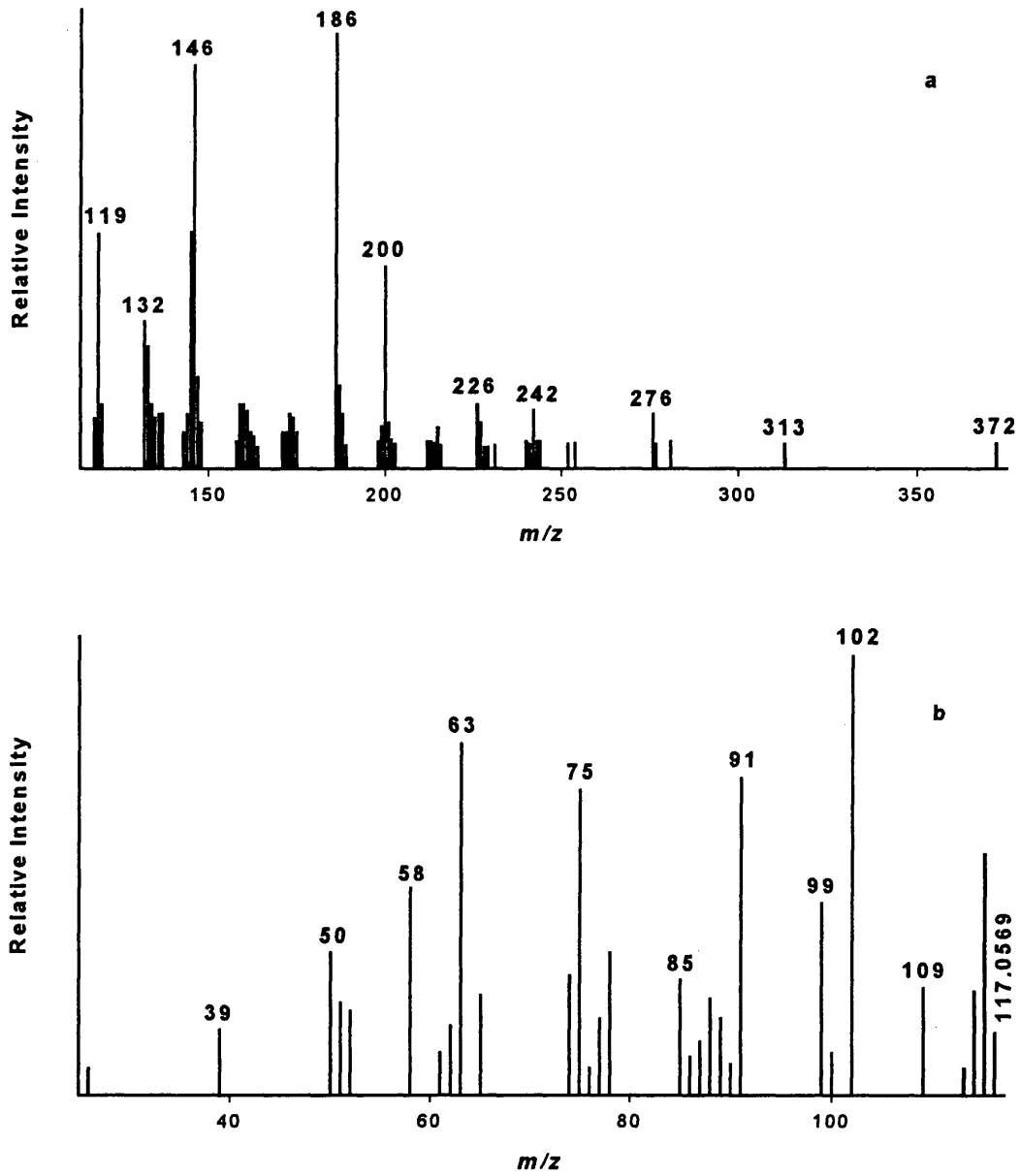


Figure A.19. DEI (a) precursor ion mass spectrum of  $m/z$  117 and (b) HR-DEI product ion mass spectrum of  $m/z$  117.0569 from *Brucella neotomae*.

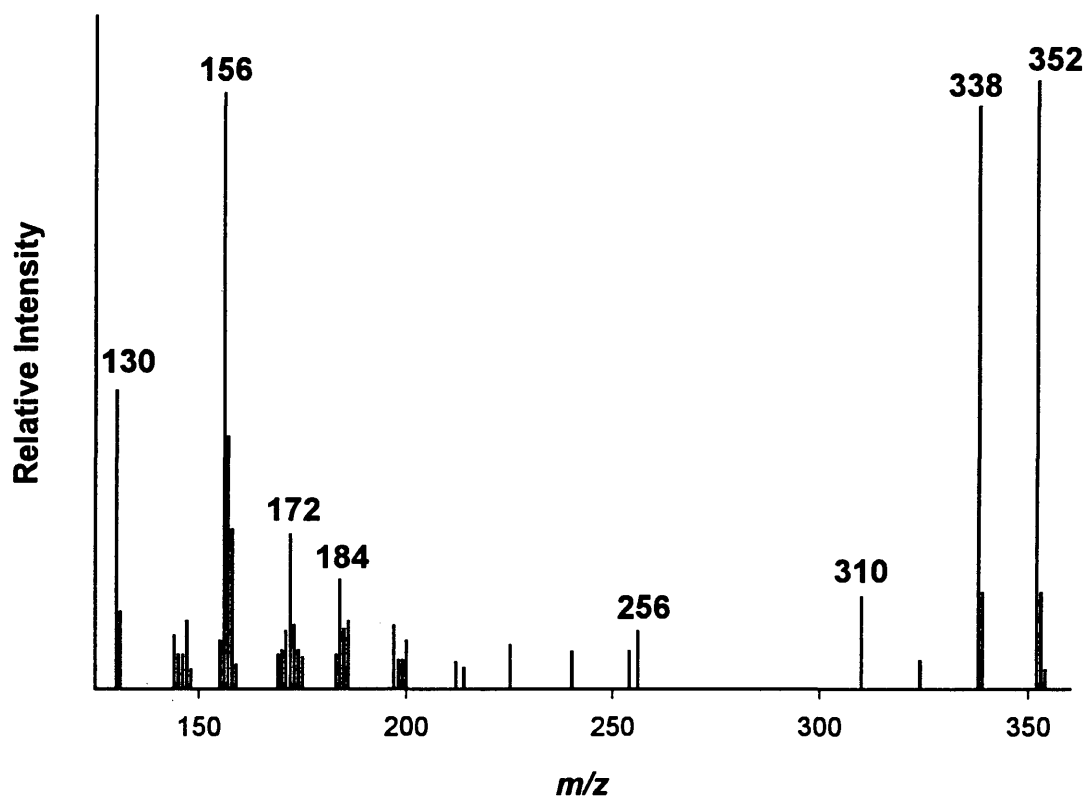


Figure A.20. DEI precursor ion mass spectrum of  $m/z$  129 from *Brucella neotomae*.

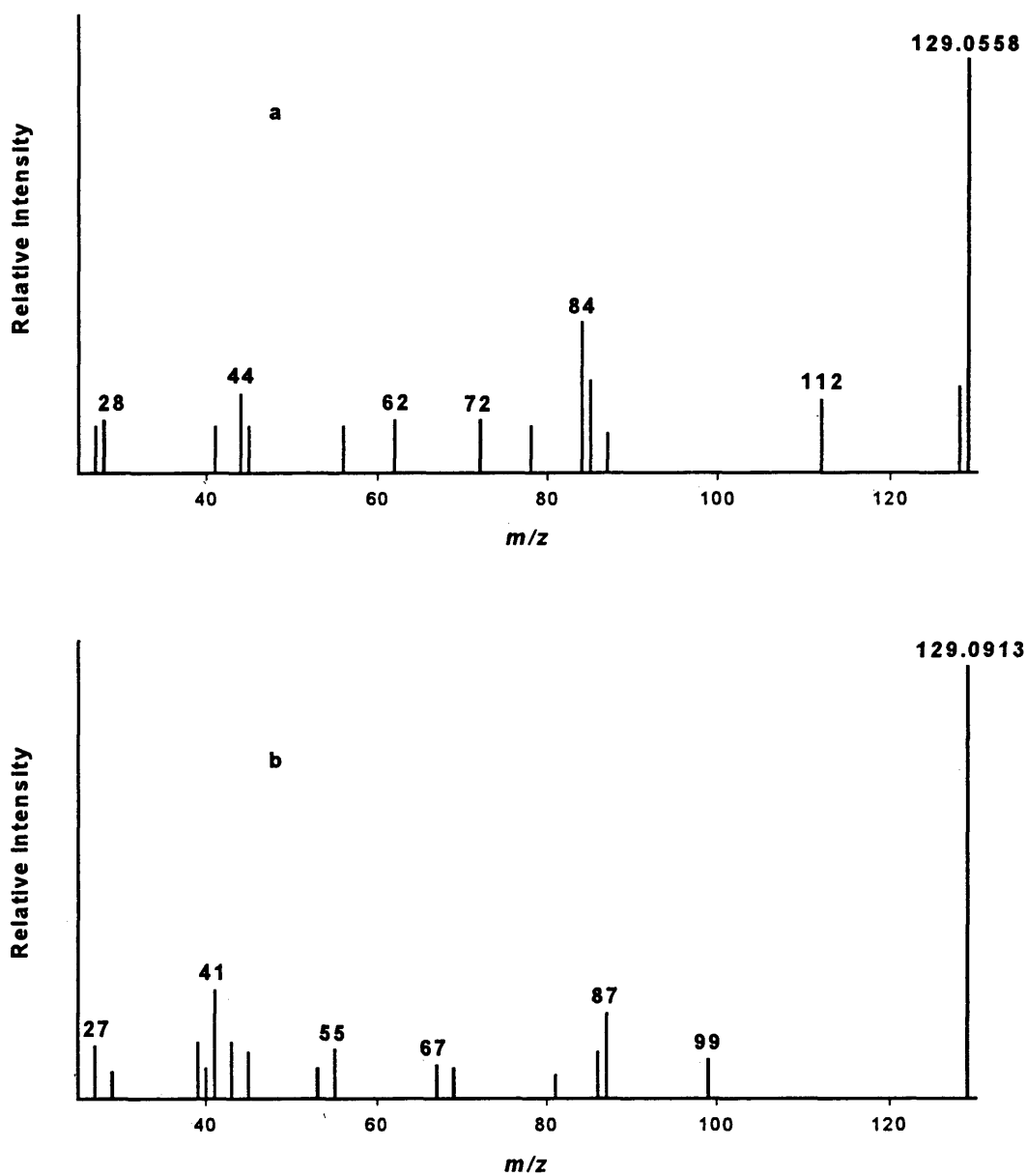


Figure A.21. HR-DEI product ion mass spectra of (a)  $m/z$  129.0558 and (b)  $m/z$  129.0913 from *Brucella neotomae*.

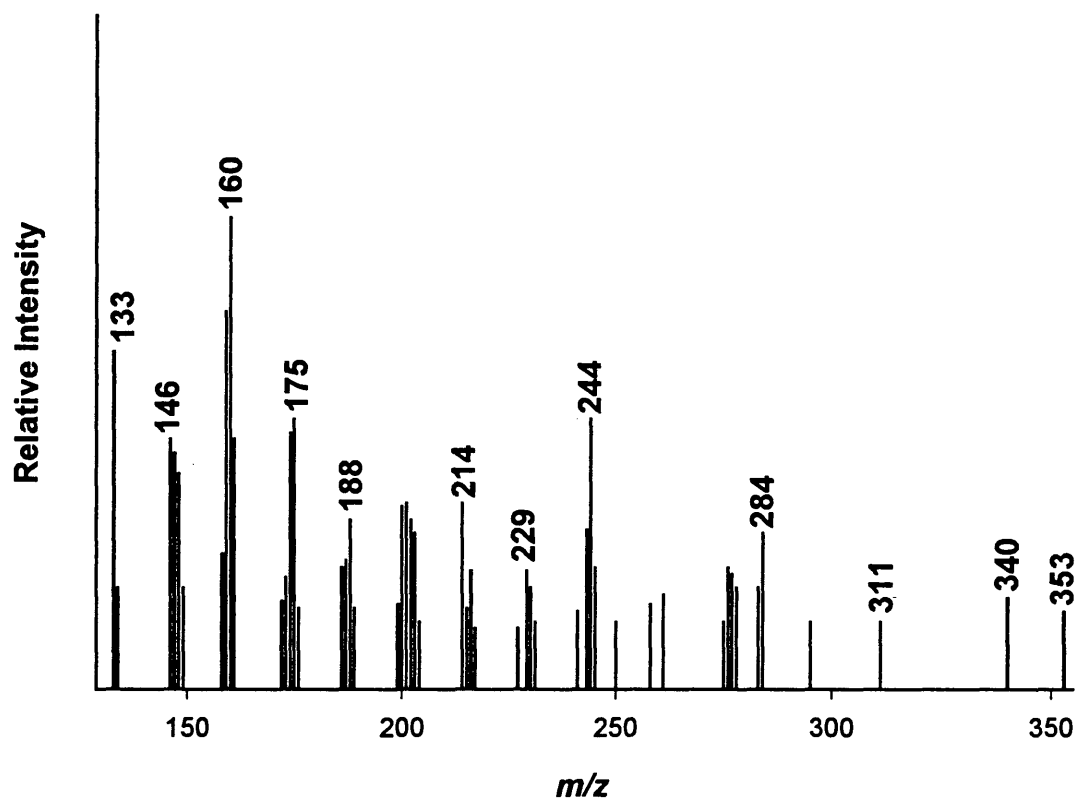


Figure A.22. DEI precursor ion mass spectrum of  $m/z$  131 from *Brucella neotomae*.

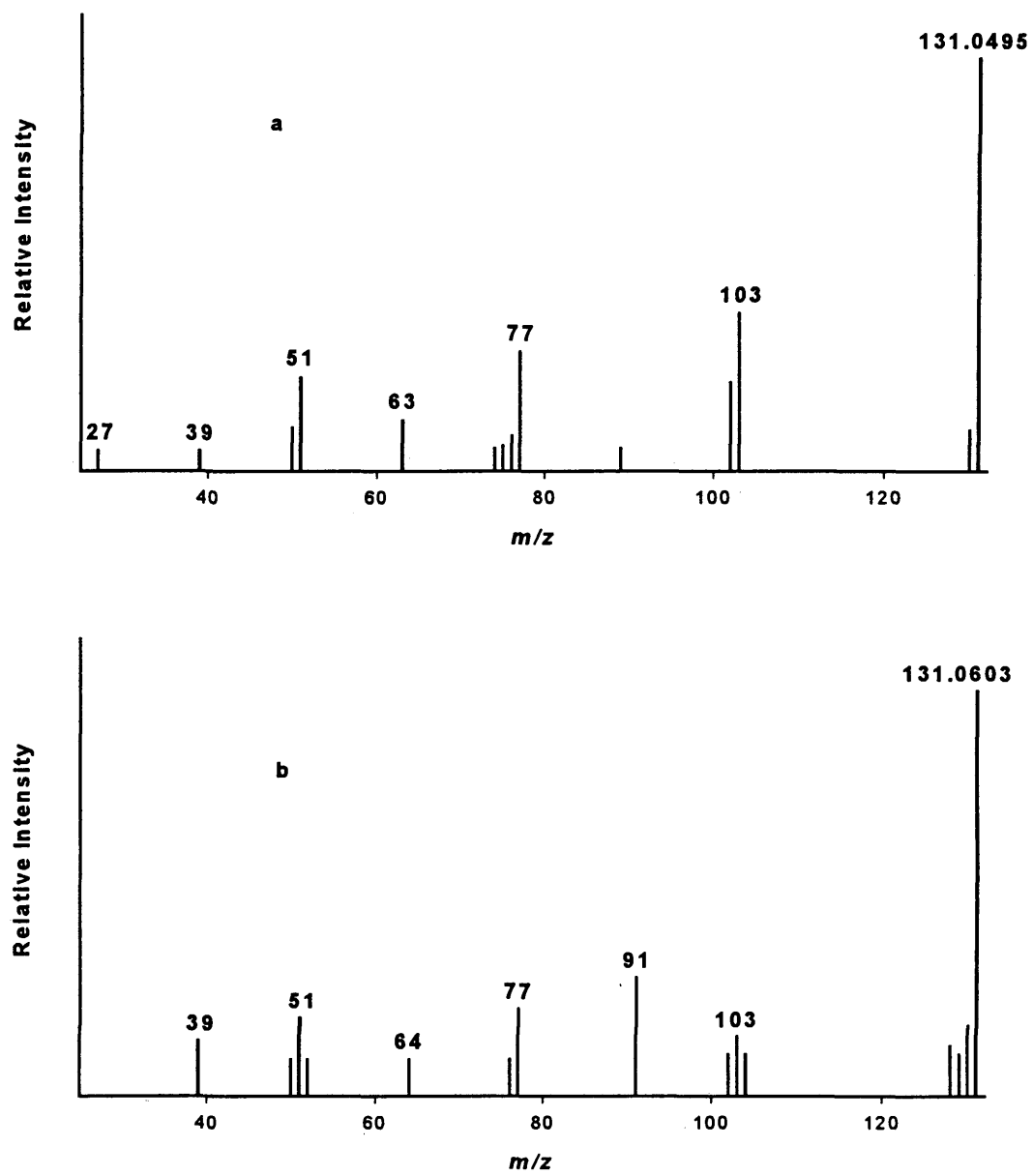


Figure A.23. HR-DEI product ion mass spectra of (a)  $m/z$  131.0495 and (b)  $m/z$  131.0603 from *Brucella neotomae*.